INTEGRATED REAL TIME STUDIES TO TRACK ALL PHYSICAL AND

CHEMICAL CHANGES IN POLYIMIDE FILM PROCESSING

FROM CASTING TO IMIDIZATION

A Dissertation

Presented to

The Graduate Faculty of The University of Akron

In Partial Fulfillment

of the Requirements for the Degree

Doctor of Philosophy

Emre Unsal

December, 2013

INTEGRATED REAL TIME STUDIES TO TRACK ALL PHYSICAL AND

CHEMICAL CHANGES IN POLYIMIDE FILM PROCESSING

FROM CASTING TO IMIDIZATION

Emre Unsal

Dissertation

Approved: Accepted:

_____   _____
Advisor   Department Chair
Dr. Mukerrem Cakmak   Dr. Robert Weiss

_____   _____
Committee Member   Dean of the College
Dr. Mark Soucek   Dr. Stephen Z Cheng

_____   _____
Committee Member   Dean of the Graduate School
Dr. David Simmons   Dr. George R. Newkome

_____   _____
Committee Member   Date
Dr. Coleen Pugh

_____
Committee Member
Dr. Chrys Wesdemiotis

ABSTRACT

Physical and chemical changes during the complex multi-step thermal imidization reaction were investigated including all processing steps (solution casting, drying and imidization), using newly developed highly instrumented measurement systems. These instruments allowed us to observe the dynamic relationship between the bound solvent evaporation that causes relaxation and chain orientation during the imidization.

Drying and imidization of PMDA-ODA solutions in NMP were investigated by a novel custom designed measurement system that tracks real time weight, thickness, surface temperature, in-plane and out-of-plane birefringence. At low temperature drying stage (T<120°C), the weight and thickness reductions occurred rapidly as a result of solvent evaporation. All the parameters started leveling off while the out of plane birefringence steadily increased and reached a plateau at longer drying times. When the temperature was increased for imidization reaction (T=200°C), additional weight loss accompanied by temporary reduction of birefringence was observed due to evaporation of bound solvent as solvent molecules decomplexed from the polymer chains and plasticized the film. During the latter stage, out-of-plane birefringence rose rapidly as the polymer chains increasingly became oriented with their chain axes were preferentially

oriented in the film plane. Throughout the whole process the in-plane birefringence remained zero. For the first time, these real time measurements allowed us to quantitatively show the dynamics between chain relaxation due to evaporation of the decomplexed solvent molecules, and orientation development due to decreased chain mobility caused by imidization reaction and increasing Tg for the PMDA-ODA/NMP solutions. In addition, the dynamics of this interplay was investigated by varying the processing conditions: initial casting thickness and drying temperature.

Chemical conversion, bound solvent and chain orientation that take place during thermal imidization of uniaxially constraint PMDA-ODA polyamic acid precursor film was investigated up to 200°C using real time measurement system that combines true stress, true strain, in-plane birefringence and temperature with polarized ultra-rapid scan polarized FT-IR spectrometry (URS-FT-IR). Upon heating, initially isotropic solution cast film developed stress and birefringence from the beginning while the solvent is decomplexed and evaporated. At a critical temperature (~130°C) onset of imidization reaction was observed as stress going through a maximum. Beyond this point, the evaporation and conversion took place simultaneously with steady increase in birefringence. At the end of the experiment, 80% conversion is achieved with 3% bound solvent remaining in the system.

ACKNOWLEDGEMENTS

TABLE OF CONTENTS

Page

KEY WORDS

polyimide, real-time, stretching, imidization, mechano-optical, PMDA-ODA, structural characterization, spectral birefringence, IR dichroism, orientation, IR spectroscopy

List of abbreviations

PMDA - pyromellitic dianhydride

ODA - 4,4'-oxydiphenylamine

NMP - N-Methyl-2-pyrrolidone

PAA – Poly(amic acid)

PI – Polyimide

DMAc – Dimethylacetamide

DMF – Dimethylformamide

MDA – Methylene dianiline

YI – Yellowness index

CTC – Charge transfer complex

CTE – Coefficient of thermal expansion

URS-FTIR – Ultra rapid scan Fourier Transform infrared spectroscopy

PM-IRLD – Polarization modulation infrared linear dichroism

LIST OF TABLES

LIST OF FIGURES

xiii

xv

CHAPTER I

INTRODUCTION

There is a rapid increase in interest and research to synthesize and
develop high performance and high temperature polymeric materials to meet the
requirements for advanced materials in industries such as aerospace,
automotive, and electronics. These applications require such materials that are
not only superior in one matter but a combination of many.[1] To meet these
requirements scientists have developed many polymeric materials including
polyimides and their derivatives.

Polyimides are a group of polymers that exhibit desirable properties in
many diverse areas. The superior properties of polyimides can be listed as;
excellent mechanical properties, low dielectric constant, low relative permittivity,
high breakdown voltage, low losses over a wide range of frequency, good
planarization, good processability, easy purification, wear resistance, radiation
resistance, inertness to solvents, good adhesion properties, low thermal
expansion, good hydrolytic stability and long term stability. These properties
make them attractive to varied industrial applications such as inter-metal
dielectric, high temperature adhesive, photoresist, nonlinear optical material,
membrane and Langmiur-Blodgett (L-B) film. The applications of polyimides

range from aerospace to microelectronics to optoelectronics to composites to fiber optics.[2]

Although the first aromatic polyimide was first synthesized at 1908, the commercialization started later at 1950s and early 1960s by DuPont. Their researchers were the first ones to develop a successful commercial route to high molecular weight polyimides.[2] Following this, a wide range of derivatives with tailored properties found their way to market.

These superior properties of polyimides have created processability problems in the industrial applications and turned into a large disadvantage for mass production with conventional melt polymer production methods like injection molding or extrusion. For example, rigid phenyl groups and imido ring pairs that constitute the backbone of the aromatic polyimides are responsible for high T_g values and high solvent resistivity. These properties also decrease their solubility making them processable only by solution processing with strong acids.

Due to the processability problems listed above, several distinct synthesis routes have been developed for the preparation of polyimides (Figure I-1). These routes lead to different properties in the films.[3] The reasons for these different properties can be stated as: starting from monomeric state in the solution, there is a series of often concurrent physico/chemical processes taking place before the final film is produced. These include evaporation of the solvent, concurrent imidization, orientation due to collapse of polymer chains and densification and consequent shrinkage (Figure I-2 & Figure I-3). It has been rather difficult to

explain these differences as the mechanistic differences that occurred during the complete processing cycle has not been understood well as most researchers studied the films by conventional off-line characterization methods after all the complex sequence of processes has taken place.
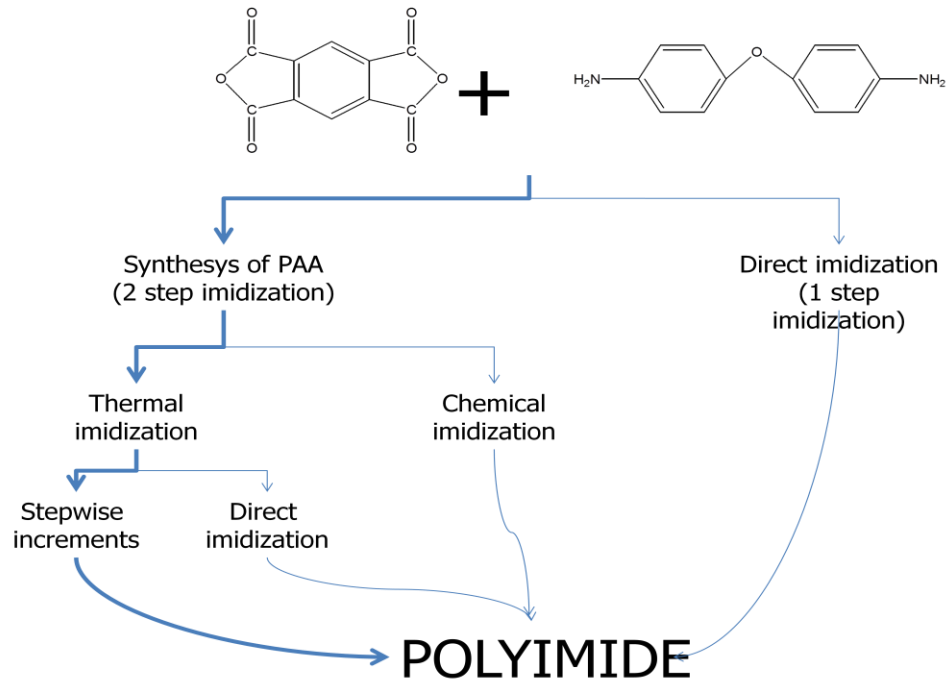
Figure I-1 Different imidization techniques

Since the excellent properties of polyimides are a result of combination of both chemical structure and final morphology of the products, it is important to understand the structural evolution within the material during imidization process, which directly affects the final thermal, mechanical and optical properties.[3] Additionally, given that these properties are a result of chemical structure and final morphology, it is not realistic to have a single definitive scheme for imidization and generalize it to all polyimides. As noted earlier, even for the same

type of chemical structure, different imidization routes can lead to different properties at the end. Due to this reason the focus of this research will be primarily based on pyromellitic dianhydride (PMDA) and oxydianiline (ODA) systems in N-Methyl-2-pyrrolidone (NMP) as solvent, which are commercially available from Sigma-Aldrich. The imidization process chosen among many other possibilities is the thermal treatment (both stepwise increment and ramp heating), which will cover all steps starting from poly(amic acid) precursor to the formation of polyimide.

To overcome the complexity of the imidization process, online measurement systems that can characterize the multifarious properties of polyimides during imidization is required. Since all steps in imidization process (solution casting, drying and imidization) contribute to the final structure development of films, it is necessary to monitor and characterize each of these steps separately.

Solution casting and drying of a polymer solution is a complex phenomenon that directly influences the final properties of the films produced with this method. The changes during drying process include solvent loss, gel-film collapse, thickness reduction and shrinkage. Our group designed a wind tunnel shaped solution drying system that is capable of real-time monitoring of temperature, weight, thickness and in-plane and out-of-plane birefringence of polymer cast solution (Figure I-2).

For the imidization process, in the recent years our research group has developed and modified further several well-built-custom design on-line measurement techniques, which include the measurement of mechanical properties at various temperatures; optical properties as well as electrical properties (uniaxial only) simultaneously when the samples are deformed both uniaxially and biaxially. These systems allow the measurement of birefringence, that can be related to orientation of chains microscopically, and mechanical properties such as true stress and true strain facilitating linkages between microscopic and macroscopic properties of materials. In other words, during deformation (or pure heating and holding) orientation of the chains can be tracked real-time. Besides, uniaxial stretching machine makes measurements of conductivity, where the electrical properties can be during deformation studies (Figure I-3).

In addition to these real-time measurements listed, an FTIR system that is capable of rapid scanning (up to 1000 scans/s) for the whole mid-IR range is equipped to the one of the uniaxial stretching machines, which was mainly used to determine the degree of imidization during different experimental conditions and solvent content real time. This FTIR system is also capable of measuring the dichroic ratio of the selected functional groups. This measurement will allow monitoring the orientation of selected functional groups during imidization process.
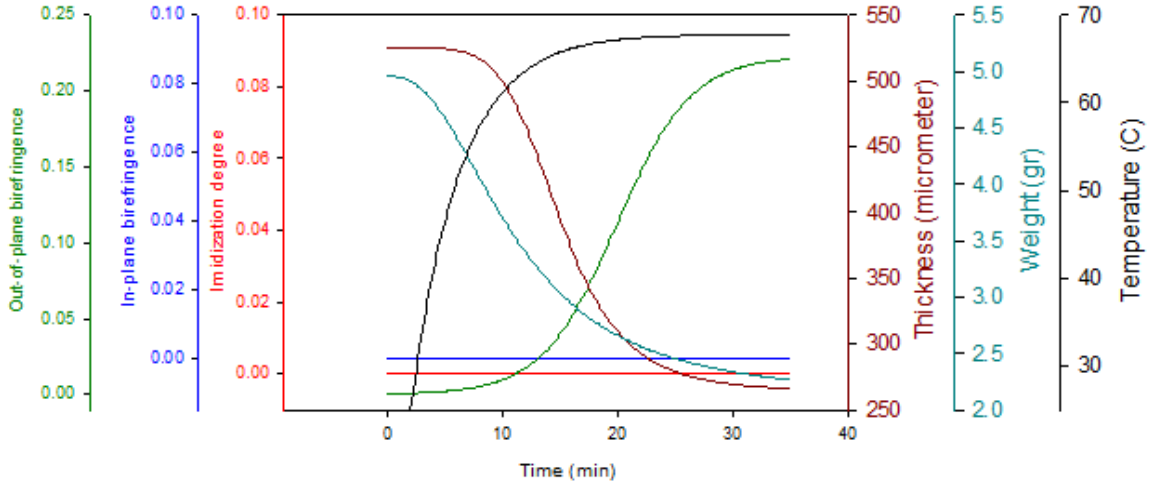
Figure I-2 Examples of changes during drying of polymer solutions that can be quantitatively measured by the designed drying equipment.
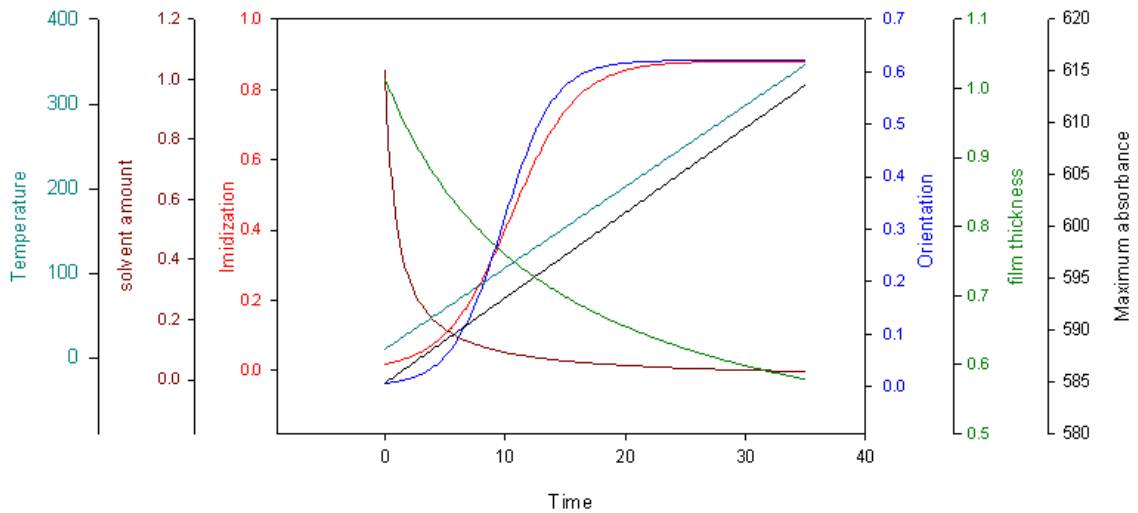
Figure I-3 Examples of changes during stretching/holding/heating of polymer films that can be quantitatively measured by the designed uniaxial stretcher.

As a summary the main scope of this work is to understand deeply the underlying changes in molecular mechanisms during the course of casting

6

evaporation/imidization/orientation processes process with the help of these powerful on-line measurement techniques validated with the offline characterization techniques. This will make it possible to correlate the experimental conditions or different imidization routes to the final structure of polyimide system to their macroscopic physical properties. Additionally this will create a control on the imidization process to have a fine tuning of the final polyimide product with desired optical, mechanical and thermal properties.

CHAPTER II

LITERATURE REVIEW

It is very difficult to summarize the complex nature of polyimides and imidization process in one heading. For this purpose, the literature review section is divided into two large sections. First section will give information on chemistry related issues of imidization process such as synthesis and imidization followed by synthesis of transparent polyimides. The second section will be on the structural development and characterization of polyimide films. This section will give information of processes that are required to produce high quality polyimide films and their characterization methods including a separate section for IR spectroscopy.

2.1.   Polyimides

Polyimides are the group of polymers that exhibit desirable properties in many diverse areas. The superior properties of polyimides can be listed as excellent mechanical properties, low dielectric constant, low relative permittivity, high breakdown voltage, low losses over a wide range of frequency, good planarization, good processability, easy purification, wear resistance, radiation resistance, inertness to solvents, good adhesion properties, low thermal expansion, good hydrolytic stability and long term stability. This wide range of

properties make them attractive and have called attention to varied industrial

applications such as inter-metal dielectric, high temperature adhesive,

photoresist, nonlinear optical material, membrane and Langmiur-Blodgett (L-B)

film. The applications of polyimides range from aerospace to microelectronics to

optoelectronics to composites to fiber optics.[2]

Although the first aromatic polyimide was first synthesized in 1908, the

commercialization started later in the 1950s and early 1960s at DuPont. In

DuPont's Film Department at the Experimental Station in Wilmington, Delaware,

C. E. Sroog and Andy Endrey were the first ones to develop a successful

commercial route to high molecular weight polyimides[2]. This was achieved by

synthesizing a soluble polymer precursor called a poly(amic acid) and then

converting this precursor to polyimide by heating or chemical treatments resulting

in Kapton® polyimide (Figure II-1). After this point research and development on

this family of polymers increased due to extensive interest in various applications

and resulted the appearance of new and improved polyimides with different

characteristics.
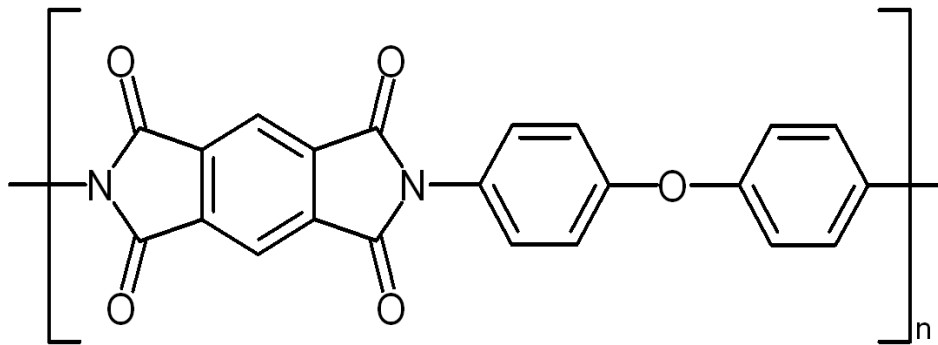
Figure II-1 Structure of Kapton® Polyimide

Massive research in the last years in chemistry and characterization of polyimides enabled countless possibilities to reach the end product by various methods. However aromatic polyimides gained the attention of academy and industry over other types due to more desired properties and formed the major category of such materials. Because of these reasons this study and review will focus on mainly chemistry and processing conditions of aromatic heterocyclic polyimides and more precisely on thermal imidization of pyromellitic dianhydride (PMDA) and 4,4'-oxydianiline (ODA) systems in N-Methyl-2-pyrrolidone (NMP) (Figure II-2).
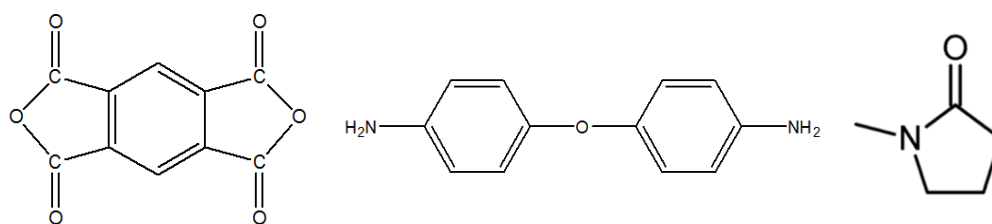
Figure II-2 Chemical structures of PMDA, ODA and NMP

2.1.1. Basic Properties

Polyimides consist of repeating units that are connected by an imide linkage. Imide linkages are formed by connecting two carbonyl groups to a primary amine group (Figure 2-3).

$$R'-\overset{\overset{\displaystyle O}{\|}}{C}-\underset{\underset{\displaystyle R}{|}}{N}-\overset{\overset{\displaystyle O}{\|}}{C}-R''$$
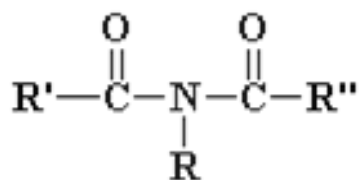
Figure II-3 Imide group

Imides are generally synthesized by the reaction of ammonia or a primary ammine with carboxylic acids or acid anhydrides. If this imide group is polymerized the resultant product is called a polyimide. Polyimides can be separated into two large categories depending on the chemical structure of the repeating unit: linear polyimides and aromatic heterocyclic polyimides.

Linear polyimides consist of many repeating units in the form of linear chains (Figure II-4). These polyimides generally show weaker properties compared to the aromatic ones.

$$\left(\!R-\overset{\overset{\displaystyle O}{\|}}{C}-\underset{\underset{\displaystyle R}{|}}{N}-\overset{\overset{\displaystyle O}{\|}}{C}\!\right)_{n}$$
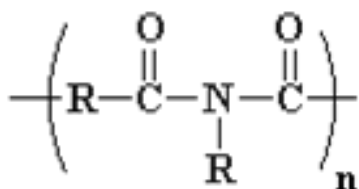
Figure II-4 Repeating unit of linear polyimides

Aromatic polyimides consist of several aromatic rings in their repeating units with a heterocyclic imide group. Heterocyclic compounds are cyclic units that include carbon and atoms other than carbon in the ring structure. These

11

aromatic heterocyclic polyimides are typical commercialized polyimides, due to their excellent properties coming from strong intermolecular forces.
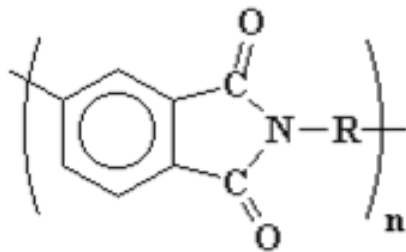
Figure II-5 Repeating unit of aromatic heterocyclic polyimides

2.1.2. Synthesis and Imidization of Aromatic PIs

The majority of polyimides consist of insoluble and infusible rigid aromatic chemical structures. As a result, it is challenging to synthesize and process polyimides with conventional methods. DuPont scientists were the first ones to overcome this disadvantage and produce aromatic polyimides on a bulk scale via a two step polymerization. This synthetic scheme was accepted by the market and enabled product to be commercially available.

The synthetic scheme consists of synthesizing a soluble precursor called a poly(amic acid) from the reaction of a dianhydride and a diamine and their precursor is further converted into polyimide via thermal treatment or chemical treatment (Figure II-6). Decades after DuPont's invention, the two-step imidization method is still the most widely practiced procedure in polyimide synthesis. Although this reaction scheme seems a collection of simple elementary reactions, all these reactions result in a very complex process at the end. [1–11]
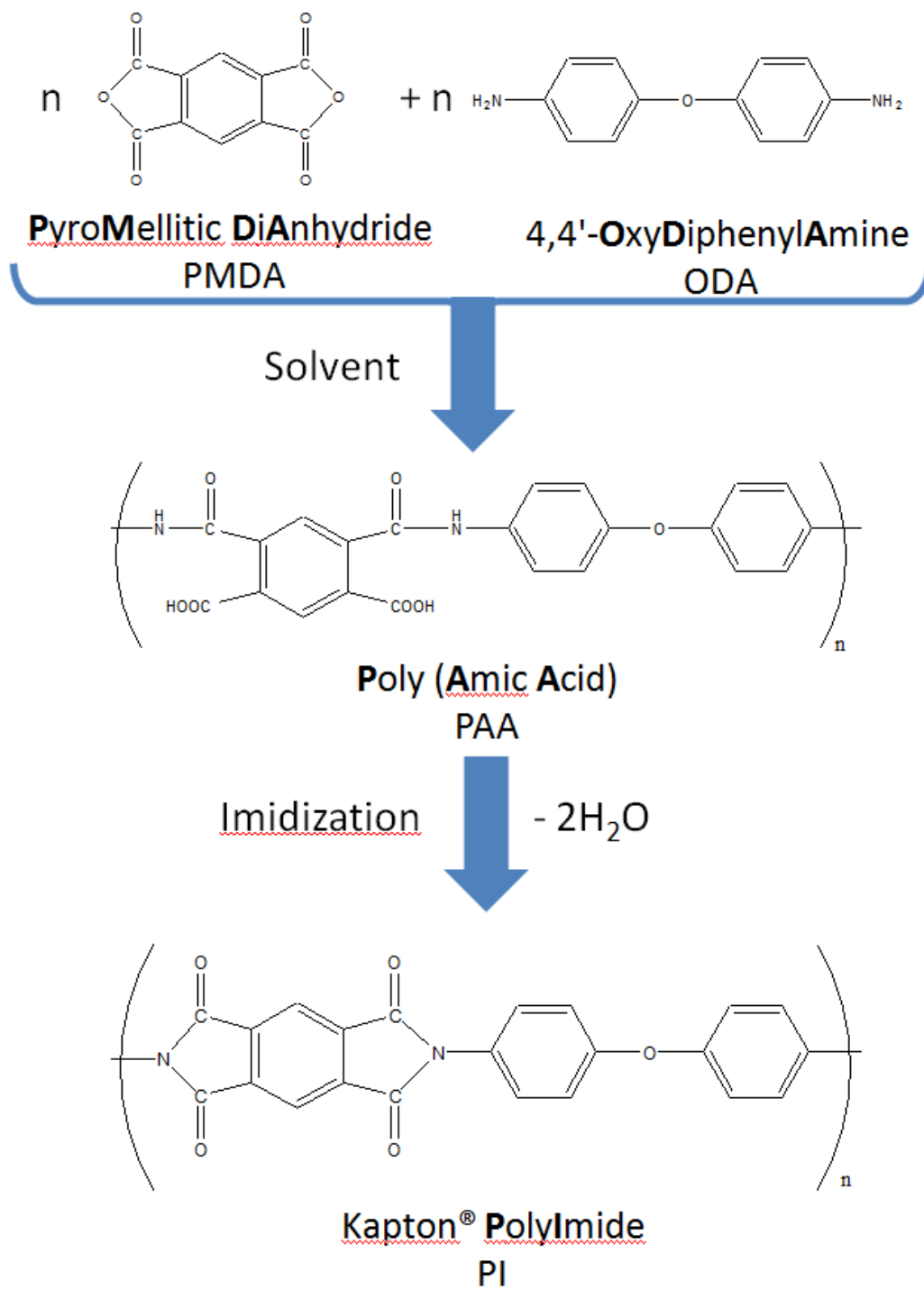
Figure II-6 Reaction Scheme of Kapton

The complexity of the synthesis can be affected by many factors, particularly from reaction conditions to as subtle as mode of monomer addition. One needs to pay great attention to small details in synthesis reaction in order to achieve a high molecular weight product at the end. These details include choice of monomer, solvents, reaction conditions, side and intermediate reactions. [1, 2, 6, 10]

Processing conditions on imidization adds another dimension to the complexity of the whole process mentioned above. On the two-step imidization scheme, after the synthesis of poly(amic acid) is completed, this product needs to be converted into polyimide via heat or chemical treatment. Each of these schemes has different effects on the final physical, optical and mechanical properties of the polyimide. [2, 3, 7, 8, 12,13]

This discussion will continue by giving brief information on synthesis of poly(amic acid)s for PMDA ODA systems and will mainly focus on processing conditions and imidization of poly(amic acid)s to polyimides. Other imidization techniques such as chemical imidization and direct (one step) imidization will also be mentioned briefly.

2.1.2.1. Poly(amic acid)s precursors

Poly(amic acid)s are obtained by reactions of diamines with dianhydrides in dipolar aprotic solvents such as NMP, DMAc or DMF (Figure II-7) at ambient

15

temperatures.[2, 10] The ratios of reacting diamines and dianhydrides are reported to be fairly close to the stoichiometric ratios.[11]
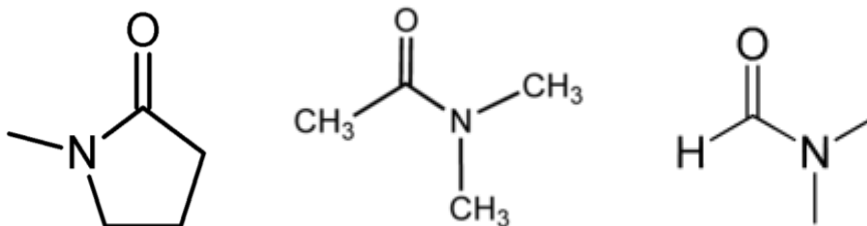
Figure II-7 Chemical structures of NMP, DMAc and DMF

Reaction occurs through a nucleophilic attack of the amino group on the carbonyl carbon of the anhydride group. This reaction is followed by a ring opening mechanism in the anhydride ring to form an amic acid group. [2, 10]
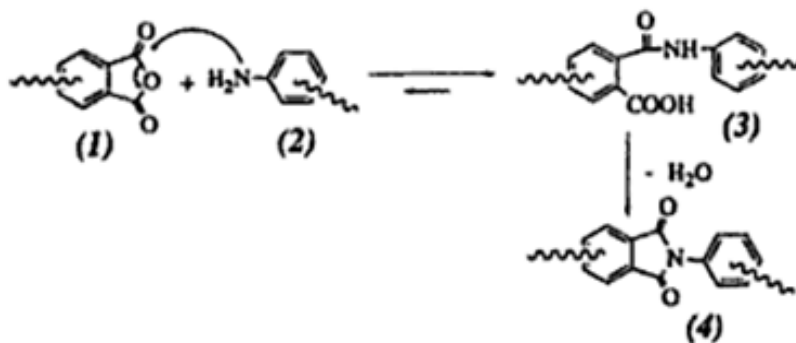
Figure II-8 Reaction mechanism of imide formation

Synthesis of poly(amic acid) is a reversible reaction as indicated by the arrows above. Forward reaction rate is several orders of magnitude greater than the reverse reaction rate. However in order to achieve high molecular weight

products, it's necessary to use high purity monomers. Another important factor is the order of reactions. The forward reaction in dipolar solvents is a second-order reaction and the reverse reaction is a first-order reaction. At high concentrations of monomers, the reaction equilibrium shifts to the right and high molecular weight poly(amic acid) product is achieved. [1, 2, 10, 11, 14]

Solvent also plays an important role in synthesizing high molecular weight poly(amic acid). Most commonly used solvents are DMF, DMAc and NMP, which are all Lewis' bases (Figure II-7). Following table summarizes the basic properties of these solvents (Table 2-1).[15] The starting reaction solution is basic and as the reaction proceeds and poly(amic acid) is formed the resulting final product is an acid. During the reaction, a strong acid-base interaction is observed between the amic acid groups and the amide solvent molecules. This interesting property of the solution mixture is the main force of exothermicity and the major driving source for the reaction. Considering this characteristic of the reaction, rate of formation of poly(amic acid) is generally faster with solvents that are more basic and polar.[1, 2] The solvents summarized in Table 2-1 share a high boiling point temperature and high dipole moment values in common where higher dipole moment values are an indication of high polarity.

Table II-1 Properties of common solvents for PAA

Solvents	Boiling Point (C)	Dipole Moment (Debye)	Refractive index
NMP	202	4.09	1.4700
DMF	153	3.82	1.4269
DMAc	165.5	3.79	1.4356

Indeed Solomin et al. noted that the rate of reaction for phthalic anhydride and 4-phenoxyaniline is increased with solvent basicity in order of THF<acetonitrile<DMAc in the ratio of 1:2.5:200. Following table (Table II-2) represents the rate constants for corresponding solvents.[16]

Table II-2 Rates of amic acid formation at 30°C and effects of solvents. k_1 is the rate constant of second-order forward reaction.

Solvents	k_1 (1/mol*s)
DMAc	0.085000
Acetonitrile	0.001020
THF	0.000387

Although the formation of poly(amic acid) is mainly dependent on the reactivity of monomers and the nature of the solvent, there are other very crucial reactions assisting to main reaction. These side reactions create undesired side

products and have an important effect on the final molecular weight of the product. In order to achieve a high molecular weight product, it is desirable to keep these side reactions in minimum. [1, 2, 10]

The most important side reaction is the hydrolytic degradation of poly(amic acid) chains even at ambient temperatures. In equilibrium conditions, the solutions of poly(amic acid) contain poly(amic acid) and small amount of anhydride groups. This small amount of anhydride group has a crucial role in the hydrolytic degradation of poly(amic acid) chains. In the presence of water, the anhydride groups are hydrolyzed to form ortho dicarboxylic group. This chemical group remains stable in solution and does not revert back to anhydride. Since the amount of anhydride decreases in the solution, more of it has to be produced to preserve the equilibrium condition. This condition shifts the reaction backwards causing a reverse reaction (from poly(amic acid) to form dianhydride and diamine) to replace lost anhydride in the solution. Although the amount of dianhydride is very small, this reaction chews the polymer chains affecting the molecular weight directly as well as entanglement and viscosity. [1, 2, 6, 10]

Figure II-9 Orthodicarboxyylic acid

The main source of water in the reaction solution are due to solvents and monomers that are not highly pure. The imidization reaction also generates water in the system. Conversion of poly(amic acid) groups to the polyimides produces one molecule of water for each imide group formed. One can argue that the imidization therefore the formation of water is relatively slow at ambient temperatures. However, as mentioned above, even the presence of a small amount of water in solution has an important role over a long period of time, causing a gradual decrease in molecular weight.

This gradual decrease is investigated in detail by Frost and Kesse.[17] Their system was 11% DMAc solution of PMDA-Methylene dianiline (MDA) PAA. The solution was kept at 35°C for 21 days which converted 20% of amic acid groups into imide groups. The corresponding amount of water that was generated during the reaction was 0.19%. To investigate this effect, they prepared experiments where water was deliberately introduced into the poly(amic acid) solution. Figure II-10 shows the viscosity changes when the solvent is dried (anhydrous), when the solvent is used as received (0.12% H_2O) and when additional water is introduced to the system (4.4% H_2O). As expected the anhydrous system showed a lesser decline compared to the other two conditions and the decline in viscosity increases as water amount in the system is higher.
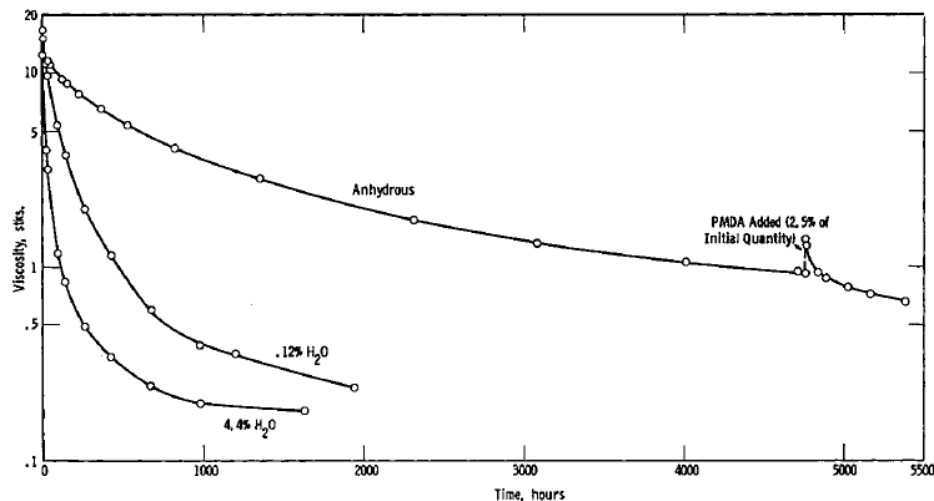
Figure II-10 Effect of water on viscosity of 10% DAPE-PMDA in DMAc at 35C

This study demonstrates that solutions of poly(amic acid) should be kept refrigerated in less humid environments when long term storage is necessary. This is necessary to prevent the small amount of reverse reaction and to maintain a high molecular weight for further processing, especially in imidization step.

2.1.2.2. Thermal Imidization of PAAs

The conversion of poly(amic acid)s to polyimides is mostly accomplished via the thermal imidization route. This thermal transition is preferable done in the solid state instead of viscous solutions of poly(amic acid). Solid state is preferred because of the necessity to create thin objects, such as films, coatings, fibers and powders. In general imidization is performed on dried films of poly(amic

21

acid)s by heating to final temperatures up to 250-400°C, depending on the stability and physical properties of the polymers (like glass transition temperature). The choice of thin films and gradual heating is commonly preferred over thick films and rapid heating due to the possibility of formation of bubbles and voids in the final polyimide film.

In the literature there is no exact recipe for how to achieve full imidization. People used different routes to achieve high conversions. Although the schemes are different, they can be categorized in two main types. One type is heating, gradually to 250-350°C depending on the type of the polyimide. [4, 8, 12, 18] Another route is by a gradual-stepwise heating (Figure II-11). [19–26] In this scheme, poly(amic acid) films are heated to certain elevated temperatures and stabilized at preferred temperatures by annealing for selected times. One example to this scheme would be gradual heating to 100°C and keeping at 1 hour, followed by gradual heating to 200°C and keeping at that temperature for another hour and finally gradual heating to 300°C. [22]
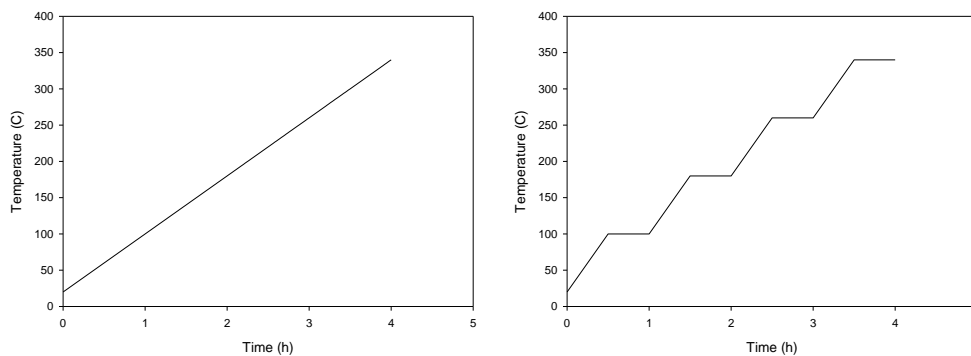
Figure II-11 Gradual and Stepwise heating profiles for thermal imidization

Even though the thermal imidization scheme seems easy and basic, the

process itself is very complicated. Complexity of the reaction comes not from the

elementary chemical reactions but from the dynamically changing physical

properties, such as diffusion rate, chain mobility, solvation, generation of by-

products, orientation of chains and acid-base interactions. Such a complex

system makes it difficult to analyze the system with simple and offline methods.

There are several common properties in imidization being independent

from the thermal route followed. A typical imidization graph for gradual heating is

shown in Figure 2-12.
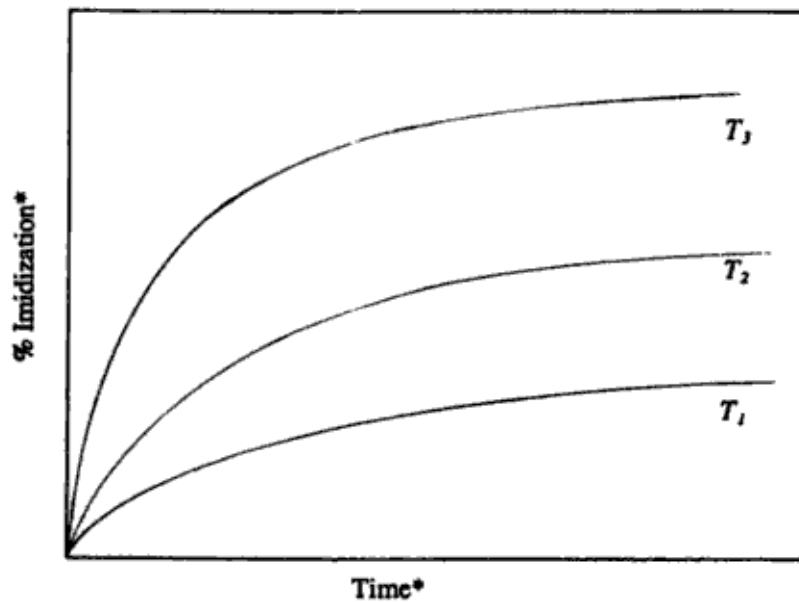
Figure II-12 Schematic representation of typical isothermal imidization
kinetic curves at various temperatures being T1<T2<T3. * Arbitrary Scale

The initial stages of imidization proceed much faster than the later stages and

reach a plateau. This behavior is common in any diffusion limited kinetic process.

23

As expected imidization proceeds faster and yields are higher at higher temperatures.

There are several dynamic reasons for this behavior as mentioned before. First of all the amount of bound solvent in the system plays a crucial role in determining the imidization kinetics. The effect of solvent on the system will be explained in more detail in the next section, since it is the main factor in determining the imidization rate. Second, the Tg of the system approaches that of the PI, which is higher than that of the PAA-NMP system. This prevents chains to move freely by stiffening them and the rate slows noticeably. The last reason is a consequence of the previous event the favorable conformation for the poly(amic acid) groups is precluded when the imide group is formed; the unfavorable conformation needs to first rotate to a favorable conformation and then form the imide group. This motion is difficult when stiff polyimide groups are formed.[10]

2.1.2.2.1.   Solvent Effect

Residual solvent is the main factor determining heating rate during thermal imidization and a gradual heating is necessary to prevent the formation of bubbles as mentioned before. Diffusion and evaporation of bound solvent and water that is produced during the cyclization reaction are the main reasons for this phenomenon. When a solution of PAA is cast with a high boiling point solvent (Table 2-1) is dried at ambient temperatures to a stable film state, the

resulting film may still contain a substantial amount of solvent depending on the drying conditions and thickness of the film. In the literature bound DMAc it is stated as 25-30% [26] and bound NMP is generally stated as 40-50%.[27]

Kreuz et al. reported that drying a DMAc solution of PMDA-ODA poly(amic acid) at ambient temperatures result in products that contain 28% solvent. For films tested by TGA at 170°C - 200°C, 29% to 32% weight losses were observed (Figure II-13). [26]
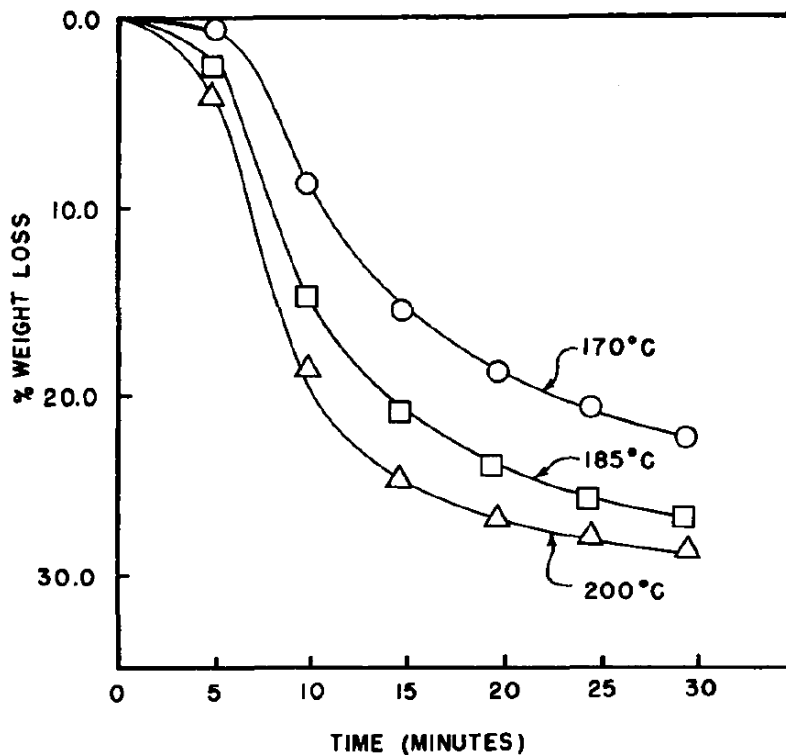
Figure II-13 Weight losses of PAA films with DMAc as solvent.

However, an investigation of imidization by infrared spectra revealed that only 80% conversion is achieved at the temperature range of 170°C - 200°C.

This conversion is also responsible for producing water coming from the decondensation reaction occurring during the cyclization of the 5 membered imido ring, which produces around 7% (by weight) water. This observation concludes that the weight loss is not only coming from the solvent but as well from the by-product water. Kreuz suggest that one mole of DMAc is associated with each carbonyl function. From this assumption the weight loss coming from the solvent would be 29.4% and the total weight loss including formed water would be 36% for 100% imidization. The formation of water or the presence of bound solvent makes it difficult to monitor the amount of imidization or amount of bound solvent alone by just tracking the weight changes for the PAA systems.

Particularly in the initial and intermediate stages of imidization, this substantial amount of solvent in the PAA matrix makes the reaction medium not a completely solid medium but rather a very viscous concentrated solution. The presence of the solvent plays an important role as reported by many researchers.[18,26–31] Imidization proceeds faster in the presence of dipolar amide solvents. This effect is attributed to the specific solvation to allow the favorable conformation of amic acid group to cyclize. This conformation is important since the adjacent COOH and NH groups react with each other during the imide ring formation. It may also be explained by the plasticizing effect of the solvent to increase the mobility of the reacting functional groups. The favorable property of amide solvent also suggests that its basicity to accept protons may be responsible for the specific effect. The proton of the carboxylic group is strongly hydrogen bonded to the carbonyl group of the of the amide solvent. The

26

cyclization of o-carbozyamide group results in dehydration bonding and release of the solvent molecule along with water of condensation.

Kreuz et al. further analyzed the kinetics of imidization and reported that the imidization rate increases rapidly with increasing temperature and has a rapid initial cyclization followed by a slower cyclization process. Similar results are also observed in thermal imidization of other poly(amic acid) structures. They concluded that there might be several reasons contributing to this behavior, such as the amount of bound solvent in the system assisting imidization.

Another reason is, as Kreuz assumes, imidization of the poly(amic acid) proceeds in two consecutive 1st order reactions, where the first stage is faster and second stage is slower (Figure II-14). They calculated the activation energies for fast cyclization as 26 kcal/mole and for slow cyclization as 23 kcal/mole, where the values are not significantly different. However, when they calculated the entropy of activation they found that for fast reaction, it is -10 e.u.and for slow reaction its -24 e.u, which they believe is a significant difference and responsible for the different imidization rates. They tried to explain this phenomenon by selected favorable conformation of amic acid and amide groups and solvents contribution to this conformation change.
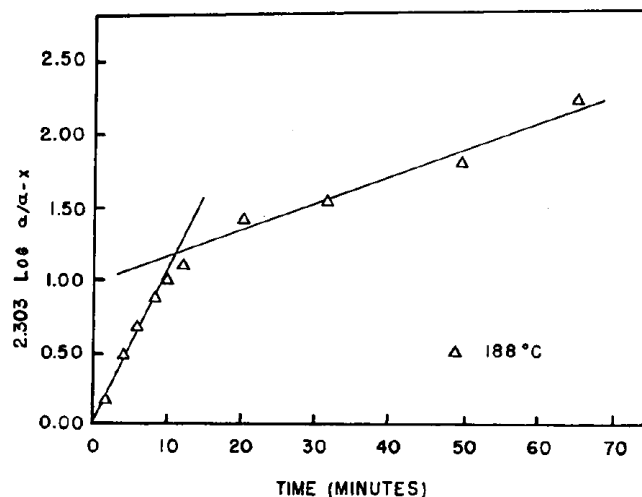
Figure II-14 Logarithmic plot of conversion of PAA

In order for the imidization reaction to take place, both amic acid and amide groups have to face on together. During imidization chain stiffness in the matrix increases due to the conversion of relatively flexible poly(amic acid) groups to rigid polyimide groups. This increase in chain stiffness decreases the ability of the amide groups to orient themselves easily and perform the imidization reaction. DMAc assists in favorable orientation for ring closure. As the film is heated the solvent evaporates and its loss before full conversion retards imidization rates.

To support the idea of solvent assisting the imidization reaction researchers began to investigate the corresponding model compounds. They synthesized the model compounds of poly(amic acid)s in high boiling solvents. Kreuz et al. followed the cyclization of the N phenylphthalamic acid (Figure II-15) and observed that they are soluble over the entire imidization reaction. There

28

was no deviation in the rate of reaction for conversions greater than 75%.

Compared with polymeric samples, the conversion of model compounds was

much faster at 150°C. In order to achieve similar conversion values with the

polymer, a higher temperature was required. This observation was important to

understand the role of the solvent in polymeric systems. They performed the

imidization reaction in solid phase for N-phenylphthalamic acid at 150°C and

found that only 42% conversion was achieved in 80 minutes whereas same

conversion values was achieved in 12 minutes in DMAc.[26]
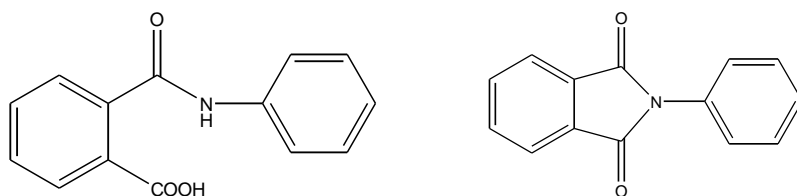
Figure II-15 N phenylphthalamic acid and corresponding imide

Brekner and Feger studied the interactions between the amic acid groups

and solvents used for imidization.[28] They used NMP as solvent and N

phenylphthalamic acid (Figure II-15) for the model compound for poly(amic acid).

They used TGA to investigate the system. Figure II-16 shows the results of

typical TGA diagram for diamic acid reactions.
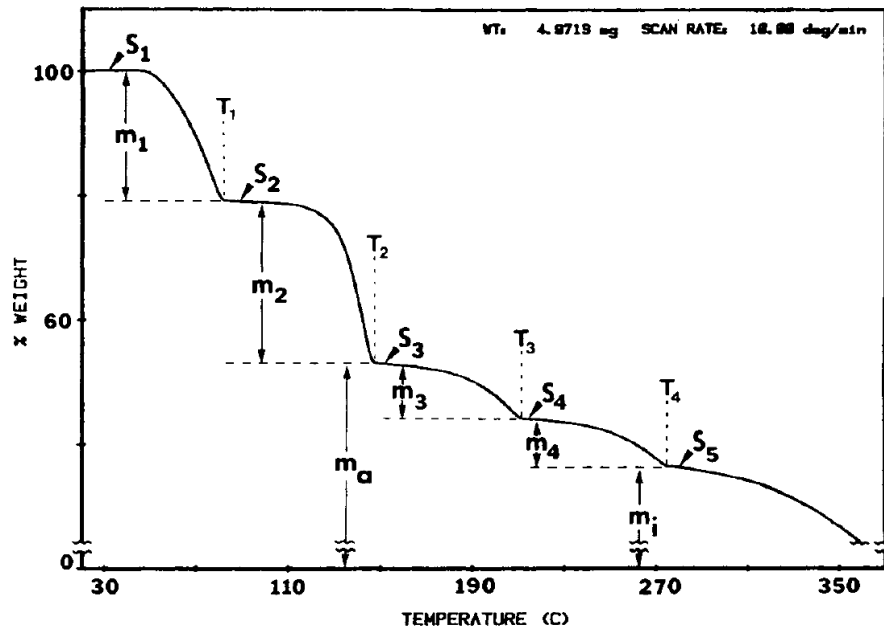
Figure II-16 TGA cure plot of diamic acid/NMP comlexed material

In the graph above, m values corresponds to relative weight losses in each step and T values are the temperature values. S values correspond to samples collected for polarizing microscopy and IR to investigate crystallization and imidization.

They observed that the ratio of m_a/m_2 remains constant and is independent of PMDA/aniline ratio in preparation. They also gathered samples volatilized from these steps and investigated with GC/mass spectroscopy. This experiment revealed that steps m_1 and m_2 are releasing pure NMP. Hence these two distinct NMP losses are an indication of two distinct interactions between diamic acid and NMP molecules.

30

The investigation of samples S_1 and S_2 ($T_1 = 39°C$) with polarizing microscopy and FT-IR revealed that both samples were highly crystalline and no imide formation was observed. In samples S_2 they observed the formation of a new carbonyl bond at 1661 cm^{-1} indicating that molecular environment of one carbonyl group is changing compared to S_1 samples. They assigned this carbonyl group to the amide carbonyl group and concluded that 2 different amide groups exist.

There was no indication of crystallinity and solvent with sample S_3. The following peak assignments were made from the FT-IR spectra of the samples in Figure II-17.

- o A = 1709 cm^{-1} = acid carbonyl stretching
- o B = 1680 cm^{-1} = carbonyl stretching of complexed NMP
- o C = 1661 cm^{-1} = amide carbonyl stretching
- o D = 1629 cm^{-1} = amide carbonyl stretching
- o E = 1600 cm^{-1} = aromatic ring stretching
- o F = 1550 cm^{-1} = amide II band
- o G = 1498 cm^{-1} = aromatic ring stretching
- o H = 1450 cm^{-1} = C-O stretching
- o I = 1408 cm^{-1} = NMP CH2 bending
- o J = amide III band range
- o K = acid group absorbance range

In the FTIR spectrum of samples S_1, S_2 and S_3 it was observed that all carbonyl absorbance shifted to lower wavenumbers. This observation supports the idea that initially the samples of S_1 consists of carbonyl groups complexed with NMP molecules. As temperature increases some of the

31

complexed NMP on the carbonyl groups is set free hence forming a new carbonyl peak at the lower wavelength of 1661 cm^{-1}. The presence of previous peak results that both conformations exist in samples of S_2. Finally with further heating samples S_3 all complexed NMP molecules are removed and all carbonyl peaks shifted to lower wavelengths indicating that only one carbonyl group environment is present on sample S_3 which is decomplexed from NMP molecules. The removal of NMP can also be traced by disappearance of the 1408 cm^{-1} peak (Figure II-17).
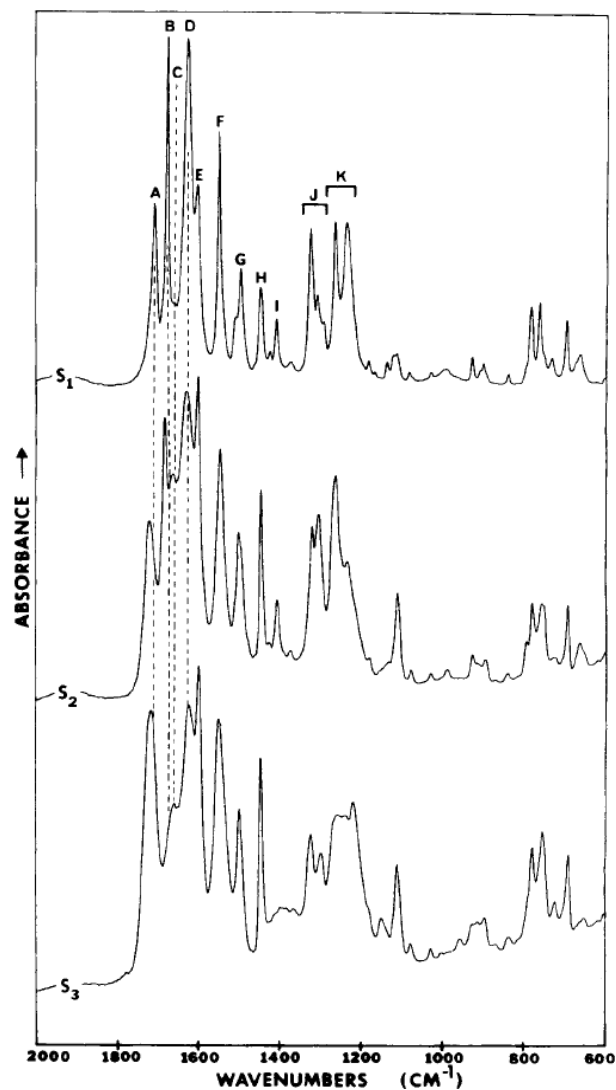
Figure II-17 FTIR spectra of samples S1, S2 and S3 in the range of 2000-600 cm-1 range

By all these observations they conclude that samples S_1 are ¼ complexes and S_2 are ½ complexes of diamic acid/NMP. Quarter (¼) complexes are not as stable as ½ complexes and in fact ¼ complexes lose NMP already if kept under vacuum even at room temperature. However addition of more NMP to the system reverts back to ¼ complexes. They calculated the decomplexation enthalpy for

these complexes and found that first step is 20 ± 2 kJ/mol for NMP. This value corresponds to complexation enthalpies of one hydrogen bonding per NMP molecule. They approximated the second decomplexation step as 55 kJ/mol. This relative high value corresponds to greater thermal stability for ½ complexes and indicates two hydrogen bonds per NMP molecule.

Furthermore they concluded that there are four possible sites that have the potential in participating hydrogen bonding with NMP molecules. These are two amide groups and two carboxylic acid groups. Compared within the molecule, the acid groups are better proton donors than amide groups. This difference leads to formation of two distinct NMP complexes with different thermal stabilities. As temperature increases, NMP molecule bonded to amide groups is released first. The amide groups forms another hydrogen bonding with another NMP molecule that is already bonded to carboxyl group or makes an inter-chain or intra-chain hydrogen bonding with the carbonyl group. More heat supplied to the system and remaining NMP molecule is set free via decomplexation from diamic acid group.
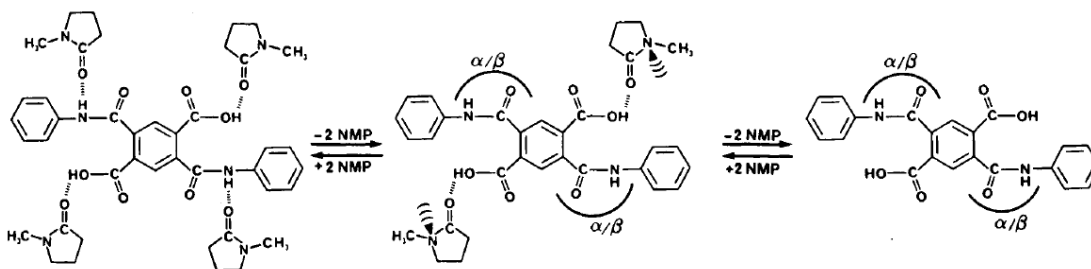
Figure II-18 Complexation/decomplexation process: a/b indicates the possibility of two different molecular surroundings

Brekner and Feger also investigated the cure of corresponding poly(amic acid) of the model compound (PMDA-ODA). [29] Quarter (¼) and half (½) type of complexes as well observed in the polymeric form and thermal stabilities of these complexes found to be very similar to the ones in model compound. Baking of poly(amic acid) films above room temperature and below 85°C resulted films with ½ complexes and no imidization occurs at these temperatures. Imidization started to be observed at temperatures above 102°C. At 144°C after 36 minutes of curing the final films still contains more than 11wt% NMP. As mentioned above, at 129°C in the corresponding model compound all complexed NMP was removed from the system. This slow removal of NMP at higher temperatures compared with the model compound is not due to the complexation/decomplexation mechanism but rather the decrease in the solvent diffusion rate as imidization proceeds in the poly(amic acid) films. As a result in polymeric systems solvent removal and imidization proceeds side by side and removal of solvent is delayed compared to model compounds investigated.

Feger investigated the curing of polyimide films obtained from poly(amic acid)s of PMDA-ODA in NMP with dynamic mechanical thermal analysis (DMTA) (Figure II-19).[32] Prior to experiments, the films were cured around 85°C and ended up ½ complexes of PAA/NMP system. From the graph it was concluded that there are two distinct processes one starting around 110°C and one above 350°C. As previous results he concludes that the first process is the decomplexation of bound NMP from the system. Further heating to temperatures above 300°C revealed a second process. This process is attributed to molecular

packing of chains as temperature reaches the glass transition of polyimide and increases the chain mobility.
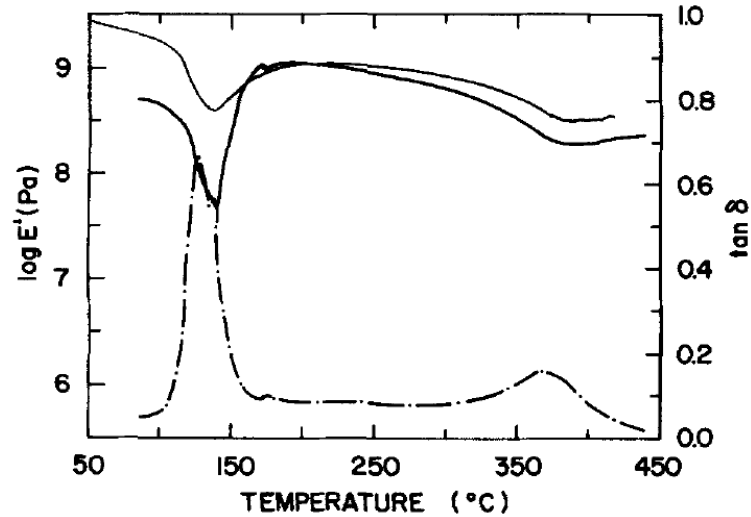
Figure II-19 Typical DMTA trace of the thermal cure of poly(amic acid)films at 5C/min.

Feger attributes the decomplexation of NMP form the poly(amic acid) groups as a plasticizing effect on polymer matrix. In addition to this effect, decomplexed poly(amic acid) chains become more flexible. Feger also mentions as imidization proceeds the formation of water also contributes to plasticizing effect of bound NMP created. These two effects side by side promotes imidization.

As a support to this approach, the term accelerator is used for high boiling point co-solvents for the conversion of poly(amic acid)s to polyimides by Frayer.[33] In his patent he claims that the use of co-solvent accelerates imidization and permits lower processing temperatures for applications of polyimides (Table II-3).

36

N-cyclohexyl-2-pyrrolidone (CHP) was chosen for high boiling point solvent

(BP=250°C) for the system.

Table II-3 % Conversion of Polyimides followed by FT-IR with a heating
rate of 10°F/min. None = No co-solvent accelerator

Temperature (°F)	None	10 % CHP	Time (min)
200	2.0	2.0	0
250	2.0	9.0	5
300	2.0	16.5	10
350	3.1	30.5	15
400	14.3	40.4	20
450	35.3	66.2	25
500	62.6	85.7	30
550	81.2	96.4	35
570	87	98.5	40

Feger also investigated the effect of heating rate on imidization. It was

found that the onset of decomplexation process stays constant as expected

being independent of heating rate. However the plasticization process changes

strongly with heating rate. This is attributed to a competition between the

imidization and diffusion rate of solvent.

Hsu and Liu performed a similar study to investigate the effect of solvent during thermal imidization for polyimide resins. [27] They examined the NMP as a solvent in PMDA-ODA PAA with varying the amount of solvent in the system. They proposed that there are free NMP molecules as well as bound solvent in a poly(amic acid) film dried at ambient temperatures. As temperature increases these molecules plasticize the film and facilitate imidization and they will evaporate. As temperature increases NMP molecules that are H-bonded to amide groups will become free since their decomplexation energy is lower. These molecules will also plasticize the film before evaporating. At this point past of the amide groups that are set free is converted to imide group. Further temperature increase results the decomplexation of NMP molecules H-bonded to acid groups are set free and film is plasticized again. The majority of the imidization takes place during this stage. Additional heating will result in fully imidized solvent free polyimide films (Figure II-20).
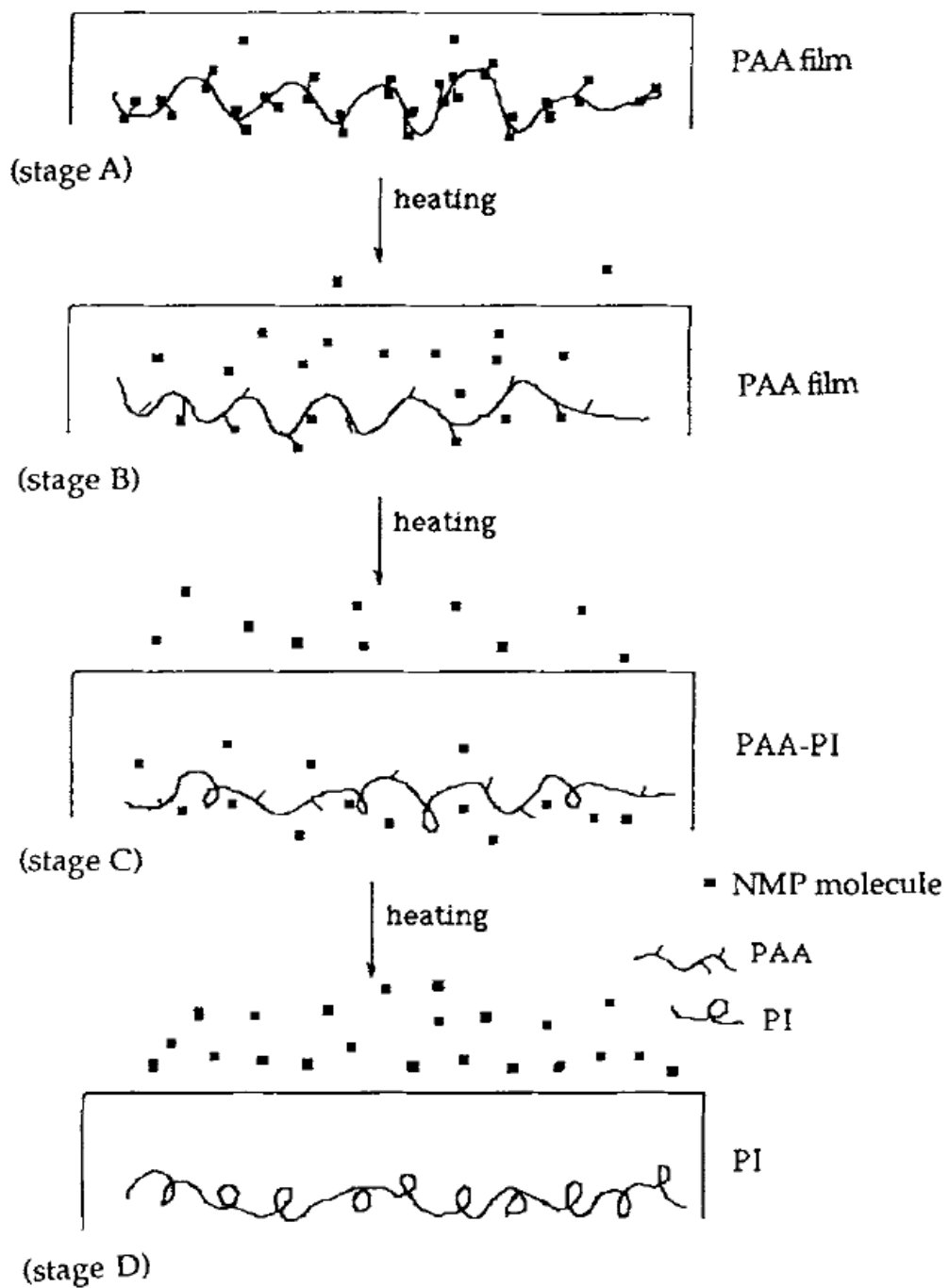
Figure II-20 Schematic illustrating the formation of NMP from PAA solution and imidization

2.1.2.2.2.   Tg and conformational factors

The glass transition temperature (T_g) of the poly(amic acid)/NMP solution changes during imidization. The diffusion and evaporation of the solvent as well as conversion of relatively flexible poly(amic acid) chains to more rigid imide chains increases the T_g of the system.

Kotera et al. reported the T_g of the PAA/NMP system as 107°C where they used modulated DSC to make the observation. [23]

As imidization proceeds, chains of poly(amic acid) are being converted to polyimide. When imidization is partially occurred, this creates poly(amic acid) groups and polyimides on the same chains, resulting a copolymer of PAA and PI. As imidization proceeds, the T_g of the system shifts from T_g of PAA to T_g of PI. T_g of a copolymer can exist between two extreme states, block copolymer or a random copolymer. T_g of a block copolymer can be expressed as simply adding the contribution of each component. On the other hand T_g of a random copolymer can be explained by Fox's equation as follows

$$\frac{1}{T_g} = \left\{ \frac{w_{PAA}}{T_g(PAA)} \right\} + \left\{ \frac{w_{PI}}{T_g(PI)} \right\} \tag{1}$$

where, w_{PAA} is the weight fraction of PAA, w_{PI} is the weight fraction of PI. T_g of the fully imidized polyimide film was found to be 420°C.[34] Following graph shows the two extreme conditions for possible T_g variations in PAA/PI copolymer. [23] The observed values correspond to the predicted Fox's equation. This result also

concludes that the imidization reaction from PAA to PI proceeds randomly on polymer chain.
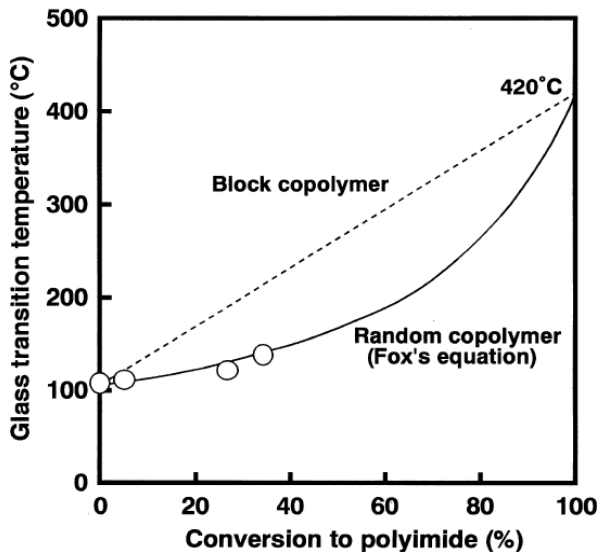
Figure II-21 Relationship between Tg of poly(amic acid) PMDA-ODA cast from NMP solution and the conversion to PI

Similar to bound solvent and physical properties of the medium, chemical structure also plays an important role on thermal imidization. As mentioned before, the slower rate in imidization can also be attributed to unfavorable conformations of amic acid and amide groups. In order for imidization to proceed the amic acid and amide groups has to be close and facing together. The initial and fast step in imidization consumes all the favorable conformations (Figure II-22 – a). In the second slow step, the unfavorable conformation (b) has to rearrange to conformation (a) for imidization to take place. [10]

41
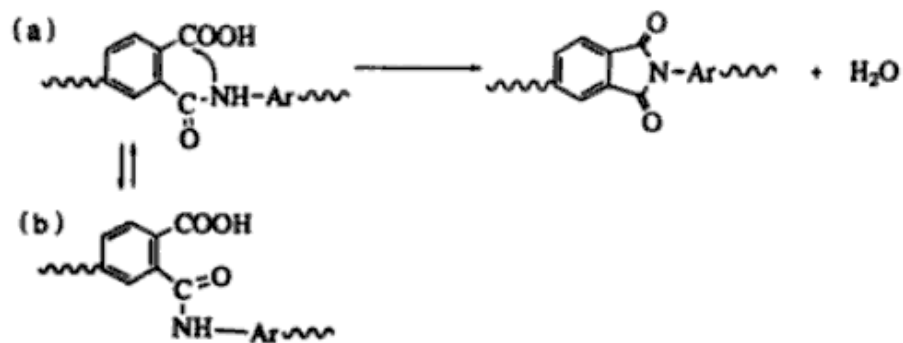
Figure II-22 Mechanism of thermal ring closure of amic acid to imide

The effect of conformational structure was investigated in detail by Verbicky and Williams.[35] Their study focused on the relationship between the structure of the amic acid group and thermal ring closure reactions. The imide formation reduced as the steric bulk of the alkyl substituent in the phthalamic acid increases (Table II-4).

Table II-4 Thermal reactions of N-Alkylphthalamic acids

R	Number of β-carbon	% Yield	
		Imide	Anhydride
$-CH_3$	0	100	0
$-CH_2CH_2CH_2CH_3$	1	100	0
$-CH_2\overset{\displaystyle CH_3}{\underset{}{C}}HCH_3$	1	98.9	1.1
$-CH_2\overset{\displaystyle CH_3}{\underset{\displaystyle CH_3}{C}}-CH_3$	1	97.6	2.4
⟨H⟩	2	82.2	17.8
$-\overset{\displaystyle CH_3}{\underset{}{C}}HCH_3$	2	66.3	33.7
$-\overset{\displaystyle CH_3}{\underset{}{C}}H \cdot CH_2CH_3$	2	65.3	34.7
$-\overset{\displaystyle CH_3}{\underset{\displaystyle CH_3}{C}}-CH_3$	3	12.0	88.0
$-\overset{\displaystyle CH_3}{\underset{\displaystyle CH_3}{C}}-CH_2CH_3$	3	0	100

2.1.2.3. Chemical Imidization of PAAs

Another method to synthesize polyimides is chemical imidization. In the case of manufacturing fibers or molding powders, chemical imidization is chosen instead of thermal imidization due to low energy requirements. However the necessity of using dangerous reagents, this technique is rarely used for other applications.[1, 36]

Similar to thermal route, this process also includes a two step mechanism. First step is the synthesis of soluble precursor poly(amic acid). Second step is the distinctive step that separates the thermal and chemical imidization. Instead of heating the poly(amic acid) solution at elevated temperatures, dehydrative cyclization of poly(amic acid) chains is carried by chemical reagents at ambient temperatures. [37–42]

These chemical reagents are composed of a mixture of dehydrating agents and base catalysts. Most common dehydrating agents are acid anhydrides such as acetic anhydride and propionic anhydride. For base catalysts pyridine, trialkylamines and methylpyridine can be used. Among these reagents acetic anhydride/pyridine pair is commonly used. For solution imidization metal carboxylates are also added to the solution with dehydrating agent and base catalyst. [36-38, 43,44]

As happens in thermal imidization, conversion of poly(amic acid) to polyimide with chemical imidization not only yields imide groups but also several

44

side products such as isoimides and o-carbxyamides. It is necessary to treat the final product thermally at high temperatures to complete the imidization by converting isoimide and o-carboxyamide groups to imide groups. Also this treatment helps removal of the any residual solvent. [1, 36]

2.1.2.4. Charge transfer complex (CTC) formation

Charge-transfer complexes (CTC) or electron donor-acceptor (EDA) complexes are molecular compounds resulting from the association of an electron-donor molecule (D) with an electron-acceptor molecule. This interaction generally results in a fractional or total transfer of the electron from donor molecule to acceptor molecule. The attraction between the molecules is created by electronic transition into an excited electronic state, resulting a stabilizing force for the molecular complex.

These electrostatic interactions between the two partners vary in strength. It can be classified as a weak interaction where only a partial electron transfer occurs as in dipole-dipole interactions, dipole-induced dipole type or dispersion forces. It can be classified as a strong interaction as happens in ionic interactions where a total transfer of the electron occurs. The donor-acceptor complexation is an equilibrium reaction. In the macromolecules these interactions are usually weak complexes. [45]

In the formation of electron-donor-acceptor complex, the electron is transferred from the ground state of the donor to the excited state of the

45

acceptor. This transition usually requires less energy than the transitions of individual donor and acceptor molecules.

Regardless of its nature (inter or intra-molecular, small or macromolecules) the formation of CTC complex always appears as a new and unique absorption band in the UV or visible domain of the spectrum different from the individual molecules. This band can show a peak maximum or can be a shoulder appearing and can be observed in both solution and solid state (Figure II-23).
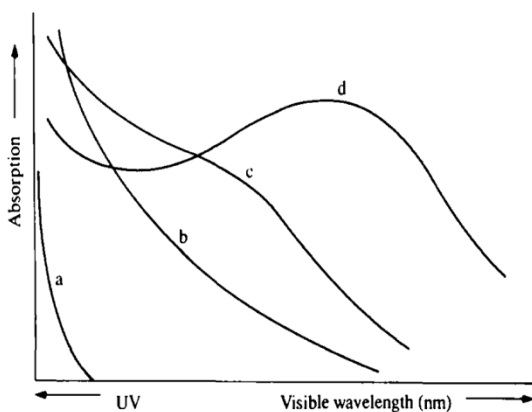
Figure II-23 Absorption of the macromolecular complexes. (a) absorption spectrum of an individual component, (b) supplementary absorption due to complex formation, (c) CT absorption band with a wide shoulder (d) CT absorption with a net maximum

The complexation can be used as a method for shifting the photoconductivity spectrum of photo-conducting polymers in to visible domain. The position of the absorbance band can be determined by the following formula,

$$hv_{DA} = I_p - E_a + W \tag{2}$$

where I_p is the ionization potential of the donor molecule, E_a is the electron affinity of the acceptor molecule and W depends on the columbic attractions and the environment. The position of the absorption band of the complex can be effected or modified by the solvent due to its effect on W. [45]

Dine-Hart and Wright studied the CTC complexes in model imides, (including different substitutions on the phenyl ring) and reported that formation of such complexes has an important influence on the properties of the materials such as melting point, solubility and absorption spectra (Figure II-25).

They suggested that the central ring (A) in dianhydride part is electron deficient due to the four carbonyl groups surrounding it, and N-phenyl groups (B) are electron rich due to the electron donating power of the nitrogen (Figure II-24). This electron acceptor and donor character results a highly polarized chain structure. Also the N-phenylphthalimide and –C6H5 substituent is coplanar with the imide ring, which concludes the possibility of formation of intermolecular charge-transfer complexes. They concluded that the intense yellow color of the compounds is a result of this characteristic. [46]
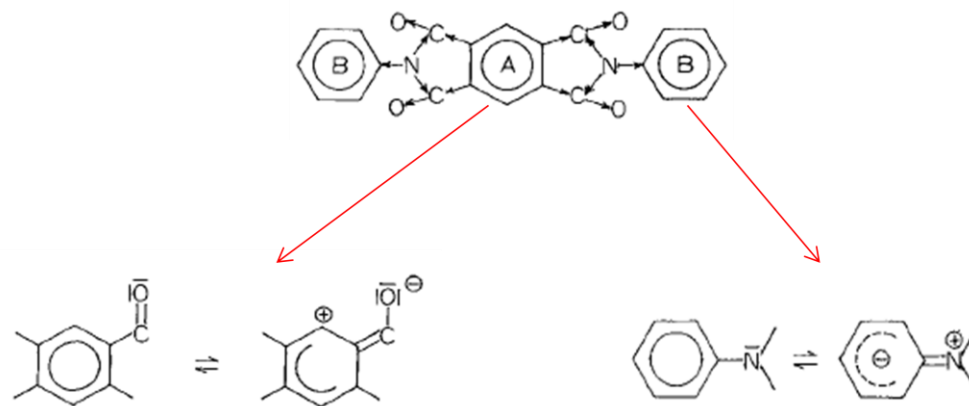
Figure II-24 Polar nature of imide structure

Sample No.	Substitution	Method of preparation	Structure
8	*o-*	B	
9	*m-*	A	
10	*p-*	A	
11	*o-*	B	
12	*m-*	A	
13	*p-*	A	
14		B	
15	*o-*	B	
16	*m-*	A	
17	*p-*	A	
18	*o-*	B	
19	*m-*	B	
20	*p-*	B	

Figure II-25 Imide samples with possible substitutions on the aromatic ring

48

To prove the explanations on the effect of molecular linearity on the formation of inter molecular charge-transfer complexes, Dine-Hart and Wright synthesized imide samples with different substitutions on the phenyl ring to disturb the planarity of the molecule. (Figure II-25) They observed that the para substituted compounds didn't disturb the planarity of the molecules and these molecules have an intense yellow colors, highest melting point temperatures, and low solubility in solutions. Meta isomers have smaller melting point temperatures and higher solubility values compared to para units. However they still exhibit yellow color, indicating that the meta substitution disrupted the order but the molecules are still planar and formed charge-transfer complexes. On the other hand ortho substituted isomers (Figure II-26) disturbed the planar structure; therefore close packing, of the molecule due to steric hindrance. This resulted near white color, low softening point and high solubility for these compounds. (Figure II-27)
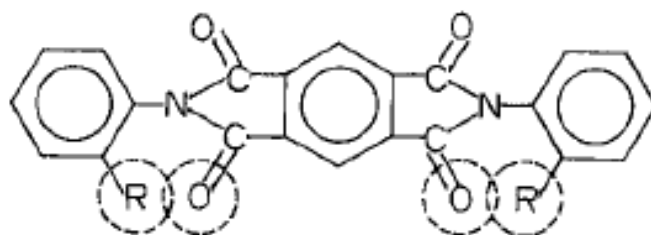
Figure II-26 Ortho-substituted imide structure and steric hindrance
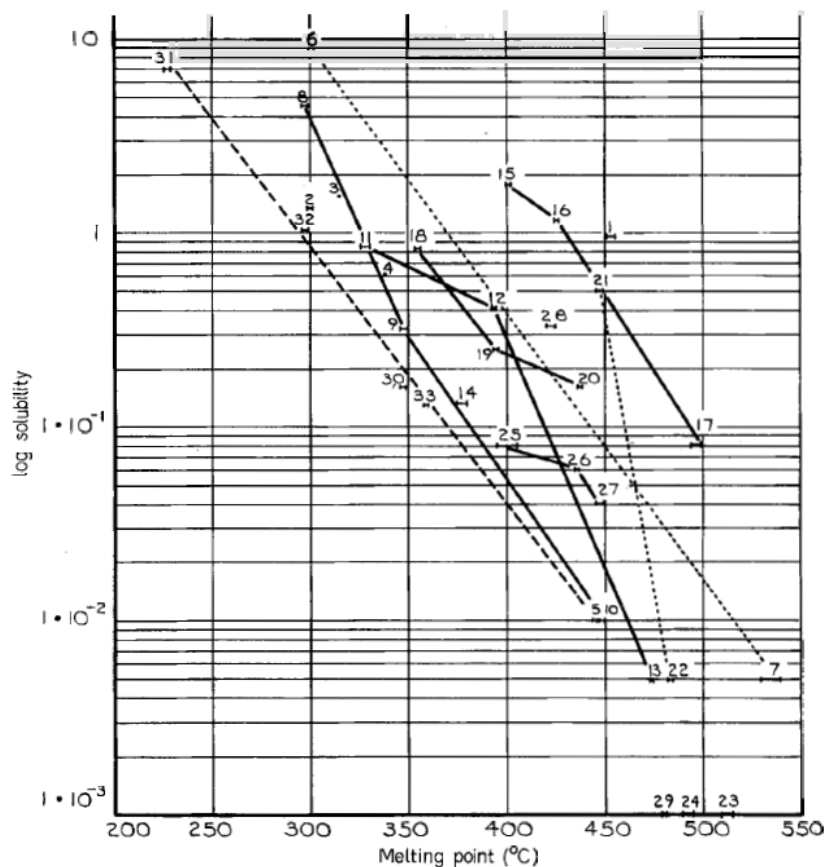
Figure II-27 Relationship between log solubility (g in 10g of refluxing DMF)
and melting point of aromatic imides

Kotov et al. reported that polyimides may form charge transfer complexes

in their model compounds. Diamine residues contained in the polyimide chains

retain their electron donor properties and can form CTC when small molecules of

electron acceptor units introduced into the system. Similarly polyimides can also

form CTC with the electron donor molecules due to diimides which is an electron

acceptor. Hence a polyimide chain consists of alternating electron donor and

acceptor molecules, which can form CTCs, and this interaction in polyimides is

responsible for the color and other, particularly semi-conductor properties, in

50

polyimides. They were the first ones to discuss inter-chain and intra-chain CTCs in polyimides. Intermolecular (inter-chain) charge transfers in CTC formed by acceptor and donor structural elements of adjacent macromolecules; whereas intra-molecular charge transfer occurs from the upper filled π-orbit of the donor residue of diamine to the vacant π-orbit of the imide ring.[47] They also concluded that it is very difficult to separate the relative effect of inter and intra molecular charge transfer on the UV-Vis absorption spectra.
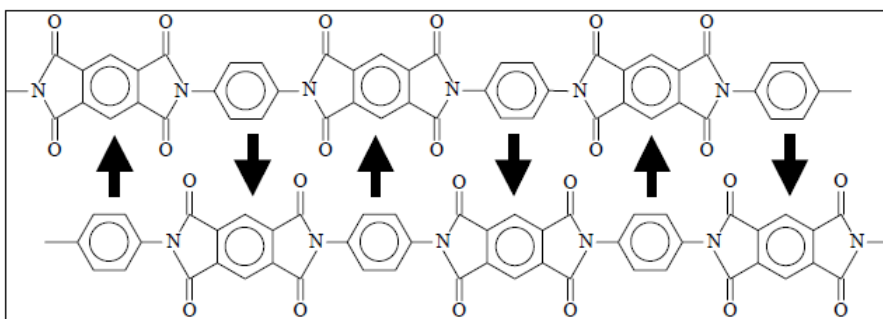
Figure II-28 Idealized inter-chain CTC formation

Intermolecular CTC interactions are not only resulting intense light color, but they are also considered as s a physical crosslink between the polyimide chains, responsible for decreasing the solubility, increasing the chain rigidity, and high T_g values of the polymers. Figure II-28 (look Figure II-24) shows the idealized interactions between the dianhydride and diamine groups. However this idealized alignment will not occur over more than a few repeat units. [1, 48]

Many researchers tried to reduce these inter-chain interactions in order to produce polyimides that can be melt-processed, having solubility in various

solvent, lower dielectric constants, and transparencies in the UV-Visible regions.[49–52]

Transparency is very important in the fields of space applications and optical instruments including Liquid crystal displays as optical retarder layers. For the space applications a film having low absorption to cosmic rays is required to be used in solar cells. It is necessary to develop materials that are heat resistant, colorless and transparent in UV-Vis region. Commercial aromatic polyimide films are 70% transparent (thickness dependent) at the solar wavelength of interest (500nm). In addition to this problem, polyimide films are aging in the space environment which lowers the transparency further down to 30%. [49-51]

Coloration is a serious problem in the development of optical components such as cables and filters for communication systems and liquid crystal display boards, where high resistance and high reliability is necessary for the materials used. Transparencies of commercial polyimides are indicated by yellowness index (YI). Most of the marketed polyimides have high YI. (Table II-5) YI of polyimides should be lower than 10, in order to be used for optical instruments. Polycarbonate, which is used widely in optical instruments, has YI of 7. [49]

Table II-5 Yellowness index of several commercial polyimides

Polyimides	Yellowness index (YI)
PMDA-ODA	129
Upilex-S	125
LARC-TPI	50

St. Clair et al. also attributed the coloration to inter-chain and intra-chain interactions and to solvent resistance of polyimides, due to formation of CTC. They proposed, in order to produce colorless and soluble polyimides, it is necessary to separate or completely remove the chromophoric centers from the polyimide chains. Also both inter-chain and intra-chain electronic interactions, that cause absorptions in the UV-Visible region, should be prevented by introducing bulky electron-withdrawing groups and separator groups in the polyimide structure. For bulky electron-withdrawing groups they used $-CF_3$ or $-SO_2$ groups and for separator groups they used $-O-$ linkages (Figure II-29 and Figure II-30) that can reduce the electron affinity and overall conjugation in the polymer chain. Incorporation of electron withdrawing groups in the diamine portion of the polymer structure is particularly beneficial in reducing the formation of inter-chain and intra-chain charge transfer complexes which cause large absorptions in the UV-Visible range. Incorporation of large, bulky groups into either the diamine or dianhydride monomers reduce the

amount of chain-to-chain electronic interactions and thereby lessens

charge transfer complex formation. This directly affects the transparency

and solvent resistivity of polyimide films. (Table 2-6 and Figure II-31) [50, 51, 53]
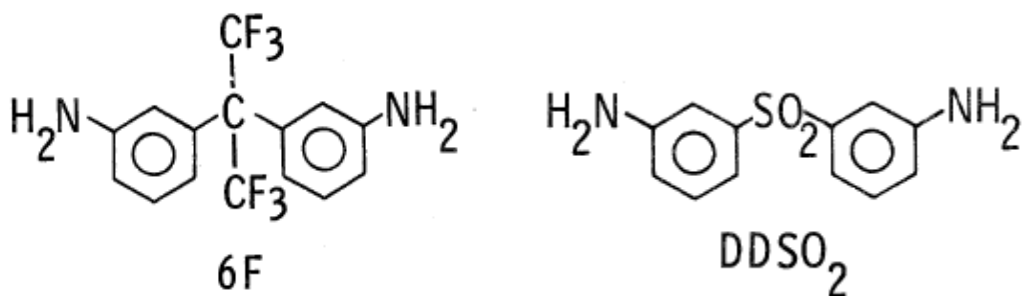
Figure II-29 Examples of aromatic diamine monomers
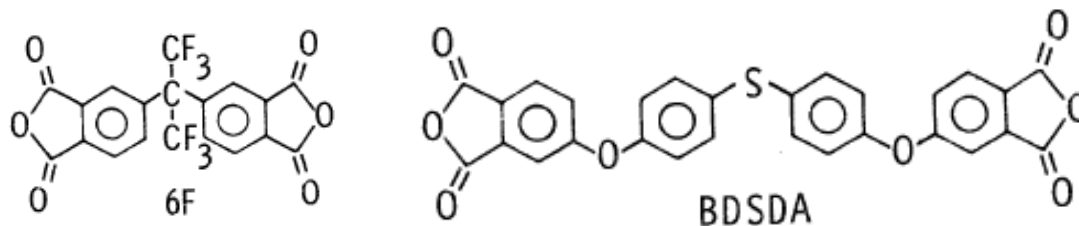
Figure II-30 Examples of aromatic dianhydride monomers

Table II-6 Solubility of transparent polyimide films

Polymer	Film Solubility[a] in		
	DMAc	CHCl$_3$	Diglyme
6F + APB	P. Sol.	P. Sol.	P. Sol.
6F + 3,3'-ODA	Soluble	Soluble	Soluble
6F + BDAF	Soluble	Soluble	I
6F + DDSO$_2$	Soluble	Soluble	I
6F + 3,3'-6F	Soluble	Soluble	Soluble
ODPA + APB	P. Sol.	P. Sol.	I
ODPA + 3,3'-ODA	Soluble	Soluble	I
ODPA + BDAF	P. Sol.	P. Sol.	I
ODPA + DDSO$_2$	P. Sol.	I	I
BDSDA + APB	P. Sol.	P. Sol.	I
BDSDA + BDAF	Soluble	Soluble	Soluble
BDSDA + DDSO$_2$	Soluble	P. Sol.	I
BTDA + APB	I	I	I
BTDA + BDAF	I	I	I
BTDA + DDSO$_2$	I	I	I
PMDA + APB	I	I	I
PMDA + BDAF	I	I	I
PMDA + DDSO$_2$	I	I	I

[a]Performed on 1% w/w solutions; P. Sol. = partly soluble;
I = insoluble
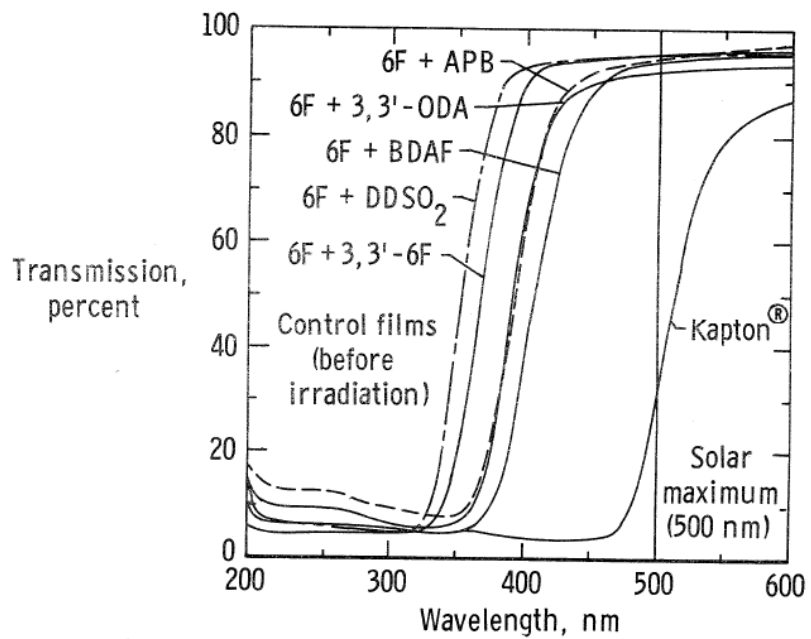
Figure II-31 UV-Visible spectra of 0.5 mil 6F-containing polyimide films before irradiation

They concluded that among the colorless polyimides they synthesized, 6F-DDSO$_2$ has similar heat properties with commercial aromatic polyimides. When compared with the Kapton polyimide, there is no sacrifice in heat resistance of transparent polyimide. (Figure II-32 and Figure II-33) [53]
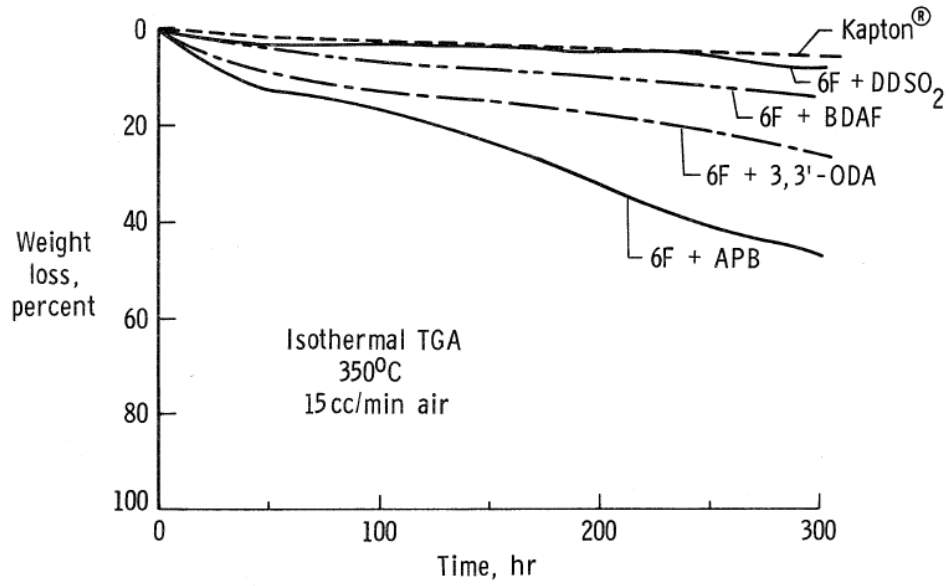
Figure II-32 Isothermal weight loss of 6F-containing polyimide films at 350C in air
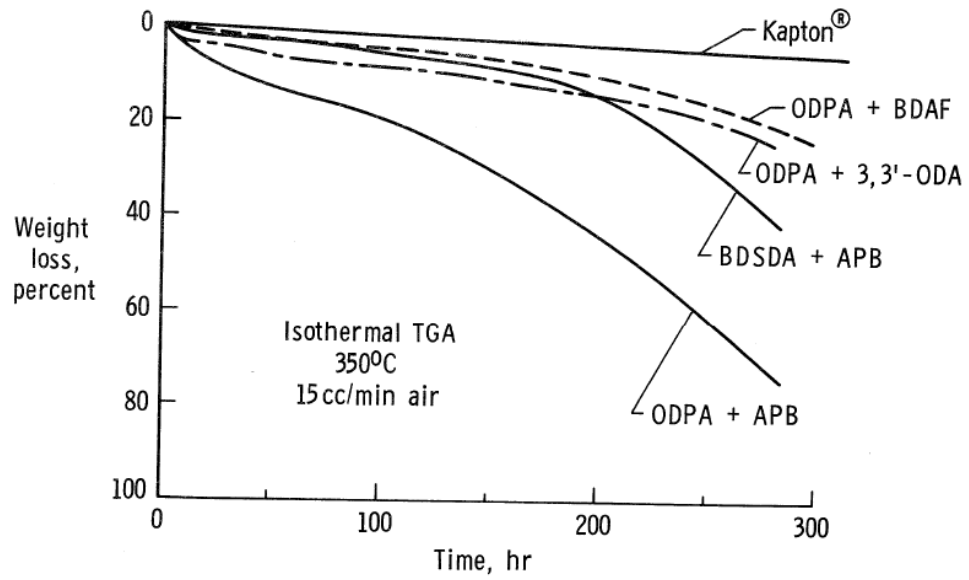
Figure II-33 Isothermal weight loss of ODPA and BDSDA-containing films at 350C in air

2.2.   Vibrational Spectroscopy of Polymers

Vibrational spectroscopy is one of the most widely used techniques for identification and characterization of materials in which polymers constitutes a major category. Vibrational spectroscopy can be separated into two main subcategory; Infrared and Raman spectroscopy. Both spectroscopic methods can be used to identify materials and to determine the molecular microstructure and morphology of the complex polymers.

IR absorbance and Raman scattering intensities are linearly proportional to the number density of species giving rise to that band. As a consequence these methods can be used for quantitative analysis in polymers. Bands in interest need to be calibrated or normalized with respect to an internal or external invariant band in the spectrum or film thickness for some applications.

Vibrational spectra of polymers are sensitive to changes in environmental effects near the groups that are in interest. This means when developing any quantitative method it must be remembered that it is sensitive to copolymer sequence, tacticity, molecular conformation, molecular orientation and configuration. This dependence results both advantages and disadvantages since the properties listed above can be investigated (after necessary calibrations are done) using vibrational spectroscopic technique.[54,55]

2.2.1. Dichroism and Molecular Orientation

Many post processing techniques, such as stretching, fiber spinning, and blow molding etc., produce polymer products (films, fibers and bottles) that are oriented in selective orientations. This directional orientation during the fabrication process may result in some desired end use physical properties in polymer products, for example directional stiffness, gas permeability, and optical properties. Similar to birefringence measurements, polarized IR and Raman spectroscopy are useful and practical tools for investigating polymer anisotropy that is caused by these post processing techniques.

The reason that IR spectroscopy is a useful tool to investigate the polymer anisotropy arises from the nature of the interaction between the incident infrared radiation and transition moment vector of the vibration bands. The absorption of infrared radiation is caused by the interaction of the electric field vector of the incident radiation, **E**, with the transition moment vector, **M**, of a particular vibration mode. If linearly polarized radiation is used to obtain the IR spectrum, the absorbance A_i for the band association with the vibration *i* is proportional to the square of the scalar product of M_i and **E**:

$$A_i \propto \sum(M_i \cdot E)^2 \propto \sum(M_i\,E)^2\cos^2\gamma \qquad (3)$$

where γ is the angle between the transition moment and the electric field vectors. Equation above shows that the absorbance is highest when **M** and **E** are parallel and is zero if they are perpendicular. For isotropic samples the absorbance is independent of polarization of the incident radiation since the

summation is over all randomly oriented absorbing molecules. (Note: in Figure

II-34 angle γ can be defined as θ+β) [54-56]
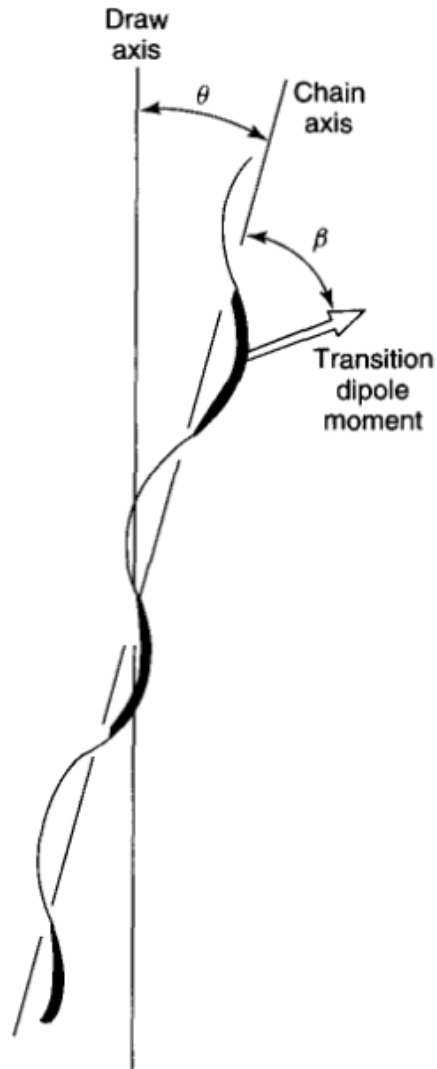
Figure II-34 Definition of the angles that describe the chain orientation
function and the dipole transition angle in a uniaxially oriented polymer.

The purpose of any vibrational spectroscopic investigation is to determine

the total averages of the angles that describe the orientation of the various

polymer chain directors with respect of the macroscopic reference axes of the samples.

For studies of IR dichroism, oriented samples are examined with the IR beam polarized horizontally or vertically by reference to the axes of the sampling plane in spectrometer. The sample reference axes are normally aligned parallel to these spectrometer axes. The sample reference axes may be chosen by using crossed polarizers to coincide with the principle optical axes of the refractive index ellipsoid. For a fiber or uniaxially oriented film, the axes of interest correspond to the direction of draw and any perpendicular to the draw. For a biaxially oriented film, the axes in the film plane are often chosen as machine direction (MD) and transverse direction (TD). [54-56]
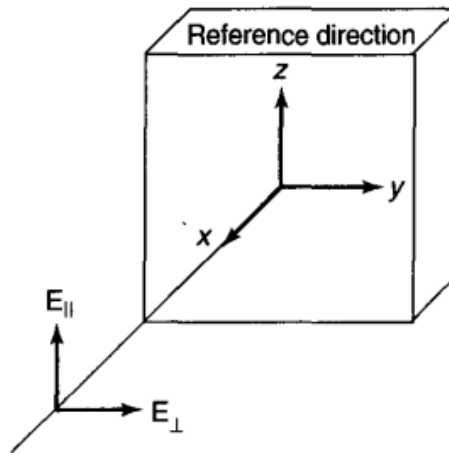
Figure II-35 Measurements at normal incidence. Geometry of incoming IR beams at the sample and definition of the reference direction and x, y, z coordinate system.

The anisotropic optical absorption of oriented samples, so-called dichroism, can be analyzed by measuring spectra using light polarized parallel and perpendicular to the fixed reference direction. This type of experiment is called infrared linear dichroism (IRLD). Parameters commonly used to characterize the degree of optical anisotropy in oriented samples are the dichroic ratio, D:

$$D = \frac{A_{||}}{A_{\perp}} \tag{4}$$

and the dichroic difference ΔA:

$$\Delta A = A_{||} - A_{\perp} \tag{5}$$

where $A_{||}$ and $A_{\perp}$ are the interrelated absorbance of the investigated band measured with the radiation polarized parallel and perpendicular to the reference direction. The intensities for these absorptions are given by the following equations following the Equation 3 as;

$$A_{||} = \left[ME_{||}cos\gamma\right]^2 \tag{6}$$

$$A_{\perp} = [ME_{\perp}sin\gamma]^2 \tag{7}$$

where M is the transition moment vector, $E_{||}$ and $E_{\perp}$ are the parallel and perpendicular electric field vector of the incident radiation, and γ is the angle between the draw axis and the transition moment vector (γ=θ+β) (Figure II-36). [56, 57]
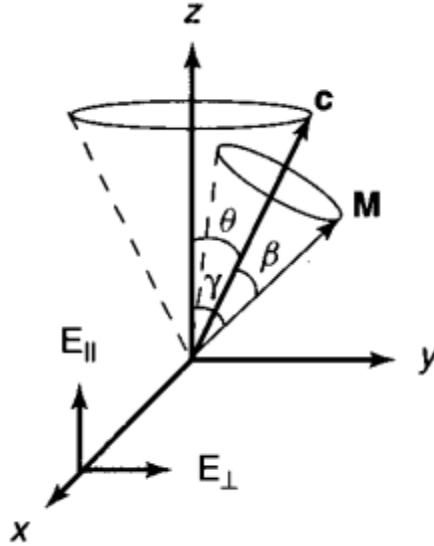
Figure II-36 Geometric representation for the nested axially symmetric distributions of orientation of the transition moments M about the molecular axis c (β angle) which is distributed around the reference direction z (θ angle).

By measuring the dichroic ratio, the degree of chain orientation can be estimated by using the orientation function f for the uniaxially oriented samples;

$$f = \frac{3<cos^2\theta>-1}{2} = \frac{(D-1)}{(D+2)} \times \frac{2}{(3cos^2\beta-1)} \tag{8}$$

this can be also rearranged into;

$$f = \frac{3<cos^2\theta>-1}{2} = \frac{(D-1)}{(D+2)}\frac{(D_0+2)}{(D_0-1)} \tag{9}$$

where, $D_0 = 2cot^2\beta$. [56-58]

For uniaxial orientation, measurements parallel and perpendicular to the single unique reference axis suffice; for biaxial orientation, polarized spectra must be recorded parallel to the three independent reference axes. The most

important advantage of the IR dichroism is that, since the IR spectra is selective to chemical groups; it allows determining orientation for these specific chemical groups. This selectivity property of IR radiation makes it possible to monitor both the selective phase in a matrix and the matrix itself. For thick polymer samples, where the absorbance will become an issue, FTIR-ATR method can also be used to investigate structural development. [59]
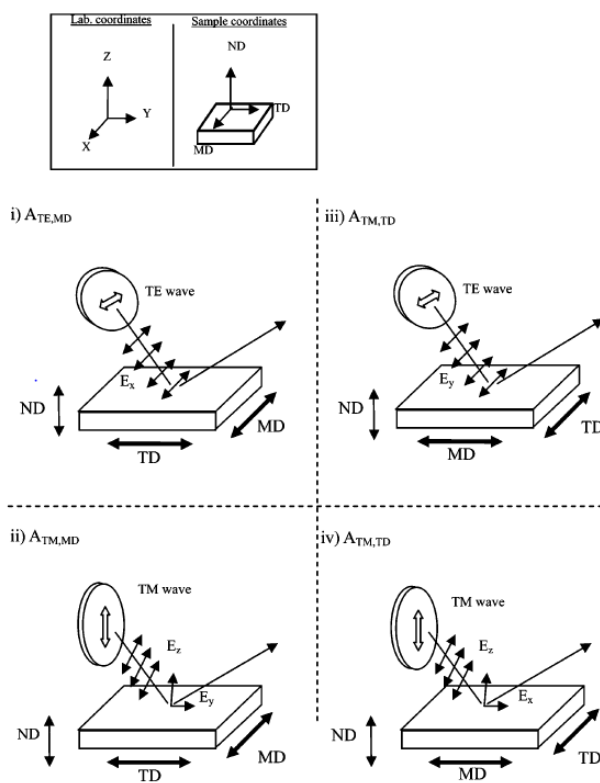
Figure II-37 3D orientation analysis with ATR.

Compared with the IR spectroscopy, Raman scattering can provide more detailed information on molecular anisotropy. Unlike IR absorptions, Raman spectrum results from inelastic photon scattering, which can be related to the changes in the polarizability of the chemical bonds. Polarizability is a tensor

quantity, which makes it more complex to interpret the data compared to single dipole angle (IR spectra characteristic), but in principle it provides more information. In addition to this complexity some experimental difficulties caused Raman spectra to become unfavorable for dichroism measurements. [60–62]

The objective of most industrial investigations is to characterize the effects of process variables such as draw temperature, rate, and extent on molecular orientation. Determining the dichroic ratio and then the orientation function for some one-way drawn samples requires simply that the absorbance of appropriate orientation sensitive bands be measured with the mid-IR radiation electric vector parallel and perpendicular to the sample draw axis. For weakly absorbing bands or for thin samples these may be measured in transmission.

PET is one of the most extensively studied polymers by IR dichroism that is commercially available. As the polymer chains in PET are extended, the glycol unit can undergo a conformational change from the *gauche* to the more extended *trans* form. Specific orientation parameters may be interpreted to describe preferential orientation of the aromatic rings into the sample plane, or preferential orientation of the chain axis with respect to the sample. Figure II-38 shows the IR absorbance and Raman scattering spectra recorded from uniaxially oriented PET. Parallel and perpendicular refers to the alignment of the electric field vector of the radiation with respect to the draw (chain) axis of the polymer. [62–64] In the figure (Figure II-38) absorption around 1020 cm^{-1} is almost parallel to the chain axis, while the 875 cm^{-1} band is almost perpendicular. For Raman 1615 cm^{-1} has

parallel character while as might be expected the vC=O has greater intensity in the perpendicular view.
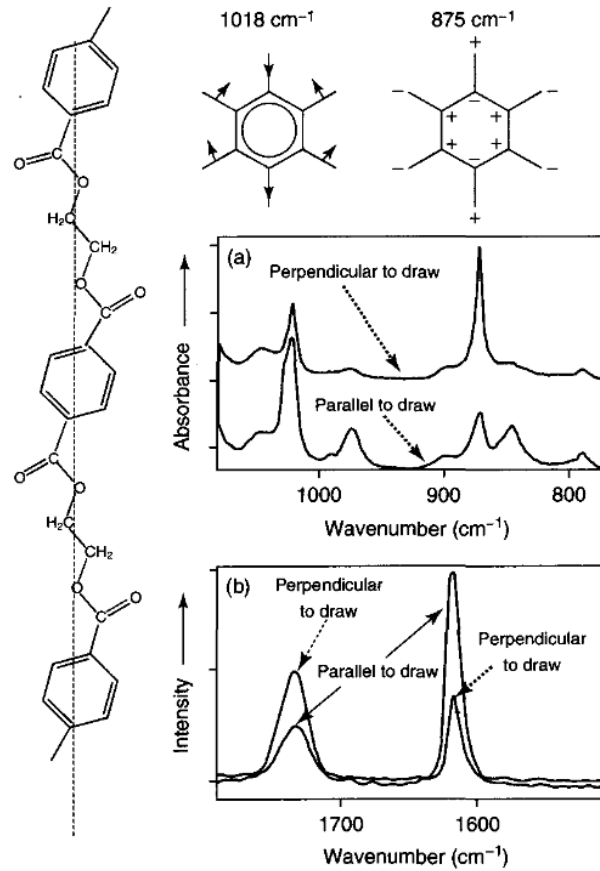
Figure II-38 PET orientation (a) IR absorbance and (b) Raman spectra recorded from uniaxially oriented PET.
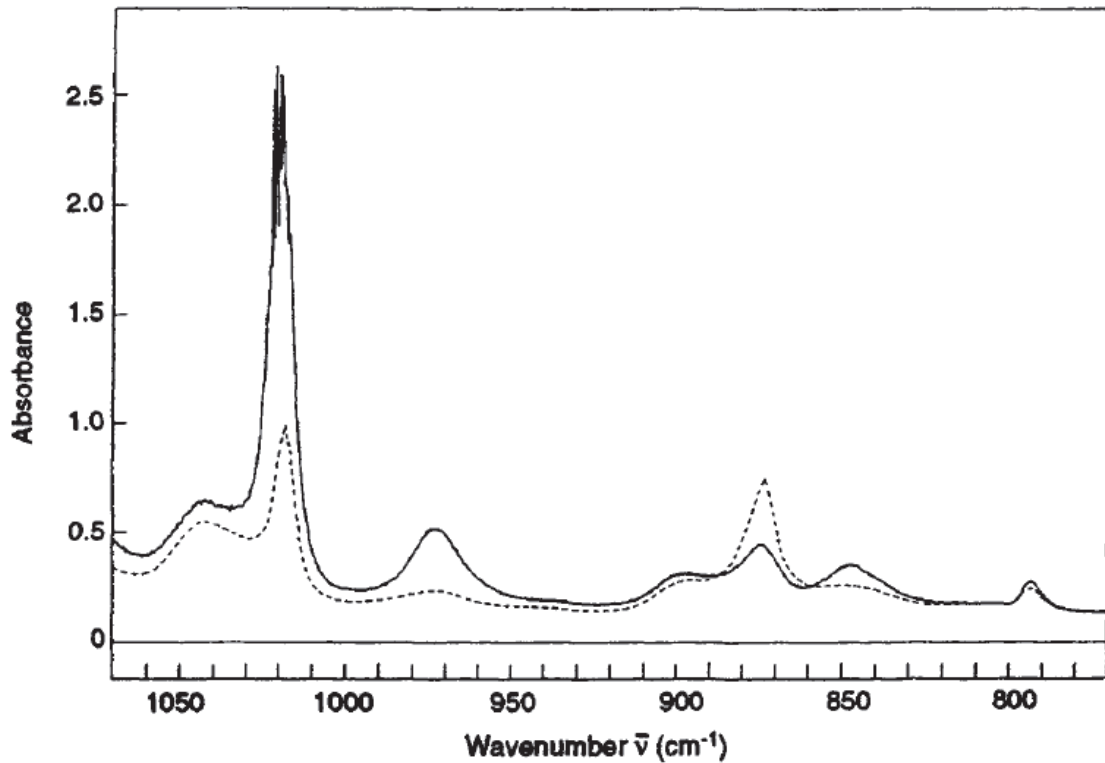
Figure II-39 Dichroic infrared measurements on a film of biaxially oriented PET

Spectrum in Figure II-39, which corresponds to biaxially oriented PET, is very similar to Figure II-38 (a). However as mentioned before, in order to calculate the orientation function of a biaxially oriented sample, dichroism measurements with respect to all 3 major axes has to be made with additional calculations required.

All examples discussed up to this point were performed with samples that were already stretched and the measurements were taken offline after the deformations are already performed to the samples. Dichroism measurements

can also be done in real-time during performing FTIR scans while samples are being deformed.

2.2.2. Time-Resolved Ultra-rapid-scan FTIR

A conventional FTIR instrument uses interferometer to generate and collect spectrum of samples. Interferometer consists of a light source, two mirrors (one of them is stationary and one of them moving at constant velocity), a beam splitter and a detector. Working principle of an interferometer is: the light coming from the source is split into two identical beams by the beam splitter. One beam will travel and reflect back from the stationary mirror and the other beam will travel a different path and reflect back from the moving mirror. Reflected beams will be recombined at the beam splitter. (Figure II-40)
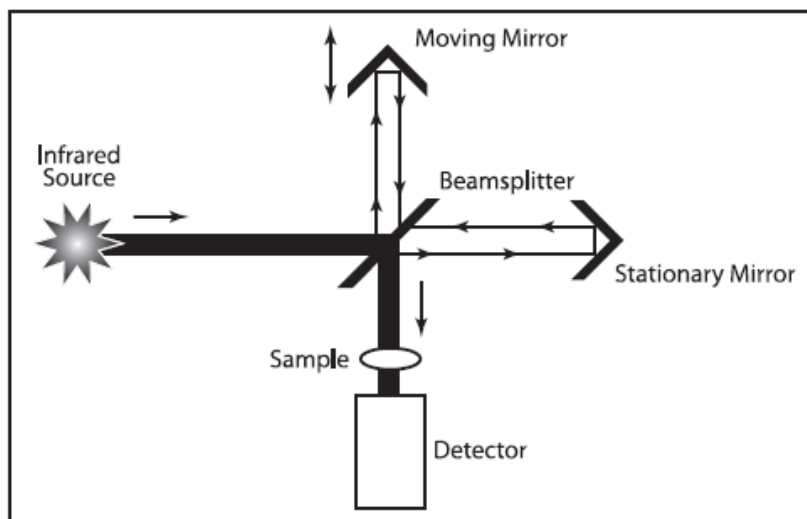
Figure II-40 Interferometer Diagram [65]

The beam reflected back from the moving mirror has traveled a different distance compared to the stationary mirror and this difference in the optical path length creates a phase difference between the two waves. When these two waves combine together at the beam splitter, due to the phase difference, the result could be either constructive or destructive. These recombined waves create the interferogram and it interacts with the sample. Some portion of this interferogram will be absorbed by the sample and remaining portions will be transmitted to the detector. Detector reads the information coming from a range of wavelength simultaneously and this signal is transmitted to the computer. In the computer, Fourier transform and subtraction of the background spectrum operations are performed to get the resultant transmittance spectra of the sample. The x axis on the spectra typically showed in wavenumbers (units in cm^{-1}), which is a product of the Fourier transformation of the interferogram.

The resolution of the time scale of the FTIR instrument highly depends on the velocity of the moving mirror. In order to achieve higher scan rates, the non-stationary mirror has to move very fast. The limiting factors for the speed of this mirror are the motor that moves it linearly and the weight of the mirror unit itself. Taking these limitations into considerations typical FTIR instrument can reach scan times down to 40 ms, operating at 4 cm^{-1} resolution. [66]

These values are good enough to record spectral changes in many systems. However some systems require faster data collection rates, since the experiments are non-repeatable and they occur in very short period of times, such as combustion or ultra-fast deformation experiments. If the time-scale of the

spectral change is higher than the time-scale of the interferometer response, the FTIR instrument can be used to record all the changes real time. However if the time-scale of the spectral change is smaller than the interferometer response, the spectral response can be misjudged since the scan rate of the instrument is not high enough.

Many scientists tried to overcome the issue of producing faster FTIR measurements by changing the structure of interferometer or more specifically trying to move the non-stationary mirror faster. Several methods have been developed during these researches but Manning introduced a technique that enhanced the duty cycle and time resolution of the data collection compared to conventional FTIR spectrometers. [66–68]

As described before, the speed of the experiment time-scale is determined by the moving mirror velocity. If it can be moved faster, the experiment time decreases. The key point that Manning introduced was to use a rotary motion to generate the path difference coming from the moving mirror instead of linear back and forth motion. This setup has two major advantages, first the moving mirror can have a circular disk shape which makes it lighter and second it can be rotated at higher speeds to generate the path difference between the separated beams. He describes the key features of the technique in his patent. [66] In Figure II-41 **1** represents the source and **5** is the generated beam from the source. **10** is labeled as beam splitter and it splits the original beam **5** into two beams **6** and **7**. Beam labeled as **6** travels a fixed distance and is reflected back from a fixed mirror labeled as **50**. Beam **7** travels a variable path and it first hits the rotating

mirror **200** and reflected to the cube-corner retroreflector **30** to the mirror back

through **3'**. Beam **3'** is reflected from the surface of **200** to the mirror **40** at a right

angle and the beam returns the reverse side by following its original path. The

two beams **6** and **7** are recombined at the beam splitter **10** and transferred to the

detector **2**. [66]
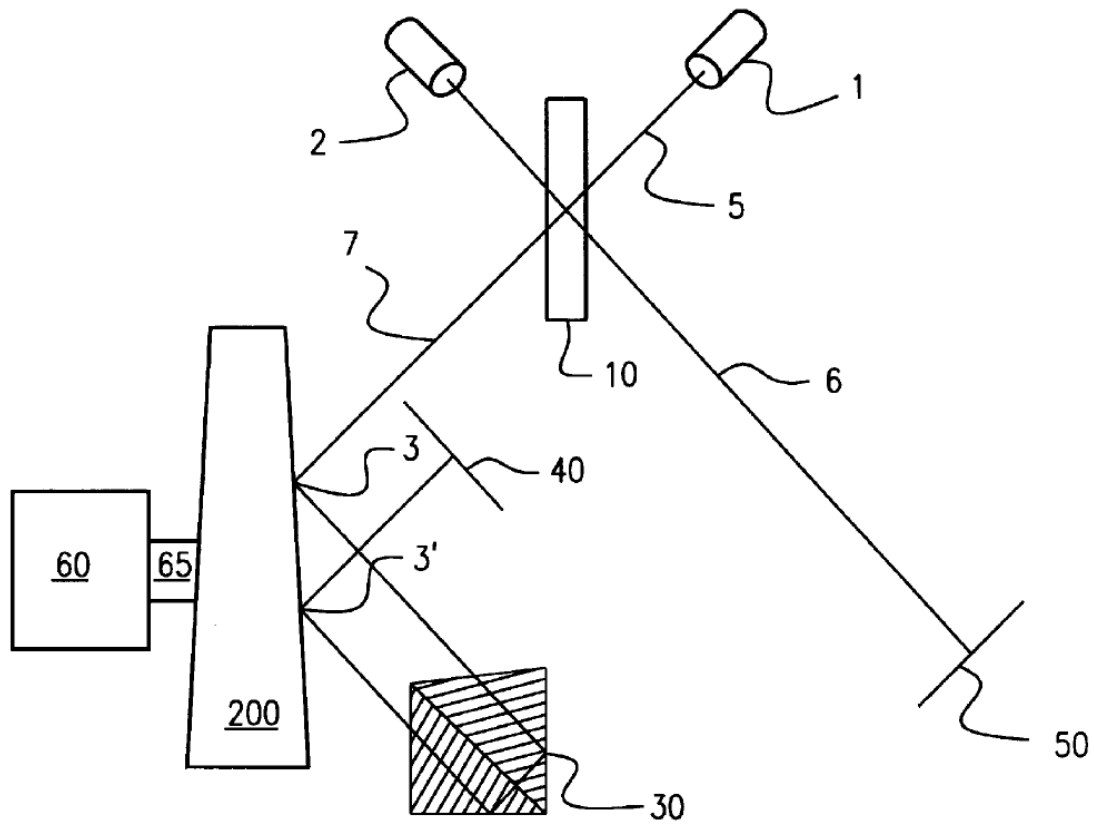
Figure II-41 Two dimensional representation of the ultra-rapid-scanning
interferometer

Rotating mirror **200** can vary the path length of the second beam by the

motion of the motor **60**. The two units are connected through a shaft labeled as

65. The rotation speed can be controlled by the applied voltage or current to the motor **60**. [66]

The speed of this concept has been proven by Griffith and Manning, by examining the spark-initiated combustion of ethane and methane in air. They used a very similar setup that described above and they reported a rate of scan of 150 scans per second. [67]
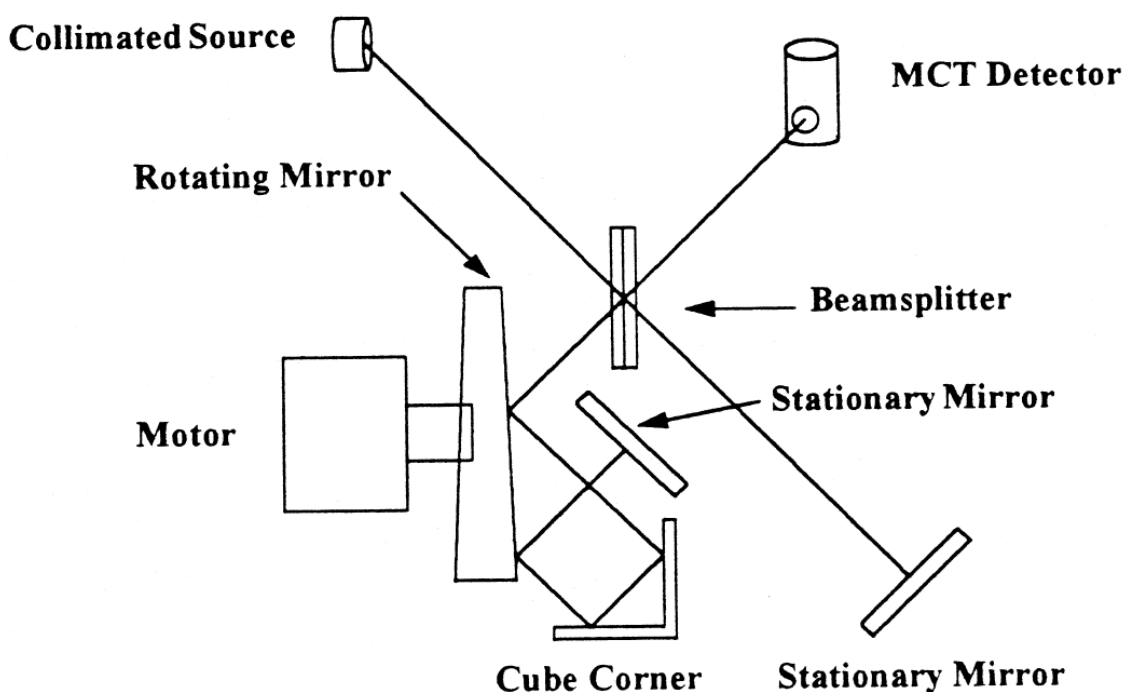
Figure II-42 Two dimensional representation of the ultra-rapid-scanning interferometer used for the experiment

150 scans per seconds correspond to 6.7 millisecond separation between each scan. Figure below (Figure II-43) shows the collection of spectra that are separated by 13 millisecond time lapse and spectra 1 and 2 shows results before the spark initiation. Spectra 3 is after the spark at 7 ms, 4 is 20 ms, 5 is 33 ms

and 10 is 99 ms. By this experiment they proved that this instrument can be used to record FTIR spectra of rapid reactions or processes. [67]
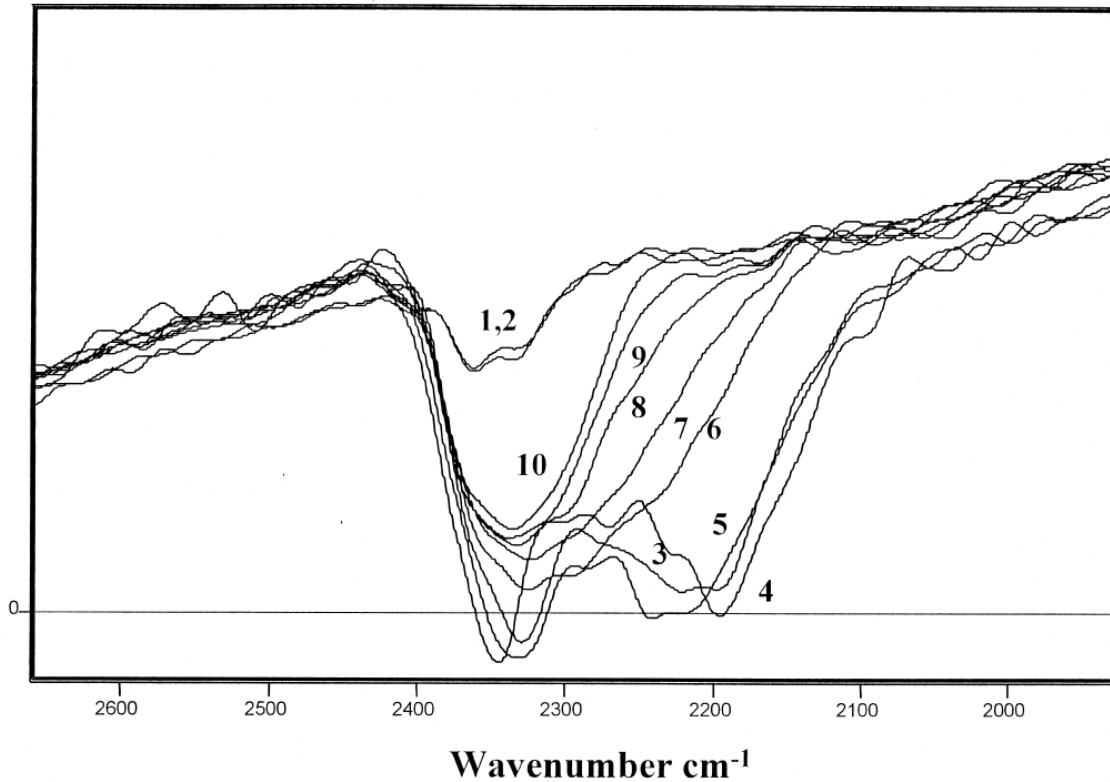
Figure II-43 Series of spectra collected before and after spark-initiated combustion of ethane.

The same system has been evaluated by Pellerin et al. [69] to measure real-time orientation behavior of PET, PS and PS/PVME blends during irreversible macroscopic deformation. They also recorded the relaxation behavior following the deformation with a time resolution of 20 ms. The results were compared with the polarization modulation infrared linear dichroism method (PM-IRLD) by Pellerin et al. [69]
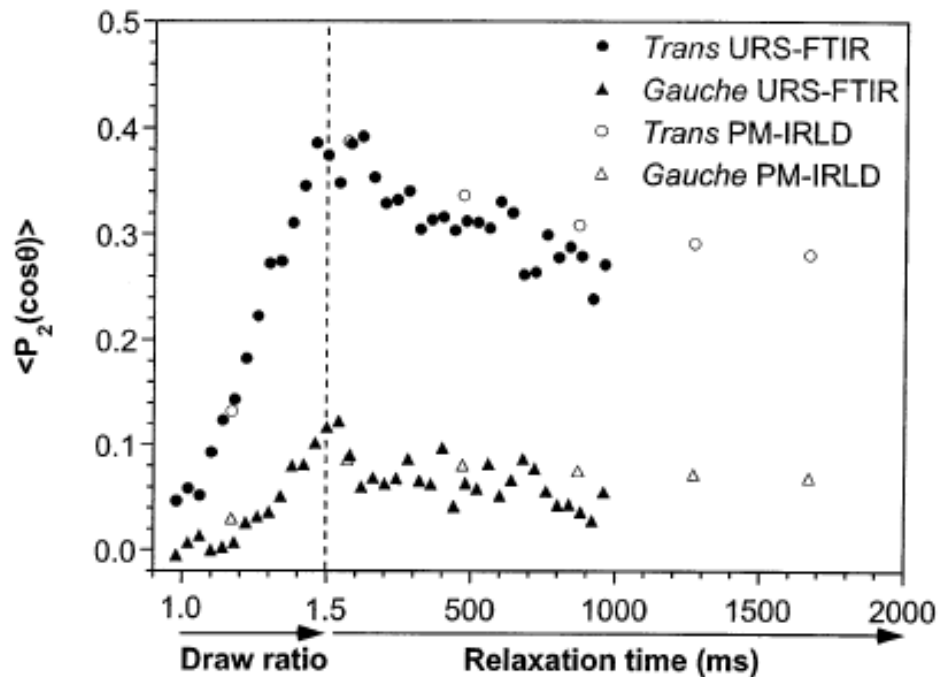
Figure II-44 Orientation function of gauche and trans conformers of PET during and after deformation at 90C measured both by URS-FTIR and PM-IRLD

Figure II-44 shows the orientation function for the trans and gauche bands as a function of draw ratio during the deformation and as a function of time during the relaxation period. If the two methods are compared, URS-FTIR and PM-IRLD, it can be seen that the two measurement methods are in good agreement. However it can be noted that the PM-IRLD fails to provide sufficient data points compared to the URS-FTIR. This can lead to misjudged orientation function calculations. [69]

Similar agreements have been observed for the PS and PS/PVME blends too. Figure II-45 shows the orientation function of PS and PS/PVME blend as a function of draw ratio and relaxation time afterwards. The total time for the

experiment is reported as 1360 ms. In this experiment PM-IRLD method could

generate one data point in every 1.6 s and URS-FTIR method could generate 1

data point in every 20 ms, which shows the significant enhancement of the

method over time resolution of FTIR measurements.
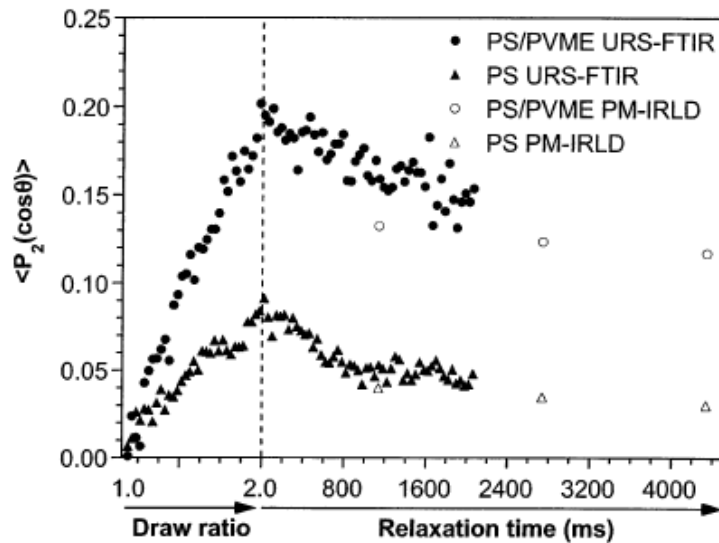
Figure II-45 Orientation function of PS and 70/30 PS/PVMe blends during and after deformations at T_g+15C determined by URS-FTIR and PM-IRLD

On their later work Pellerin et al. increased the time resolution of the URS-

FTIR instrument. [70] Similar to their earlier work, they measured the deformation

and relaxation behavior of PET films above and below its T_g. They again used

the two methods, PM-IRLD and URS-FTIR in synchronous, to see the agreement

between them. As reported on their previous work [69], the two methods have a

good agreement.
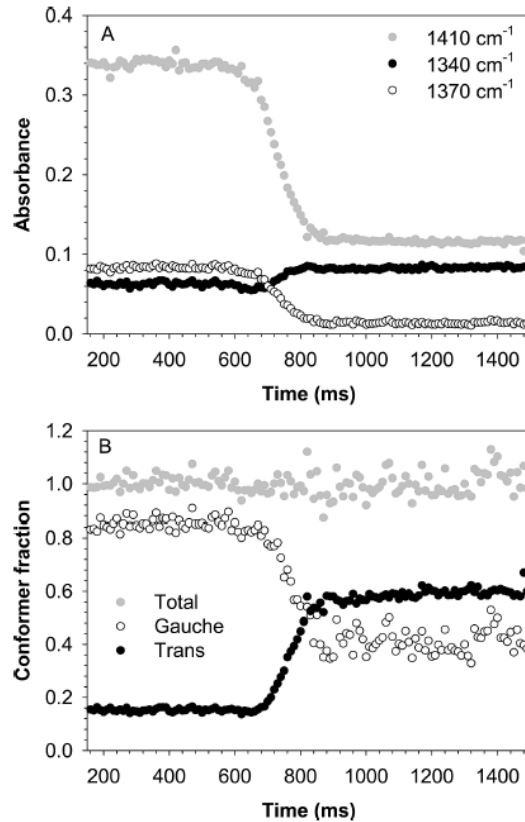
Figure II-46 Evolution of (A) the structural absorbance of the bands in interest and (B) the fraction of gauche and trans conformers calculated from these bands for a PET deformed at room temperature

Figure II-46 shows the structural absorbance of the trans and gauche bands in PET films. These films were deformed at room temperatures very rapidly. The total experiment time for deformation is 1500 ms. The spectra were collected at a rate of 100 scans per second, resulting a 10 ms time resolution. Graph (B) in Figure II-46 shows that the different conformers can be tracked by this method independently.

Figure II-47 shows the real time evolution of orientation function calculated from dichroic ratio of trans conformers during the deformation of PET films at

76

room temperature by using the Equation 9. They noted that the initial sample is anisotropic initially that might be caused by the blow molding process.
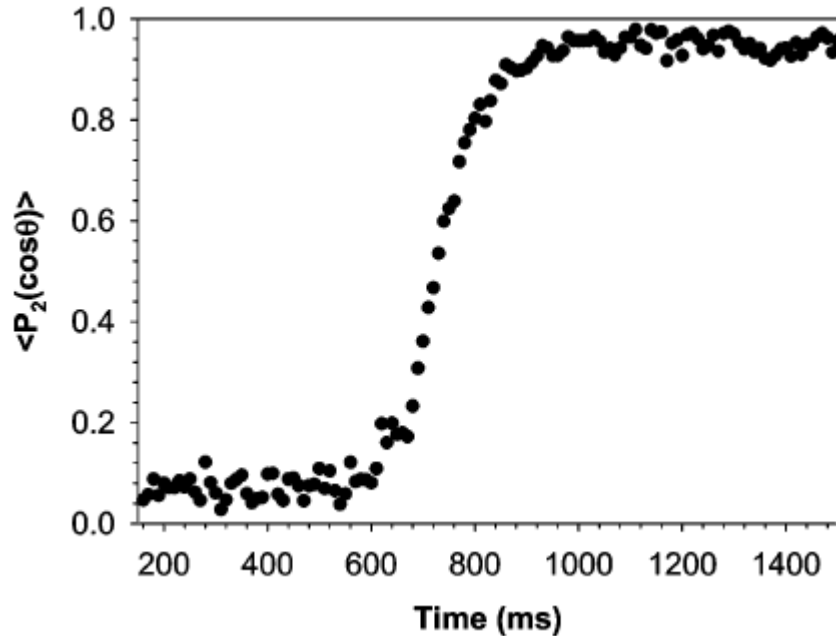
Figure II-47 Evolution of the orientation function for the trans conformers during deformation of PET at room temperature

These results concluded that the rapid deformation of polymers can be tracked by the URS-FTIR method. The results obtained from this method were in good agreement with the PM-IRLD measurements. However URS-FTIR is superior to the PM-IRLD method when the time resolution of the two methods taken into consideration (400 ms vs. 10 ms).

2.2.3. Infrared Spectroscopy of Polyimides

Infrared spectroscopy can be used to examine the formation of polyimides by monitoring the curing study of poly(amic acid) precursor. Also it can be used to track the amount of residual solvent, which plays a crucial role on imidization kinetics. Dichroism measurements can reveal the information on degree of orientation on poly(amic acid) samples and polyimides.

2.2.3.1.   Determination of imidization

Degree of imidization can be determined by Infrared spectroscopy. As previously discussed, during imidization amic acid groups are turning into imide groups. Amic acid and imide groups absorb infrared light at different frequencies and give rise to separate absorption bands. By tracking the intensities of these bands, one can determine the degree of imidization of the samples. [18, 25, 38, 71–79]

Table II-7 Important infrared absorption bands of compounds of imidization

	Absorption band (cm^{-1})	Intensity	Origin
Aromatic imides	1780	Strong	C=O asym. stretch
	1720	Very strong	C=O sym. stretch
	1380	Strong	C-N stretch
	725		C=O bending
Amic Acids	2900-3200	Medium	COOH and NH$_2$
	1710	Strong	C=O (COOH)
	1660 amide I	Strong	C=O (CONH)
	1550 amide II	Medium	C-NH
Both in amic acid and imide	1500	Strong	Breathing mode of aromatic ring
Solvent (NMP)	1408	Medium	NMP CH$_2$ bending

As it can be seen from the Table II-7, several characteristic absorption bands can be used for determining imidization. Strongest absorptions occur in the region of C=O (symmetrical stretching, around 1720 cm^{-1}), but this band overlaps with strong carboxylic acid band of poly(amic acid) (1700 cm^{-1}). Other useful two bands, C=O asymmetric stretching and bending at 1780 cm^{-1} and 725 cm^{-1} respectively, are overlapping with the anhydride absorptions if the product

has little amounts as impurity or it can also be generated as a side product during imidization process. [72, 73]

In addition to these problems, Pryde showed that C=O bands located at 1780 and 730 cm-1 are affected by the degree of molecular orientation in the film, which increases significantly during imidization process. [80]

The use of these peaks to determine the imidization degree of films requires further corrections due to overlaps and molecular orientation effects. Amic acid peaks generally appear as broad peaks, due to the strong hydrogen bonds, particularly with the residual solvent. However they can be used for qualitative analysis.

In his later work, Pryde showed that C-N stretching peak at 1380 cm^{-1} is not overlapping with any other absorption bands or is not affected by the molecular orientation of the polyimide chains. He suggested that, intensity of the C-N stretching peak can be normalized with respect to the aromatic ring stretching at 1500 cm^{-1}, used as an internal standard. This peak is not affected by molecular orientations of imidization. [81]

Following equation can be used to determine the imidization % of the samples;

$$Degree\ of\ imidization = \frac{\frac{A(1380\ cm^{-1})_T}{A(1500\ cm^{-1})_T}}{\frac{A(1380\ cm^{-1})_{T\prime}}{A(1500\ cm^{-1})_{T\prime}}} \qquad (10)$$

where the upper fraction is the imidization value at temperature T and lower fraction is the ratio of the peaks for the fully imidized sample.

A typical imidization curve calculated by the equation above can be seen in the graph below (Figure II-48). Li et al. showed the results for two separate peaks both coming only from the imide absorptions (1378 and 588 cm^{-1}). The calculations were done by preparing samples that are heated to defined temperatures by 10°C/min and held at the set temperature for 60 minutes. Samples were cooled to the room temperature and ratios of the imide peaks were determined offline by FTIR. Their results and many others show that the imidization reaction is almost completed around 200°C. Further heating to 400°C or 450°C is required to push imidization above 95% and get rid of the residual solvent. [78]
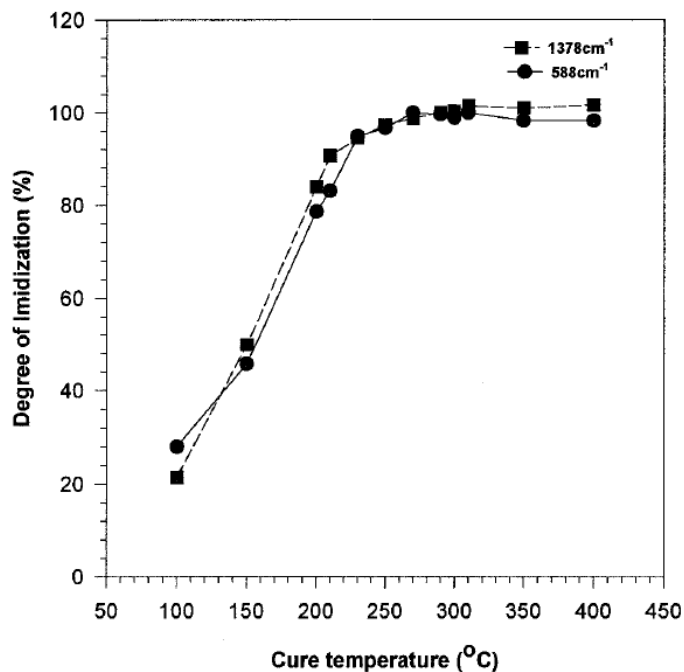
Figure II-48 Degree of imidization determined by using peaks at 1378 and 588 cm^{-1}.

Shin et al. monitored the imidization reaction of PMDA-ODA with a time-resolved FT-IR instrument. They heated poly(amic acid) samples with 2°C/min to 350°C and recorded the FTIR spectra of film at determined temperatures. Figure II-49 shows typical IR spectra collected during the imidization reaction as a function of temperature. It can be seen that the as temperature increases amide I and II peaks disappear and –CN– imide peak appears. Also aromatic ring absorption stays constant in the temperature range. [18]
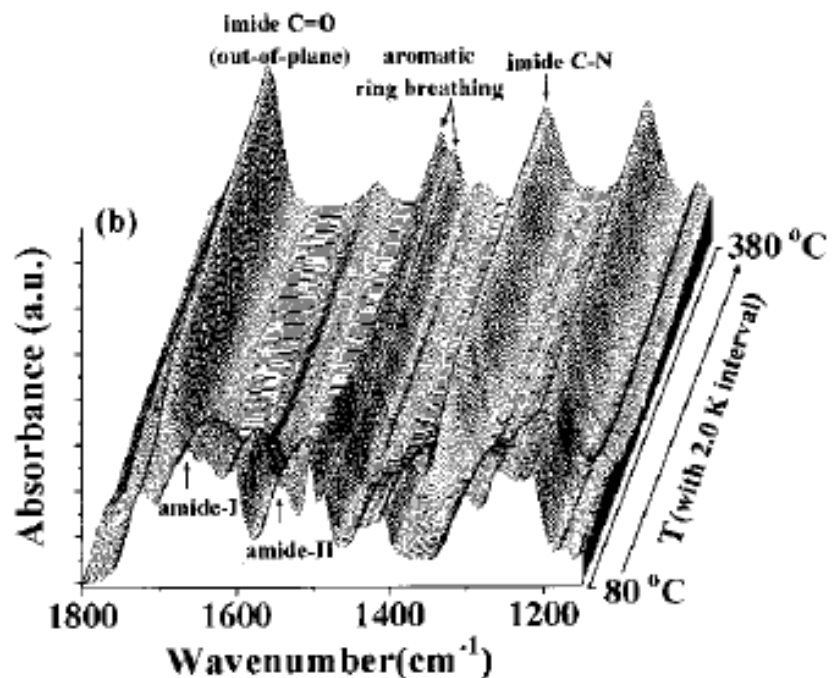
Figure II-49 Typical IR spectra monitored during the imidization as a
function of temperature

Figure II-50 shows the imidization degree that is calculated real time from
the data observed in Figure II-49. It can be noted that the imidization starts
around 120°C and 93.5% imidization is completed at 210°C. Further heating to
300°C pushes imidization to higher values and degrading starts around 380°C.
Figure II-50 also shows the derivative of the imidization with respect to
temperature. Second curve shows a maximum value around 150°C, which
indicates that the imidization reaction occurs at a maximum rate. [18]
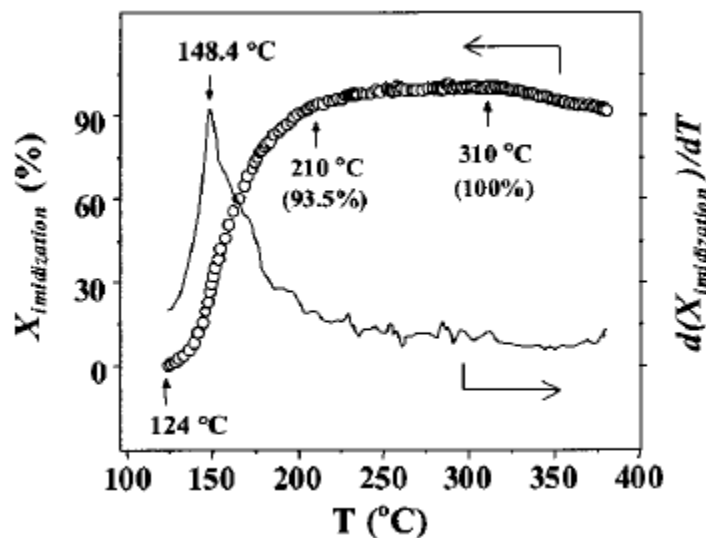
Figure II-50 Degree of imidization and its derivative as estimated from the variation of the imide -CN- stretching band measured during imidization of PMDA-ODA at 2.0°C/min

2.2.3.2. Determination of Residual Solvent Content

Amount of residual solvent can be determined by the IR spectroscopy. Solvent NMP has a distinct peak at 1408 cm^{-1} coming from the CH$_2$ bending vibrations. Thomson et al. also determined the peaks around 1680 and 985 cm^{-1} are originated due to the residual solvent molecules in PAA films. [72, 73] The details of this characterization have been discussed on the previous sections of this dissertation. (2.1.2.2.1 Solvent Effect)

2.2.3.3. Determination of orientation

The development of in-plane orientation in polyimides can be determined by using FT-IR spectroscopy. Parallel and perpendicular polarized IR light can be used to measure dichroic ratio of several groups on the polyimide chains. Kim et al. showed that C-N stretching vibration around 1380 cm-1 can be used to track orientation of polyimide chains. Since the direction of transition moment of this vibration is parallel to the director of the imide segments, it can represent the orientation of polyimide chains (Figure II-51). [82]
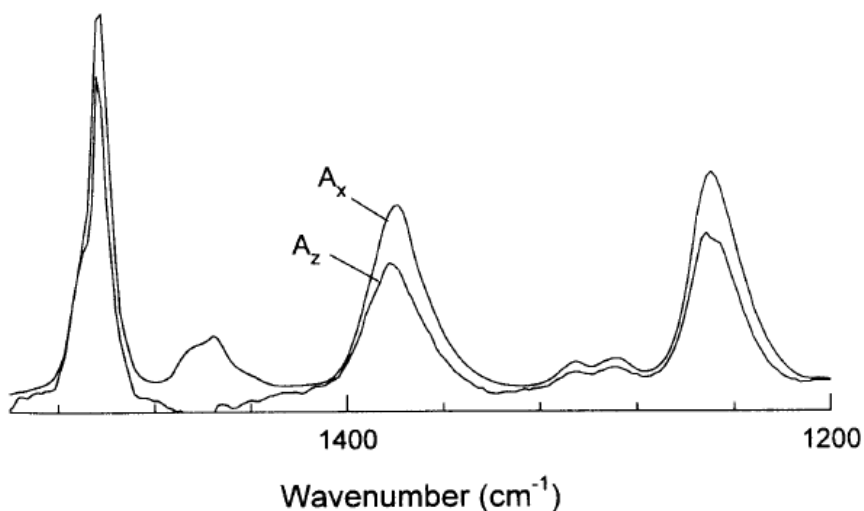
Figure II-51 Parallel and perpendicular polarized IR spectra of polyimide film

Sawa et al. also tried to measure the dichroic ratio in processed polyimide films. The anisotropy to the films is introduced by rubbing them with rayon cloth in *y* direction. They compared the results for nonrubbed and rubbed samples by

recording the FTIR spectra both parallel and perpendicular polarized. The peak

intensity values for the two samples were different for all peaks under

investigations for parallel polarized light (1720 cm^{-1} for C=O, 1500 cm^{-1} for

aromatic ring, and 1240 cm^{-1} for C-O-C). [83]
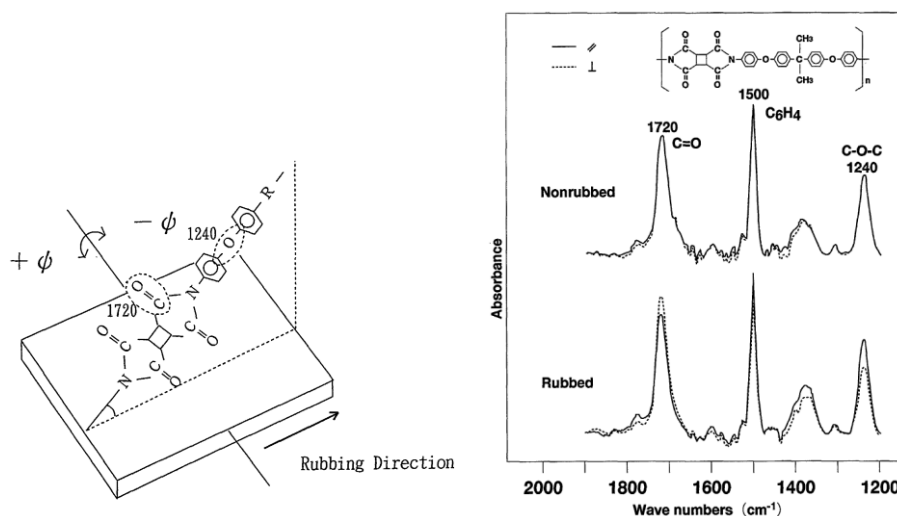
Figure II-52 Dichroic ratio measurements of anisotropic PI film

2.2.4. Raman Spectroscopy of Polyimides

Cure of poly(amic acid) has been extensively investigated by many

scientists using FTIR as mentioned on the previous sections. Different from

others, Jonhson and Wunder tried to monitor the imidization reaction by using

FT-Raman spectroscopy, rather than FTIR.[84] Figure II-53 below shows the FT-

Raman spectra of 10 µm films of as-cast PMDA-ODA poly(amic acid), cured at

135°C for 5, 30 and 120 minutes. In the graph X represents the solvent peak,

poly(amic acid) C-O is mark with *, polyimide peaks are marked with the arrow,

and Θ represents the aromatic ring vibration. Going from spectra A to C, solvent peak disappears and poly(amic acid) peak decreases. Polyimide peaks become stronger as imidization proceeds. They tried to normalize these peaks with respect to aromatic ring vibration, but the intensity of the aromatic ring vibration is not remaining constant as imidization proceeds. Considering this effect, FT-Raman measurements can be used to get qualitative data but quantitative results such as % conversions cannot be calculated by this method. [84] They also observed that, curing temperatures above 135°C, resulted disappearance of some peaks, which should be present on the FT-Raman spectra.
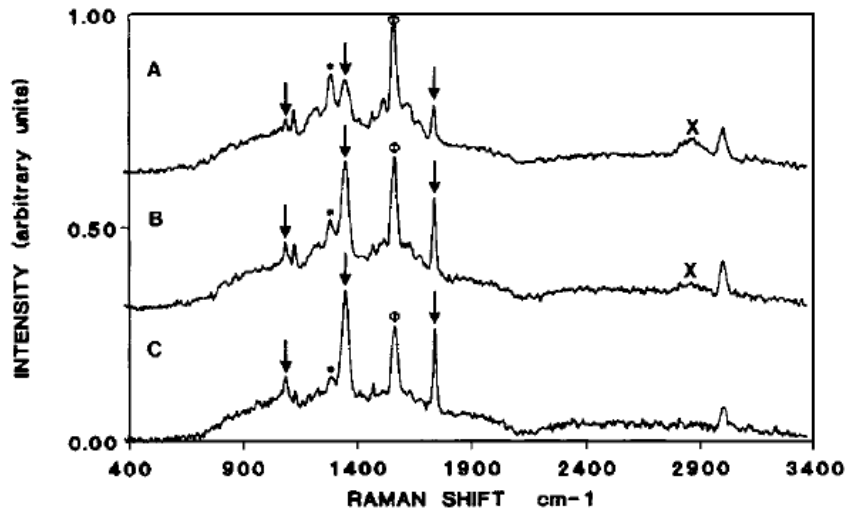
Figure II-53 FT-Raman spectra of 10 μm films of as cast PMDA/ODA poly(amic acid) cured at 135°C for (A) 5 min; (B) 30 min; and (C) 120 min.

2.3. Structural Characteristics and Orientation Development during Two-Step Imidization

Structural characteristics of any polyimide product (films, fibers, foams etc.) are influenced by several factors. These factors can be separated into two large groups; chemistry related features and processing conditions. Chemistry related features can be listed as; types of monomers used to synthesize the poly(amic acid) precursor and polyimide, solvent type (its interaction with the precursor such as H-boding and boiling point temperature), molecular weight, molecular weight distribution, and solution concentration (viscosity). Processing conditions have an influence at the morphology of the final product through the imidization type selected (i.e. chemical imidization vs. thermal imidization), curing conditions of the polyimide (free standing vs. constrained films), cast surface that the poly(amic acid) solution is applied, final cure temperature, thickness of the film, and environmental conditions (such as humidity, vacuum etc.). Among all these factors affecting the final morphology of the polyimide products, the main focus on this section will be on the influence of the curing conditions of poly(amic acid) precursor. [85]

2.3.1. Process of preparing polyimide films

The detailed synthesis scheme for polyimides through two-step procedure was explained in previous sections (CHAPTER II2.1.2 Synthesis and Imidization of Aromatic PIs). As a quick reminder, in the two-step synthesis scheme, first a soluble precursor named poly(amic acid) is synthesized by the reaction of tetracarboxylic dianhydride and diamine. This synthesis is carried away in a polar aprotic solvent at relatively low temperatures (30-60°C). Following this step, poly(amic acid) precursor is converted to final polyimide product by heating to higher temperatures (300-400°C). The heating step can also be separated into two steps. First, the film is heated to 200°C, to remove the solvent and imidize the sample simultaneously. The excess heating to 300-400°C is required to remove any residual solvent bound to the film and push the imidization above 95% (heating to 200°C will cause imidization degrees close to 90-95%). The major steps in this procedure can be listed as;

    i.   Synthesizing the poly(amic acid) precursor

    ii.   Casting the solution onto a substrate

    iii.   Drying the solution to remove excess solvent and peeling the film from substrate

    iv.   Curing the poly(amic acid) film to remove any remaining solvent and complete the conversion to polyimide

Each of these steps has considerable effect on the final morphology of the polyimide product and the impact of each step has to be considered carefully.

Following sections will give detailed explanations and their effects on structure development on polyimides during the imidization process (except the first step since synthesis is not on the scope of this dissertation).

2.3.1.1. Solution Casting

The poly(amic acid) precursor solution can be applied onto a substrate by various methods. The most common methods can be listed as spin coating and solution casting (by hand or by blades). Solution casting of poly(amic acid) precursor by blades will be the main focus in this section. A motor-driven blade casting method is preferred over other methods (hand casting or hand-drawn blades) due to the production of films with more uniform thicknesses.

The main objective of casting the solution of poly(amic acid) precursor is to produce uniform, detect-free polymer layer onto a substrate. The final morphology of the polyimide might be affected from the casting method applied. The literature has reported that the solution casting with blades induces orientation on the air-solution interface as well as solution-substrate interface due to shearing effect that is introduced to the polymer solution due to the movement of the casting blades. [85] Prest and Luca showed that during the solution casting, polymeric chain backbones are preferentially aligned in the plane of the film and this effect might introduce birefringence for the optically anisotropic films. They took this explanation one step further and calculated the values of stresses that developed during solvent casting process by measuring the birefringence and

using the stress optical rule (SOC). [86] Detailed explanation of stress optical rule can be found elsewhere. [87] However they discovered that the calculated stresses are bigger than the introduced stress during casting process and they concluded that drying process of the solution introduces additional stresses to the cast films.

On a later work, Greener et al. studied the optical properties of solvent cast polymer films of several systems. They studied the effect of two casting procedures on the final optical properties of the films. The first casting method they studied was named as free casting, where a polymer solution was on top of a flat-surfaced glass cup without applying any hydrodynamic stress on the liquid. The second method, named as blade casting, is regular procedure where a knife blade was used to spread the liquid over the surface and some hydrodynamic stress was generated during casting procedure. [88,89]

They observed that, being independent of casting procedure all films were isotropic in the plane of the film ($\Delta n_{xy}=0$), and anisotropic in the transverse direction ($\Delta n_{xz}= \Delta n_{yz}\neq 0$). Also the data observed from both casting methods were independent of initial concentration, volume, and casting thickness. They also concluded that the polymer chains are aligning parallel to the film plane, where the orientation in *x-y* direction is completely random in both casting methods. The agreement of the results between free casting and blade casting results that the stresses generated during the blade casting method did not contributed the *x-y* orientation of the film.

On the other hand, it was observed that out-of-plane birefringence values were different for the two casting methods. Blade cast films exhibited higher birefringence values compared to the free casting films (measurements were done when films were fully dried). Figure II-54 shows the out-of-plane birefringence values as a function of dried film thickness of polystyrene (PS) and tetramethyl polycarbonate (TMBPA). From the graph two conclusions can be revealed. First, blade casting method produced higher birefringent films compared to the free casting method. Second, the birefringence on the films is a function of the film thickness and as the dried film thickness increases birefringence values decreases. The rate of decrease is higher in the free casting films compared with the blade casting films. The effect of dried film thickness will be explained further in the next section.
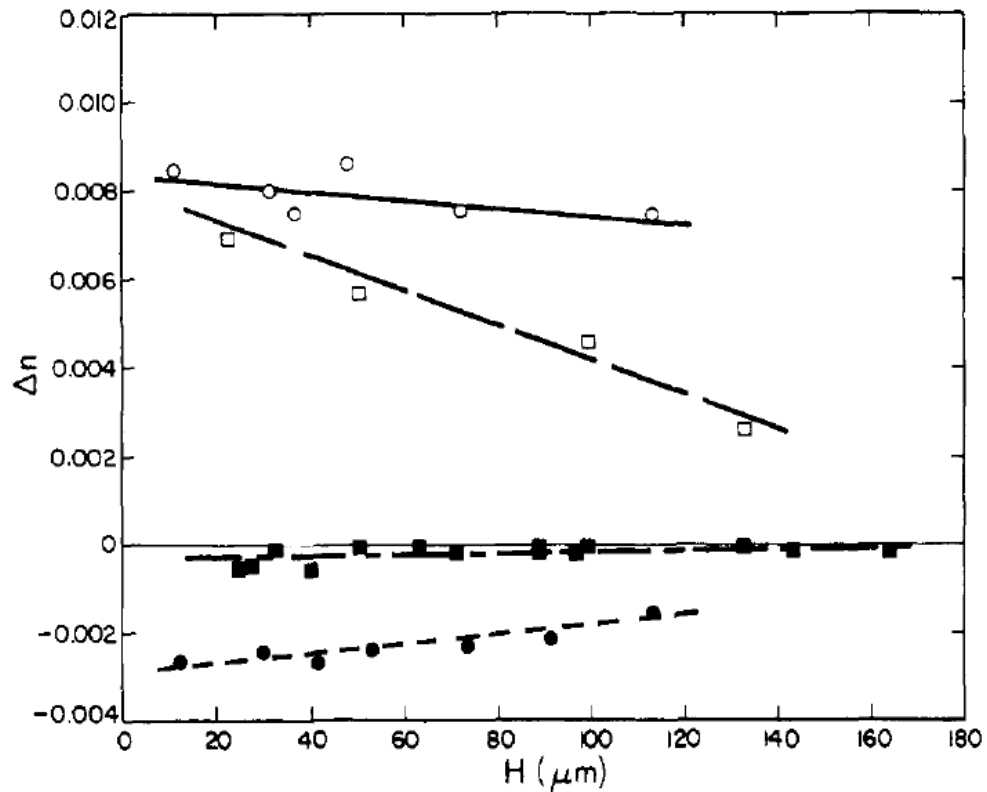
Figure II-54 Transverse birefringence vs. dry film thickness showing the effect of casting method. TMBPA: ○ BC method, □FC method. PS: ●BC method, ■FC method

2.3.1.2. Drying the PAA film

The objective of the drying process is to remove any excess solvent from the cast precursor solution so the film can be handled independently and peeled from the carrier without failure. The parameters that controls this step and affects the structural development in polyimide films can be listed as; solvent amount (viscosity), solvent boiling temperature (vapor pressure), polymer-solvent interaction, glass transition temperature of the solution, imidization temperature,

thermal stability of poly(amic acid), drying time and temperature, drying rate, and environmental conditions (such as humidity, air flow rate etc.).

Drying of the solution cast films are generally performed by hot air convection or by conduction through a hot surface. To produce uniform, high quality, and self-standing poly(amic acid) films, it is important to have a uniform temperature distribution on the solution. Solvent molecules that are generated from the film have to be removed and the cast solutions have to be oriented perfectly horizontal. The air flow rate and drying temperature should be adjusted such that the formation of the skin layer on top section of the film should be prevented. Solvent and water molecules trapped under the skin layer might cause bubbles on the surface of the film. Also drying rate is a function of not only the diffusion rate of the solvent but also the imidization rate at the selected drying temperature. Since the polyimide chains exhibit bigger stiffness than the poly(amic acid) chains, it will be harder for solvent molecules to diffuse out as sample imidizes.

Similar to casting step, drying step has an influence on the final structural development of the solution cast poly(amic acid) films as well as any other solution cast films. As mentioned on the previous section (2.3.1.1 Solution Casting) solution casting produces films with zero birefringence in the plane of the films and non-zero birefringence on the out-of-plane directions.[90] Cherkasov et al. noted that two conditions can be responsible for this behavior which are showed figure below. (Figure II-55) [91] The polymer chains can be either oriented parallel or perpendicular to the surface of the film. They proposed that, when the

chains are oriented parallel to the surface the angle v in the figure, should

change between 123°>v>57°and the orientation parameter should have a

negative value (S=-0.5 is perfectly planar orientation). If the chains are aligned

normal to the film surface, the angle should change between 57°>v>-57° and the

orientation parameter will have a positive value. As a result, the sign of the order

parameter is an indicator for the ordering type. In Figure II-56, they showed that

the all solution cast films possess negative values of order parameter *S* and they

concluded that the chains are aligned parallel to the film surface. Also polyimide

films in the graph exhibited very high order parameter values indicating almost

perfectly planar orientation of the polymer chains. In their work of investigating

anisotropy in solution cast poly(amic acid) and polyimide films, Russell et al.

concluded similar observations. [92]
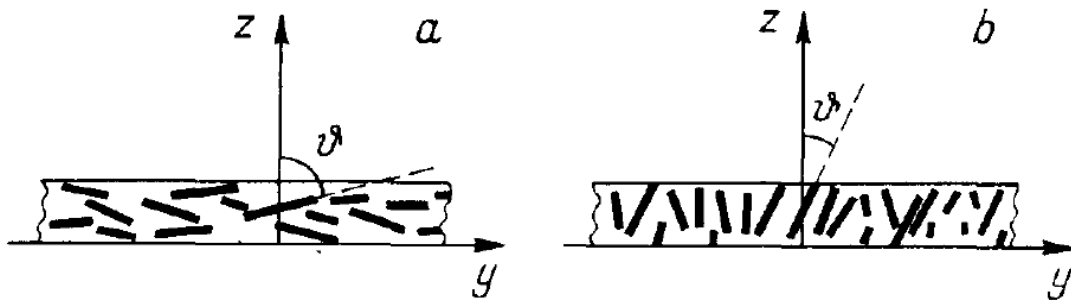
Figure II-55 Possible types of ordering in surface layers of polymer films
causing birefringence: a-plane ordering; b-normal ordering
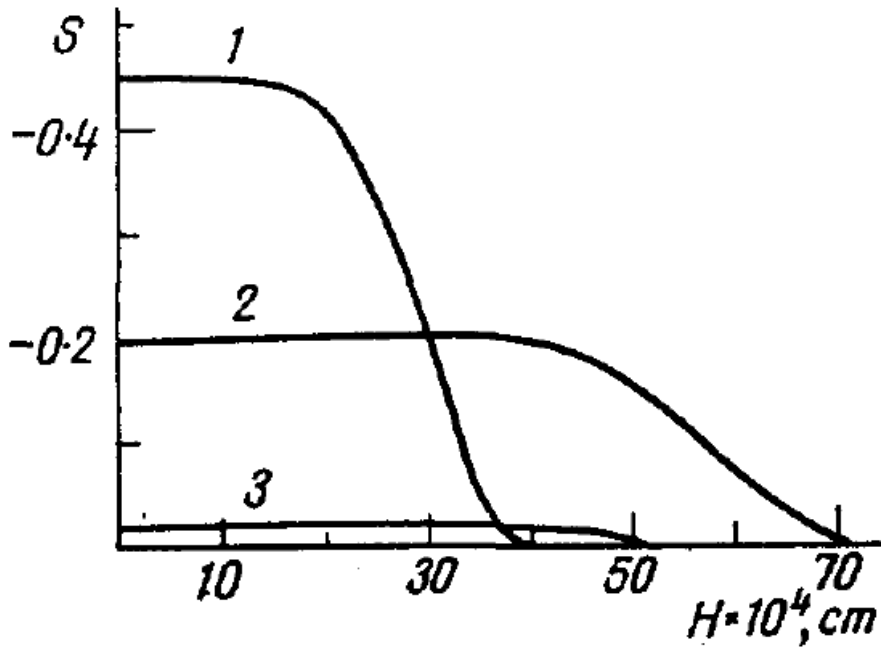
Figure II-56 Relation between the orientation factor of ordering
$S=0.5(3\cos^2\theta - 1)$ and thickness H for (1) PI, (2) CLPS, (3) PS films

Coburn et al. suggested the following explanation; the evaporation of the

solvent from the cast films causes shrinkage on the cast films. If the polymer

solution is constrained during the solvent loss, shrinkage can result orientation

development in the constrained directions. Coburn et al. named this process as

gel-film collapse as illustrated figure below. (Figure II-57) Spin coated or blade

casted solutions on a substrate are constrained parallel to the casting surface

and shrinkage due to solvent mostly occurs in the thickness direction. As the

solvent loss continues, the film becomes at a stage where it can sustain stress as

a film and further solvent loss results alignment of precursor chains parallel to the

surface of the substrate. Stresses developed due to shrinkage introduce more

anisotropy to the film. Although there is anisotropy in the thickness direction, in-

96

plane orientation of the film can be isotropic or anisotropic depending on the

casting conditions. [85, 93,94]
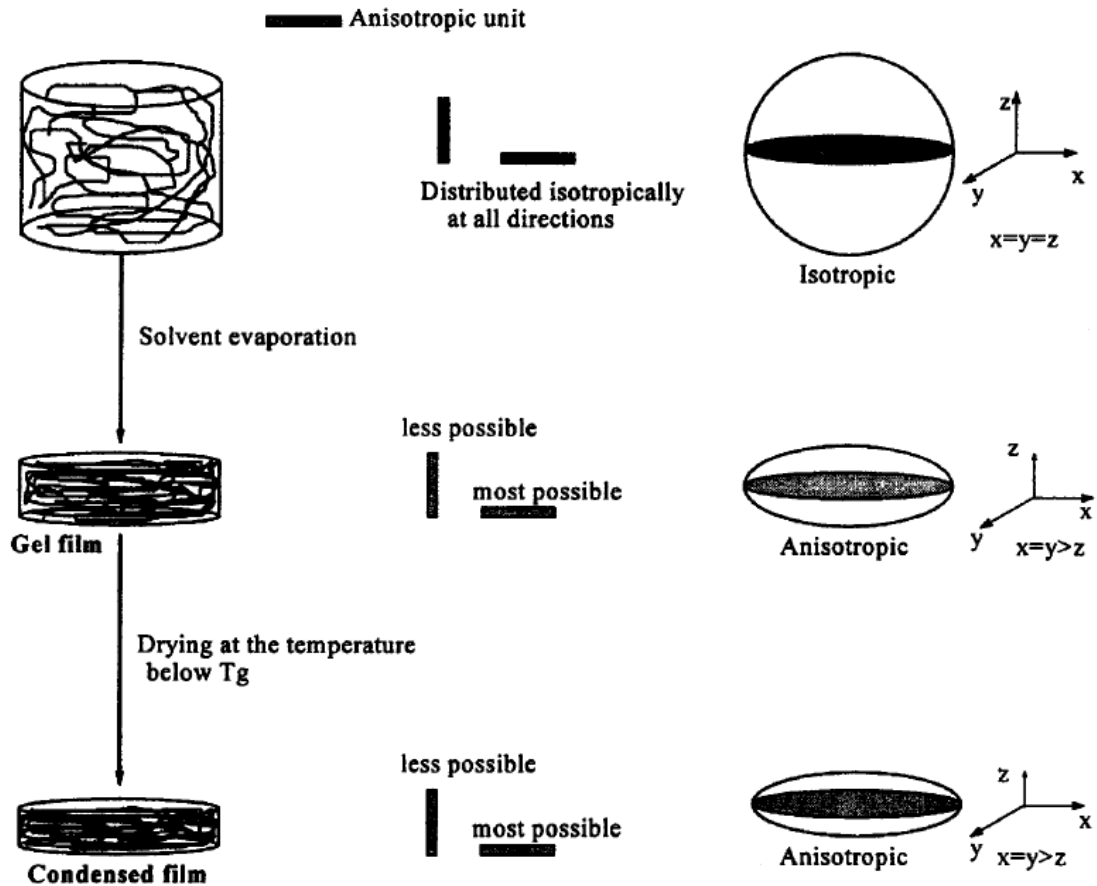
Figure II-57 Development of anisotropy in polyimide films during solvent casting

Prest and Luca, explained this behavior as a competition between the

planar conformation of chains introduced by drying and tendency of chains to

orient randomly. This competition can be affected by various factors, including

initial thickness of the cast, dry film thickness, solvent type, casting temperature,

T_g of the system, M_w of the polymer, surface energy of the substrate and SOC of the polymer. [85, 86, 88, 89, 93, 95] All these factors are affecting the relaxation times of drying chains directly.

The effect of dry film thickness has an influence on the development of orientation in solution casting films, which is also mentioned in the previous section (2.3.1.1 Solution Casting). Machell et al. and others investigated this effect and they concluded that the out-of-plane birefringence is inversely proportional to the thickness of the dry films. As the thickness of the film increases, the level of orientation in the film decreases and after a critical thickness value, this relation levels off. [88] Prest and Luca concluded that this observation suggests the existence of a thin skin region with highly oriented chains and as thickness increases its contribution to averaged orientation decreases. [86, 95] Figure II-58 shows this relation for bisphenol A polycarbonate (PCl) cast from dichloromethance (DCM) as solution for both free casting and blade casting method. [88]
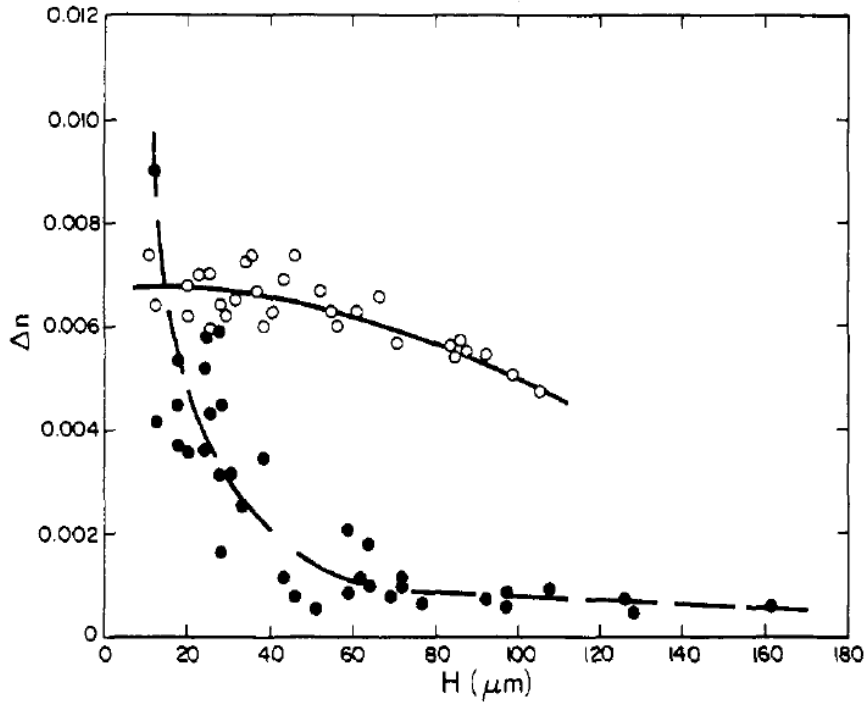
Figure II-58 Transverse birefringence vs. dry film thickness for PCI cast from DCM

Compared with the film thickness, solvent type has a smaller effect on the orientation development on the solvent cast films. In general, slow evaporating, higher boiling point solvents produce smaller birefringence. This can be explained by the plasticizing effect of the solvent on the polymer chains. If solvent has a higher boiling point, it will evaporate slower and it will result a slower freezing of the polymer chains. [86, 88, 89, 95, 96] Echigo et al. investigated the effect of solvent on birefringence on polyimide films prepared from NMP and THF/MeOH solvents and they observed films prepared from THF/MeOH solvent produced smaller birefringence values. (Figure II-59) They also suggested that

the nature of the solvent might also have a role on in plasticizing effect of the solvent over polymer chains. [96]
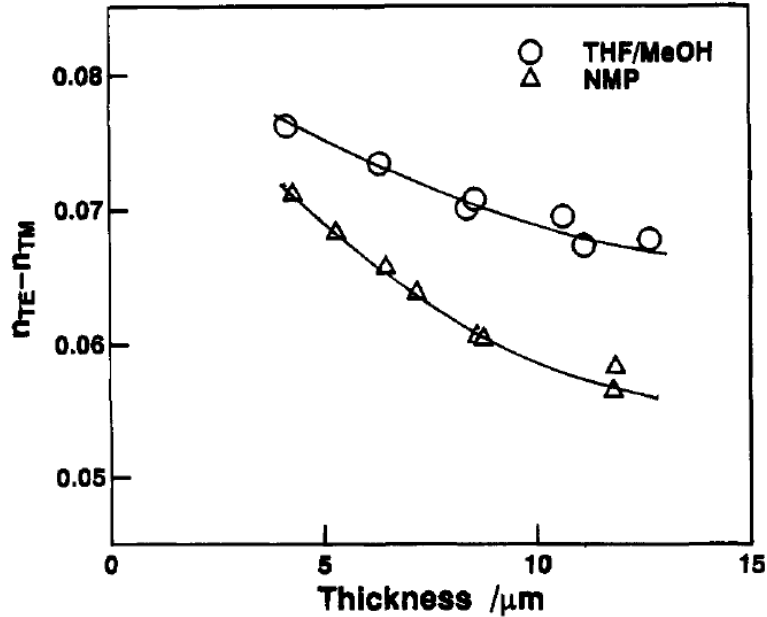
Figure II-59 Dependence of birefringence of PI(NMP) and PI(THF/MeOH) films on thickness

The molecular weight of the polymer also has an effect on the orientation development of solution cast films. Figure II-60 shows the birefringence of different molecular weight PS films as a function of dry film thickness. It can be noted from the graph that the orientation decreases as the molecular weight decreases. This can be attributed to the more entanglements for higher molecular weight polystyrene chains which freeze the system earlier and prevents the relaxation of the polymer chains as solvent evaporates. [86, 95]

100
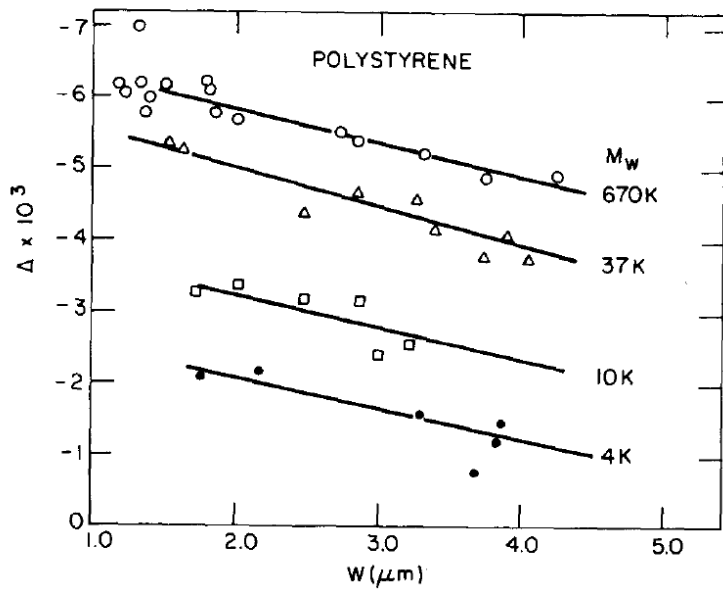
Figure II-60 Birefringence of different molecular weight PS as a function of thickness

The effect of casting temperature on the orientation development is shown in Figure II-61. [95] From the data, it can be concluded that as the T_c getting closer to the T_g of the system, birefringence decreases. This is due to the slower freezing process of the polymer chains at closer temperatures to the T_g. [88, 95]
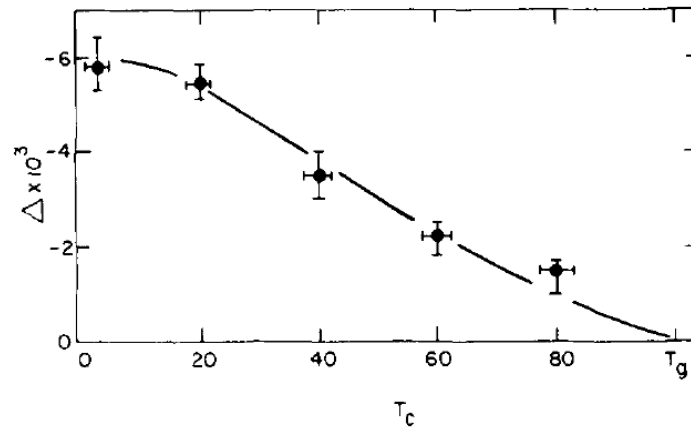
Figure II-61 Birefringence of PS as a function of casting and drying
temperature

Last of all the role of the casting substrate is investigated by Machell et al.

They used Teflon, aluminum, glass and polyethylene surfaces and compared the

orientation development of solution cast films on these surfaces. The surface

energies of these substrates in the decreasing order is

glass>aluminum>polyethylene>Teflon. [88] The data for this experiment can be

seen in the Figure II-62. It can be concluded that the birefringence decreases

with decrease in the surface energy of the substrate.
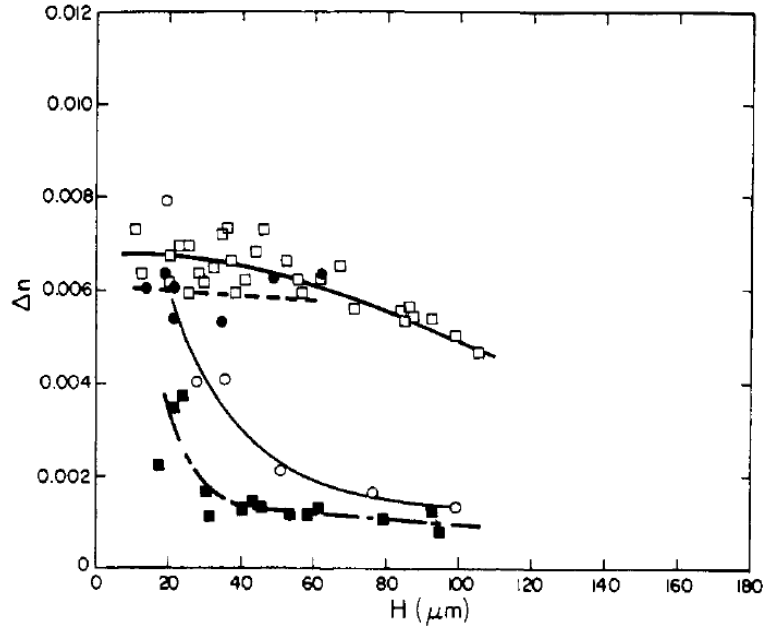
Figure II-62 Birefringence vs. dry film thickness showing the effect of
casting substrate for PCl casted from DCM ○ polyethylene, □glass,
●aluminum, ■Teflon substrate

As a summary, applying a polymer solution onto a surface is followed by

solvent evaporation and as solvent evaporates the volume of the solution

decreases and the polymer chains collapse. At the early stages of the

evaporation, relaxation times of the polymer chains can respond to the solvent

loss on the film and can still possess isotropy. However, as more solvent is lost

from the solution, several consequences are observed. First of all, the viscosity

of the system decreases which is followed by a decrease in the chain relaxation

ability. More solvent loss results in a locking mechanism by affecting the T_g of the

system and hence the relaxation times of the polymer chains. Other factors

effecting the out-of-plane orientation of solution cast polymer films can be listed

as molecular weight of the polymer, casting temperature, film thickness and

surface energy of the substrate. These factors and their effects on the orientation development (out-of-plane) on the dried film can be summarized in a table. (Table II-8) [85, 86, 88-90, 92, 93, 95–102]

Table II-8 Contributing factors to orientation in solvent cast films

	Change	Δn_{th}
Dry film thickness	↑	↓
Solvent boiling point	↑	↓
Casting temperature	↑	↓
T_g of the polymer	↑	↑
M_w of polymer	↑	↑
Surface energy of substrate	↑	↑
SOC of polymer	↑	↑

2.3.1.3. Imidization of PAA film

The main objectives of this step are to remove any residual solvent that is present on the poly(amic acid) film, and to perform the conversion of amic acid groups into imides. Curing (or imidization) plays the most important role on determining final properties of polyimide products.

For example, type of imidization results different properties on the polyimide films even for the same chemical compositions. Russell et al. found that films that are cured chemically possess almost 3 times higher birefringence than films prepared by thermal imidization. [92]

The focus of this section will be on the polyimide films that are cured thermally and a detailed explanation of imidization process is given on the previous sections of this dissertation (2.1.2.2 Thermal Imidization of PAAs). As mentioned on that section, ramped imidization (first heating the samples to around 200°C and then further heating it to 350-400°C) is preferred over other methods due to a more successful solvent removal and achieving higher degrees of imidization. Processing time, temperature and heating rate are the most important variables that control thermal imidization.

As discussed on the previous sections, the solution casting and drying processes are introducing out-of-plane anisotropy resulted primarily from shrinkage effect due to solvent evaporation. For polyimide films, on top of all these complications, conversion of relatively flexible and soluble poly(amic acid) groups into rigid and insoluble polyimide groups adds another dimension. As explained on the previous sections of this dissertation (2.1.2.1 Poly(amic acid)s precursors and 2.1.2.2.1 Solvent Effect), dried PAA films have considerable amount of residual solvent due to H-bonding interactions of amic acid groups with NMP molecules. During imidization these solvent molecules have to decomplexed from the amic acid groups and evaporate. At the same time the conversion of these amic acid groups to imide groups takes place and due to this

reaction water is released as a byproduct, which also evaporates from the film. This complex scheme of imidization has an influence and also itself is influenced by already previously developed orientations on the film due to solution casting and drying processes. The chains in polyimides are strictly restricted to relax due to solvent loss and conversion to rigid imide groups. In addition to this, solvent loss, water loss as a byproduct and conversion of amic acid to imide introduces more shrinkage to the film, resulting higher orientation values.

Elsner reported that, another reason for stress development on polyimide films is the CTE difference between the polyimide film and the substrate that it is cured on. During the thermal imidization the poly(amic acid) films are heated to 400C for curing, and sometimes with the substrate that they are casted on, and while the imidized film is cooled down to room temperature, the CTE mismatch between the polyimide film and the substrate creates stress and evolution of orientation. [103]

Coburn et al. performed a similar study and investigated the stress development on polyimide films during imidization process. Similar to solution cast films, they observed zero birefringence in-plane and anisotropy in the out-of-plane birefringence. They reported the birefringence is a combination of molecular orientation due to chemical change and birefringence introduced by the residual stresses presented on the films (mainly due to mismatched CTE). To separate the effect of two they investigated the imidized samples that are adhered on the surface as well as free standing samples. Figure II-63 shows the relationship between the birefringence as a function of thickness for free standing

106

and adhered samples. As it can be concluded from the graph, adhered samples

have higher birefringence values due to the additional stress development.

Although the solution concentration was changed in a small range, they didn't

observe any effect of concentration on birefringence.

Birefringence in adhered samples can be expressed as;

$$\Delta n = \Delta n_0 + C \sigma_f \qquad (11)$$

where Δn_0 is the zero-stress birefringence due to orientation, C is the

stress-optical coefficient and σ_f is the film stress. [85, 93, 104, 105]
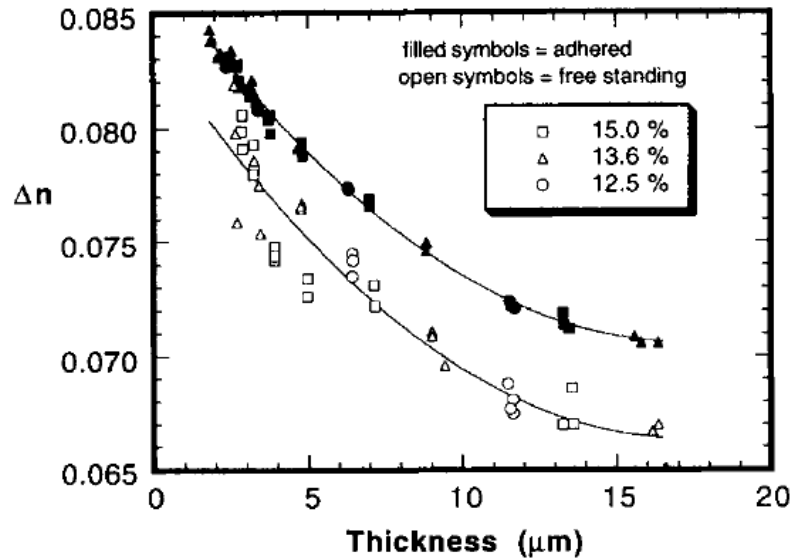
Figure II-63 Birefringence vs. thickness for free standing and adhered films

Polyimide films with different anisotropies can be achieved by controlling

the imidization degree or by controlling the stresses developed during the

imidization by constraining the poly(amic acid) film. Numata et al. showed that

107

poly(amic acid) films that are biaxially constrained exhibit higher degree of orientation compared to the free standing films. This molecular orientation development is a result of restricting the in-plane shrinkage of polyimide film. The reasons for the shrinkage can be listed as, solvent evaporation, evolution of water and its evaporation and conversion of amic acid groups to imide groups, which occupies less volume than the amic acid groups. [106,107]

Hasegawa et al. observed very similar results by using a different method. Instead of measuring the orientation factor of polyimide chains directly, they dispersed a die flat molecule within the poly(amic acid) solution. This die molecule orients itself parallel to the polyimide chains and absorbs light in the UV-visible region.[108] They confirmed the previous results by observing isotropy in the film plane of undrawn PAA and PI films are and the out-of-plane orientation is thickness dependent and decreases as thickness increases. [109,110]

Heating rate during imidization has also an effect on the final orientation of the chains. General trend is, as heating rate increases the orientation of the film decreases. [85, 93, 110] This behavior is explained by Coburn and Pottiger with the effect of heating rate on the effective glass transition of the film. (Figure II-64)
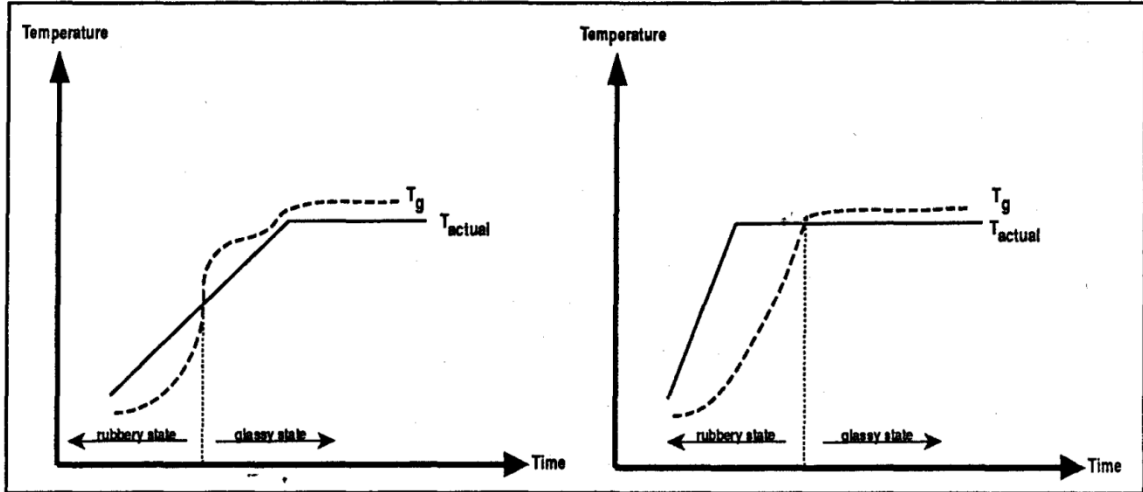
Figure II-64 Effect of heating rate on the effective glass transition
temperature for slow and fast heating rates

Relaxation of poly(amic acid) films that are partially imidized depends on

the solvent amount, degree of imidization and the temperature. If the films are

cured with slow heating rates, the effective glass transition temperature rises

faster than the film temperature. For the fast heating rates, the cure temperature

rises faster than the effective glass transition temperature of the film. For fast

heating rates, since the film temperature is above the effective glass transition

temperature, the chains can relax and produces lesser orientation. For slow

heating rates, the effective glass transition temperature of the film is above the

film temperature, so the chains are in a frozen mode and cannot relax, hence

produces higher orientation degrees.

2.3.2. Polyimides under deformations

The stiff polyimide chains doesn't allow for high stretching values. Generally precursor poly(amic acid)s are stretched at temperatures close to the room temperature (cold drawing) and are subsequently imidized.

Hasegawa et al. found that the thermally imidized uniaxially cold-drawn poly(amic acid) films give higher orientation values compared with the non-deformed samples by a factor of 3. [48, 108-111]

Ando et al. investigated the effect of chemical structure on uniaxially cold drawn poly(amic acid) films. They stretched six different PAAs and then thermally imidized these samples. They observed the birefringence values of final PI films are higher than the undrawn samples. The stiff chains showed bigger increase compared to relative flexible chains containing –O–, –CO– and –C(CF$_3$) – linkages. [112]

Samuels et al. investigated the effect of processing conditions on optical properties of polyimide films. They measured off-line three-dimensional orientation functions of cold drawn polyimide films. Figure II-65 shows the evolution of orientation function in three directions as a function of percent extension. They concluded that for the highly drawn film, the value of orientation function is only around 0.5, which indicates the chains are far from being perfectly aligned parallel to the drawing direction. This also results there is room for dramatic improvement on the orientation of chains parallel to the stretching

direction. Their measurements also agreed with the previous literature on the isotropic orientation of molecules in the plane of the film before any deformation.[13, 113–115]
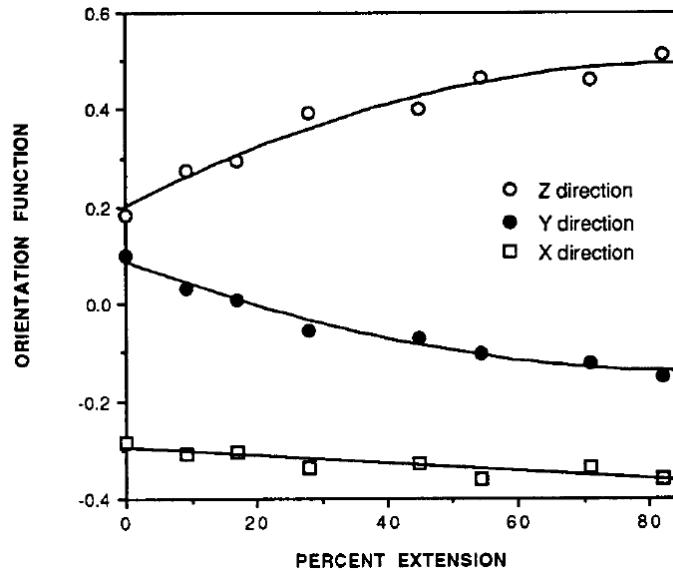
Figure II-65 3D orientation functions of drawn PI films(z= MD, Y=TD, X= ND)

Samuels et al. also conducted optical characterization studies of polyimide films as a function of film thickness, to understand the surface and bulk characteristics of the films investigated. They used two different methods; polarized microscopy (to measure the bulk refractive indices of films) and polarized refractometry (to measure three principle surface refractive indices) on a series of high refractive index Kapton polyimide films of varying thicknesses. They chose n_z as principle refractive index parallel to the optical symmetry axis in the sample plane, n_y as the principle refractive index perpendicular to the optical

111

symmetry axis in the sample plane and n_x as the principle refractive index normal to the sample plane. (Figure II-66) [113]
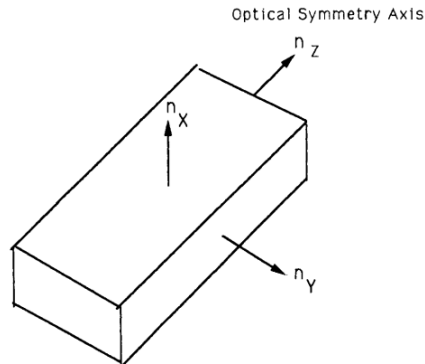
Figure II-66 Principle refractive indices in the film geometry

Figure II-67 compares the bulk and surface refractive indices of the Kapton films as a function of film thickness. It was observed that the n_z increases with increasing film thickness and up to 3 mils and decreases. On the other hand n_y decreases slightly with film thickness. They concluded that the orientation in the film plane has increasing anisotropy with thickness up to 3 mils. Also in Figure II-68, the in-plane birefringence Δ_{zy} is increasing with increasing thickness up to 3 mils. The value of n_x is smaller than other either in-plane values and it decreases constantly as the film thickness increases. However the value of Δ_{zx} is increasing, which they concluded that it is an indicator of planar orientation of molecules in the film and this orientation increases as film thickness increases up to 3 mil.

Finally from the data in Figure II-67 and Figure II-68 they indicated that the bulk Kapton films have higher anisotropy that the surface. They concluded these films are heterogeneous with slightly higher oriented region within the bulk. [113]
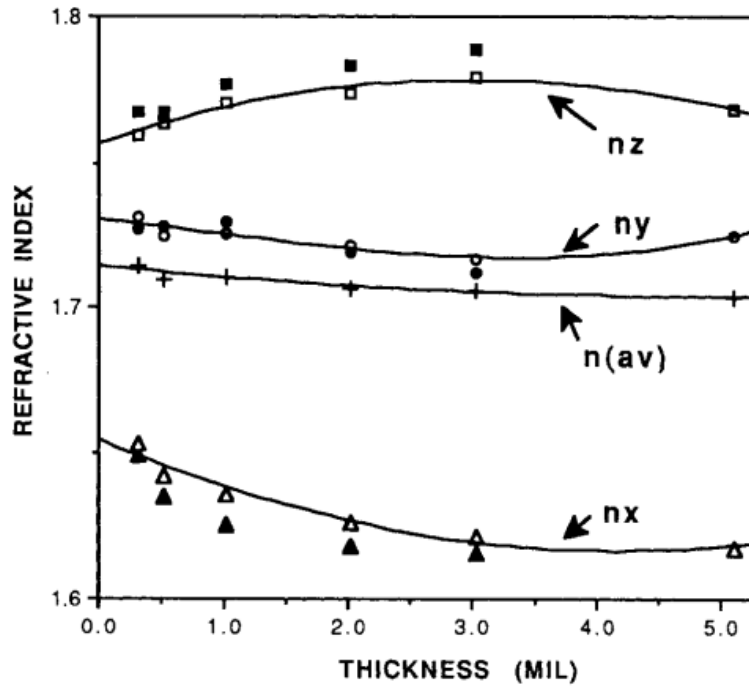
Figure II-67 Refractive indices of Kapton films as a function of film thickness (open symbols - surface; filled symbols - bulk)
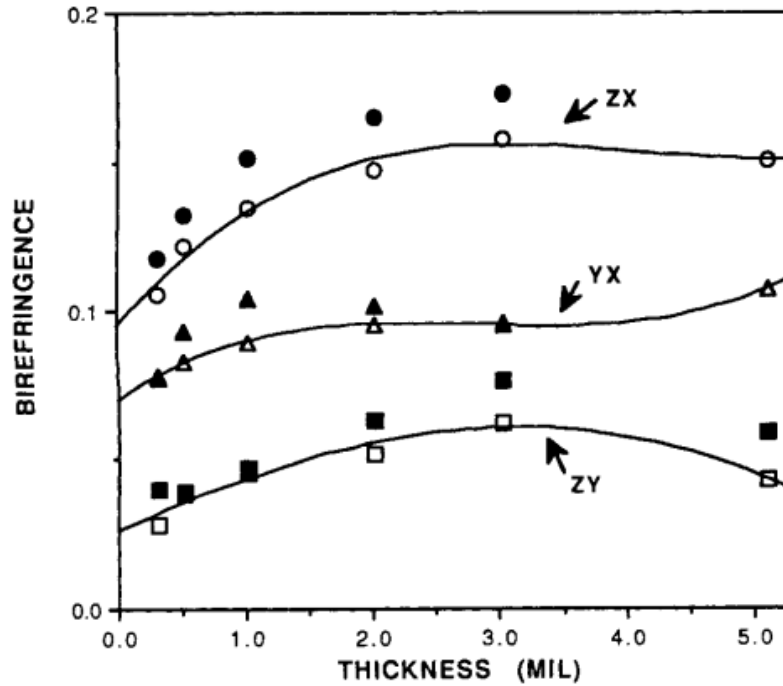
Figure II-68 Birefringence of Kapton films as a function of film thickness
(open symbols - surface; filled symbols - bulk)

In all their results the surface refractive indices and birefringence values

are slightly lower than the bulk values. In this sense, Samuels et al. results seem

to contradict the other researcher's results where majority noted the orientation of

the solution cast films decreases as a function of thickness and surface portion of

the sample has higher orientation than the bulk. The reason for this contradiction

might come from the sample preparation step, where Samuels et al. do not report

how these samples are prepared. The Kapton samples they used are provided

by DuPont Company and there is no information scheme on imidization or post-

processing of these films.

CHAPTER III

REAL-TIME MEASUREMENT SYSTEM FOR TRACKING

BIREFRINGENCE, WEIGHT, THICKNESS AND SURFACE

TEMPERATURE DURING DRYING OF SOLUTION CAST

COATINGS AND FILMS

This chapter describes the design and performance of a new instrument to track temporal changes in physical parameters during the drying behavior of solutions, as well as curing of monomers. This real-time instrument follows in-plane and out-of-plane birefringence, weight, thickness and surface temperature during the course of solidification of coatings and films through solvent evaporation and thermal or photocuring in a controlled atmosphere. It is specifically designed to simulate behavior of polymer solutions inside an industrial size, continuous roll-to-roll solution casting line and other coating operations where resins are subjected to UV curing from monomer precursors. Controlled processing parameters include air speed ,temperature, initial cast thickness and solute concentration while measured parameters are thickness, weight, film temperature, in-plane and out of plane birefringence. In this chapter we illustrate the utility of this instrument with solution cast and dried poly (amide-

imide)/DMAc solution, water-based black paint, and organo-modified clay/NMP solution. In addition, the physical changes that take place during UV photo polymerization of a monomer are tracked. This instrument is designed to be generic and it can be used for tracking any drying/swelling/solidification system including paper, foodstuffs such as grains, milk as well as pharmaceutical thin paste and slurries.

3.1 Introduction

Drying is a common method that is used by various manufacturing disciplines to produce large quantities of products. The common goal of the drying process in all different processing industries is to produce a good quality product in an optimized medium by precisely controlling the drying conditions. For instance, in food processing, the aim is to produce products with highest level of nutrient and flavors, while in polymer processing one of the aims is to produce films with uniform thickness distribution, high optical clarities and desired optical anisotropies such as in the cast of optical retarders used in construction of LCD displays.[116–118]

Typically the polymer solutions are deposited on the substrates using electro-spraying, ultrasonic coating, doctor blade casting and slot die coating to manufacture products including protective coatings, films for membranes, optical and electrical applications.[118–122] The solution is then dried via application

116

of conductive heat sources through the substrates and/or convective air flow from the free surface of the cast films.

During the drying phase, the material undergoes a series of stages as the solvent molecules diffuse to free surface and then evaporate. The details of this drying, controlled by process and material parameters, dramatically affect the final structure and properties of coatings and films. Rickert et. al.[123] reviewed the organization and assembly of macromolecules that are deposited on inorganic substrates and concluded that substrate properties, solution organization and interfacial characteristics of macromolecules are the important elements controlling the process.

As the evaporation of the solvent from the medium continues, the loss of solvent causes shrinkage that is accompanied by ensuing solidification of the material. This shrinkage mainly occurs in the thickness direction since the solution is typically constrained in the film plane on the substrate to which it generally adheres. This is manifested in significant reduction of the thickness of coating/film during drying.

Traditionally the evaluation of the final properties of the solution cast and dried films are carried out by systematic study of the process and material parameters and examining the final films through a series of offline characterization methods. The treatment of these complex physical processes as "black box" makes it difficult to develop models to quantify the dynamics of the physical/chemical processes that take place during the course of drying. These

117

offline studies, nevertheless still, reveal valuable information especially on optical properties of solution cast polymer films. Sosnowski and Weber[124] are the first ones to discuss the optical anisotropy through the thickness direction on free casting of polystyrene and poly (methyl methacrylate) solutions on glass substrate. They concluded that birefringence occurs as a result of stress development in the film and the level of birefringence depends on the solvent type and drying temperature. Cherkasov et. al.[125] also investigated orientation development on free cast (no stress on casting procedure) polymer solutions with different chemical structures and they found that the polymer chains preferentially orient parallel to the surface of the film sometime during drying. They also observed that smaller thickness values and rigid chemical structures generate higher values of birefringence. In a similar study, Prest and Luca[126,127] investigated the optical properties of polymer solutions that were cast on substrates via wire wound draw bars that leads to shearing induced stress generation in the film. They focused on the effect of film thickness, molecular weight, plasticizer content, solvent and temperature on the level of orientation in polymers. Birefringence values increase with reduction of film thickness, molecular weight increase and drying temperature decrease. The initial concentration of the solutions has little or no effect on the orientation development. In light of these observations, they concluded that the development of preferential orientation of chains parallel to the film surface is a result of a complex relationship between the relaxation time and evaporation induced chain axis alignment in the film plane.

In a later study, Machell et. al.[88] compared the effect of casting method, solvent type, casting temperature, casting substrates and timing of the peel-off step on the final optical properties of the solution cast films. In agreement with the previous studies, the films produced by all the casting methods exhibited in-plane isotropy and out of plane anisotropy and the level of anisotropy decreased as the thickness increased. They observed that casting methods also affect the final optical properties of the dried films. Blade casting method generated higher birefringence in the films as compared with the free casting method indicating that at least part of the orientation introduced by the shear flow during casting remains in the final dried film.[88,128] This occurs despite the relatively low viscosity of the casting solutions used. The solutions prepared with higher boiling point solvents generated lower birefringence films as more relaxation takes place for these films and they experience slower evaporation rates. Machell et. al. also investigated the timing of the removal of the film from the substrate and found out that the films removed before complete drying generated lower birefringence. Finally the effect of casting substrate is investigated and concluded that in general level of birefringence decreases with decreasing surface energy. [88] These "off-line" studies helped to understand the final properties but did not reveal the temporal development of mechanistic changes that occur during the course of drying.

There have been a series of modeling studies to predict the drying characteristics of the polymer solution.[129–133] The validation of these modeling studies, however, has been hampered by lack of high quality real time data.

Ataka and Sasaki[134] were the first ones who tracked the real-time weight loss during evaporation of cellulose-acetate/acetone solution for membrane production. They found that the solvent/polymer weight ratio decreases almost exponentially with time. Tantekin-Ersolmaz et. al. and Greenberg et. al.[135,136] developed an instrument that can measure both weight loss and surface temperature during the evaporation of the solvent. They quantified the amount of cooling (as much as 24°C) during the drying of cellulose-acetate/acetone solutions. They found out that the surface temperature drops quickly at the early stages of evaporation and passes through a minimum.

Payne et. al.[137] developed an apparatus to determine the stress evolution during drying of polymer and ceramic coatings. In their design, they used cantilever deflection method to calculate generated stresses as the coatings are dried in controlled air/temperature environment. They reported that generated stress decreases with increasing relative humidity levels and increasing temperature values. It was observed that final stress was not affected by chilling, final thickness and initial solution concentrations.[138] They also reported stress generation relative to weight decrease, but these results were not obtained simultaneously on the same samples, though they were obtained in identical conditions. They noted that at the initial stages of evaporation, the modulus is not high enough to support stress, and stress develops rapidly after a critical amount of solvent is evaporated.

In the following, we describe the details of an automated real time measurement instrument, designed to track the weight, temperature, thickness

coupled with in and out of plane birefringence -a first- while subjecting to convective heating.

3.2   The Casting Process

In a conventional roll-to-roll industrial solution casting and drying process, a polymer solution is delivered to a carrier via a casting blade or a slot die. The coating is then transported on a substrate through a series of drying zones that are heated by under-bed heaters below the belt and convectively heated by the air circulating system from above. In our design, we aimed to mimic this process by applying coatings and polymer solutions on a wide variety of substrates such as metals, plastics, and glass. Various initial wet thicknesses (from 25 micrometer to 1 millimeter) and dimensions can be used for the selected substrates with dimensions less than 6"in wide and 9" in length. A small motorized drawdown coater (Cheminstruments, EZ Coater, Model number: EC-200), equipped with a commercial 3" wide, double blade assembly Dr. Blade coater is used to apply the coatings onto selected substrates.

Transparency of the substrate and the coating or cast polymer is important for to real-time birefringence measurements as the spectral birefringence method operates in transmission mode. In experiments, where the optical properties are not important or cannot be measured for highly filled and/or colored samples, non-transparent substrates can be used such as steel, aluminum and ceramics. Glass substrates are selected for the experiments, where the optical properties of

121

drying solutions are crucial to measure real-time for transparent optical film

production process. The back face of the glass substrates was painted black to

improve the signal quality of the laser displacement sensor. Additionally, the

glass substrate may be coated with most of the metals or ceramics while leaving

a small portion uncoated for optical birefringence measurement. Figure III-1

illustrates the glass substrate (black) coated with polymer solution (transparent-

yellow). The red dots (indicated by arrows, L1, L2 and L3) are the projections of

the positions where the laser displacement measurements are performed. The

light blue circles (P1, P2, P3, and P4) represent the projection of positions where

the pyrometer surface temperature readings are obtained. The large circle in the

middle represents the position of spectral birefringence measurement. All real-

time measurements are performed in the close proximity to the center of cast

polymer solutions where the edge effects are avoided.
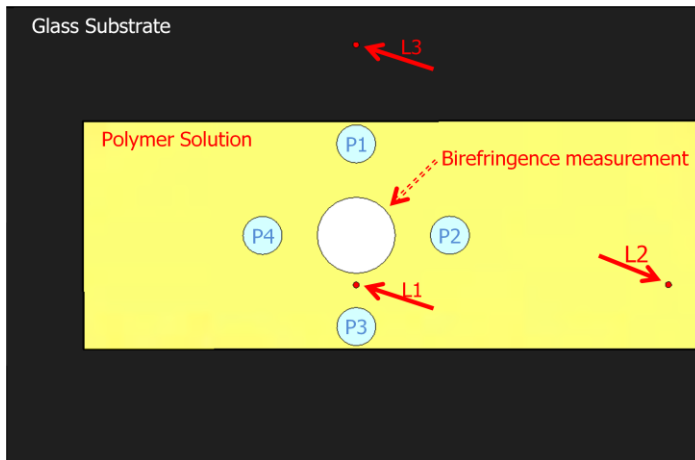
Figure III-1 Glass substrate with cast polymer solution and projections of measurement location (Pyrometers: P1, P2, P3, P4 and Lasers: L1, L2, L3).

In a typical casting procedure, the prepared polymer solution is introduced inside the reservoir of the Dr. Blade casting system. The speed on the motorized coater can be adjusted and finally the moving bar is set in motion. As the bar moves, it pushes the Dr. Blade on the glass substrate depositing desired thickness coating (Figure III-2). Coated glass substrate is then placed on top of the sample platform inside the wind tunnel for real-time measurements during drying process. This casting method is found to be very stable and it provided excellent repeatability.
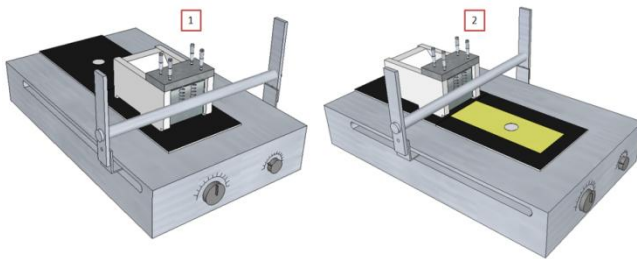
Figure III-2 Casting procedure with Dr.Blade apparatus: before (1) and after casting (2)

3.3　Drying Apparatus

The real-time measurement apparatus is shown in Figure III-3. The shape of the main body is designed as a wind tunnel to provide a uniform air flow for the drying polymer solution which is located at position 4 on a graphite platform. The frame consists of two layers of metal enclosures that are separated with a

thermal insulation material in between. Aluminum is selected for high solvent and

corrosion resistivity.
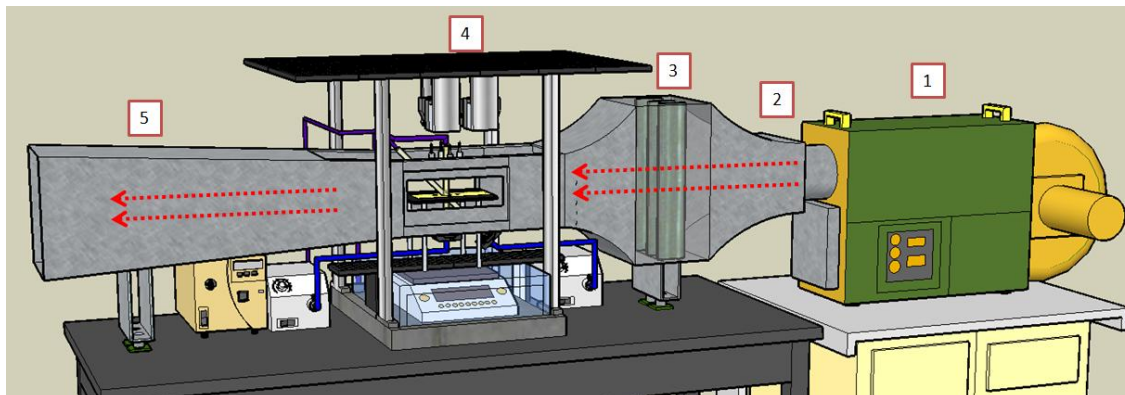
Figure III-3 Real-time solution drying platform. From right to left it is numbered as: 1) Hot air blower, 2) Connection of blower to the tunnel, 3) Vertical baffles 4) Drying sample and sensor location and 5) open end of the tunnel

Hot air blower with the model number TSK-52HT (Type 3200-17C-025Y-

LB-HT) [#1 in Figure III-3] from Taketsuna Company is capable of setting

temperatures between ambient and 500°C at air speeds up to 6 m/s. The air

blower connects to the wind tunnel at position #2. The dashed red arrows

indicate the direction of air flow inside the wind tunnel. There are three adjustable

vertical baffles [#3] that are used to fine tune the uniformity of air flowing through

the drying polymer solution. These baffles were adjusted and locked while the air

speed at various locations inside the sample position was measured by an

external anemometer. The sample and sensors' location is marked as # 4 in

Figure III-3. The downstream end of the wind tunnel is open to atmosphere [#5].

An exhaust is positioned close to this opening, to collect the solvent containing

air coming out from the wind tunnel. The exhaust inlet is separated by about 2"

from the end of this tunnel so as not to cause excess vacuum by the air handling

system.
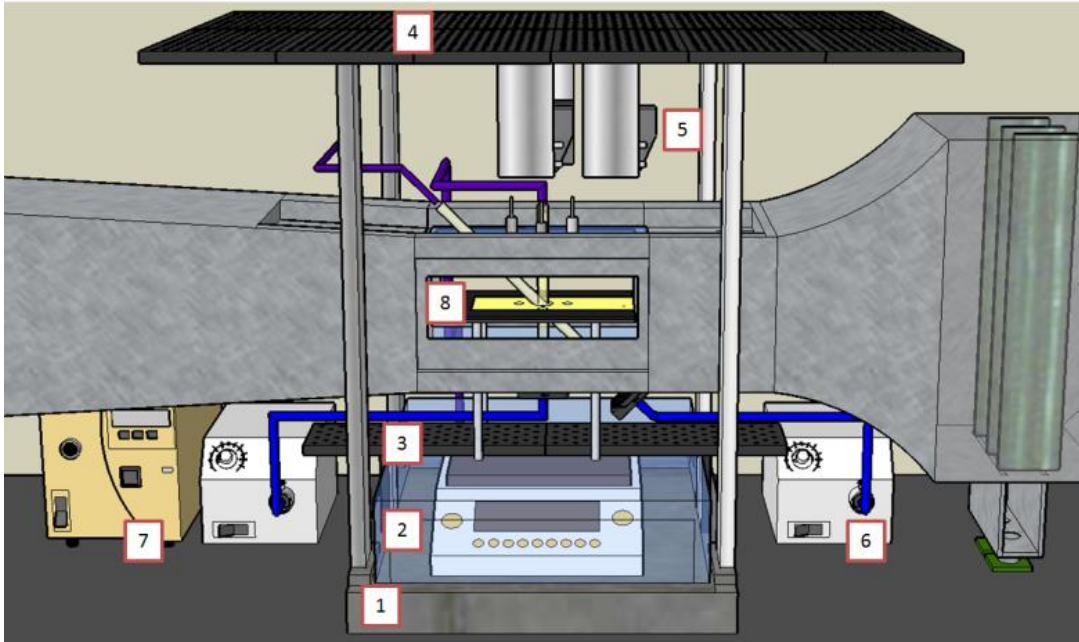
Figure III-4 Sample and sensor location 1) Cast iron base 2) Balance and plastic box 3) Small breadboard for optical components 4) Large breadboard for optical components and sensors 5) Laser displacement sensors 6) Visible range light sources 7) UV light source 8) Sample platform

The sensors for real-time measurement are positioned in the mid-section

of the wind tunnel [# 4 in Figure III-3] where the drying sample and the substrate

are introduced [Figure III-4]. All the sensors and optical components are

connected to two breadboards [# 3 and 4 in Figure III-4], one located on top and

one located at the bottom of the sample position. The top larger breadboard [#4]

holds the laser displacement sensors [# 5] for thickness measurement, bifurcated

fiber optic cables for in-plane and out-of-plane birefringence measurement and a

USB camera. The smaller breadboard [# 3] at the bottom position of the drying sample holds the fiber optic guides for visible light sources and linear polarizers. These breadboards are attached to a heavy cast iron base [#1in Figure III-4] for stability. An electronic balance with sensitivity of 0.01g (Sartorius, LA-6200 S) is placed on the cast iron base. A plastic enclosure is built around the balance, to prevent any noise introduced from air flow fluctuations in the room [# 3 in Figure III-4]. Visible and UV wavelength range light sources are marked as # 6 and #7 in Figure III-4 respectively.

The middle section of the wind tunnel is modified by creating glass windows on the sides to introduce the sample inside. Top and bottom sections of the middle portion are also replaced with anti-reflection coated glasses for observation, non-contact laser thickness monitoring and in-plane and out-of-plane birefringence measurements (Figure III-5).
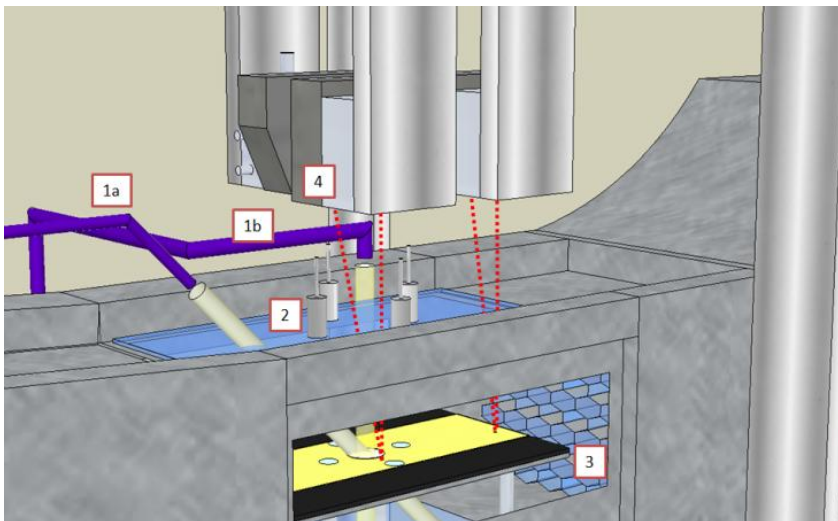
Figure III-5 Substrate with cast sample in position 1) Optical paths and fiber optic cables 2) Pyrometers 3) Honeycomb structured air diffuser 4) Position of laser displacement sensors

Real-time optical properties of the drying polymer solutions are measured

through the transparent uncoated portion located at the center of the glass

substrate (see Figure III-1). The optical system consists of visible wavelength

range light sources (Dolan-Jenner MI-152 400 nm to 700 nm), linear polarizers,

fiber optic cables and visible spectrometers (Avantes, Avaspec-NIR256-2.5). For

the measurements, 45° linear polarized light is passed through the sample and

collected by bifurcated fiber optic cables (#1a and #1b in Figure III-5, optical

paths for 0° and 45° are identified with transparent yellow tubes). For each angle,

one of the fiber optic cables is polarized parallel and the other is polarized

perpendicular to the initial polarization and the data is transferred to the

spectrometers for further calculations. The detailed instructions and the theory

behind this system have been discussed in detail in our previous publications.[139–144] Real-time in-plane and out-of-plane birefringence values are calculated by

measuring the retardation (at 546 nm) values at two different angles, 0° and 45°.

Though we picked this green wavelength (546 nm) as it is in the middle of the

visible wavelength range to demonstrate the instruments capability, the software

developed allows the measurement of retardations at any wavelength in 400-700

nm range. Another reason we picked 546 nm is that most optical compensators

(offline retardation measurement devices) are calibrated to this (546 nm).

The in-plane birefringence (Δn_{12}) is calculated by dividing the measured 0°

retardation (R_0) by the thickness values (d_m: stands for real-time thickness values

measured by middle laser) (Equation 1). The optical components are set up as;

positive in-plane birefringence values indicate higher refractive index is oriented

127

in the air flow direction; whereas negative in-plane birefringence values indicate higher refractive index is oriented in the transverse direction of the air flow for polymers. Out-of-plane birefringence (Δn_{23} where 2 is transverse or machine direction and 3 is thickness direction) is calculated using the Stein's equation[145] shown below (Equation 2).

$$\Delta n_{12} = \frac{R_0}{d_m} \tag{1}$$

$$\Delta n_{23} = \left(\frac{1}{d_m}\right) \left[\frac{R_0 - R_\theta \left(1 - \frac{\sin^2 \theta}{\bar{n}^2}\right)^{1/2}}{\frac{\sin^2 \theta}{\bar{n}^2}} \right] \tag{2}$$

In Equation 2; d_m is the real-time thickness value calculated by middle laser, R_0 is the measured 0° retardation, R_Φ is the retardation value measured at Φ degrees (where $\Phi = 45°$ in our case), and $\bar{n}$ is the average refractive index of the material. With appropriate calibration of average refractive index vs. solvent concentration in the film, we extract this value during the drying process from weight loss data.

Surface temperature is measured by four separate pyrometers (Micro-Epsilon, Model: thermoMETER-CT), focused downwards on the film very close to the center of the drying sample [#2 in Figure III-5]. They are mounted on the top glass window by drilling special mounting holes. The temperature readings from these sensors are verified with contact thermocouples. Honeycomb structure air diffuser [# 3 in Figure III-5] from Plascore, PCGA-XR1 3003 Aluminum

Honeycomb is placed inside the wind tunnel to streamline the air arriving to sample holding platform downstream and eliminate potential noise.

The thickness of the drying solution is measured by a combination of three non-contact laser displacement sensors [#4 in Figure III-5] (Keyence, Model: LK-G 152). These sensors are attached to the breadboard located on top of the sample platform. The exact measurement positions and their projections on the sample and substrate are shown with red dots in Figure III-5 (also see Figure III-1). These sensors (indicated as Laser 1 thru 3) only measure the position of the top surface of the cast solution through the laser reflection (red dots in Figure III-5 indicate the reflected laser beams from the surfaces). Laser-1 measures the displacement of the surface of drying solution in the middle of film very close to the location where spectral birefringence measurements are made. Laser-2 measures the displacement of the surface of the drying sample on the upstream towards the heater. Laser-3 measures the displacement of the surface of glass substrate and this value is subtracted from the Laser-1 and Laser-2 values for real-time thickness calculations at those locations.
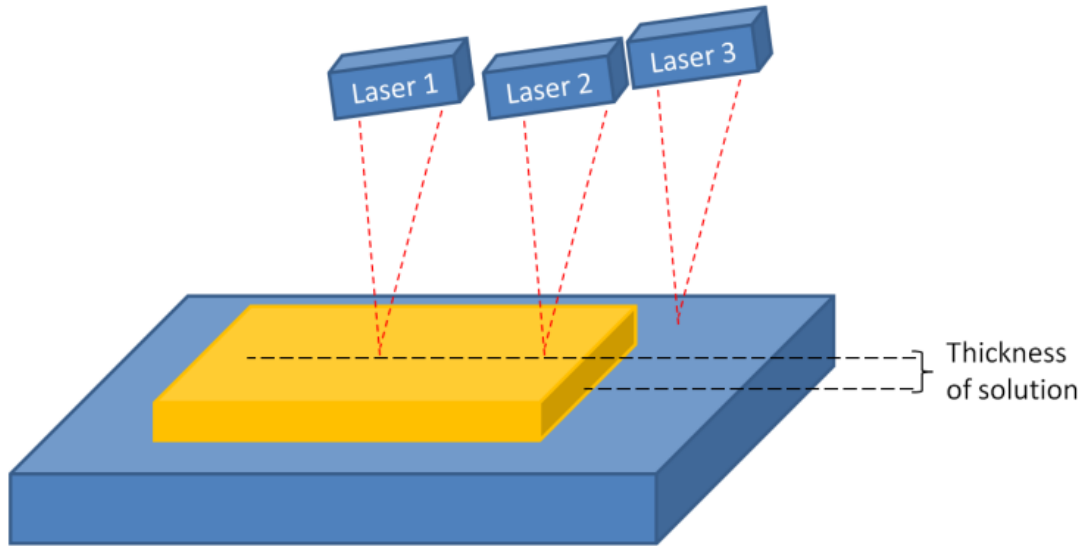
Figure III-6 Basic schematic of 3 lasers and thickness measurement of drying solution

This method eliminates the noise that might be caused from the movement of the whole sample platform at high air velocities. It also corrects for the thermal expansion of the sample platform and the glass substrate that the polymer solution is cast. The thickness value calculated from Laser-1 and Laser-3 is used for birefringence calculations.
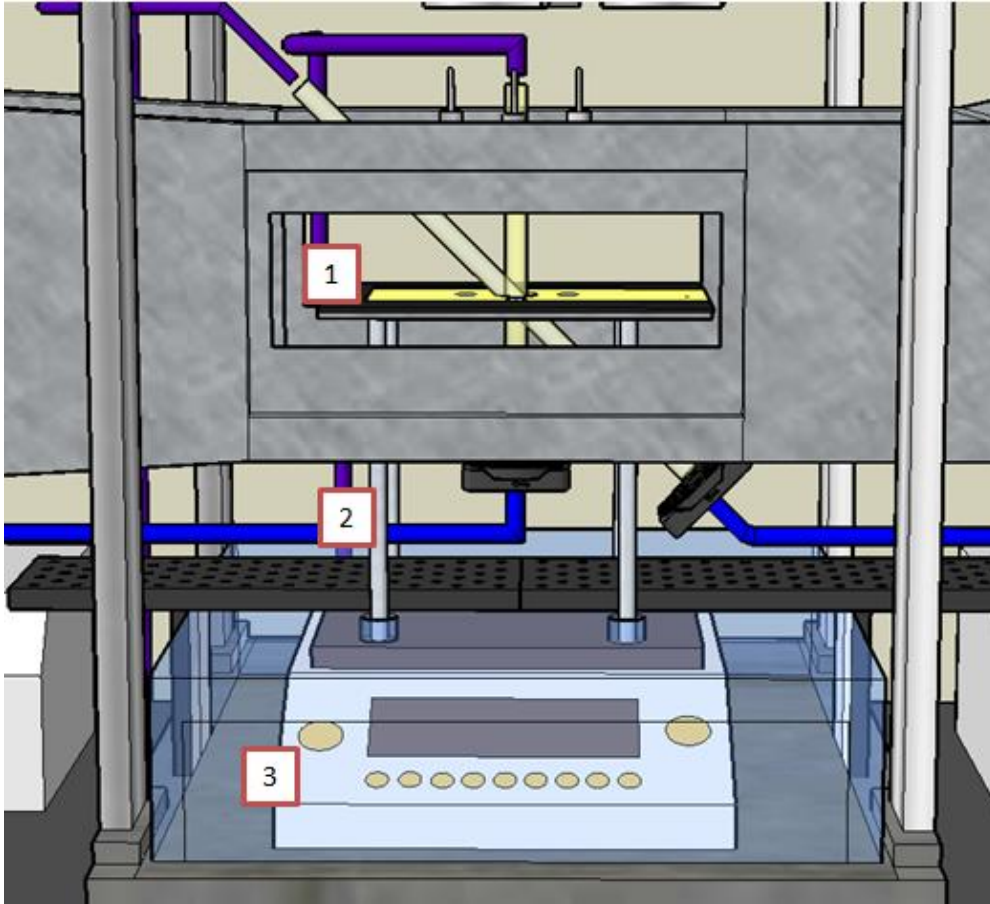
Figure III-7 Sample Platform; 1) Top of the sample platform where the substrate with the solution is introduced, 2) legs of the sample platform 3) Balance in contact with the sample platform for weight measurements

Very light weight graphite four legged table [# 1 and 2 in Figure III-7] was constructed as the sample platform. Graphite was selected due to its low thermal expansion coefficient and high thermal conductivity. The four post graphite rod-shaped legs [#2] contact directly the balance surface [#3] for the weight measurement of the drying sample. Small openings were made to bottom surface of the wind tunnel and plastic cover for these legs to go through without any contact.

A high definition USB camera (Microsoft, LiveCam 9000) is positioned to record the images and videos of the drying solution to capture the visual changes during thecourse of drying.

All these sensors are connected to a computer and the real-time data is acquired via software developed in Labview platform. Figure III-8 shows a screenshot of the GUI. This allows real-time observation of all the collected and calculated data. All the graphs are generated as a function of experiment time. The first column shows the weight [#1], three laser displacement measurements [#2] and calculated thickness values [#3] respectively in Figure III-8. The first two graphs on the second column shows the 0° and 45° optical retardation values [#4 & #5] in nanometer units. The calculated in-plane and out-of-plane birefringence values are shown at the top two graphs in the third column [#6 & #7]. The last graph in this column represents the temperature measurements of the pyrometers [#8]. The typical data acquisition rate is 4 data points/second which is fast enough to determine the transitions in the most drying processes. Currently the variables that can be tracked and recorded real-time by this system include the weight, thickness (3 laser measurements), surface temperature at four positions and in-plane and out-plane-plane spectral birefringence of drying polymer solutions.
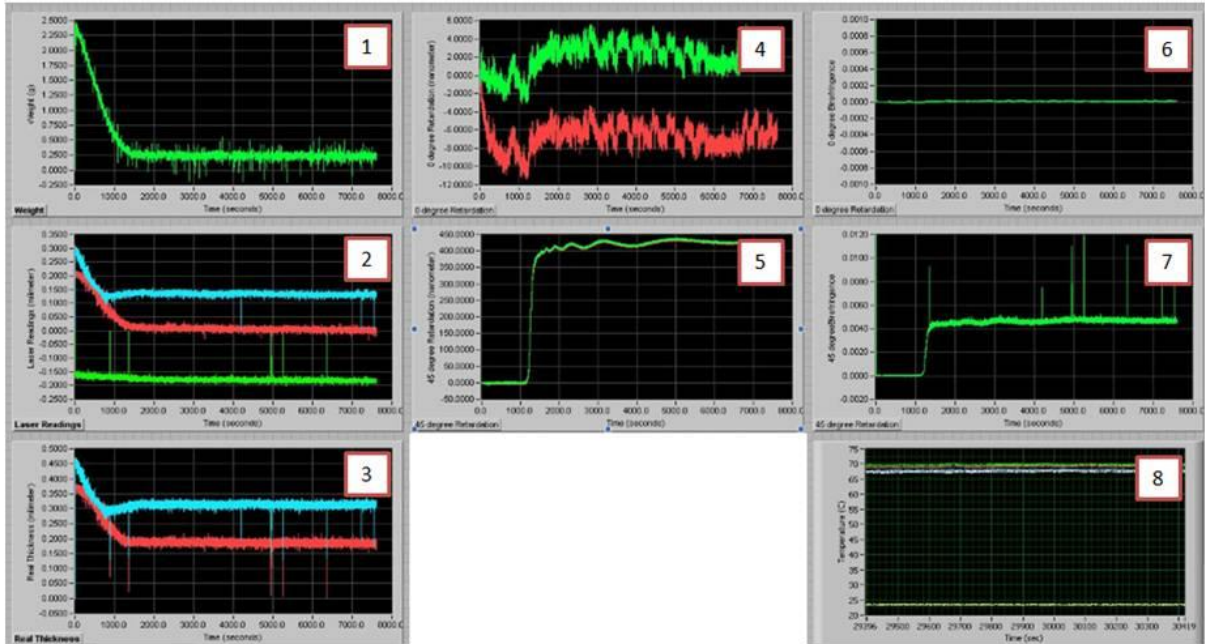
Figure III-8 GUI of the program, parameters updated real-time for observation during the experiment.

3.3.1 Photopolymerization of UV curable monomer films (solventless process)

The design of the instrument allows it to be modified further with new sensors and measurement techniques to simulate different processing methods. For example, one of the pyrometers can be replaced with a UV light source, that is introduced via a fiber optic cable, and the dynamics of real-time UV curing studies can be performed (Figure III-9). These measurements allow rapid capture of all the measurement parameters essentially tracking the kinetics of the curing process and it can help understand applications such as lamination, photocuring in liquid crystal industry and optical storage applications like holograms.[146]
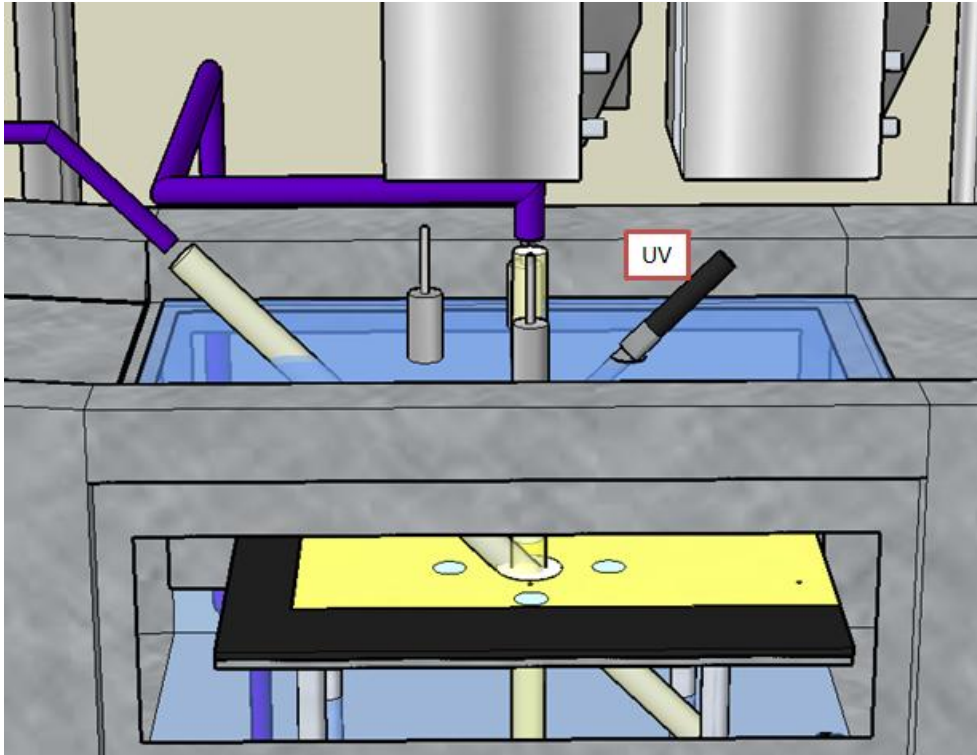
Figure III-9 UV light source modification

3.4　Validation Experiments

The honeycomb structured air diffuser is placed inside the tunnel due to the noise created in weight data acquired from the electronic balance for high air speed (~6 m/s) experiments. The graph below shows the noise levels in unloaded weight measurement system with and without the air diffuser (Figure III-10). Before insertion of the honeycomb, the weight fluctuation during a typical run was around 8g at 6m/s. After placing honeycomb structure, the noise level substantially decreased to 0.18 g. The air speed values were measured at

different locations before and after the insertion of the honeycomb structure and no significant changes were observed.
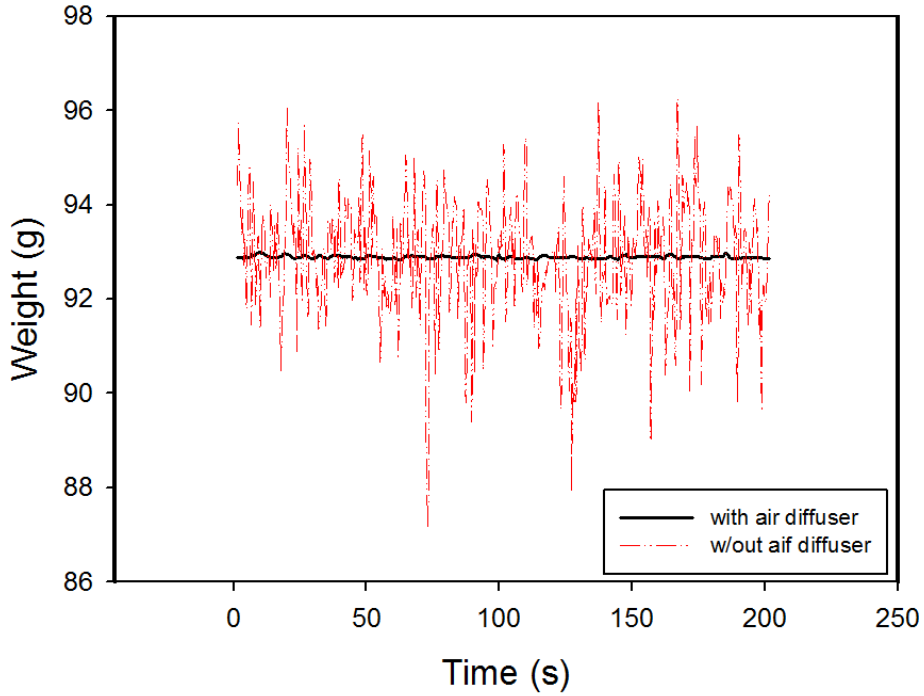
Figure III-10 Effect of honeycomb structured air diffuser at high air speed experiments

In order to test the capabilities of the real-time measurement apparatus three different solutions were cast and dried; additionally a non-solvent system of photocurable monomer was tracked during UV polymerization.

3.4.1 Poly(amide-imide)/DMAc Solution – Real time data and verification with offline methods

The first solvent based experiment was performed with a poly(amide-imide) solution (PAI) (provided by Akron Polymer Systems, APS) in Dimethylacetamide (DMAc) as solvent (Sigma Aldrich, synthesis grade) with 8 wt % concentration. 0.5 m/s air speed and 50°C drying temperature is selected as the experimental process. The system is pre-heated to desired temperature and 500 μm thick solution is cast on the glass substrate and placed on the sample platform.
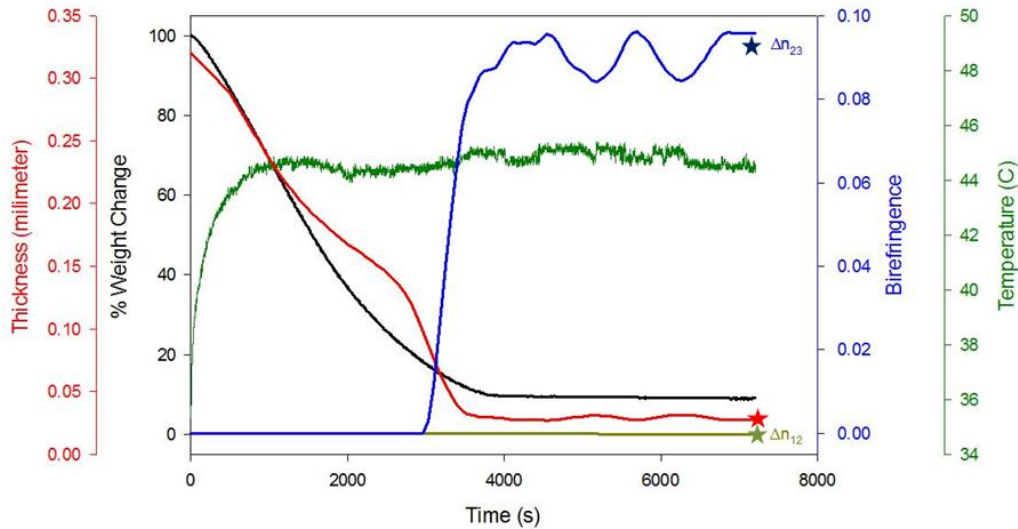
Figure III-11 Real-time drying data of PAI-DMAc solution. Filled stars indicate the offline measurements of thickness (red star), in-plane birefringence (green star) and out-of-plane birefringence (blue star) of dried film.

Figure III-11 represents the real-time % weight change (measured from the initial stage), thickness (mm), temperature (°C), in-plane and out-of-plane birefringence data as a function of time for PAI/DMAc solution drying experiment. The weight and thickness values decrease and level off beyond a critical value as solvent evaporates. The thickness data shows interference pattern below a certain thickness value. This pattern is also reflected to the birefringence data, since thickness is used to calculate the in-plane and out-of-plane birefringence. Surface temperature values remain nearly constant through the experiment after it reaches a plateau. In-plane birefringence (Δn_{12}) remains constant during the drying. This indicates that there is no in-plane preferential orientation of the polymer chains. However, out-of-plane birefringence (Δn_{23}) rapidly increases to a high value around 3000 seconds, indicating preferential orientation of the axes of the polymer chains in the film plane. This very sharp rise in birefringence in such a short period has not been reported in the past. Only the final birefringence values of dried films has been reported. [88,124–128]

The data for this experiment is verified with the offline characterization methods. The thickness of the final dried film is measured by a precision micrometer and the measured value is marked with red star on the Figure III-11.

The in-plane and out-of-plane birefringence data on final dried film is verified by using a Gaertner optical bench polariscope (Model L305; Gaertner Scientific Co.) equipped with a 7 order Babinet compensator (GSC No. 617-F). Similar to our system, Equation (1) and (2) [145] is used for the calculations and wavelength of 565 nm is used since the instrument is calibrated for this specific wavelength.

The end results for in-plane birefringence (green star) and out-of-plane birefringence (blue star) are indicated in Figure III-11. They are in very good agreement with the final values obtained on line.

TGA is used to verify the weight data and amount of remaining bound solvent is calculated and compared with the real-time experimental data. Figure III-12 represents the % solid and solvent change as a function of time, calculated from the initial concentration of the solution and the real-time weight data. At the end of the experiment, our system shows there is 12 % bound solvent with-in the film and the TGA data showed there is 17% bound solvent. This difference is mainly due to the sensitivity of the scale (0.01g). For this specific experiment, the total solid content of the cast solution is 0.3g and 0.01g difference causes 3% fluctuation on the weight data for dried film. Figure III-11 and Figure III-12 it demonstrate that the real-time measured physical parameters are very close to the values that are measured with standard offline characterization methods.
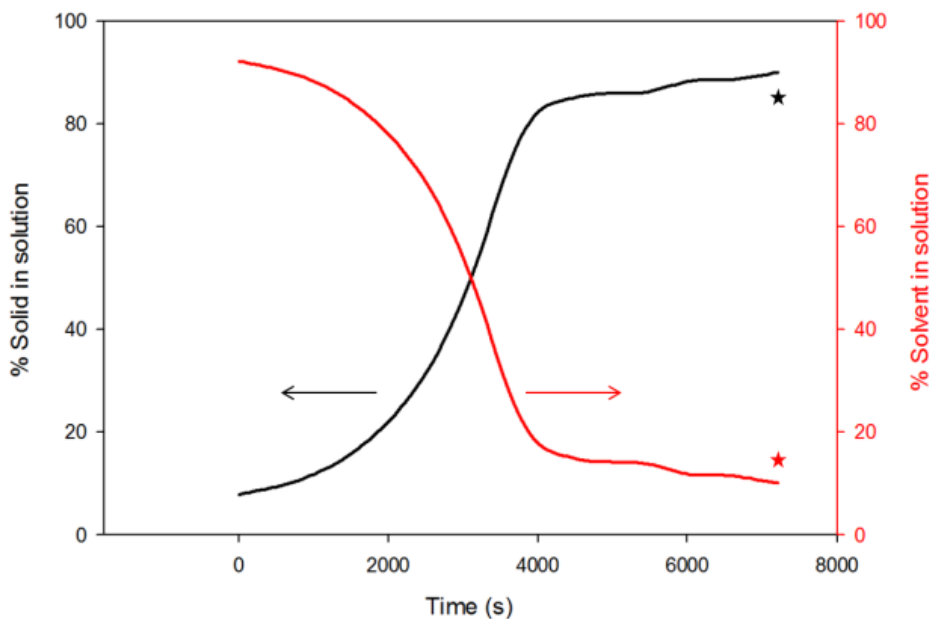
Figure III-12 % solid and % solvent calculated from the initial concentration and real-time weight data. Filled stars indicate the results of TGA for the dried films.

Figure III-13 shows a series of the images recorded with the camera for PEO in water (10 wt %) solution. The air flow direction on the picture is from right to left and formation and propagation of the drying front is observed. The front location is highlighted with an arrow in each picture. These images are captured so that we can track the movement of distinct wet/semidry boundary indicated with the arrow below. This occurs in all drying operations.
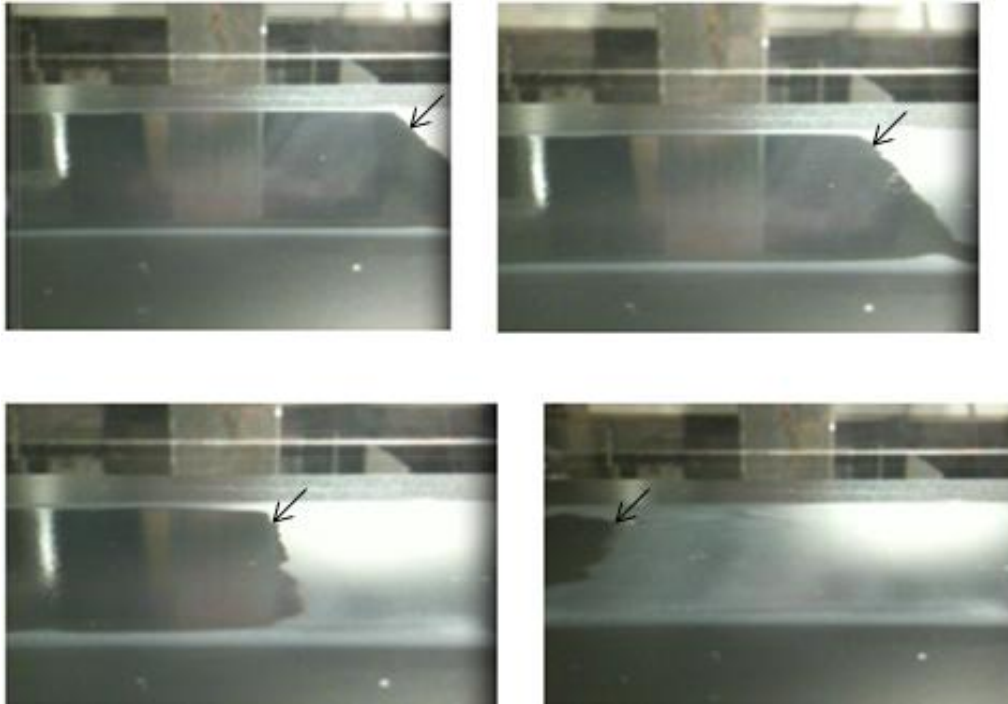
Figure III-13 Propagation of drying front in PEO-water solution traced by camera (air flow direction is from right to left)

3.4.2 Photopolymerization of Cast Film

Figure III-14 represents the real-time data of UV curing for Dr.Blade cast urethane acrylate and 5% photo-initiator mixture. No weight change was observed during these experiments where only initiation, propagation, chain transfer and termination occur in these solvent-free monomers. A total of 10% thickness change observed in these samples at the early stages of the experiment. This early stage is called precuring period. Also a sharp 3°C increase is noted on the temperature during the precuring period. The temperature continues to increase at a slower rate, which might be the heating effect due to UV lamp on the sample. The in-plane birefringence remained very

close to zero values, while a slight increase and then levelling off behavior is observed for the out-of-plane birefringence. Even though the increase was a very small value, the instrument is sensitive enough to measure such small changes for solution casting or UV curing process.
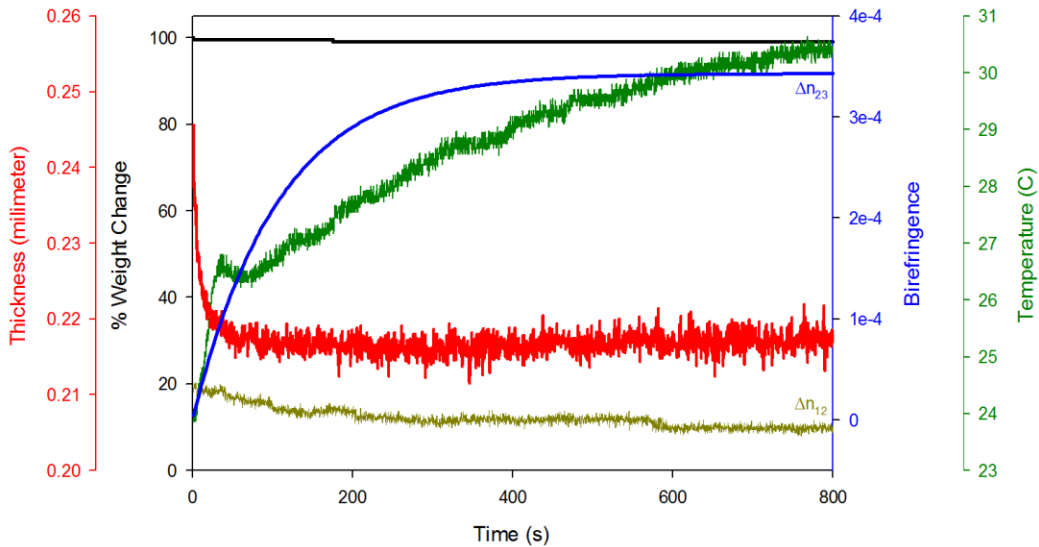
Figure III-14 Real-time measurement during UV curing of Urethane-Acrylate with photo-initiator

3.4.3 Drying of a Water-Based Paint

For this demonstration, we used commercially available water-based black paint (Glidden Ultra-Hide 1210-9990V). A thin layer of paint is cast on top of the aluminum metal substrate and dried at room temperature inside the instrument. The air speed is set to 0.5 m/s and initial cast thickness is set as 560 µm for this experiment.

Real-time weight, thickness and surface temperature data is presented at Figure III-15. The weight and thickness change was followed as the solvent evaporates. The surface temperature showed an initial decrease due to evaporative cooling, passed through a minimum and started to increase as the material solidifies and rate of solvent evaporation decreases as it is depleted in the film (Figure III-15). These results are in good agreement with the previous literature. [135,136] Due to opaqueness of the substrate and black color of this coating, the optical retardation was not measured in this system since the spectral birefringence technique we employ operates in transmission mode.
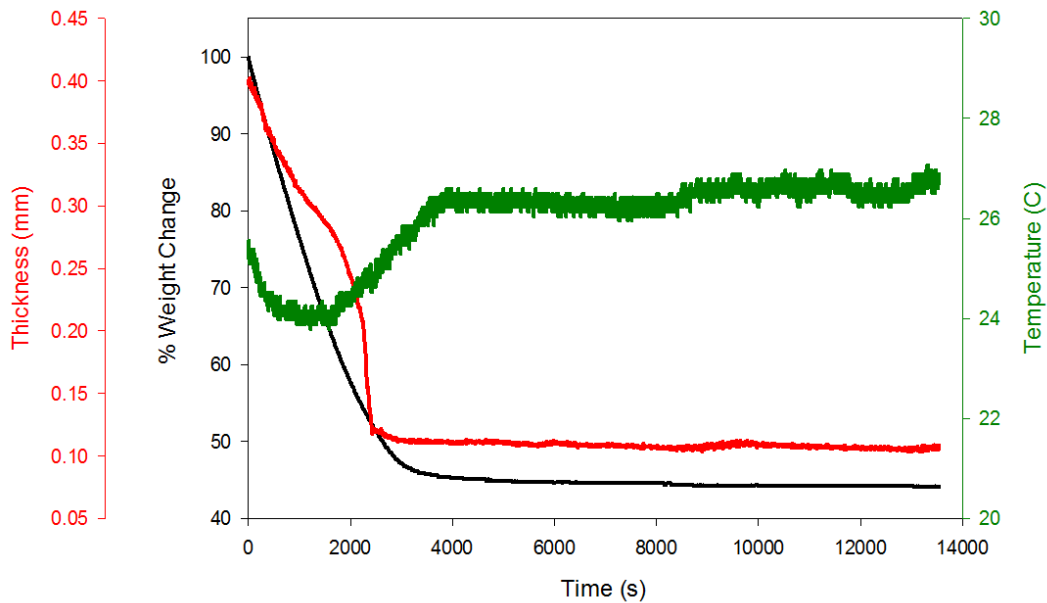
Figure III-15 Real-time drying data of water based black paint

3.4.4 Drying of Clay Solution

For the last experiment, Cloisite 30B® organo-modified clay (provided by Southern Clay Products, Inc) in NMP as solvent (Sigma Aldrich, synthesis grade) is prepared with 3 wt % solid concentration. 0.5 m/s air speed and 70°C drying temperature is selected as the process parameters. The system is pre-heated to desired temperature and 1 mm thick solution is cast on the glass substrate and placed on the sample platform.
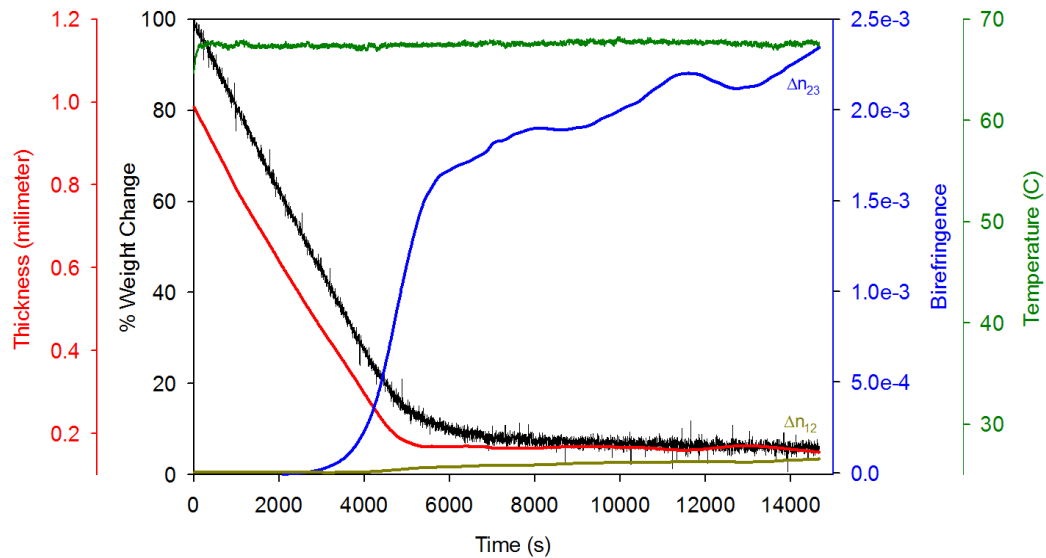
Figure III-16 Weight (g), thickness (mm) and temperature (°C) data as a function of time (s) for clay-NMP solution drying

Figure III-16 represents the real-time data for clay solution drying experiment. The weight and thickness values decrease and level off beyond a critical value as solvent evaporates and temperature remaina nearly constant throughout the experiment. Similar birefringence behavior is observed for the

143

clay solutions compared with the PAI/DMAc solutions. The in-plane birefringence values remain constant during the drying, and at a critical point, out-of-plane birefringence rapidly increases. This indicates that the there is no in-plane preferential orientation of the clay platelets whereas preferential orientation of the planes of the clay platelet in the film plane occurs. It is important to note that montmorillonite nanoplatelets has negative optical birefringence with intrinsic refractive indices reported as ($n_{out\ of\ plane}$ = 1.485 and $n_{in\text{-}plane}$=1.505-1.55)[147]

3.5   Conclusions

The instrument developed is designed to record the real time changes in physical parameters of drying of solution cast films and coatings, as well as UV curable non-solvent based systems and inorganic materials including slurries etc. A fully automated spectral birefringence measurement system was incorporated into the design of this machine for the first time. It is sensitive enough to measure very small optical retardation levels (~2-4nm) allowing this machine to be used with wide range of materials including those that exhibit small intrinsic birefringence. This instrument can be used to systematically study the effect of material variables including solvent types and mixtures and solid concentrations, and system variables including temperature, air speeda and initial thickness. In addition, the sensors are sensitive enough to track the changes in the physical characteristics of monomers during photocuring.

144

CHAPTER IV

REAL-TIME RHEO-OPTICAL MEASUREMENT SYSTEM COUPLED WITH ULTRA-RAPID-SCAN POLARIZED FT-IR (URS-FT-IR) SPECTROMETRY FOR POLYMER FILMS DURING UNIAXIAL PROCESSING

This chapter describes the design and performance of a multisensory instrument to track physical and chemical changes of thin polymer films (typically 5 μm < thickness < 100 μm) subjected to thermal and mechanical treatments. For the first time, we integrated, real-time measurements of spectral birefringence, true stress, true strain and temperature with ultra-rapid-scan polarized FT-IR spectrometer (URS-FT-IR) to quantitatively investigate the relationships between true mechanical measures and structural features at different length scales. The rheo-optical properties (birefringence-true stress-true strain) are collected at a rate of 10 data points/second and URS-FT-IR data is collected at a rate of 300 complete spectra/second. The IR dichroism measurement is performed by exposing the sample to non-polarized IR beam in transmission mode and two mutually perpendicular polarizations are separated in the detector unit(parallel and perpendicular to the stretching direction). This

made it possible to analyze the both polarizations simultaneously in the range of 500 cm-1 to 4000 cm-1 wavenumbers. Controlled processing parameters include air speed, air temperature, stretching rate, stretching ratio, stretch cycling and holding times; while simultaneously measuring optical retardation, sample width, temperature, load cell and both parallel and perpendicular IR spectra. The calibration and performance of the instrument is demonstrated with several samples undergoing uniaxial deformations. These samples include polystyrene standard, atactic polystyrene (homo-polymer), polyurethane (consists of hard and soft segments) for physical changes and polyamic acid film undergoing imidization reaction. This measurement system is particularly useful in unraveling molecular level details of complex physical and chemical events that take place during very fast deformation schemes (uniaxial stretching, retraction, relaxation, annealing) relevant to industrial processes. These include specific orientation behavior of each phase, block or filler, crystallization, relaxation and orientation state. It is also suited to track reaction rates and products in polymers undergoing thermal or photo curing.

4.1   Introduction

In polymer processing operations, multiple molecular level processes often take place concurrently.[148,149] Some examples can be listed as deformation induced orientation, thermal induced relaxation coupled with solvent evaporation and chemical reactions. Detailed analysis of this complex sequence of molecular processes by off line characterization techniques often is hampered as the earlier

processes may mask the later ones.[150] The only way to unravel these details is by phenomenon specific dynamic real time techniques. However, these are challenging either due to absence of suitable techniques or if they exist, limitations in implementation for various reasons.

The properties of polymers such as mechanical and optical are determined primarily by their chemical architecture built into and onto their backbones. While the chemical structure is fixed for a given material, the thermal history and molecular orientation can be altered by a range of post-processing techniques to tailor the final properties for the specific applications. Deformation and annealing are the most common methods that are applied to polymer films to adjust the final properties. It is critical to understand the dynamics of the molecular mechanisms during these processing steps to be able to connect the processing conditions to molecular orientation, structural hierarchy and their effects on the final properties of the films. This usually is not possible with one structural technique. A combination of multiple techniques in which each being sensitive to different aspects of the structure and mechanics is needed to derive a complete view of the materials structure. Rheo-optical measurements are a good example to this category as it combines the relation between mechanical (stress and strain) and optical properties such as birefringence and light scattering. Addition of polarized IR spectrometry to this technical toolset allows us to peer into molecular level phenomena such as segmental orientation through dichroism, crystallization and component or chemical specific other phenomenon such as thermal and photo curing.[58,151–154]

The understanding of deformation kinetics and molecular orientation is even more important and complex in multi-component systems such as semi-crystalline polymers, block copolymers, polymer blends, polymer nano-composites, polymer-fiber mixtures and materials containing residual solvents.[155–158] The optical measurements such as birefringence, provide ensemble averaged information on phase behavior, orientation of different phases for the whole system without detailed structural specificity. Polarized IR spectroscopy offers molecular specificity and their orientation of each phase of multi-component polymer systems.

There have been a number of studies on the use of IR dichroism in polymers. For example polystyrene is one of the most studied homo-polymers, in which the deformation and orientation relation have been investigated both by IR dicroism and birefringence. Jasse et. al. studied the effect of draw ratio and temperature on the dichroic ratio of atactic polystyrene films for different absorption bands[58]. They observed a linear relationship between birefringence and dichroic ratio. Nicholas et. al.[151] studied the influence of annealing temperature on polarized IR spectra of syndiotactic polystyrene, that can be either crystalline or quenched into glass. Nicholas observed that the higher annealing temperatures increase crystallinity in syndiotactic polystyrene with resulting higher orientation.[151] The orientation relaxation of different molecular weight atactic polystyrene during uniaxial stretching was studied by Richard et. al.[152] Another study of molecular orientation was conducted by Messe et al. in

148

which the effect of temperatures above T_g on relaxation time during stretching was investigated with the use of birefringence and IR dichroism.[153]

Polyurethanes are a class of polymers that provide good example for multi-component systems as they have soft and hard and soft segments in their chain backbones and tend to phase segregate into these domains. Even though the hard and soft segmental structures are semi-continuous, it was found that they exhibit distinctly different orientation response to deformation.[154,159–162] Estes et al. monitored each segment behavior in polyether-based polyurethane segments following stretching in step increments and relaxation.[154] The hard segment orientation was found to be highly dependent on strain history while the soft segments orientation generally was found to be insensitive. Increasing stretching temperature was shown to increase the orientation of both hard and soft segments gradually up to 90°C after which it decreases rapidly.[160] Annealing at sub-melting temperatures is found to enhance phase separation and lower average orientation of both segments.[161] The film thickness and presence of nano-particles do not affect the alignment of hard or soft segments.[159] Graff et al. investigated the effect of added plasticizer in polyurethane which was found to disrupt hydrogen bonding in hard segment and decrease the glass transition temperature of soft segment and diminished the ability of either domain to reorient.[163] These findings have been supported by other offline and simultaneous studies such as SAXS ,WAXD and AFM on the stretched polyurethane and polyurethane-urea samples.[162,164–166]

Morphological changes during deformation of polymers mostly manifest in the infrared spectra as formation of new peaks, band shifts or changes in the ratios of peak intensities for different polarization states due to development of absorption anisotropy leading to IR dichroism. However, bands also can shift to lower or higher frequency, because of bond deformation that is induced by the stress developed on main chains. Bretzlaff and Wool have shown the effect of stress and temperature on IR frequency shifts and band asymmetry in isotactic polypropylene.[167] Band asymmetry is linked to the existence of nonuniform molecular stress distribution. Tashiro et al. studied the relationship between stress induced frequency shifts and mechanical deformation mechanisms and were able to derive quasi-harmonic equations with lattice dynamics for planar-zigzag polyethylene, helical polyoxymethylene and isotactic polypropylene.[168,169] Structural and mechanical behavior of α and γ crystal forms of Nylon-6 have been investigated at low strain values and correlated with IR vibrational frequency shifts by Loo and Gleason.[170] Their emphasis was on hydrogen bonding and methylene chains. The different crystalline and amorphous region contributions to the shifting behavior were distinguished.

These examples demonstrate the importance of monitoring real-time rheo-optical properties of polymer systems for morphology and deformation relationships, particularly in the complex ones. Siesler developed instrumentation[164,171–174] to measure the synchronized real-time mechanical and FTIR spectroscopic changes of several polymer systems during uniaxial deformation and relaxation. Their instrumentation measured the stress and strain

on the sample via force and displacement transducers. Polarized IR measurements were introduced by a rotatable wire-grid polarizer and spectra were measured with a time lag as small as 50 ms by quickly alternating the polarizer orientation. The nominal time resolution was one interferogram (i.e., spectrum) per second at 4cm^{-1} resolution. Their instrument allowed the study of strain-induced crystallization behavior of thin polyurethane films (~15μm) during uniaxial deformation and relaxation[164,171-174], trans-gauche transformation of thin PET films during biaxial deformation[175], and relaxation behavior of PMMA blends.[176]

Nemoto et. al. also developed an instrument to measure the simultaneous stress and microscopic IR dichroism at constant elongation rates. Similar to Siesler's instrument this system also measures stress and strain via transducers. The polarized IR beam is introduced via a polarizer and photoelastic modulator (PEM), providing essentially zero delay between measurements of the two polarizations. The temperature of the stretching cell, where the sample is clamped can be adjusted from 20°C to 250°C and the elongation rate can be adjusted from 0.001 to 10 mm/min. The thickness and width values are corrected for cross-sectional area of the sample that is calculated from measured width (through a microscope) and thickness (from interference fringes). The equipment can generate one spectrum in 3 seconds at 4 cm^{-1} resolution, simultaneously capturing both polarizations.[177] Using this instrument, they investigated molecular orientation of amorphous and crystalline regions and simultaneous stress-strain relation of isotactic polypropylene films.[178–180] They also examined the

inhomogeneous deformation behavior of spherulites in isotactic polypropylene and necking formation phenomena.[181–183]

The rheo-optical measurement systems discussed thus far provide relatively slow data acquisition rates on the order of one spectrum per second. These instruments are limited by the conventional design of the interferometers, which generally require linear scan motion of a mirror to create optical path difference. The inherent slowness makes these instruments ineffective for investigation of very fast deformation rates that usually are required for roll-to-roll, continuous industrial applications. Crucial data are lost, because the time-scale of the deformations (microseconds) is poorly matched to the data acquisition speeds (seconds).

To overcome this problem, Griffiths and Manning designed a new interferometer by eliminating the linear scan mirror and replacing it with a tilted/wedged circular mirror that rotates at very high speeds (~500 Hz).[66,67,184,185] The novel optical geometry enabled actual data acquisition rates of 1.5 milliseconds at 8 cm^{-1} resolution and theoretical data acquisition rates of 1 millisecond at 4 cm^{-1} spectral resolution.[66,67,184,185] This instrument allowed them to monitor the spark-initiated combustion of ethane and methane in air with 10 ms time intervals.[67] They also investigated the effect of very fast deformation (draw rates up to 3.16 cm/s) and relaxation on the orientation behavior of uniaxially stretched PET and PS thin films. They successfully observed the gauche-to-trans transformation in PET films and orientation and relaxation of PS films with 10-40 ms time intervals via IR dichroism measurements.[69,70]

Even though the instrument was capable of generating data at very high scan rates, the data acquisition boards and computers were not be able to keep up with the data generation rates at their current state of development. This problem restricted the experiment lengths and the total acquisition times were only a few seconds.[69,70] In the intervening decade, the speed of computers has increased by about 30% per year, and memory has expanded comparably.

In this chapter, we report a novel measurement system that couples a custom-built uniaxial stretcher with an advanced version of custom-built URS-FT-IR. The uniaxial stretching machine is capable of generating real-time true stress-true strain-birefringence with data acquisition rates of 10 data points/second. The advanced URS-FT-IR instrument is capable of generating simultaneous parallel and perpendicular IR spectra at 300 scans/s with continuous total data acquisition times longer than 2 hours. For the first time, deformation and orientation of polymer chains is measured and reported by coupling the mechanical (true stress-true strain), optical (birefringence) and spectrometric (IR dichroism) information at very high speeds for long experiment times. The two data sets (rheo-optical and spectrometric) are synchronized through time stamping and results are combined by post processing of the two data sets.

4.2   General Description of the Instrument

The novel real-time rheo-optical measurement platform is shown in Figure IV-1. The equipment has two main subsystems or layers. The inner layer consists of a custom-built uniaxial stretching machine [#1] and the second (outer) layer of the equipment consists of an Ultra-Rapid-Scan FT-IR (URS-FT-IR) that is supported by a robust aluminum frame to maintain alignment between the interferometer and detector, as well as minimize the vibrations [#2]. The hot air blower [#3] is used to control and maintain the sample temperature up to 200°C. This unit is connected to the heating chamber via flexible metal tubing and ductwork that are insulated to reduce the thermal losses. Hot air is circulated through the blower to obtain higher efficiency and temperature uniformity inside the sample chamber. The air temperature and air speed can be adjusted manually. A visible wavelength spectrometer [#4] is part of the inner layer [#1] and the fiber optic cables transmit the signals to this unit for real-time measurement of in-plane birefringence of the samples during processing. Details of the stretching apparatus and URS-FT-IR are provided in the following sections.

Figure IV-1 Real-time rheo-optical measurement platform. 1) Inner layer is a custom-built uniaxial stretching machine. 2) The outer layer is a custom build URS-FT-IR spectrometer. 3) Hot air blower. 4) Visible wavelength spectrometer.

4.2.1 Uniaxial Stretching Machine

This part of the instrument holds the polymer sample and the sensors for the mechanical (true stress and true strain) and the optical (retardation and birefringence) measurements. The sample is located at the center point of the heating chamber. The heating chamber is fabricated from a high temperature mineral filled polymer material (rated for continuous operation at 200°C). On the

centers of the front and back panels of the heating chamber, 25.4 mm diameter KBr disk windows are located to enable birefringence and IR spectral measurements. In addition, two glass windows are placed at 45° angle, below the center on the front panel and above the center of the back panel for laser width micrometer measurements.

Stretching is applied by two moving crossheads that are located at the top and bottom of the heating chamber. The sample is connected to the crossheads via metal rods that pass through top and bottom holes in the heating chamber without touching. The bottom rod is connected directly to the bottom crosshead, and the top rod is connected to a metal frame that holds the load cell for force measurement . The crossheads move in opposite directions during motion and produce stretching or retraction on the sample. Because both crossheads move in opposite directions, the center position of the sample doesn't move during stretching and therefore remains at the focus of the infrared and visible beams. Real-time measurements are performed on this center of the sample that remains stationary at all times during the stretching, retracting and holding stages.

The thickness is measured indirectly through the real-time width measurement at the center point of the sample. A sub-micrometer resolution laser micrometer mounted at 45° to the horizontal, monitors the width of the sample center. By using two assumptions, (i) constant volume (or density) (Eq. 1) and (ii) transverse isotropy (Eq. 2), the real-time thickness can be calculated given that the initial thickness, width and length of the sample are known. By

using these assumptions the true strain (Eq. 3), Hencky strain (Eq. 4), true stress (Eq. 5) and birefringence (Eq. 6) can be calculated. The data on verification of the assumptions and the equipment can be found in previous publications.[140,186–191]

Birefringence is calculated by using spectral measurement method.[144,192-203] A visible wavelength light source is used coupled with a +45° linear polarizer. The polarized light is reflected thorough a metallic mirror (no change in the state of polarization) and focused on the sample. The reflected beam is 7° off-axis from the normal to the plane of the sample to allow the separation of the visible light from the IR beam. The light path distance inside the samples is corrected for the 7° angle in the birefringence calculations. The transmitted light reaches the two fiber optic cables that are supported on a holder. In front of these fiber optic cables, two analyzers (*i.e.* polarizers) are located. One polarizer is parallel to the original polarization direction (+45°) and the other is perpendicular to the original polarization (-45°). The light acquired by these fiber optic cables is transmitted to the spectrometer for recording and subsequent retardation calculations (more detailed information is given elsewhere[144,192–203]). We calculate the in-plane birefringence by simply dividing the retardation values by the real-time thickness values (Eq. #6). [145]

$$D_0 W_0 L_0 = D_t W_t L_t \tag{1}$$

$$\frac{W_t}{W_0} = \frac{D_t}{D_0} \tag{2}$$

$$True\ strain\ = \frac{Elongation}{Initial\ lenght} = \frac{L_t - L_0}{L_0} = \frac{\Delta L}{L_0} = \left(\frac{W_o}{W_t}\right)^2 - 1 \tag{3}$$

$$Hencky\ strain\ = \ L_n\left(\frac{L_t}{L_0}\right) = L_n\left(\frac{W_0}{W_t}\right)^2 \tag{4}$$

$$True\ stress = \frac{Force}{Cross\ sectional\ area} = \frac{F_t}{W_t D_t} = \frac{F_t}{\left[\left(\frac{W_t^2}{W_o}\right)D_0\right]} \tag{5}$$

$$\Delta n_{12} = \frac{\Gamma}{D_t} = \frac{\Gamma}{\left(\frac{W_t D_0}{W_0}\right)} \tag{6}$$

where; D_0 = initial thickness,

W_0 = initial width,

L_0 = initial length,

D_t = instantaneous thickness,

W_t = instantaneous width,

L_t = instantaneous length,

F_t = instantaneous force,

Γ = instantaneous retardation,

Δn_{12} = instantaneous in-plane birefringence.

4.2.2 URS-FT-IR Instrument

The main components, interferometer module and detector module are attached to a very robust extruded aluminum frame. The visible wavelength range light source that is used for birefringence measurements also is supported by this frame. The frame is wrapped around the uniaxial stretching machine so that the IR beam passes through the same region where the birefringence and width measurements are done.

The general concepts of the disk mirror interferometer have been reported previously.[67,204] The novel features of the new version are the use of a disk mirror in each arm to allow variable resolution[66,67] and vastly more powerful data acquisition hardware. Infrared data are acquired at a rate of 300 spectra/second using a multi-channel analog-to-digital converter (Eight channel. 25 MHz, Manning Applied Technology, Troy, ID). Laser zero-crossing time stamps are acquired using the Brault approach.[205] The interferometer is a variation of Michelson's design in which both the fixed and moving mirrors have been replaced with three optical elements each (Figure IV-2). The three optical elements are a disk mirror, hollow cube corner infrared reflector and terminal mirror. Michelson's design and variations thereof are used in all FT-IR spectrometers. The terminal mirrors generally are equivalent, being simply flat mirrors of good optical quality. The key attributes of the terminal mirrors are flatness and high efficiency (reflectivity). It is the interaction of the disk mirror and the hollow cube corner that make possible the high scan speeds. The disk mirror is a wedged aluminum cylinder of 12.7 mm (1/2") thickness (at the thinnest

point) that is 11.43 cm (4.5") in diameter at the largest [#1-a and 1-b]. The radius

on the thick side is tailored to provide mechanical balance such that they can be

spun at high speeds. The hollow cube corner reflector provides a transform

matrix such that the outgoing beam always is parallel to the incoming beam

(within the arcsecond, wavefront accuracy), and also is shifted from the center by

the same amount with opposite sign [#2]. The result is that after a first reflection

from the disk mirror, the infrared and reference laser [#3] beams sweep out

cones in space, where the cone half angle is equal to two times the disk wedge

angle. The cone is inverted by the disk mirror, such that the second reflection

results in a beam that is parallel to the input beam from the beamsplitter. This

allows a terminal mirror of fixed orientation to reflect the beams exactly back on

themselves. The beams incident on the terminal mirror sweep out circles, but

this beam motion is undone during the second traverse of the disk mirror/cube

corner system en route to recombination at the beamsplitter. In the case of the

instant instrument, the disk mirror/cube corner systems is duplicated in both arms

of the interferometer. The disk mirror in each arm is capable of 4 cm^{-1} operation

(*i.e.,* can produce 0.25 cm of optical path difference). The disks are mounted on

brushless motors with ceramic bearings. The phases of the brushless motors

can be independently controlled to produce up to 2 cm^{-1} resolution (*i.e.,* up to 0.5

cm of optical path difference) or as little as zero optical path difference (*i.e.,*

complete cancellation of optical path difference). Because the brushless motors

are controlled by microprocessors, the phase settings can be adjusted very

quickly. The energy of the disk mirrors can be quite significant in operation, so the instrument is enclosed in a particularly robust purge enclosure.

An understanding of the operation of an FT-IR spectrometer can be obtained by two complementary approaches. In the first, the Doppler frequency shift caused by the infrared radiation reflecting from a moving mirror is computed and found to be equal to the modulation frequency. In the second approach, the interferometer is understood to be a spectral filter, in which the rate of change of filter functions is tied to the rate of rotation of the disk mirror. The first approach looks at the rate of change of phase of the infrared radiation, while the second is more focused on the phase at any given time.

In most FT-IR spectrometers, the infrared radiation in one arm interacts with a fixed mirror, which then is called the reference arm. The radiation reflecting from a fixed mirror does not experience a Doppler shift. In the case of the novel disk mirror interferometer used herein, there are moving mirrors in both arms of the interferometer. Generally, one of the moving mirrors reduces the frequency of the infrared radiation in that arm, while the moving mirror in the other arm increases the frequency of the infrared radiation. Thus, the difference frequency between the two arms is doubled, allowing for a greater spread of frequencies across the infrared spectral range. By varying the phase between the disk mirrors in the two arms, the difference in the frequency ranges also can be adjusted, corresponding to more or less spectral resolution, with no impact on duty cycle efficiency. Typically, the Brault data processing method, including the transfer

161

function compensation, allows for a duty cycle efficiency in the range of 90 to 95%.
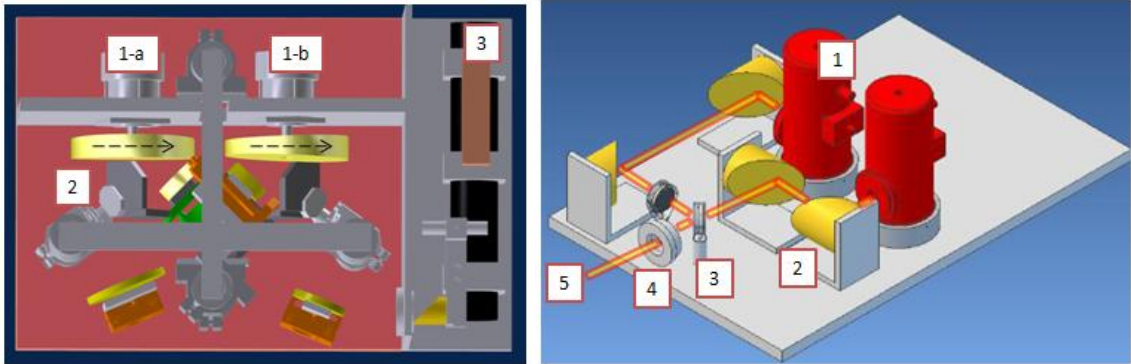
Figure IV-2 Left: Top view of the interferometer module: 1) Rotating wedge mirrors to create optical path difference 2) Hollow cube corner mirrors 3) IR source and 633 nm Helium-Neon reference laser. Right: Detector module: 1) Dewars housing two detector elements each (HgCdTe aka MCT from 400 cm-1 to 2000 cm-1 and InSb from 2000 cm-1 to 4000 cm-1) 2) Gold coated parabolic mirrors for IR beams 3) Polarizing beamsplitter 4) Entrance aperture of the detector module 5) IR Beam

The optical paths for the birefringence measurement, which uses the visible wavelength (400-800 nm) range, and the URS-FT-IR measurement, which uses the mid-infrared wavelength (2500-25000 nm) range are represented in Figure IV-3. The visible light (colored as translucent yellow in this figure) is generated by the light source [#1] and passes through a Glan-Thompson prism [#2] that is rotated to +45°. This light is reflected by a metal coated mirror [#3] and passes through the sample [#4] at a 7° angle to the normal direction of the sample surface [#8]. The angle is required to separate the optical path for the visible beam from the optical path for the infrared beam. The effect of the angle is corrected in the birefringence calculations by using the exact optical path

162

traveled by the visible light. After passing through the sample, the visible light reaches a fiber optic cable holder [#5] that holds two analyzers and two fiber optic cables. One of the analyzers is oriented parallel (+45°) and the other one is oriented perpendicular (-45°) to the initial polarization of the visible beam. The intensities for both polarizations are transmitted to the visible range spectrometer for retardation and birefringence calculations.

IR beam is generated by a conventional silicon carbide element in the custom-built interferometer module. The beam is modulated by the interferometer, and reflected by a metal-coated mirror [#7] and focused on the sample by another metal-coated parabolic mirror [#6]. The size of the IR beam on the sample is about 5mm. in diameter. The samples must have a width at least twice this diameter to ensure that both the visible and IR beams are passing through the sample during the entire stretching experiment. The parallel and perpendicular components of the beam are separated at the detector unit and directed to corresponding detector elements.
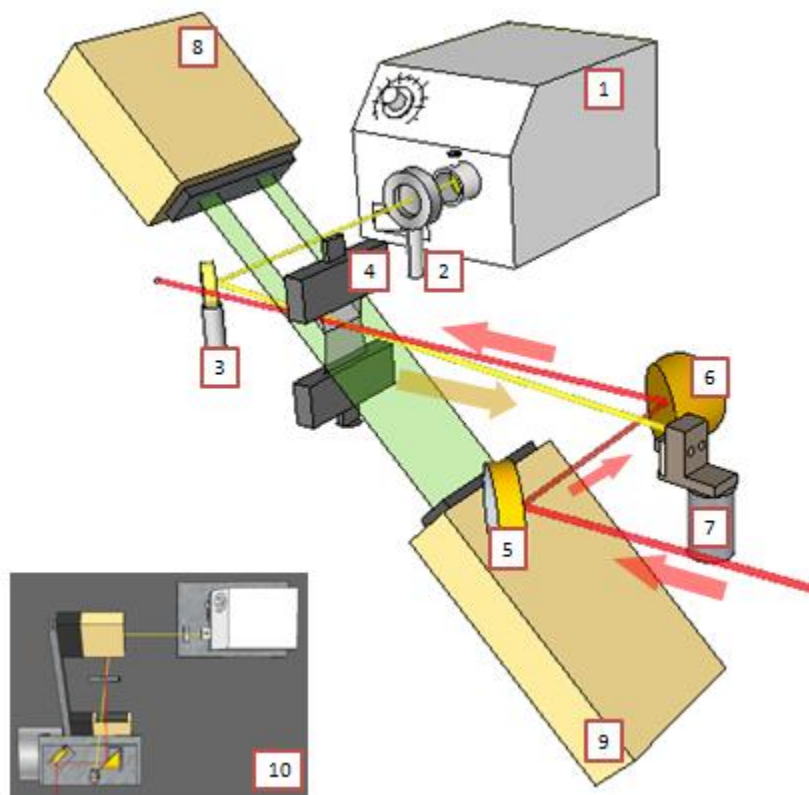
Figure IV-3 Visible and IR beam paths for in-plane birefringence and dichroic ratio measurements. 1) Visible range light source (400-800nm wavelength) 2) Linear polarizer (45°) 3) Mirror to fold the polarized light through sample 4) Sample 5) Holder for two fiber optic cables with analyzers (one polarized at +45° and the other polarized at -45°) 6) Parabolic gold-coated mirror to focus the IR beam at the center of the sample 7) Gold-coated mirror for IR beam 8)Laser micrometer receiver 9) Laser micrometer transmitter 10) Top view of the optical path, visible light makes 7° with the normal to clear from the polarized IR beams

The dichroic ratio (D) is calculated from the parallel ($A_{\parallel}$) and perpendicular ($A_{\perp}$) polarized IR absorbance values by integrating the peak area for selected chemical groups (Eq. 7). Orientation functions (f) for the selected groups can be calculated using Eq. 8 and 9 (for uniaxially oriented samples), where ψ is the transition moment angle of a specific vibration with respect to polymer chain. [206,207]

164

$$D = \frac{A_{\parallel}}{A_{\perp}} \tag{7}$$

$$f = \frac{(D-1)}{(D+2)} \frac{(D_o+2)}{(D_o-1)} \tag{8}$$

$$D_o = 2 \cot^2 \psi \tag{9}$$

4.3   Validation Experiments

4.3.1 Sample Preparation

Thin polymer films of uniform thicknesses were prepared by solution casting on substrates via blade coating. An automated coater was used to generate uniform thickness samples. The details of the coating procedure can be found elsewhere.[208] The substrate materials were selected specifically for each sample for ease of removal of dried thin films without stretching. Dumbbell shaped samples were prepared from the dried samples with the dimensions of 40 mm in length between the holding grips and 40 mm width at the centre of the film, where all the real-time measurements are performed. The initial dimensions of the samples width, thickness and length between the grips are measured with precision micrometer before mounting on the grips. These values are entered to the stretching program to be used in calculations for Equations 1-6.

Polystyrene samples were prepared from Styron D685 (Dow Chemicals, Midland, MI) with 25 weight % solids in toluene. 34 μm thick films were obtained after two days drying at room temperature.

Poly[4,4′-methylenebis(phenyl isocyanate)-*alt*-1,4-butanediol/di(propylene glycol)/ polycaprolactone], a MDI-polyester/polyester-based polyurethane from Sigma-Aldrich (CAS Number: 68084-39-9) is dissolved in THF (15 weight % solids) and cast as described to obtain 20μm thick films after final drying at ambient temperature.

Polyamic acid solutions (PMDA-ODA, 15 weight % solids in NMP) were purchased from Sigma-Aldrich (CAS Number: 25038-81-7) used as received and 5 μm films prepared by solution casting and drying at 25°C for 2 hours.

4.3.2 Polystyrene Standard Sample

NIST traceable 1.5 mil (38 microns) polystyrene standard sample ("Secondary Polystyrene Standard: 1.5 mil Polystyrene", provided by Thermo Scientific) was used to measure the performance of the equipment. The sample was measured first on a bench-top Thermo-Nicolet 380 FT-IR instrument (64 scans with 4 cm^{-1} resolution) in transmission mode. A wire grid IR polarizer is attached to the equipment to measure the two perpendicular polarizations. The same sample was measured with the URS-FT-IR instrument (300 spectra/seconds) and the two data set are compared.

Figure IV-4 shows the comparison of the two equipment for the raw data (no correction or manipulations on the data) in the range of 2000-1000 cm^{-1} respectively. The intensity level on the bench-top equipment is much higher compared to URS-FT-IR. This is due to the differences in the resolutions of the

two equipment. On the other hand, the peak positions and peak shapes match perfectly. The wavenumber values of the position of the peaks are in agreement with the calibration data provided by the NIST reports.[209,210]
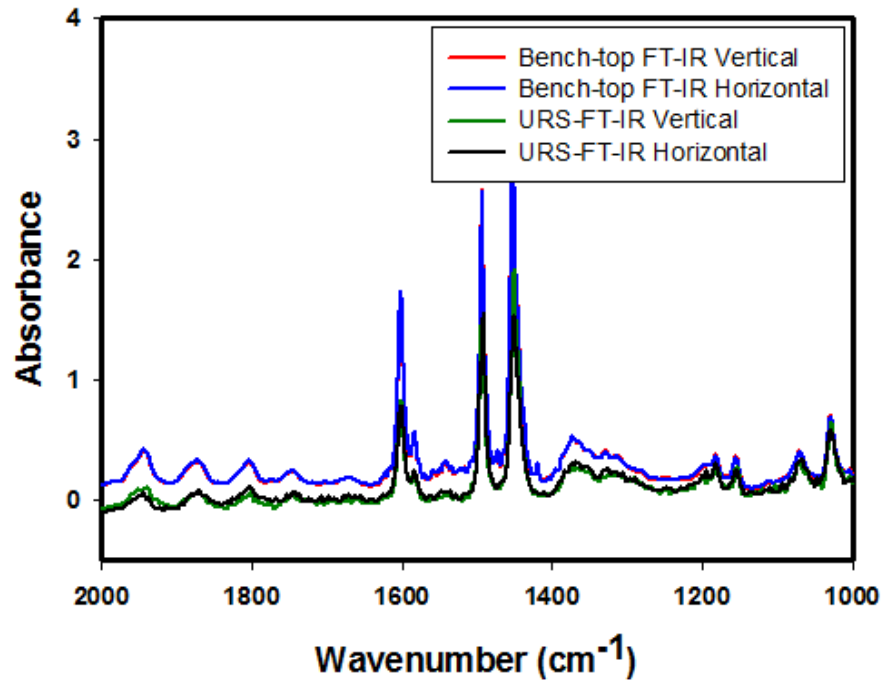
Figure IV-4 Absorbance spectra of polystyrene standard sample from 2000 to 1000 cm-1(as is spectra, no corrections or manipulations has been applied)

4.3.3 Real Time Tracking of Reacting Systems: Imidization of Polyamic acid

Polyimide films are mainly produced by thermal imidization of polyamic acid films at elevated temperatures 200°C and above. The polyamic acid films are constrained either uniaxially or biaxially to preserve their dimensional stability during the chemical conversion. The amount of conversion can be followed by FTIR spectroscopy through the disappearance of amic acid peaks followed by the formation of imide peaks. During this process, the evaporation of bound solvent is responsible for the development of internal stress and molecular orientation since the sample is constrained. The conversion reaction starts around 120°C, becomes fastest at 150°C and over 90% conversion can be achieved at 200°C.[27,85,102,211,212]

Rheo-optical system coupled with URS-FT-IR was used to monitor the physical parameters and chemical conversion for 5 micrometers thick polyamic acid film. The samples were placed in the heating chamber and they were held tightly by the grips. No stretching was applied and the temperature was increased from ambient temperature to 200°C. When the temperature reached to 200°C, the system was held at this temperature to complete the imidization reaction. Total experiment time was 1 hour.

Figure IV-5 shows the temperature, thickness and true stress and birefringence behavior as a function of time. The dashed vertical lines in both graphs indicate 150°C, where the imidization reaction is the fastest. An apparent regime change can be observed in the birefringence at this critical temperature.

The final thickness value of the imidized film was measured with a pressure

sensitive thickness gauge and marked with a red star in the graph. Final in-plane

birefringence value was verified by using a Gaertner optical bench polariscope

(Model L305; Gaertner Scientific Co.) equipped with a 7 order Babinet

compensator (GSC No. 617-F) and marked with a blue star sign on the graph. In

our system we used 546 nm wavelength to calculate the birefringence values

and the compensator was calibrated for 565 nm, which could be the slight

variation on the final values.
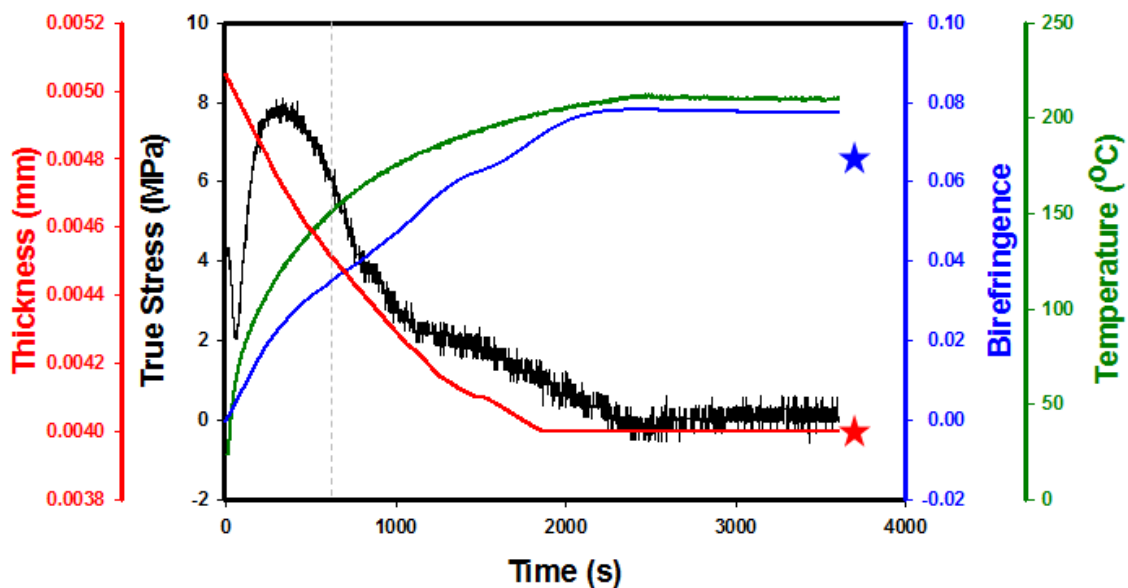
Figure IV-5 Real time results showing the temperature profile, thickness
change, true stress and birefringence development as a function of time.
150 °C is marked where the reaction rate is fastest.

Figure IV-6 shows the time evolution of vertical and horizontal polarization

spectra for imidization reaction measured by imide peak formation (centered at

1375 cm^{-1}) and the NMP solvent peak (centered at 1410 cm^{-1}) disappearance.

The vertical polarization spectra are made transparent to show there is a

difference on the area of the developed imide region that indicates the chain

orientation in the holding direction which is in good agreement with the

birefringence results. By using this information % bound solvent and %

imidization conversion can be calculated by normalizing the peak areas with a

fully imidized sample spectra.
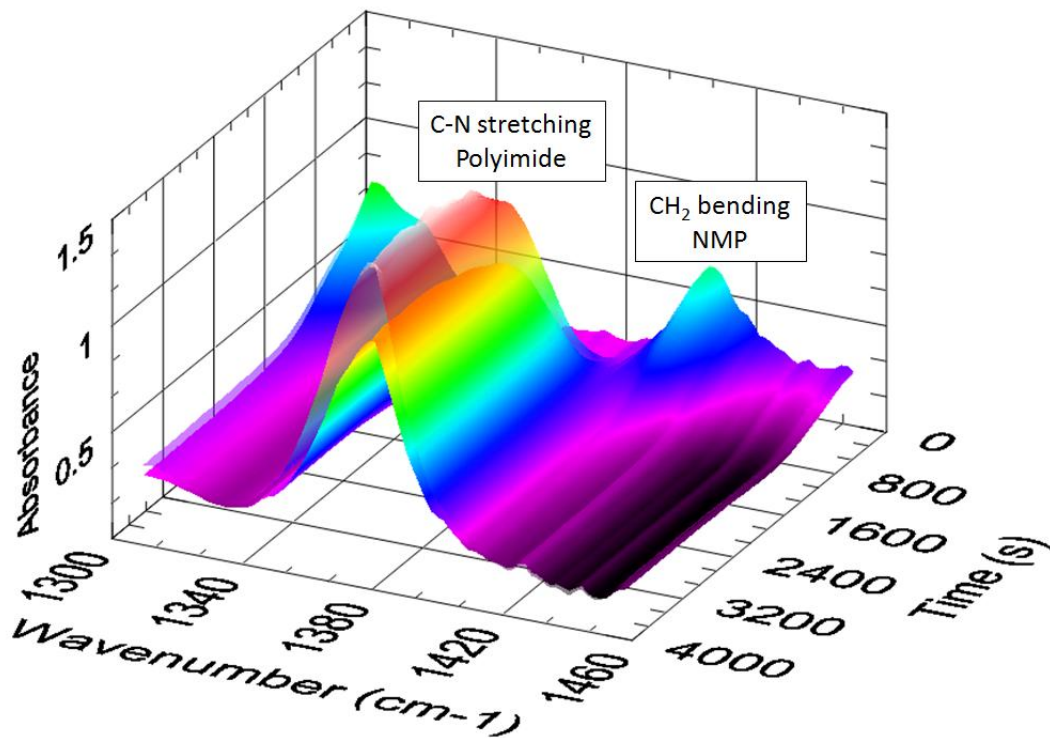
Figure IV-6 Time evolution of parallel (transparent) and perpendicular
(non-transparent) spectra showing the absorbance difference between
them.

Figure IV-7 shows the peak areas for NMP solvent region and imide

region, calculated by post processing the spectra presented in Figure IV-6.

Similar to birefringence development, when temperature reaches to 150°C the

solvent peak starts to decrease rapidly, where the imide peak slightly takes off followed by a rapid increase region and levels off. The difference on the peak areas for the imide region is also apparent here indicating preferential orientation in the stretching direction. However the solvent molecules do not exhibit such behavior.
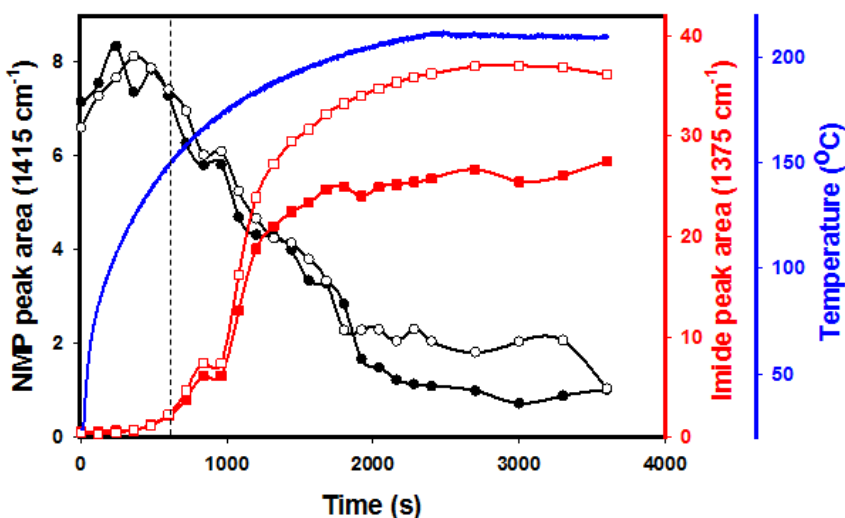
Figure IV-7 Time evolution of the peak areas for NMP (solvent, black curves) and polyimide region(red curves) as a function of time coupled with temperature data (blue curve). Open symbols belong to vertical polarization and filled symbols belong to horizontal polarization. 150 °C is marked with dashed vertical line where the reaction rate is fastest.

The infrared spectra collected from the system was verified by comparing the results with the bench-top FTIR spectrometer (Thermo-Nicolet 380 FT-IR) equipped with IR polarizer. Parallel and perpendicular polarization spectra in the range of 1800-1000 cm^{-1} wavenumbers from the two separate equipments are in good agreement (Figure IV-8).
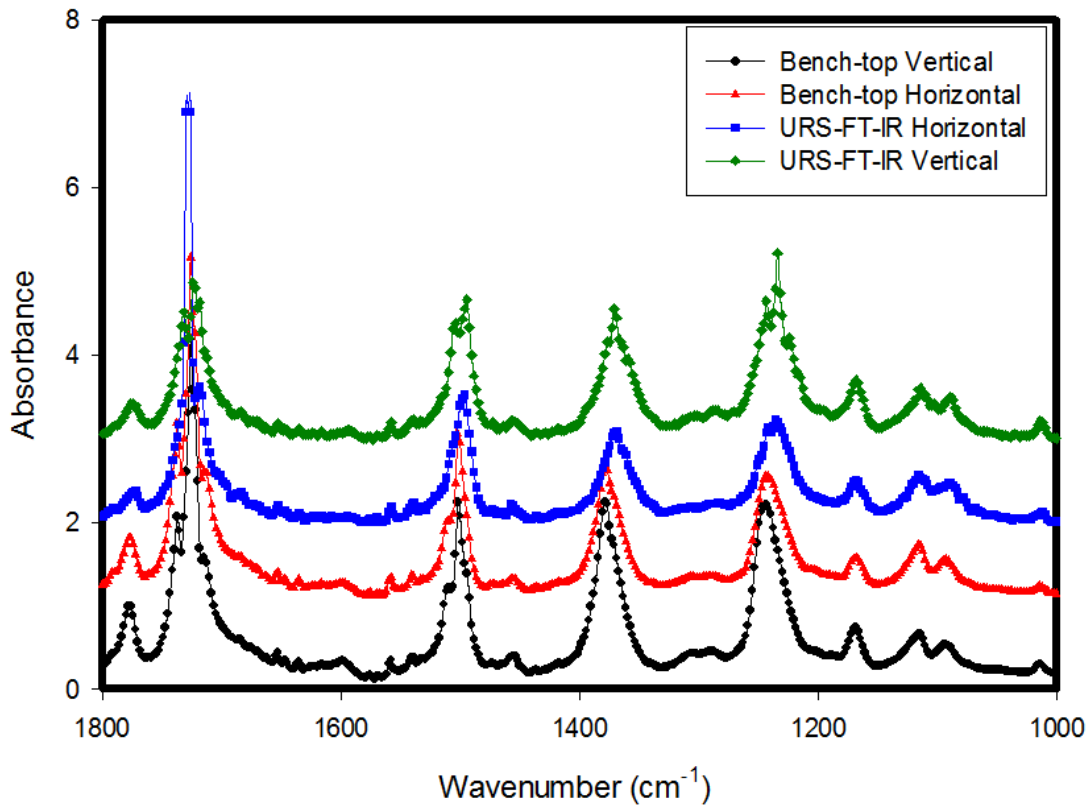
Figure IV-8 Polyimide sample equipment comparison in the range of 1000-1800 cm-1 for parallel and perpendicular polarization spectra.

The intensity levels were compared by integrating the peak areas for parallel and perpendicular polarization spectra and then calculating the dichroic ratio (equation 7) for several peak positions centered at: 725 cm^{-1}, 825 cm^{-1}, 1380 cm^{-1} and 1780 cm^{-1} (Table 4-1) for the bench-top and URS-FT-IR.

Table IV-1 Dichroic ratios calculated by bench-top and URS-FT-IR
spectrometer for several wavenumbers.

Center of the peak in wavenumbers	Dichroic Ratio ($A_{\parallel}/A_{\perp}$) calculated by Bench-top FT-IR	Dichroic Ratio ($A_{\parallel}/A_{\perp}$) calculated by URS-FT-IR
725 (cm^{-1})	0.84	1.18
825 (cm^{-1})	0.82	0.96
1380 (cm^{-1})	1.38	1.41
1780 (cm^{-1})	1.29	1.22

A comprehensive study with synchronized data for imidization kinetics, solvent evaporation, birefringence, true stress and IR dichroism behavior of this system will be discussed in details in the next chapters.

4.3.4 Real Time Tracking of Orientation: Stretching of Polystyrene

Polystyrene samples were stretched at 120°C with 30mm/min speed to 550% strain. Stretching was followed by holding to anneal and relax the sample at the same temperature for 6 minutes. Figure IV-9 shows the parallel and perpendicular absorbance changes as a function of time for the CH$_2$ symmetrical stretching region on the main chain of polymer molecules centered at 2870 cm^{-1} (range of 2750 to 2990 cm^{-1}). The transition moment angle for this band is selected as 90° and the orientation function is calculated as a function of time using the spectra shown in Figure IV-9.[58] The synchronized data for true stress, birefringence and orientation function as a function of time and Hencky strain are

represented in Figure IV-10 and Figure IV-11. As noted above, the sample was stretched followed by a holding period of 6 minutes. The latter was marked with dashed line in the graph.
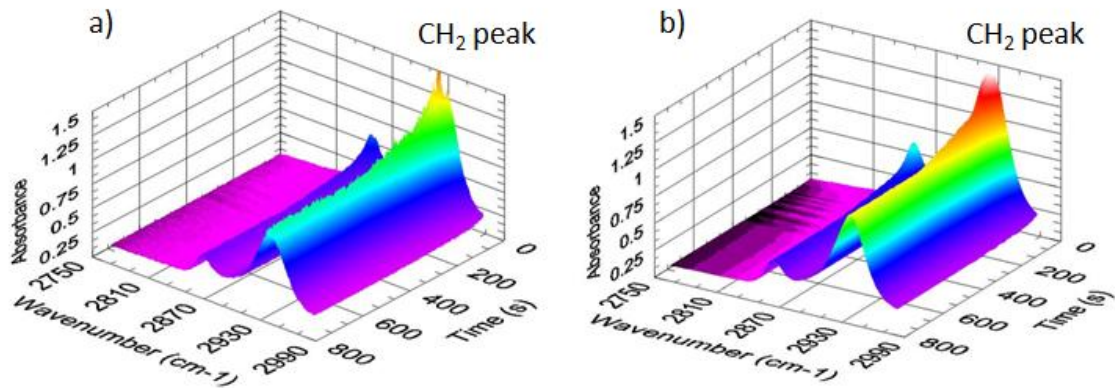
Figure IV-9 Real-time FTIR spectra of polystyrene in the 2750-2900 cm-1 range during stretching (initial 330 sec) and subsequent holding (final 360 sec). a) Time evolution of perpendicular polarization spectra b) Time evolution of parallel polarization spectra

The results are in good agreement with the literature.[58,151,152] Lawrence et. al. studied the effect of elongation on birefringence and showed a typical stress-strain curve for engineering stress and strain values.[213] Lefebvre et. al. studied the orientation function of polystyrene as a function of draw ratio at different strain rates.[214] Their results lead to an interpretation of the orientation function trend as function of strain rate. The orientation function increases with increasing strain rate. The same conclusion was made by Kiyoichi et. al.[215] Polystyrene has a negative intrinsic birefringence due to the presence of bulky side aromatic groups.[216] During stretching of polystyrene, the true stress and orientation of the main chain increases as indicated by the decrease in birefringence.
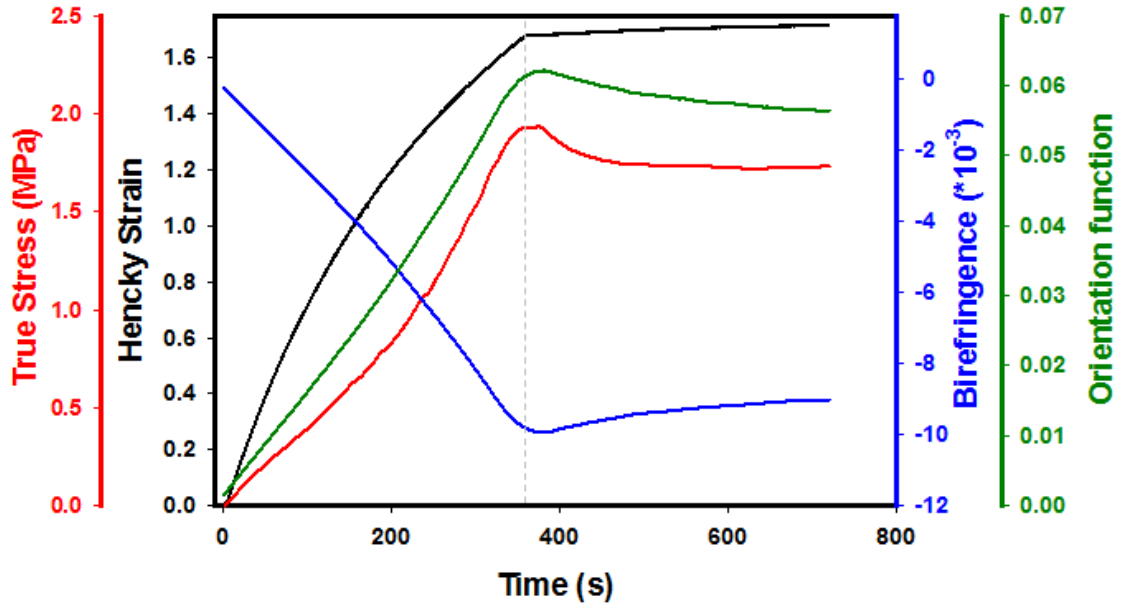
Figure IV-10 True stress, Hencky strain, birefringence and orientation function for the polystyrene film calculated by IR dichroism versus time(s). Holding stage is marked with the dashed line.

Two separate orientation functions are calculated for polystyrene; one using the IR dichroism data (unfilled circles) and one using the measured birefringence values (filled circles) and shown in Figure IV-11. The orientation functions calculated by IR dichroism and birefringence data follow same trend. Orientation function from birefringence was calculated by Equation 10 which is the ratio of the measured birefringence (Δn_{12}) and intrinsic birefringence (Δn°).[217–219] For polystyrene intrinsic birefringence is taken as -0.16. Orientation function from IR dichroism was calculated by using the equations 7-9.

$$f = \frac{\Delta n_{12}}{\Delta n^{\circ}} \qquad\qquad (10)$$
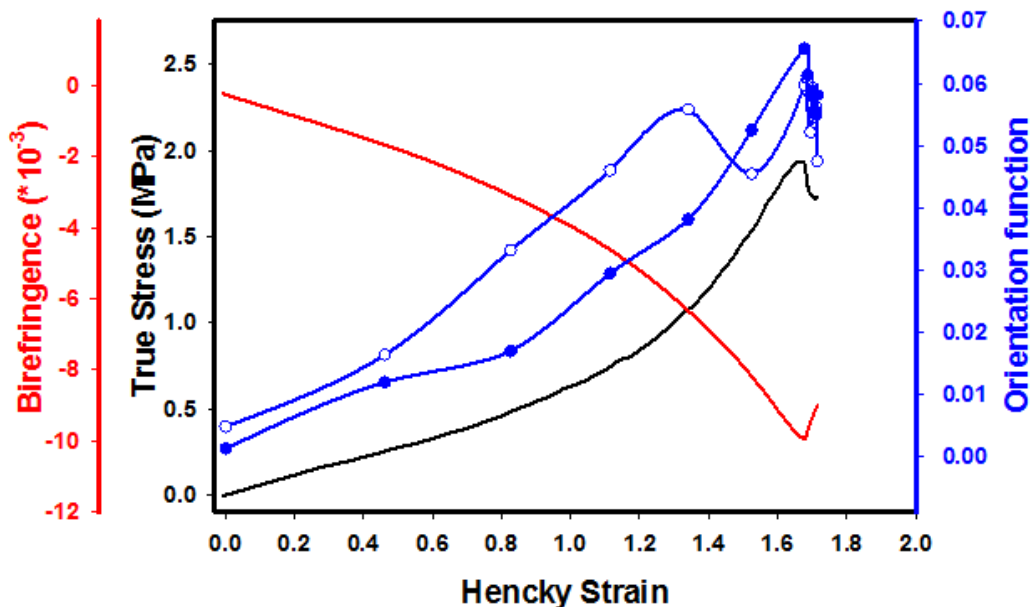
Figure IV-11 True stress, birefringence and orientation function for the polystyrene film calculated by IR dichroism (unfilled circles) and birefringence (filled circles) versus Hencky strain plots.

4.3.5 Real Time Tracking of Orientation in Multiphase Systems: Stretching of Polyurethane

Polyurethanes are a class of polymers that provide good example for multi-component systems as they have soft and hard and soft segments in their chain backbones and tend to phase segregate into these domains. Even though the hard and soft segmental structures are semi-continuous, it was found that they exhibit distinctly different orientation response to deformation.[154,159–162] Estes et al. monitored each segment behavior in polyether-based polyurethane segments following stretching in step increments and relaxation.[154] The hard segment orientation was found to be highly dependent on strain history while the

176

soft segments orientation generally was found to be insensitive. Processing details including stretching temperature[160] ,annealing[161] , presence of plasticizer was found affect the orientation.[163] These findings have been supported by other offline and simultaneous studies such as SAXS ,WAXD and AFM on the stretched polyurethane and polyurethane-urea samples.[162,164–166]

For this study, polyurethane samples were stretched at a draw rate of 50mm/min to 300% strain followed by 5 minutes holding at room temperature.

Figure IV-12 represents the parallel and perpendicular absorbance changes as a function of time for the 2650-3600 cm^{-1} region. The NH stretching vibration of the in urethane linkage is used to characterize the orientation of hard segments and the asymmetric CH_2 stretching is used to describe the prepolymer segments (polyether, polyester etc.) which form soft segments with absorptions appearing around 3320cm^{-1} and 2935cm^{-1} respectively. The transition moment angles are taken to be 90° for both vibrations indicated by Zbinden and Fraser.[220,221] The orientation functions are calculated for each segment under these assumptions and plotted against time and Hencky strain along with the stress and birefringence changes on the overall sample as shown in Figure IV-13 and Figure IV-14 respectively.
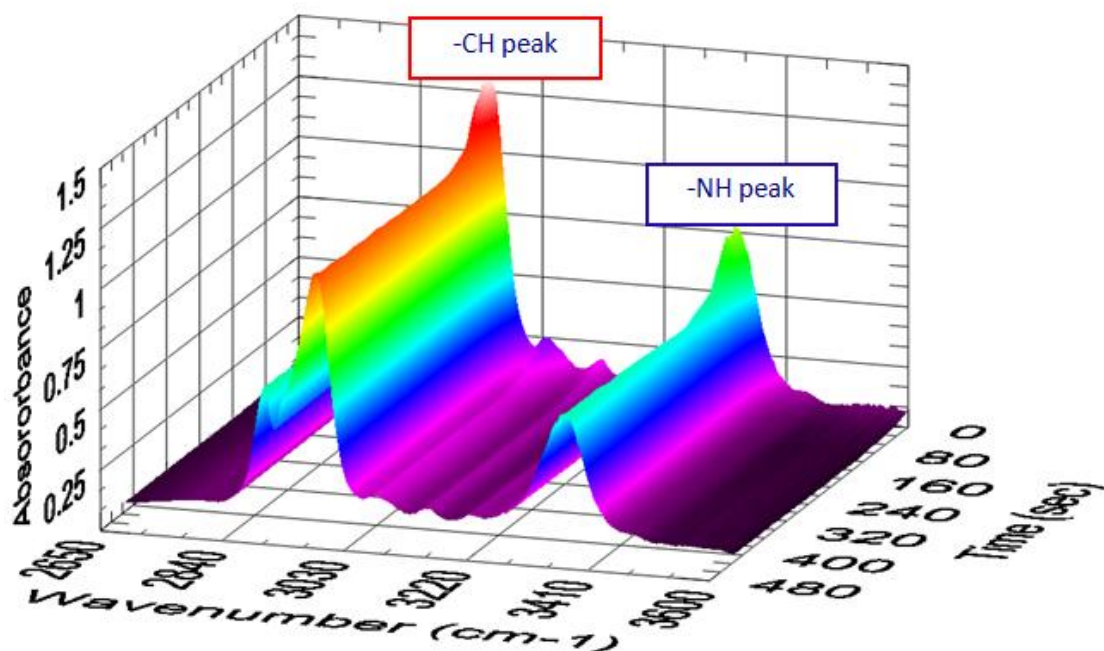
Figure IV-12 Time evolution of parallel polarization spectra in the range of 2650-3600 cm-1 for polyurethane sample. Initial 90 seconds of stretching followed by holding (next 300 sec).

Although similar degrees of orientation have been observed for hard and soft segments, their contributions are different during the experiment. The rheo-optical behavior of the overall material and orientation behavior of each segment can be divided into three distinct strain regions separated by dashed lines in Figure IV-13.
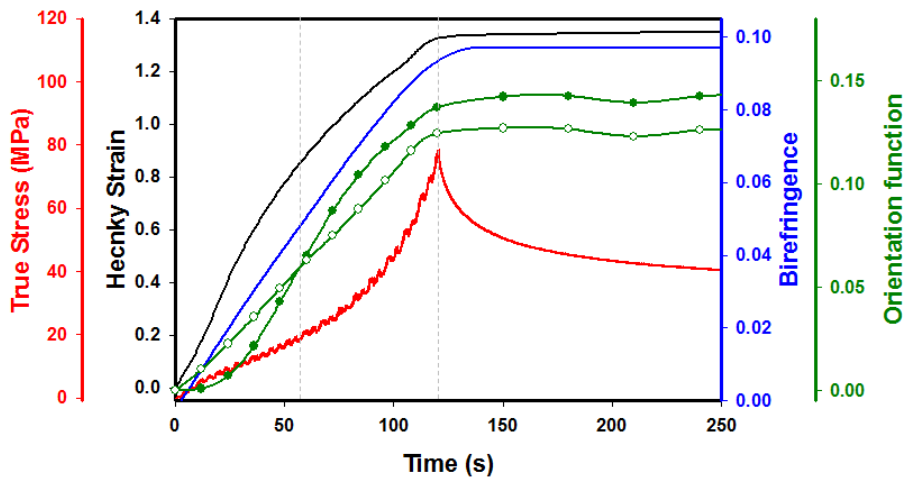
Figure IV-13 True stress, Hencky strain, birefringence of the polyurethane overall film and orientation function of the hard (NH absorption bands, filled circles) and soft (CH2 absorption bands, unfilled circles) segments versus time (s).

At low strain levels, reorientation of soft segments (CH_2 region) is greater than hard segment (NH region) reorientations (Figure IV-14). Upon application of deformation, the soft segments begin to orient immediately while hard segments remain unoriented until around 40% strain beyond which it also begins to rise. The onset of strain hardening is observed at 90% strain where the hard segment orientation function crosses over the soft segment orientation function. These results are in good agreement with the reported behavior of similar materials in the literature.[154]
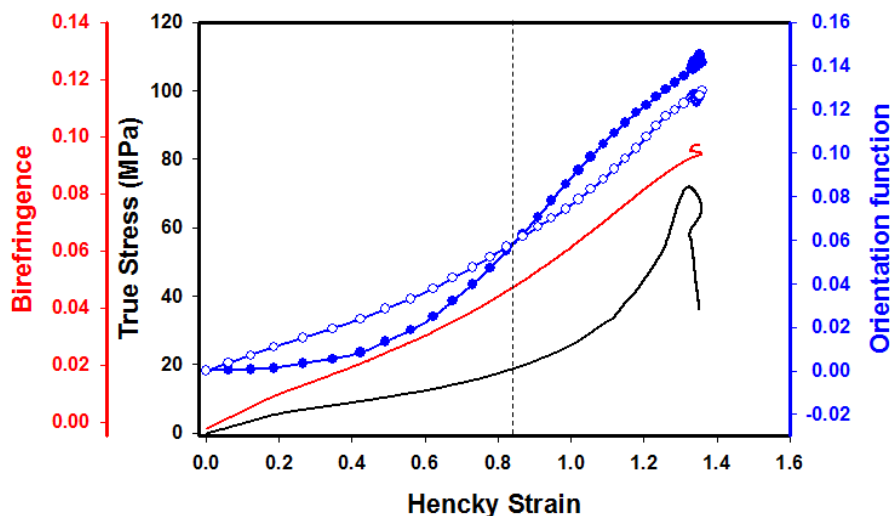
Figure IV-14 True stress, birefringence of the polyurethane overall film and orientation function of the hard (NH absorption bands, filled circles) and soft (CH2 absorption bands, unfilled circles) segments versus Hencky strain. Crossover of the hard and soft segment orientation functions on the critical strain value is marked with the dashed line.

4.4   Conclusions

The new integrated instrument allows real-time tracking of true stress, true strain, birefringence and IR dichroism of films undergoing uniaxial stretching, relaxation annealing or chemical reaction. Using these data chain and segmental orientation of different phases and crystallization and the chemical reaction kinetics can be tracked real time. The URS-FTIR makes it possible to investigate very fast deformations at speeds up to 200 mm/min with a data acquisition rate of 300 complete spectra/second.. This instrument can be used to systematically study the effect transient behavior during heating, stretching,

180

relaxing and cooling providing valuable information on understanding of physical

changes during complete film processing cycle.

CHAPTER V

REAL TIME CHARACTERIZATION OF PHYSICAL CHANGES IN
POLYIMIDE FILM PROCESSING FROM CASTING TO
IMIDIZATION

Drying and imidization of PMDA-ODA solutions in NMP were investigated by a novel custom designed measurement system that tracks real time weight, thickness, surface temperature, in-plane and out-of-plane birefringence. At low temperature drying stage, the weight and thickness reductions occurred rapidly as a result of solvent evaporation. All the parameters started leveling off while the out of plane birefringence steadily increased and reached a plateau at longer drying times. When the temperature was increased for imidization reaction, additional weight loss accompanied by temporary reduction of birefringence was observed due to evaporation of bound solvent as solvent molecules decomplexed from the polymer chains and plasticized the film. During the latter stage, out-of-plane birefringence rose rapidly as the polymer chains increasingly became oriented with their chain axes were preferentially oriented in the film plane. Throughout the whole process the in-plane birefringence remained zero. For the first time, these real time measurements allowed us to quantitatively

show the dynamics between chain relaxation due to evaporation of the decomplexed solvent molecules, and orientation development due to decreased chain mobility caused by imidization reaction and increasing Tg for the PMDA-ODA/NMP solutions. In addition, the dynamics of this interplay was investigated by varying the processing conditions: initial casting thickness and drying temperature.

5.1 Introduction

Polyimide films exhibit good thermal stability, high mechanical strength and chemical resistance. These properties allow their use in harsh industrial applications including automotive, aerospace and electronics.[50,51,53,222–224] Common polyimides are not soluble in solvents and they degrade when heated due to their high T_g. Because of these restrictions, a two step process was developed to produce high quality polyimide films.[39–41,225,226] First, a precursor polyamic acid (PAA) is synthesized that is soluble in polar, high boiling point solvents such as NMP (N-Methyl-2-pyrrolidone), DMAc (Dimethylacetamide) and DMF (Dimethylformamide).[11] In the second step, PAA is converted to polyimide through thermal imidization.[4,5,225] This part of the process can be divided into three sections; i) solution casting of polyamic acid precursor on to a substrate via blade coating or slot die casting, ii) drying of precursor to form partially dried film, and iii) thermal treatment to form polyimide film.[24,211,227] The critical temperatures for the thermal imidization are,120°C where imidization reaction starts and 150°C where the rate of conversion is the fastest.[18] As the temperature reaches 200°C,

90% of conversion is achieved. 100% conversion is reached at higher temperatures, typically 300°C - 450°C range depending on the chemical structure.[4]

During the multi-step imidization process, solvent evaporation, polymer chain orientation, chemical conversion and water loss due to the chemical reaction, all take place concurrently.[32,102,228] Because of these changes, films experience weight loss, thickness reduction, temperature change, change in rate of diffusion for solvent molecules and change in chain mobility leading to birefringence development (Figure V-1). It is very difficult to predict the effect of each processing step on the final properties due to the simultaneously changing physical and chemical parameters that are interrelated. Majority of characterization for the polyimide films has been performed on the samples that were already imidized after all these events have taken place.[7,13,99,105,114,229–231] These offline characterization measurements provided valuable information on final properties that develop as a result of complex events. However, little is known about these sequences of structural/mechanistic details that occur during the course of imidization process.
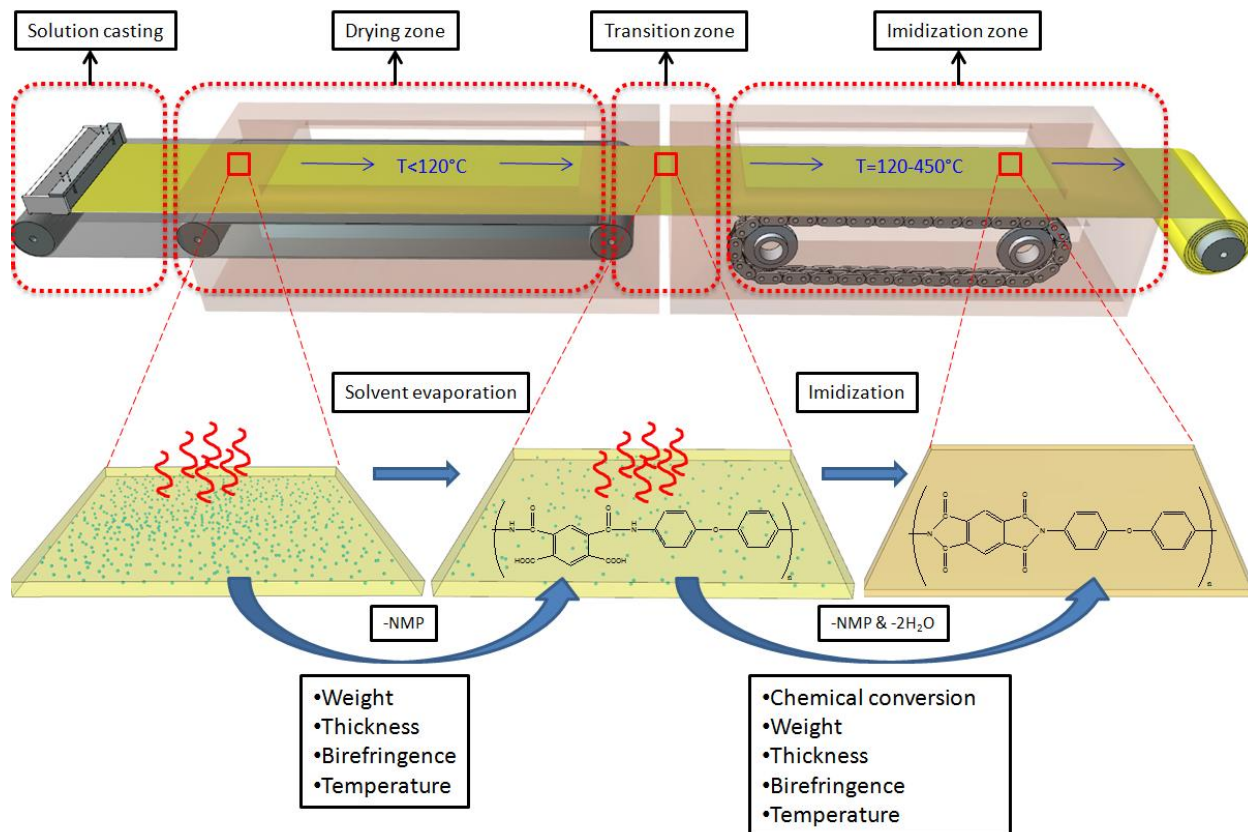
Figure V-1 Roll-to-roll polyimide film process and physical and chemical changes during the process

For high quality thin polyimide film production, a stepwise increase in temperature is preferred. The cast solution is first dried at temperatures below 120°C to form PAA film followed by imidization reaction at higher temperatures. It was found that, PAA films that are dried at low temperatures contain 30%-50% bound solvent.[26,27] Model compound studies for these PAA-solvent systems have revealed that the PAA molecules form complexes with the polar solvent molecules via hydrogen bonding.[18,26–31] There are four potential sites that can participate in hydrogen bonding on the backbone of the PAA chains, consisting of two carboxylic acid groups and two amide groups. The binding energies for these

groups are different, which creates the formation of two distinct solvent complexes with different thermal stabilities. It was reported the formation of 4:1 (solvent:PAA repeat unit) and 2:1 (solvent:PAA repeat unit) complexes depending on the processing conditions, such as casting thickness and drying temperature.[28,29]

The presence of bound solvent plays a critical role during the imidization reaction.[27,96] After drying and formation of PAA solid-like structure with high solvent content, the film is heated to imidization temperature and the bound solvent starts to decomplex from the carboxylic acid and amide groups. The solvent molecules bonded to amide groups are released earlier due to lower bonding energy compared to that of carboxylic acid group which is a better proton donor.[28,29] The release of the solvent molecules has several effects. First, it plasticizes the film, causing PAA chains to relax. Secondly, due to release of the solvent molecules, the active carboxylic acid and amide groups become free for imidization reaction to occur. Hence, decomplexation of these solvent molecules is the driving factor for the imidization reaction. The T_g of this highly viscous medium is much lower compared to that of a fully imidized film and during the reaction it changes with increasing degree of imidization and loss of solvent.[23] Increase in T_g and formation of rigid imide groups decrease the chain mobility that causes the development of spontaneous molecular orientation parallel to the film surface during the process.[92,108,109,111,232–235] This orientation development has significant influence on the final properties of films such as modulus, mechanical anisotropy, thermal expansion coefficient and optical

186

anisotropy as reflected in out-of-plane birefringence.[25,106,107,236,237] The imidization conditions, such as imidization temperature, heating rate and time, also play an important role in the development of morphology and final properties of these films.[8,85,93,98,238]

Analysis of such a complex process and evaluation of final physical and chemical properties by off-line characterization techniques can be misleading as the later processes may hinder the details of the early steps. A comprehensive study of this multi-step interrelated processes (formation of PAA-solvent complexes, decomplexation of the hydrogen bonded solvent molecules and subsequent imidization reaction) is required for a complete understanding of the effects of processing conditions on the evolution of structural and mechanical anisotropy in polyimide films.

In this chapter, we report a comprehensive study that investigates the real time dynamics of the imidization reaction, covering all the stages of this complex process from solution casting of polyamic acid to polyimide film formation. During this study a wind tunnel shaped highly instrumented drying station was used. This instrument is equipped with sensors to track real-time weight, thickness, surface temperature and in-plane and out-of-plane birefringence during solution drying of polymer films.[208] The polyamic acid conversion to polyimide was studied with all the physical changes monitored during the process and the effect of processing parameters on the structural development was investigated by varying the initial casting thickness and drying temperature for the first time.

5.2   Experimental

5.2.1   Materials

Polyamic acid solution (PMDA-ODA, 15 weight % solids in NMP) purchased from Sigma-Aldrich (CAS Number: 25038-81-7) and used as received. The solution was cast on glass substrates using a motorized drawdown coater equipped with a commercial 3" wide casting blade. The cast solutions were 7" in length and 3" in width.

5.2.2   Measurement system

The details of the measurement system (Figure V-2) used in this experiment was reported elsewhere.[208] In summary, it is a combination of a hot air blower, wind tunnel shaped frame and sensors for tracking physical changes. Hot air blower can operate at temperatures up to 500°C and air speeds up to 4.5 m/s at the sample location. The direction of the air flow is shown by the red dashed lines. The blower is connected to the wind tunnel shaped drying tunnel. This shape provides a uniform air flow at the center of the tunnel where the drying sample and sensors are located.
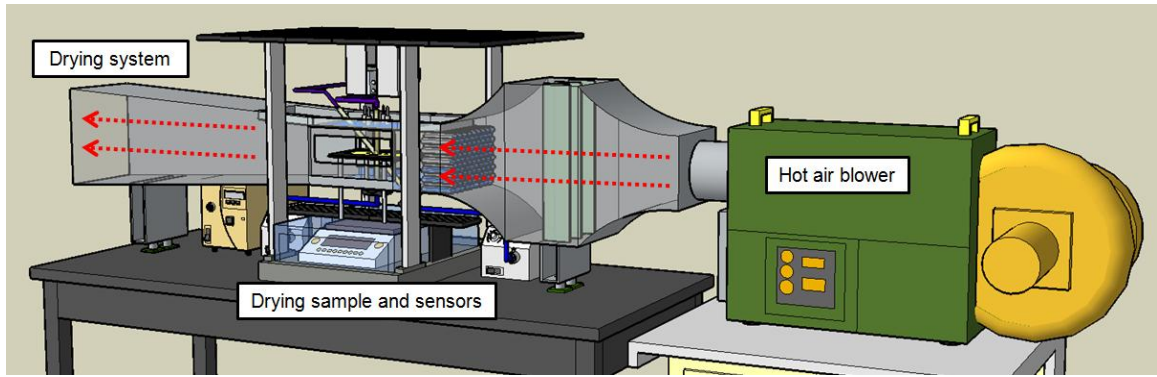
Figure V-2 Wind tunnel shaped drying system

Drying sample and the sensor locations are shown in Figure V-3. Polymer solution is cast on a glass substrate and placed on a sample platform that directly sits on a balance to measure the real-time weight of the drying solution. The sample thickness is measured by a combination of three laser displacement sensors. These lasers measure the displacement of the glass substrate top surface and the drying sample top surface at two locations (upstream of the air flow and mid section of the solution). By subtracting the two values, the thickness of the drying solution is calculated at two locations. Surface temperature of the drying solution is measured by four pyrometers that are located very close to the center of the drying solution.
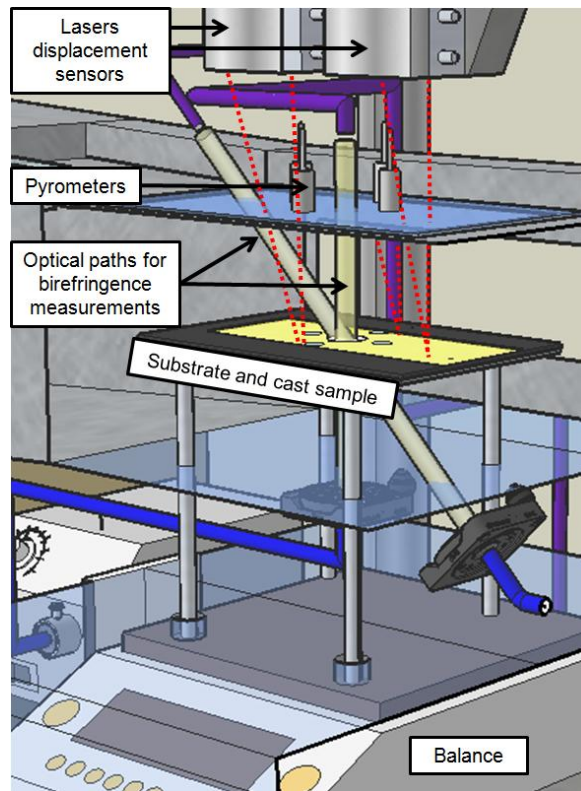
Figure V-3 Drying sample, sensors and measurement locations

Real-time birefringence is measured by spectral birefringence method.[141,143,144,186,187,189,190,192–200,202,203,239] The in-plane and out-of-plane birefringence is calculated by measuring the 0° and 45° retardation values. The optical light paths for these measurements are shown with yellow transparent tubes in the figure below.

For the in-plane and out-of-plane birefringence (Δn_{12} & Δn_{23})calculations Stein's equations are used (Eq. 1 & 2).[145]

$$\Delta n_{12} = \frac{R_0(t)}{d(t)} \qquad\qquad (1)$$

$$\Delta n_{23} = -\frac{1}{d(t)}\left[\frac{R_0(t) - R_\phi(t)\sqrt{1 - \dfrac{\sin^2\phi}{\bar{n}^2}}}{\dfrac{\sin^2\phi}{\bar{n}^2}}\right] \qquad (2)$$

where, $R_0(t)$ is instantaneous 0° retardation, $d(t)$ is the instantaneous thickness, $R_\phi(t)$ is retardation value at angle Φ (45° in this case), and $\bar{n}$ is the average refractive index of the drying solution. The average refractive index was estimated from the weight change. A linear relation was assumed with respect to concentration for the calculations. Refractive index of solvent and imidized PMDA-ODA films were measured as 1.47 and 1.72 respectively by Abbé refractometer at 633 nm. The initial concentration of the solution was 15 weight % solid and refractive index of the solutions was 1.507. The refractive index of pure polyamic acid form of PMDA-ODA film could not be measured, as this material always forms complexes with the solvent molecules. If the temperature was increased to evaporate the solvent, the imidization reaction started and the material was no longer purely polyamic acid. Hence for this study, the refractive indices of polyamic acid and polyimide of PMDA-ODA were accepted as 1.72 at 633 nm.

We recently showed the development of anisotropy through the thickness direction of solution cast polymer films experimentally by measuring the birefringence through thickness and refractive index values at both the air-

solution interface and substrate-solution interface directly. It was observed that the use of average refractive index value for the out-of-plane birefringence calculations caused only a 5% deviation from the actual birefringence values that were calculated directly from the developed gradient during drying. [240]

5.2.3 Experimental parameters

A typical industrial roll to roll polyimide film processing stages are illustrated in Figure 1.[241–245] After the blade coating or slot die casting of the solution, it enters into drying zone. In this zone, the material is dried to remove the excess amount of high boiling point solvent. The temperature is kept below 120°C where no imidization reaction takes place.

When the film is sufficiently dried, it is separated from the carrier and passes through a transition zone. In this zone, the temperature starts to rise to imidization temperature, in the range of 120-450°C depending on the chemical structure and desired imidization degree. In this zone, the sample is constrained for dimensional stability to prevent shrinkage due to solvent loss and imidization reaction. After this stage it travels deeper into the imidization zone where the temperature is kept constant at higher values for imidization to complete and remove all the remaining bound solvent.

Our real time measurement system is capable of applying all the conditions listed and measure the physical parameters changing during each

stage of the industrial processing step. These measurements include real time

weight, thickness, surface temperature, in-plane and out-of-plane birefringence.

5.3   Results

To experimentally simulate the actual imidization process, PAA/NMP

solution was cast on glass substrate at room temperature, placed on top of the

sample platform inside the preheated chamber and data acquisition was started.

The sample was first dried for 4 hours at low temperatures and then the

temperature was increased to the imidization temperature, 200°C for the next 4

hours. The air speed was kept constant at 0.5 m/s during the experiment.

5.3.1   Imidization verification

To verify the chemical conversion, imidization of the PMDA-ODA samples

were measured at different temperatures for 5 µm thick films. The solution cast

polyamic acid films were kept in a vacuum oven at different temperatures for 60

minutes. The IR spectra of these samples were compared with the fully imidized

film that was kept at 180°C for 45 minutes and 350°C for 60 minutes. Figure V-4

shows the results calculated by equation 3, using the imide peak area (CN

stretching) at 1380 cm^{-1}, normalized with the aromatic ring stretching peak area

at 1500 cm^{-1}. This peak is not affected from the chemical change. This ratio was

normalized with the ratio of the fully imidized film.

$$Degree\ of\ imidization = \frac{\left(\dfrac{1380\,cm^{-1}{}_T}{1500\,cm^{-1}{}_T} \right)}{\left(\dfrac{1380\,cm^{-1}{}_{T'}}{1500\,cm^{-1}{}_{T'}} \right)} \qquad (3)$$

The graph shows, about 90 % conversion is achieved at 200°C, which is in good agreement with the literature. [2,18,27,85,102]
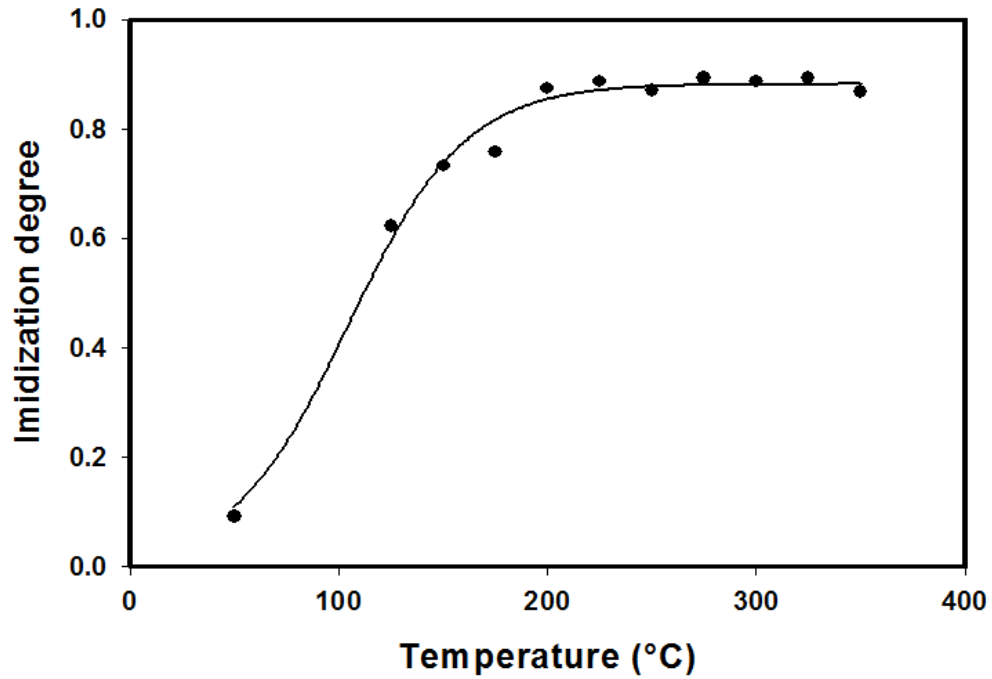
Figure V-4 Imidization degree of 5 micrometer PMDA-ODA films as a function of temperature. About 90 % conversion is achieved at 200°C.

5.3.2 Overview of the process
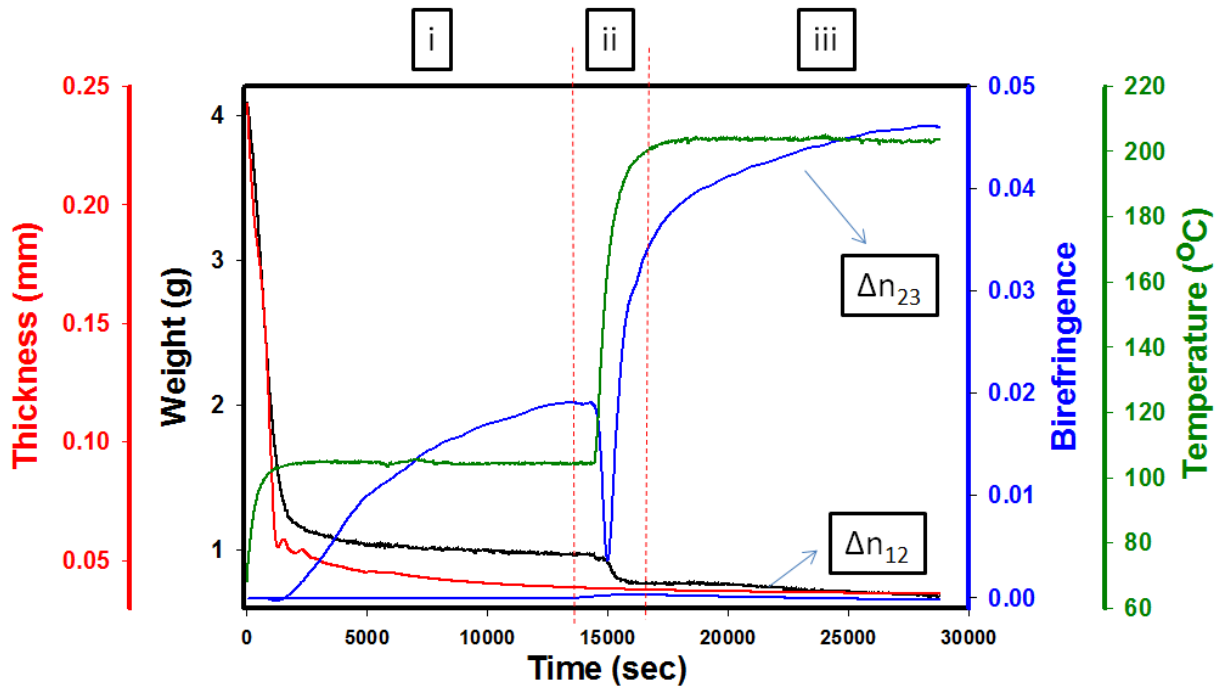
Figure V-5 Whole imidization process with all regimes marked i) drying regime, ii) transition regime and iii) imidization regime

As Figure V-5 shows, the first 4 hours of the experiment corresponds to solution casting and drying of the PAA solution (i), where the temperature was kept low to prevent imidization. In ensuing stage, the temperature was raised to 200°C and we continued to track the physical parameters during this transition (II) into imidization (III) stages as the temperature was increased. During the drying stage (i), the weight and thickness values decreased rapidly due to solvent evaporation (Figure V-6). This caused simultaneous solidification and shrinkage mainly in the thickness direction as the film is constrained in the x-y plane as it is adhered to the substrate. As the drying proceeds, the in-plane birefringence

remains zero, indicating the preservation of in-plane isotropy. Beyond a critical

drying stage, the out of plane birefringence starts to increase. This is affected by

the competition between the relaxation and reorientation of the polymer chains in

the plane as the film is undergoing compression during

drying.[89,91,95,124,126,128,130,246,247] This competition is apparent in Figure 6. Initial

sections of the drying were solvent rich, which indicates the relaxation times are

shorter and both the in-plane and out-of-plane birefringence values remained

very close to zero. As the drying proceeded (t~2000 seconds) the rate of weight

and thickness loss started to level off while the onset of out-of-plane

birefringence development was observed. At this point the sample can support

stresses and the relaxation times increase. After 4 hours, the evaporation of

solvent substantially decreases. At this stage the partially dried sample contains

about 30-40% solvent by weight.
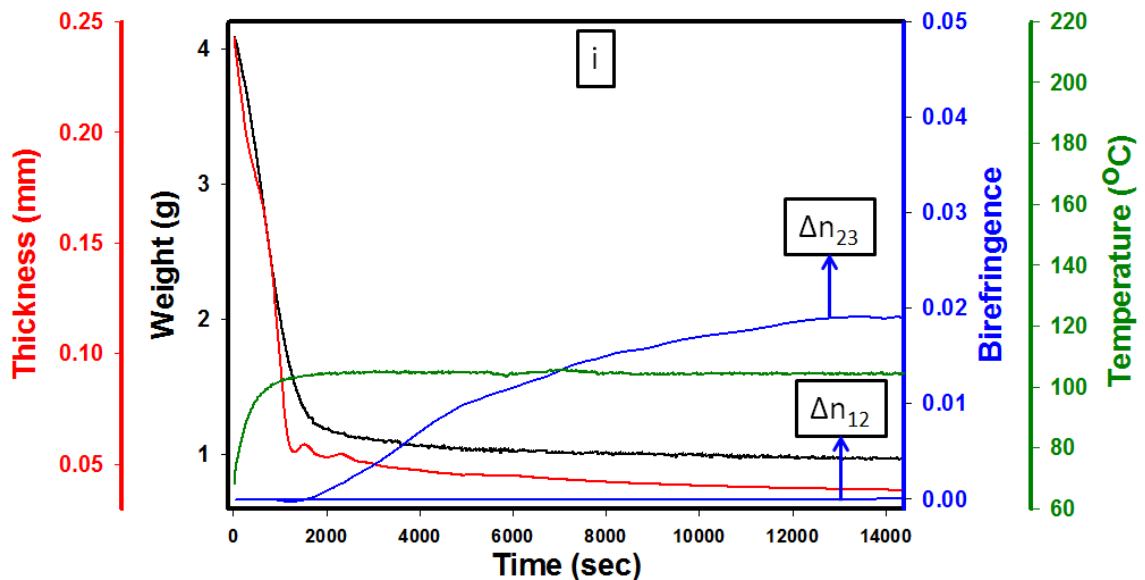
Figure V-6 Regime I drying zone

The details of the transition zone, where the temperature is increased from 100°C to 200°C, is shown in Figure V-7. As the temperature gradually increases, additional weight loss and thickness reduction is observed associated with the evaporation of the bound solvent. We also observe the temporary decrease of out of plane birefringence before beginning to increase again beyond 15000 sec. This decrease is attributed to the plasticization effect of the decomplexed bound solvent, leading to relaxation. However, at a critical temperature value(~150°C-160°C), the rate of the imidization reaction increases sufficiently enough that decreases the chain mobility, as a result of the formation of rigid polyimide chains as well as increased T_g due to evaporation of bound solvent. At this point, out-of-plane birefringence increases at a higher rate as compared to the previous drying section. Weight loss indicates the continuation of the evaporation of the bound solvent and the evaporation of the water that is formed during the reaction. Transition zone clearly shows that the orientation development is a balance between the solvent evaporation induced relaxation and the continual orientation of polyimide chains parallel to the film surface as the chain mobility decreases due to imidization reaction and consequent increase in T_g.[23,85,93,98,101,238]
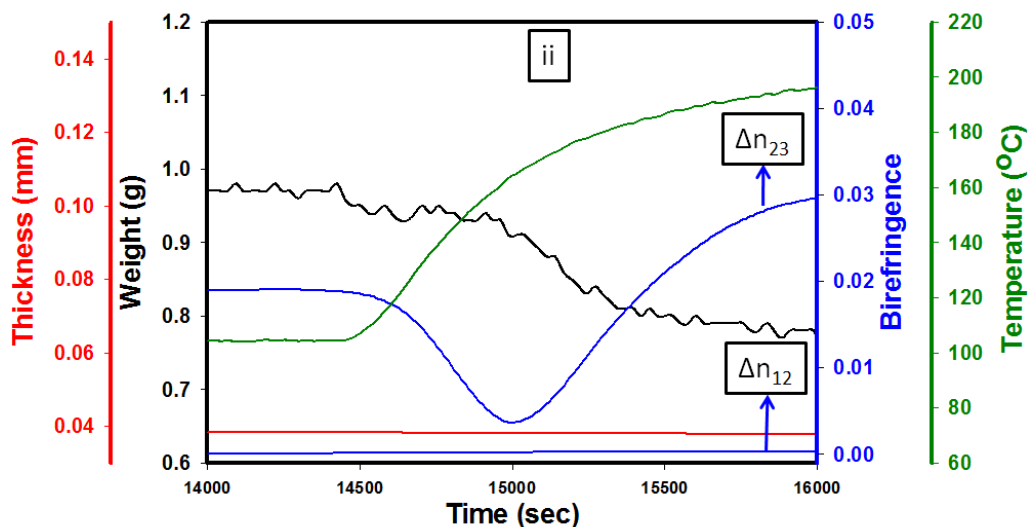
Figure V-7 Regime ii heating zone

The final stage is shown in Figure V-8. The weight, thickness and out-of-plane birefringence values start to level off as the evaporation of all the bound solvent. The leveling off of the out-of-plane birefringence also indicates the imidization reaction slows down significantly. The formation of high T_g polyimide molecules and the evaporation of almost all solvent and water molecule formed during the reaction rapidly decreases the chain mobility.
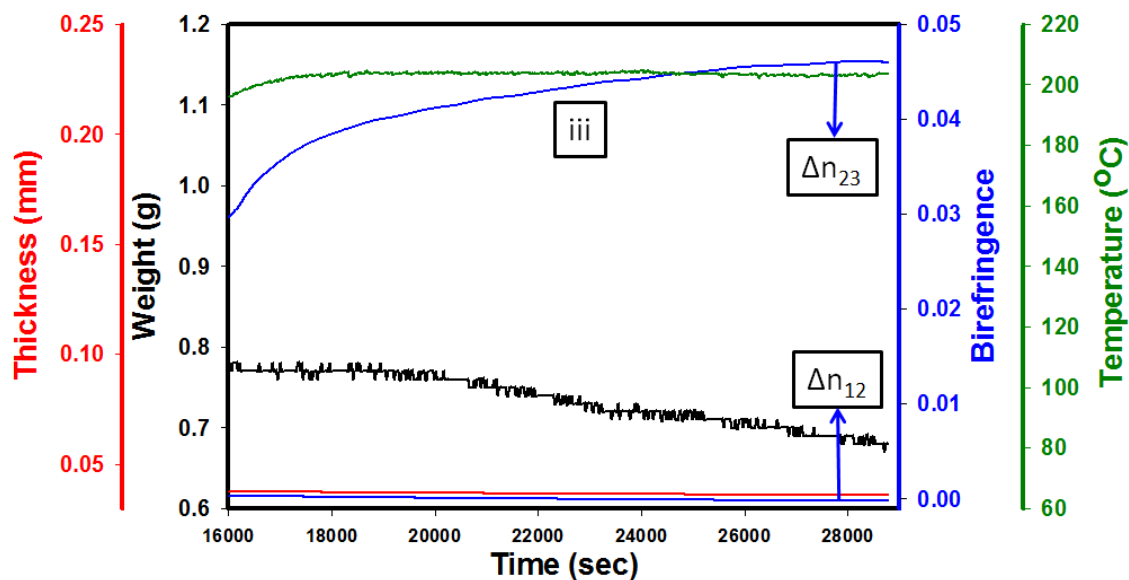
Figure V-8 Regime iii imidization zone

5.3.3 Influence of thickness

To ascertain its influence on drying behavior, we prepared films with 500 μm, 250 μm and 100 μm casting thickness. In the first step the temperature was kept at 100°C at 0.5 m/s air speed and the films were dried for 4 hours. In the next 4 hours, the temperature was increased to 200°C to for the imidization reaction. At this temperature approximately 90% of the imidization has been achieved. Real-time data for weight, thickness, surface temperature and in-plane and out-of-plane birefringence values were measured during the process.

As expected (Figure V-9-a, Figure V-9-b) as the casting thickness decreases, weight loss occurs faster due to higher evaporation rate of the solvent as shorter path lengths the solvent molecules has to travel to reach the surface

and evaporate. Figure V-9-c shows the section of the process where the

temperature started to increase to imidization temperature of 200°C. The

temperature increase causes decomplexation of the bound solvent leading to

additional weight loss mentioned earlier. The % weight losses for 500 µm, 250µm

and 100µm thick cast solutions are 21%, 26% and 37% respectively between

13000 and 17000 seconds.
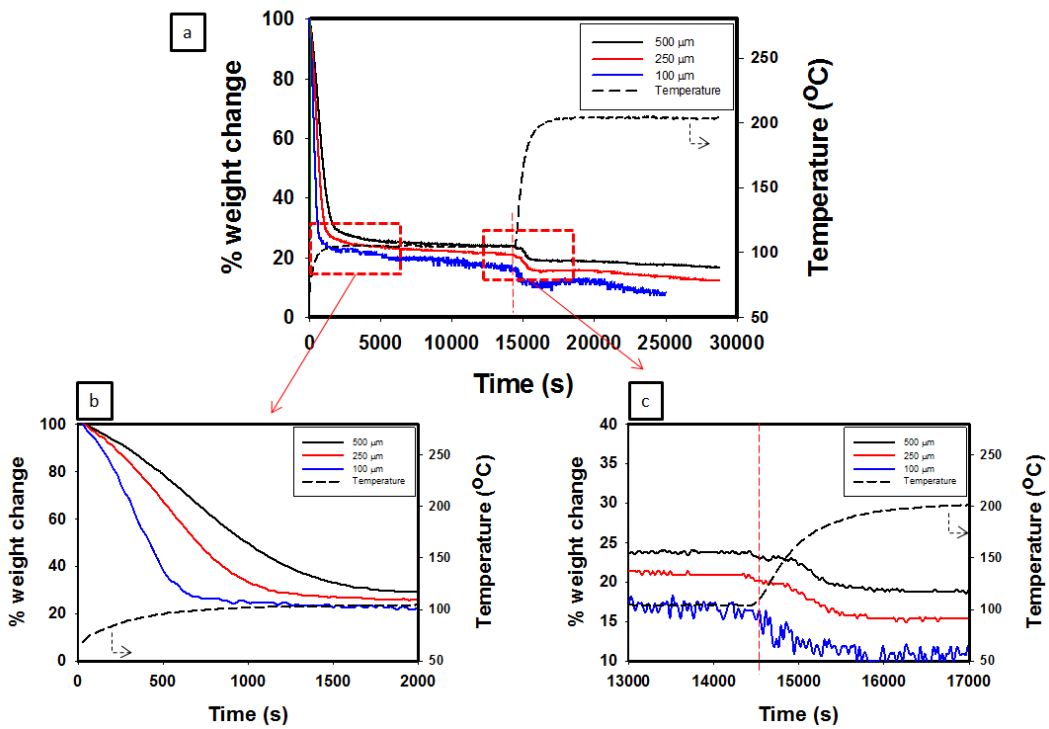
Figure V-9 Effect of thickness on weight change during the process

Thickness change during the initial stages of the process for different

initial casting thicknesses are shown in Figure V-10. Similar to weight loss, the

rate of thickness loss is faster as the initial casting thickness decreases. When

the temperature was increased to 200°C for imidization reaction to take place, no

clear change in the thickness values was observed for all thicknesses (inset graph in Figure V-10). However, since the weight loss (Figure 9) indicates the evaporation of solvent, the thickness values should decrease. Laser displacement sensors failed to detect the thickness change during the temperature increase, which is mainly due to the sensor sensitivity. The final thickness values for 500 μm, 250μm and 100μm thick cast solutions were measured as36μm, 21μm and 10μm respectively via off-line thickness gage after the process.

Figure V-10 Effect of thickness on % thickness change during imidization

Overall in-plane and out-of-plane birefringence development for all three thicknesses are shown in Figure V-11-a. During the process, the in-plane birefringence remained zero and out-of-plane birefringence increased with the decreasing initial casting thickness.

201
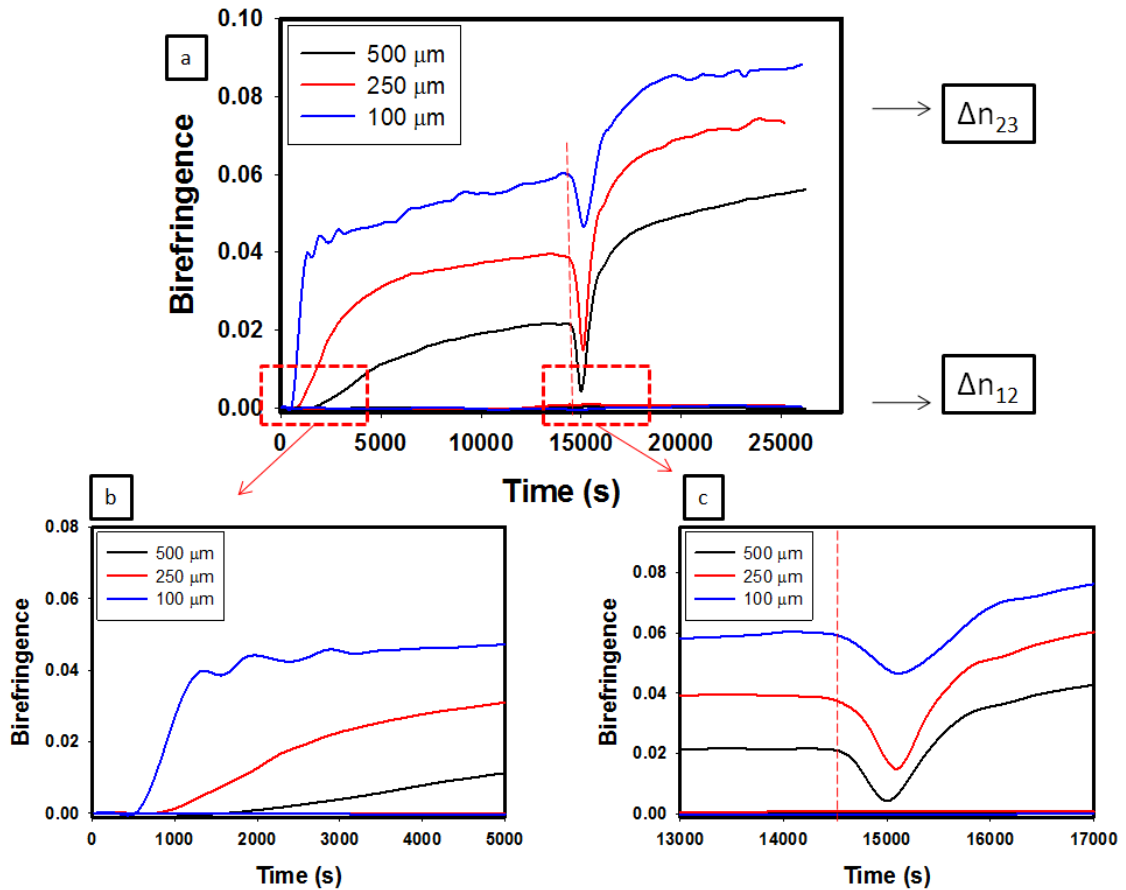
Figure V-11 Effect of thickness on in-plane and out-of-plane birefringence behavior during imidization

Initial 5000 seconds of the process is shown in Figure V-11-b where the cast solutions were dried at 100°C. This temperature is below the temperature range where little or no imidization occurs during drying. The development of the out-of-plane birefringence is attributed mainly due to the shrinkage of the film in the thickness direction since it is constrained in the x-y plane of the glass substrate. The increase of birefringence values with decreasing thickness is attributed to the rapid reduction of relaxation rates with reduced initial thickness

leading to increased overall orientation as the evaporation rate of the solvent decreases. (Figure V-9 and Figure V-10).

Figure V-11-c shows the period where the set temperature is increased to 200°C for imidization reaction to occur. The orientation in this section starts to decrease initially because of the plasticization effect of the decomplexed solvent molecules as temperature increases. However as the temperature continues to increase the rate of imidization reaction increases and dominates the orientation development. This scheme is similar for all three thicknesses, with a slight delay in the 100 µm film. The reason for this delay might be the low content of the bound solvent in this sample. As mentioned earlier, the decomplexation process of the solvent assists in the imidization reaction in two ways, making the chains mobile and releasing the active groups that participate in the rigidifying imidization reaction. Since the 100 µm film possesses the lowest amount of solvent, the chain mobility is slightly lower in this system which might be the reason for the shift. The changes in the behavior for 500 µm and 250 µm samples occur nearly at the same time.

Similar to the drying behavior, the final birefringence value increases with decreasing thickness. All these observations are in good agreement with the literature. [89,91,95,124,126,128,130,246,247]

5.3.4 Influence of drying temperature

It is possible to control the processing mechanisms and fine tune the final properties of polyimide films by changing the drying temperature. The influence of drying temperature was investigated by using five different temperatures, 100°C, 120°C, 140°C, 160°C and 200°C for 4 hours, followed by temperature increase to 200°C for the next 4 hours. Real-time data for weight, thickness, surface temperature and in-plane and out-of-plane birefringence values were measured during the process. The experiment conditions are summarized at the Table V-1.

Table V-1 Temperature profiles applied

Name	Drying Temperature (4 hours)	Imidization Temperature (4 hours)
PI-100/200	100°C	200°C
PI-120/200	120°C	200°C
PI-140/200	140°C	200°C
PI-160/200	160°C	200°C
PI-200/200	200°C	200°C

Weight change (%) during the overall process for different drying temperatures is shown in Figure V-12. Figure V-12-b focuses on the first 2000 seconds of the process where majority of the solvent evaporation took place. As expected, increasing the temperature leads to higher rate of weight loss. Also

higher temperatures result in lower weight that indicates more solvent is removed from the medium at this stage. Figure V-12-c focuses on the temperature increase region after 4 hours of drying. All the samples that had different drying temperature were increased to 200°C to finalize the imidization reaction. The weight loss on the 100°C and 120°C is apparent and the 140°C, 160°C, 200°C samples does not exhibit this decrease which indicates the solvent evaporation took place at earlier stages at higher temperatures. The percent weight changes also indicated that the higher temperature drying results in the lower solvent content remaining in the films.
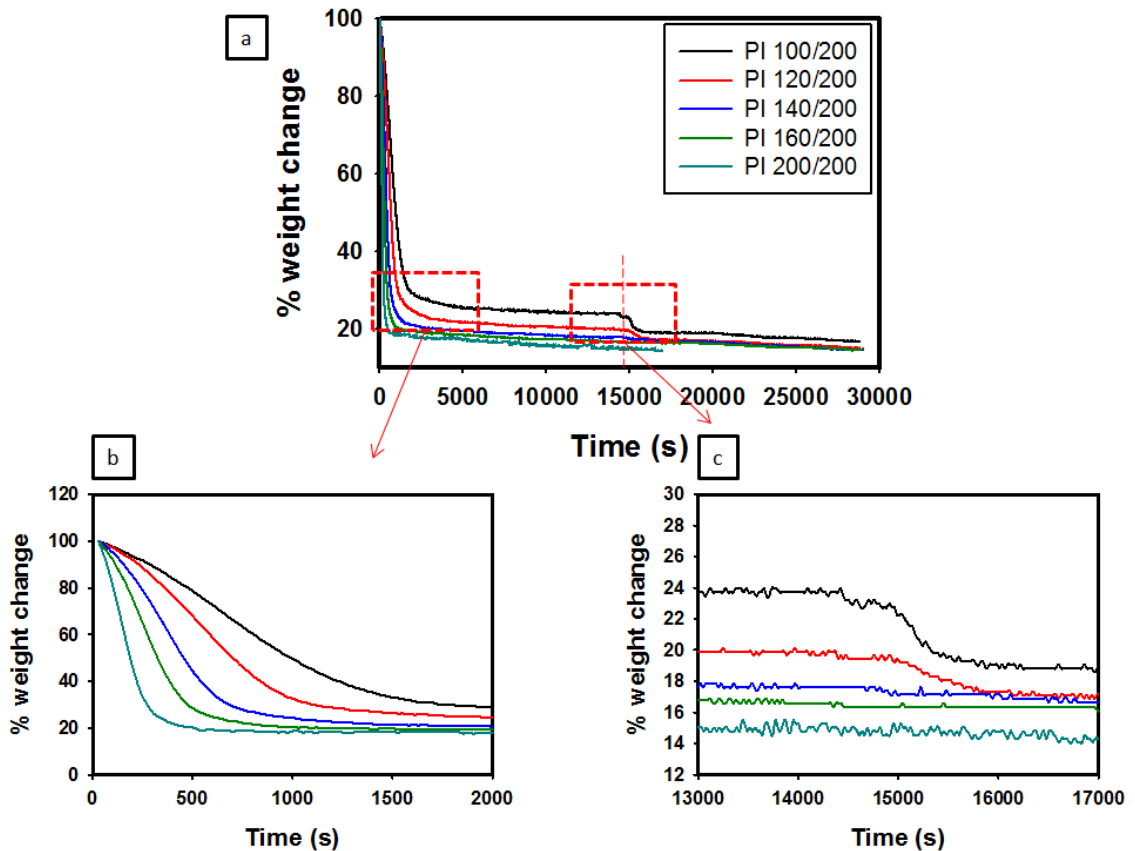
Figure V-12Effect of drying temperature on % weight change on imidization process

Thickness change during the initial stages of the process for different drying temperatures is shown in Figure V-13. Similar to weight loss, the rate of thickness decrease is higher for the higher drying temperatures. Similar to previous observations, when the temperature was increased to 200°C for imidization reaction to take place, no change in the thickness values was observed for different temperatures (inset graph in Figure V-13). Since the weight loss (Figure V-12) indicates the evaporation of solvent for the lowest two drying temperatures100°C and 120°C, the thickness values for these temperatures should also decrease slightly. Again, laser displacement sensors failed to detect the thickness change during this stage. The final thickness values for 100°C, 120°C, 140°C, 160°C and 200°C were measured as 36μm, 37μm, 34μm, 33μm and 28μmrespectively via off-line thickness gage.
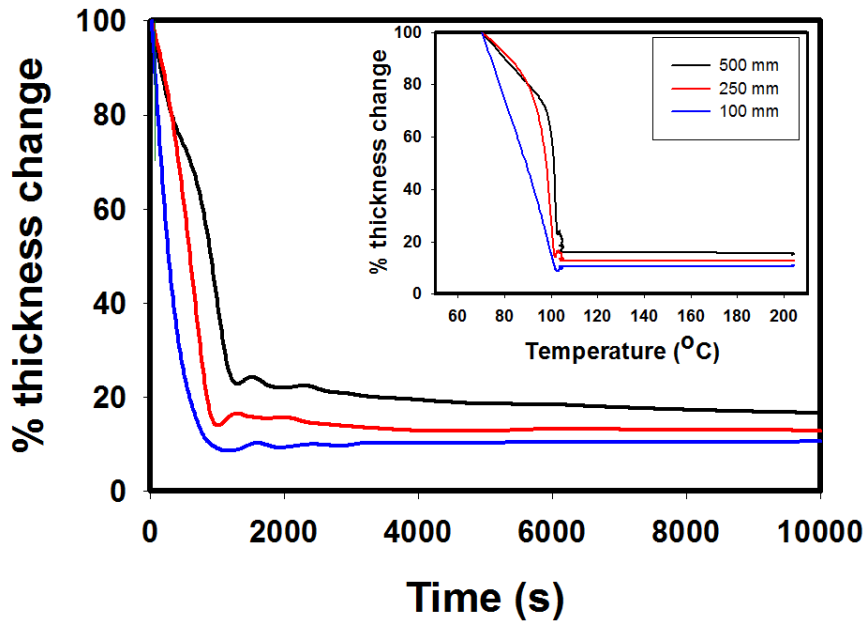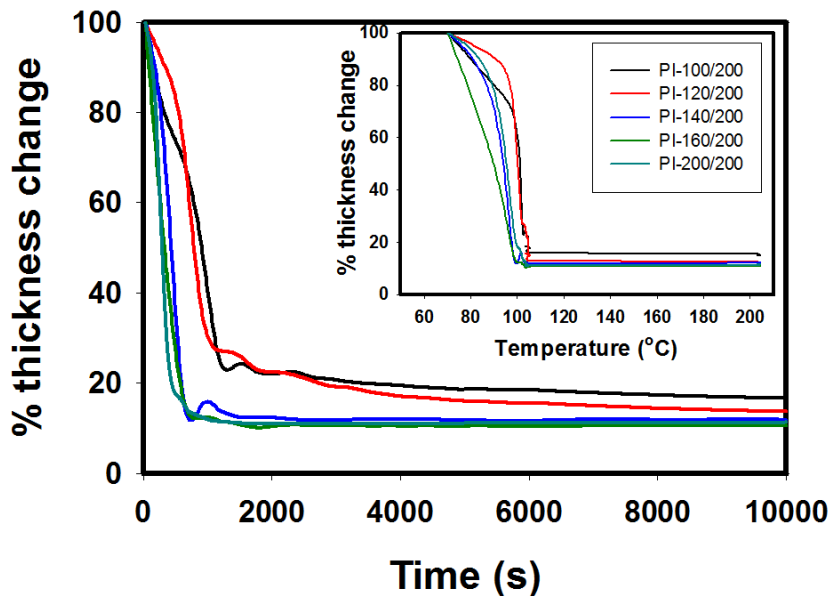

Figure V-13Effect of drying temperature on % thickness change during imidization process

In-plane and out-of-plane birefringence developments for all drying temperatures are shown in Figure V-14-a. Overall; the in-plane birefringence remained nearly zero for all samples and out-of-plane birefringence increased with the increasing drying temperature throughout the process.
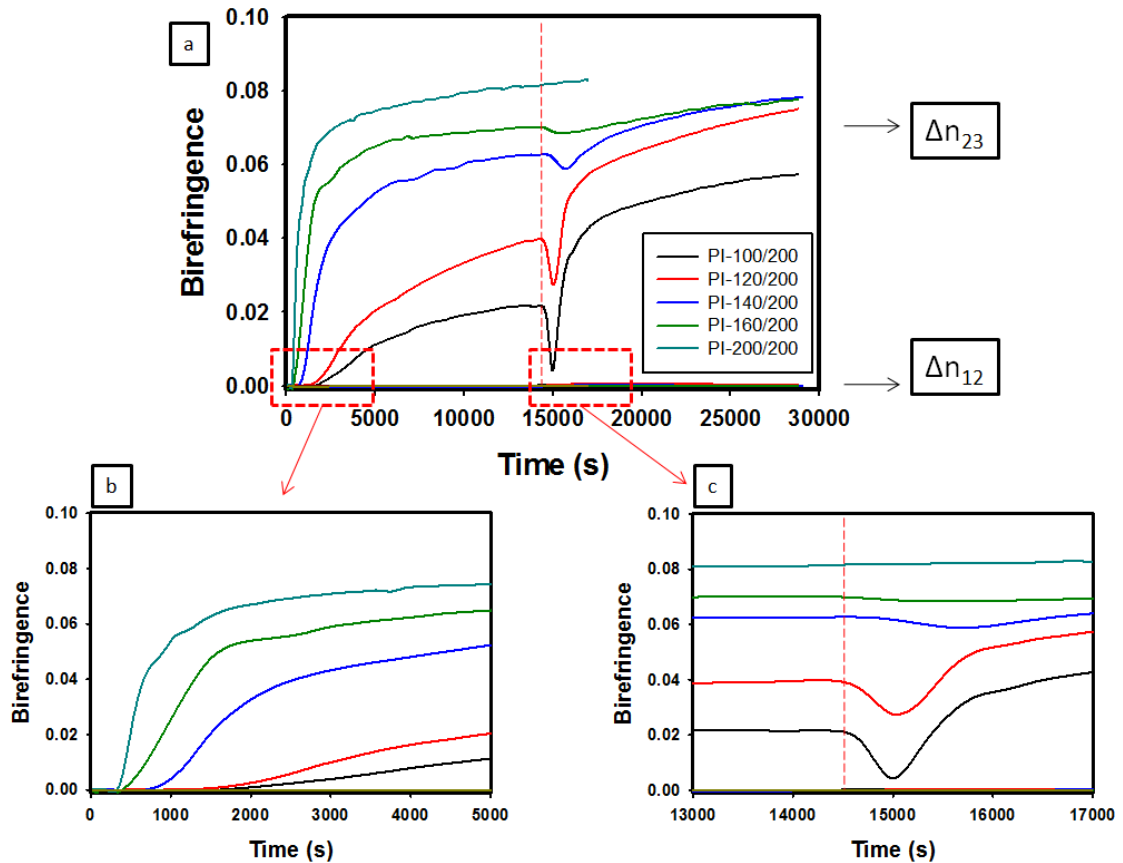
Figure V-14Effect of drying temperature on in-plane and out-of-plane birefringence development during imidiziation process

Figure V-14-b shows the initial 5000 seconds of the process where the cast solutions were dried at different temperatures. The 100°C sample is below the imidization temperature and 120°C is the onset temperature for imidization reaction. The imidization reaction is fastest at150°C, so 140°C and 160°C were

selected because they were just above and below of this value. Continuous

200°C was applied during the last experiment. The evaporation of solvent and

simultaneous imidization reaction occurred at the same time for the samples

dried at 140°C, 160°C and 200°C. The development of the out-of-plane

birefringence during this experiment had two main reasons. The first one was the

evaporation of the solvent and the shrinkage of the film in the thickness direction

since it was constrained in the x-y plane. This increase is induced by the

orientation of the polymer chains parallel to the film surface as mentioned

earlier.[89,91,95,124,126,128,130,246,247] The second reason is the simultaneous

imidization reaction for the temperatures higher than 120°C. Both of these

processes decreased the mobility of the polymer chains and the relaxation times

were much higher as the drying temperature was increased and orientation

behavior dominated.

Figure V-14-c shows the region where the set temperature was increased

to 200°C for imidization reaction to occur. For the 100°C and 120°C drying

temperatures, the out-of-plane birefringence value initially decreased because of

the plasticization effect due to the decomplexed solvent molecules. However as

the temperature continued to increase, the rate of imidization increased and

dominated the orientation development. The samples dried at 140°C and 160°C

showed very small relaxations, indicating the evaporation of the majority of the

solvent molecules took place earlier in the process and the evaporation of the

remaining solvent was not enough to enhance enough chain mobility to decrease

the orientation levels substantially, as seen on the lower drying temperatures (100°C and 120°C).

Similar to the drying behavior, the final birefringence value increased with increasing drying temperature. All these observations are in very good agreement with the literature. [89,91,95,124,126,128,130,246,247]

5.4   Discussion

The details of imidization process are summarized in Figure V-15. At point a on the graph (t=0 seconds) the dilute PAA solution includes both free and H-bonded solvent molecules. Between points a and b, rapid weight loss indicates the evaporation of the non-bonded free solvent molecules from the medium. At point b, the rate of weight loss becomes very small and evaporation decreases substantially. During this stage a drying front that separates the liquid region from the glassy region starts to enter into the birefringence measurement area in the direction of air flow. As more solvent evaporates, from point b to c, polymer solution solidifies and starts to support the stresses formed during drying. Drying front and the glassy region travels through the film and passes from the birefringence measurement area. At this stage the relaxation times are slowed down and as a result out-of-plane birefringence value continues to increase, indicating orientation of the PAA molecules parallel to the film surface. At point d, the polyamic acid film is formed that has substantial solvent content in it. These solvent molecules form complexes with PAA chains. At this point, the T_g of the

209

system increased to the ambient temperature due to evaporation of the non-bonded solvent and the chain mobility decreases considerably leading to leveling off of out-of-plane birefringence. There is very little or no imidization up until this point. When the temperature is increased right after the point d, the bound solvent molecules start to decomplex from the PAA chains and travel through the thickness to the surface of the film and evaporate. The decomplexed solvent molecules spend some time in the medium as they travel and this reflects as a time lag on the weight loss. Travelling free solvent molecules and increasing temperature plasticize the environment which result a decrease in the out-of-plane birefringence up until point e. At this point, the rate of the imidization reaction increases significantly because the evaporation of solvent increases the chain mobility and exposes the reactive ends for the imidization reaction. Carboxylic acid and amide groups become active as the decomplexation continues from the PAA chains. The rapid formation of the rigid polyimide chains and their orientation parallel to the film surface started to dominate the relaxation induced by the solvent evaporation and water formation due to the reaction. It is clear from the graph that the imidization induced molecular orientation and solvent evaporation occurs simultaneously, because, while birefringence is increasing after point e, the weight continues to decrease slightly. At certain imidization conditions, it is apparent that the drying induced orientation is lost completely when the temperature is increased to imidization temperature. As the experiment reaches point f, the weight loss and birefringence increase level off

as the T_g increases and chain mobility diminishes. At point f, most of the solvent evaporated and the conversion to polyimide is about 90%.
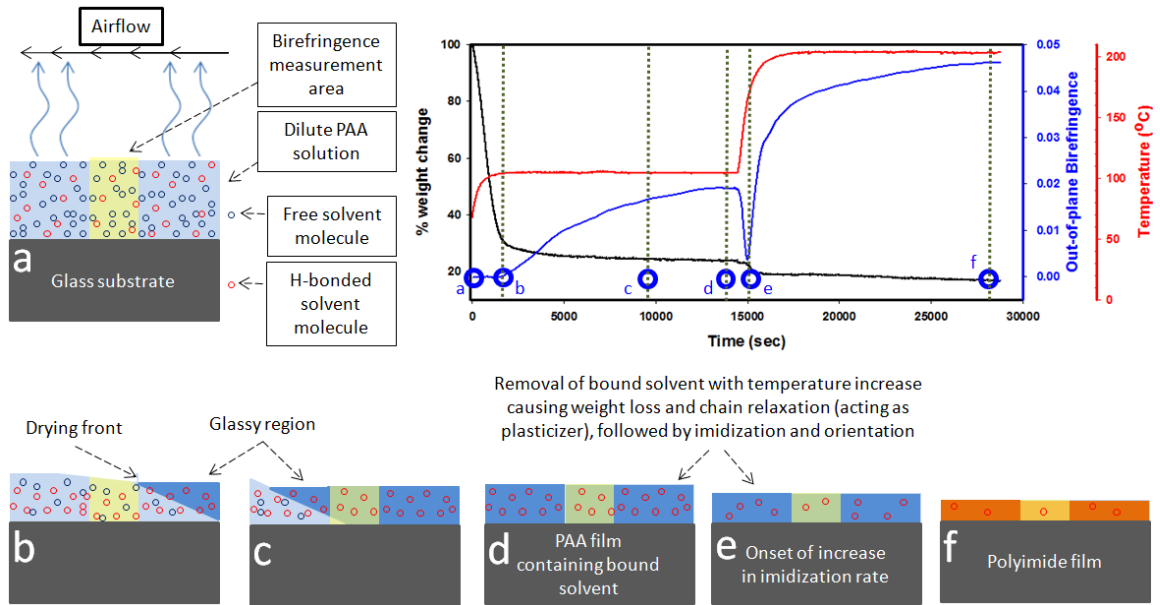
Figure V-15 Overview of the process

5.5   Conclusions

The dynamic relationship between the relaxation and chain orientation has been observed real-time on the imidization process of PMDA-ODA/NMP solution. At low temperature drying stage (T<120°C), orientation occurs due to preferential orientation of polymer chains parallel in the plane of the film. At early stages of imidization (120°C<T<150°C) temporary decrease of birefringence due to chain relaxation caused by the evaporation of the decomplexed solvent molecules was observed. At higher temperatures (T>150°C) optical anisotropy development

dominates due to decreased chain mobility as a result of imidization reaction and increasing T_g.

It was shown how this competition between the two events was affected independently for each stage (drying, transition and imidization) in the imidization process by changing the processing parameters. The level of orientation development, weight loss and solvent evaporation was affected by the changing processing conditions such as initial casting thickness and drying temperatures. This study showed that it is possible to fine tune the final orientation level during the drying and imidization stages simply by changing the processing conditions without the necessity of post-processing techniques.

CHAPTER VI

REAL-TIME IMIDIZATION KINETICS: RHEO-OPTICAL

MEASUREMENTS COUPLED WITH IR DICHROISM

Physical and chemical changes including chemical conversion, bound solvent and chain orientation that take place during thermal imidization of uniaxially constraint PMDA-ODA polyamic acid precursor film was investigated up to 200°C. Real time measurement system that combines true stress, true strain, in-plane birefringence and temperature with polarized ultra-rapid scan polarized FT-IR spectrometry (URS-FT-IR) was used. Upon heating, initially isotropic solution cast film developed stress and birefringence from the beginning while the solvent is decomplexed and evaporated. At a critical temperature (~130°C) onset of imidization reaction was observed as stress going true a maximum. Beyond this point, the evaporation and conversion took place simultaneously with steady increase in birefringence. At the end of the experiment, 80% conversion is achieved with 3% bound solvent remaining in the system.

6.1   Introduction

Polyimide films are being used in harsh industrial applications including automotive, aerospace and electronics due to their excellent thermal stability, high mechanical strength and chemical resistance.[50,51,53,222–224] High quality polyimide films are produced via two-step process:[39–41,225,226] First, a precursor polyamic acid (PAA) is synthesized that is soluble in polar, high boiling point solvents such as NMP (N-Methyl-2-pyrrolidone), DMAc (Dimethylacetamide) and DMF (Dimethylformamide).[11] In the second step, PAA is converted to polyimide through thermal imidization.[4,5,225] Thermal imidization of PAA is a three step process, where PAA solution is first cast on a substrate followed by formation of partially dried film and finally thermal treatment to form polyimide film.[24,211,227] For PMDA-ODA in NMP system, imidization reaction starts at 120°C and conversion is fastest at 150°C.[18] At 200°C, 90% of the conversion is achieved and the temperature needs to be increased to 300°C - 450°C for full conversion and complete evaporation of the bound solvent.[4]

Imidization reaction is a multi-step complex process where solvent evaporation, chain orientation, chemical conversion and water loss due to the chemical reaction, all take place often concurrently (Figure VI-1). [32,102,228,241–245] Because of this complexity, it is challenging to predict the final properties of polyimide films and how they are affected by the process conditions particularly optimization of temporal profile of thermal treatment. So far, the polyimide films were characterized by offline characterization techniques often after all these

interrelated physical and chemical changes took place. [7,13,99,105,114,229–231] Even though important details were gained from these observations, details of temporal interrelationships between physical/chemical phenomena remain unclear. As a result, off-line characterization techniques may be misleading as one dominant step can hinder the details of the other steps during the complicated structural/mechanistic developments.
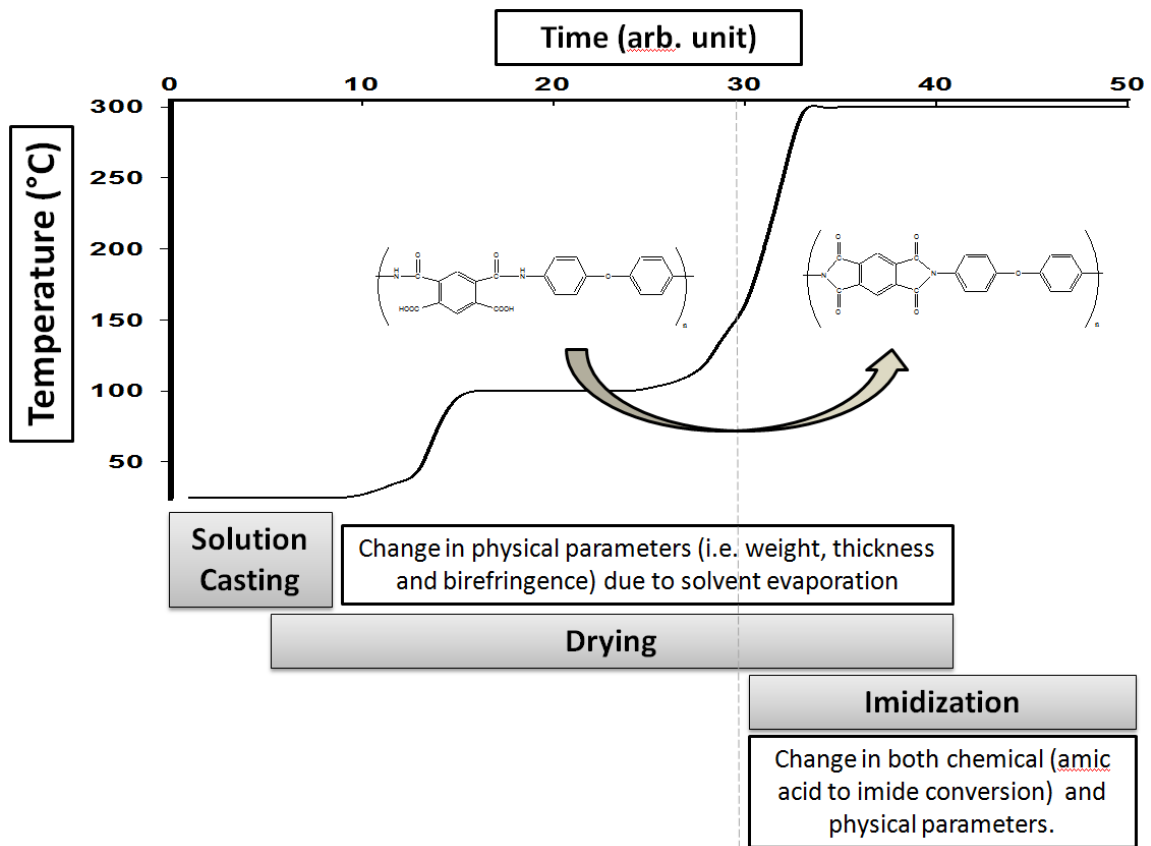
Figure VI-1 Complexity of imidization: Simultaneous solvent evaporation and imidization

Low temperature drying of PAA solution results in the formation of PAA films with bound solvent content 30-50% by weight. [26,27] Model compound

studies revealed the PAA can form complexes with the polar solvent molecules via hydrogen bonding with the ratios of 4:1 (solvent:PAA repeat unit) and 2:1 (solvent:PAA repeat unit) depending on the processing conditions.[18,26–31] There are four possible hydrogen bonding sites on the repeating unit of the PAA chains, two carboxylic acid groups and two amide groups with two distinct thermal stabilities, amide group having the lower bonding energy. When the temperature is increased for imidization reaction, the bound solvent starts to decomplex from the PAA chains starting from the amide groups. [28,29] During decomplexation, the unbounded solvent molecules release the active groups for reaction to occur and cause plasticization as they travel through the thickness to evaporate. The T_g of the medium increases gradually due to evaporation of solvent and imidization reaction, that forms more rigid imide groups compared to amic acid groups. [23] PAA films are generally constrained uniaxially or biaxially to prevent shrinkage during imidization and this causes development of internal stress and spontaneous molecular orientation. [27,92,96,108,109,111,232–235] This orientation causes polyimide films to develop mechanical, thermal and optical anisotropy in the plane or through the thickness direction, depending on the processing conditions and constraints imposed on the films.[8,25,85,93,98,106,107,236–238]

IR spectra are utilized to determine imidization reaction, bound solvent amount and chain orientation (via polarized IR spectra). The chemical conversion commonly is tracked via formation of imide peaks at 1780 cm^{-1} (-C=O asymmetric stretching) 1380 cm^{-1} (-CN stretching) and 725 cm^{-1} (-C=O bending). The solvent amount in the system can be tracked with the 1408 cm^{-1} peak that

belongs to the NMP CH$_2$ bending.[27,28] Peaks centered at 1500 cm^{-1} and 1005 cm^{-1} belong to aromatic ring, which are not affected during the chemical reaction. These are used as an internal standard for calculations to compensate for the thickness reduction due to solvent evaporation. The ratio of the selected imide peak to the reference aromatic ring peak is normalized with the same ratio of the fully imidized film to calculate total conversion (Equation 1).[2,6,18,27,85,102] Polarized IR spectra was also utilized to determine the orientation development and level of anisotropy through dichroic ratio of the selected peaks.[248,249]

$$Degree\ of\ imidization = \frac{\left(\dfrac{1380\,cm^{-1}_{T}}{1500\,cm^{-1}_{T}}\right)}{\left(\dfrac{1380\,cm^{-1}_{T'}}{1500\,cm^{-1}_{T'}}\right)} \tag{1}$$

In this chapter, we report direct measurements of the real time imidization reaction kinetics for the thermal imidiziation of the solution cast and dried PAA thin films using a uniaxial stretcher instrumented with ultra-rapid-scan FT-IR equipment and spectral birefringence. This system allowed us to measure the real-time mechanical behavior (thickness, temperature, true strain and true stress), optical properties (in-plane birefringence and IR Dichroism for selected peaks) and chemical changes (evaporation of bound solvent and imidization reaction). Such a complete study is required to completely understand the complex molecular mechanism taking place during the thermal imidization of polyamic acid films with high content bound solvent (30-50%).

6.2   Experimental

6.2.1   Materials

Polyamic acid solution (PMDA-ODA, 15 weight % solids in NMP) purchased from Sigma-Aldrich (CAS Number: 25038-81-7) and used as received. The solution was cast on a commercial solution casting line on top of a carrier. 6" wide casting blade with 50 µm initial cast thickness was used and the solution was dried at 40°C for 1 hour. Dried thin samples (thickness = 13 µm) were peeled off from substrate and big dog-bone shaped samples were punched out from cast film. The dimensions of the films that were used for thermal imidization were 40 mm in length (between the grips) and 40 mm in width.

6.2.2   Measurement system

The details of the measurement system (Figure VI-2) used in this experiment was reported elsewhere.[239] This system is a combination of a uniaxial stretcher with two IR spectrometers generating and determining two full spectra with polarizations oriented along the stretching (vertical) and along the transverse direction (horizontal) simultaneously at 300 spectra/second.
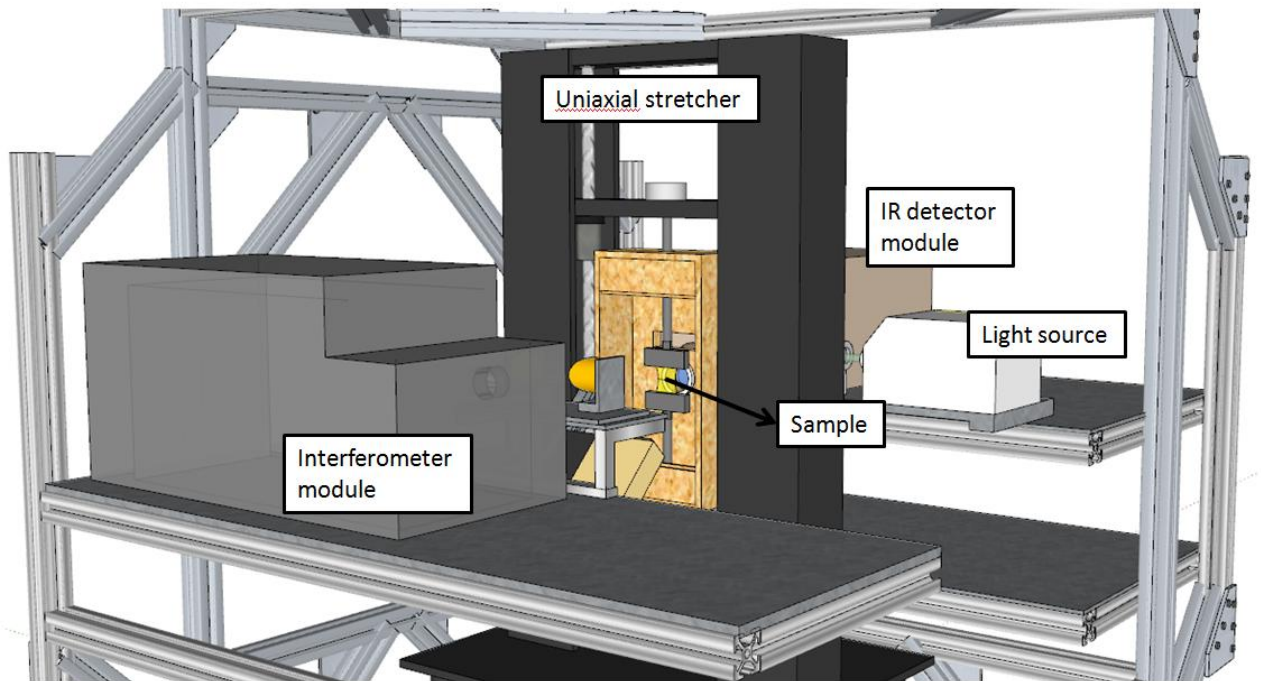
Figure VI-2 Uniaxial stretcher coupled with URS-FTIR

The uniaxial stretcher is equipped with sensors and a heating chamber to measure the load, temperature, width (through laser micrometer at mid symmetry plane) and optical retardation (Γ) of the sample (through built in spectral birefringence system) during heating, stretching, relaxing or annealing up to temperatures 200°C (Figure VI-3). From the measured raw data, real-time true strain (and Hencky strain), true stress, thickness and in-plane birefringence (Δn_{12}) can be calculated using the equations below (Equations 2-7). For the birefringence calculations, we used the spectral birefringence technique that allows the measurement of the birefringence at the full visible wavelength range and the values are reported at 546 nm.[141,143–145,186,187,189,190,192–203,239] Equation 2 (constant density) and equation 3 (transverse isotropy) are the assumptions used

to calculate the real-time thickness data through the width measurements. The data verification on the thickness calculation can be found in the previous publications. [140,186–191] Even though the density changes during imidization reaction due to solvent evaporation and chemical conversion, offline measurements provided the error contributed by this assumption on the thickness calculation is small for these thin films (<10%).

$$D_0 W_0 L_0 = D_t W_t L_t \qquad (2)$$

$$\frac{W_t}{W_0} = \frac{D_t}{D_0} \qquad (3)$$

$$True\ strain = \frac{Elongation}{Initial\ lenght} = \frac{L_t - L_0}{L_0} = \frac{\Delta L}{L_0} = \left(\frac{W_0}{W_t}\right)^2 - 1 \qquad (4)$$

$$Hencky\ strain = L_n\left(\frac{L_t}{L_0}\right) = L_n\left(\frac{W_0}{W_t}\right)^2 \qquad (5)$$

$$True\ stress = \frac{Force}{Cross\ sectional\ area} = \frac{F_t}{W_t D_t} = \frac{F_t}{\left[\left(\frac{W_t^2}{W_0}\right)D_0\right]} \qquad (6)$$

$$\Delta n_{12} = \frac{\Gamma}{D_t} = \frac{\Gamma}{\left(\frac{W_t D_0}{W_0}\right)} \qquad (7)$$

where; D_0 = initial thickness,

                 W_0 = initial width,

                 L_0 = initial length,

                 D_t = instantaneous thickness,

                 W_t = instantaneous width,

                 L_t = instantaneous length,

F_t = instantaneous force,

Γ = instantaneous retardation,

Δn_{12} = instantaneous in-plane birefringence.
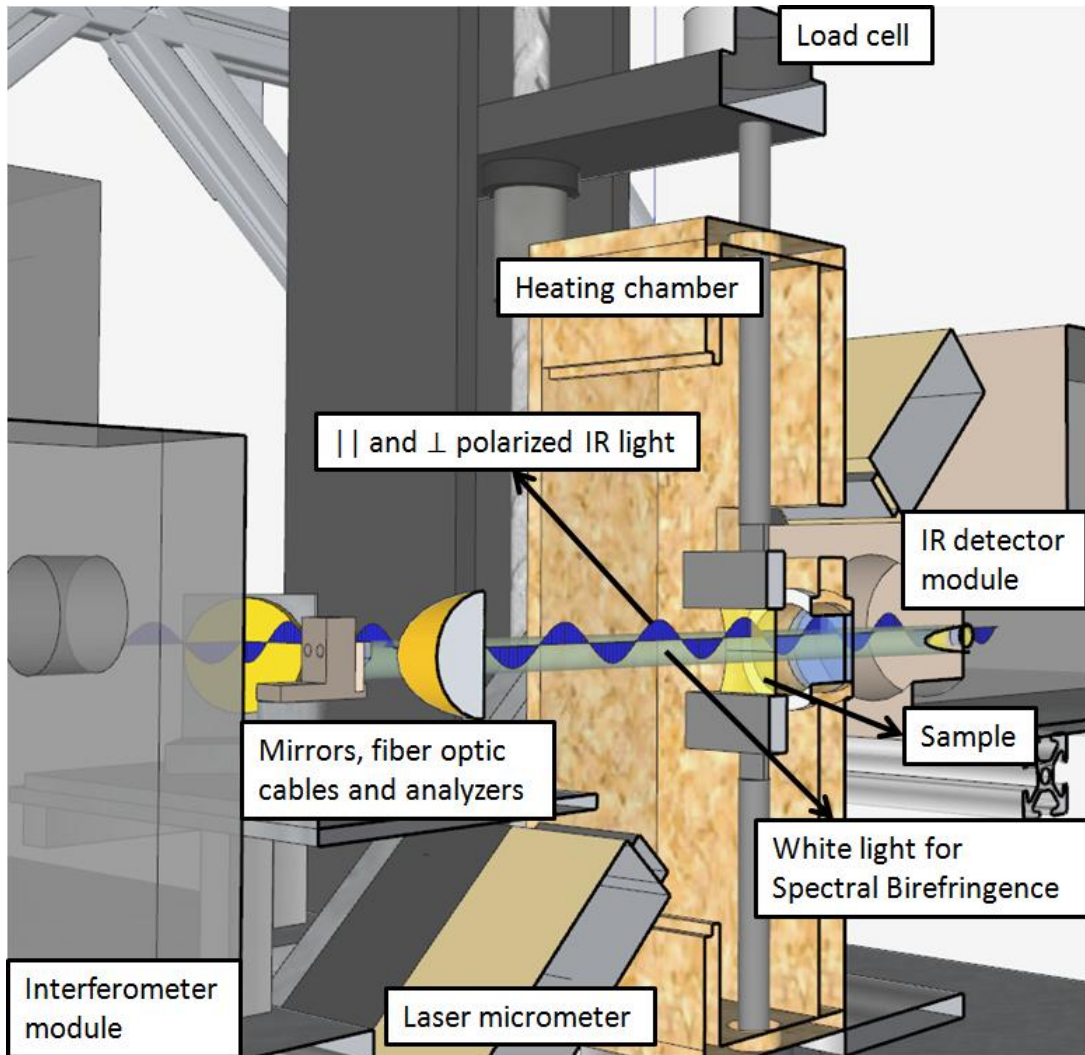
Figure VI-3 Infrared module, detector module, sample and sensor positions

The ultra-rapid-scan FTIR (URS-FTIR) unit is mounted on an independent frame surrounding the uniaxial stretcher (Figure VI-2). The interfometer is a

custom build design that is capable of generating 300 complete spectra/second with a wedged rotating disk mirror.[239] The sample inside the heating chamber is exposed to non-polarized IR beam through KBr windows in transmission mode. The parallel and perpendicular polarizations are separated in the detector unit, which provides us to analyze the both polarizations simultaneously and calculate the dichroic ratio (D) and orientation functions (*f*) of the selected molecular groups by integrating peak areas for parallel ($A_{\parallel}$) and perpendicular ($A_{\perp}$) polarized IR absorbance values Equations 8-10 shows the calculations used for the uniaxially oriented samples.

$$D = \frac{A_{\parallel}}{A_{\perp}} \tag{8}$$

$$f = \frac{(D-1)}{(D+2)} \frac{(D_o+2)}{(D_o-1)} \tag{9}$$

$$D_o = 2 \cot^2 \psi \tag{10}$$

where ψ is the transition moment angle of a specific vibration with respect to polymer chain. [206,207]

The data from uniaxial stretcher (rheo-optical measurements of true stress, true strain and birefringence) and URS-FTIR (polarized spectra for chemical changes and orientation function calculations) are time stamped and the two data sets are synchronized by post-processing. Furthermore, certain peak analysis required the deconvolution of the peaks for more accurate calculations, due to shoulders or overlapping on the multiple peak areas, which was done manually for selected number of spectra.

6.3   Results

A control experiment was utilized to compare both the machine and material performance before and after the imidization process. Two samples were prepared by solution casting of PAA/NMP solution and dried at 40°C for 1 hour. From this sample 13 μm PAA and fully imidized samples prepared. For imidization the PAA samples were kept at 175°C for 45 minutes and 350°C for 1 hour inside a vacuum oven. The IR spectra were measured for these samples using bench-top FT-IR spectrometer (Thermo-Nicolet 380 FT-IR). Figure VI-4 shows the changes in the peak positions those specifically belong to PAA and PI between the wavenumbers 1800-600 cm^{-1}. After the thermal imidization, no trace of PAA and solvent was observed. This fully imidized film was used as a reference for partially imidized films for the calculation of the imidization conversion for the real-time experiment. 1780 cm^{-1} peak is used to calculate the chemical conversion, the peak at 1408 cm^{-1} is used to calculate the amount of residual solvent in the system and peak at 1010 cm^{-1} is used as internal thickness reference for the calculations and marked on the Figure VI-4.
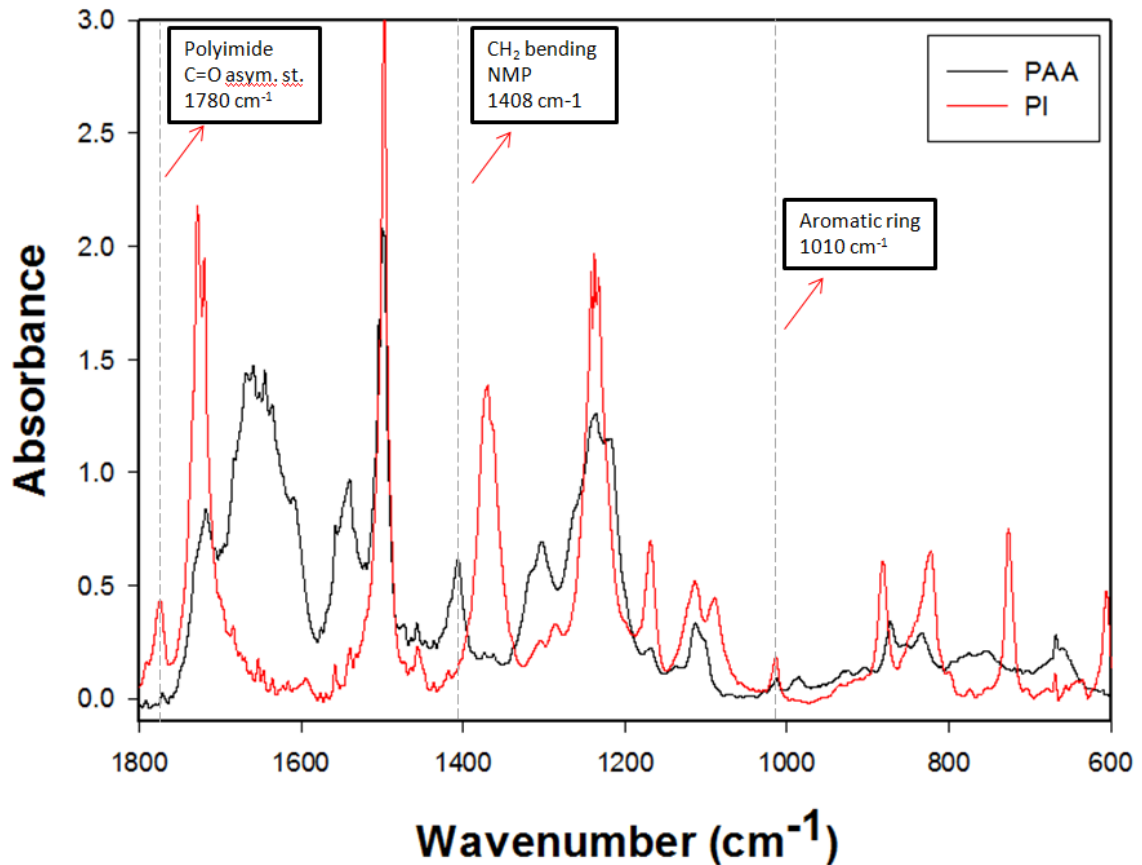
Figure VI-4 Polyamic acid to polyimide conversion, selected peaks to quantify the solvent evaporation and chemical conversion.

Real-time thickness, temperature, true stress, in-plane birefringence and IR spectra are measured with the explained measurement system for PAA thermal imidization. Partially dried PAA samples are clamped uniaxially in the machine direction and inserted inside the system. The sample is attached roughly with very small force (<0.1 N). The temperature is increased from room temperature (~20°C) to imidization temperature 200°C and it is kept at this temperature for 10 more minutes (green curve in Figure VI-5).
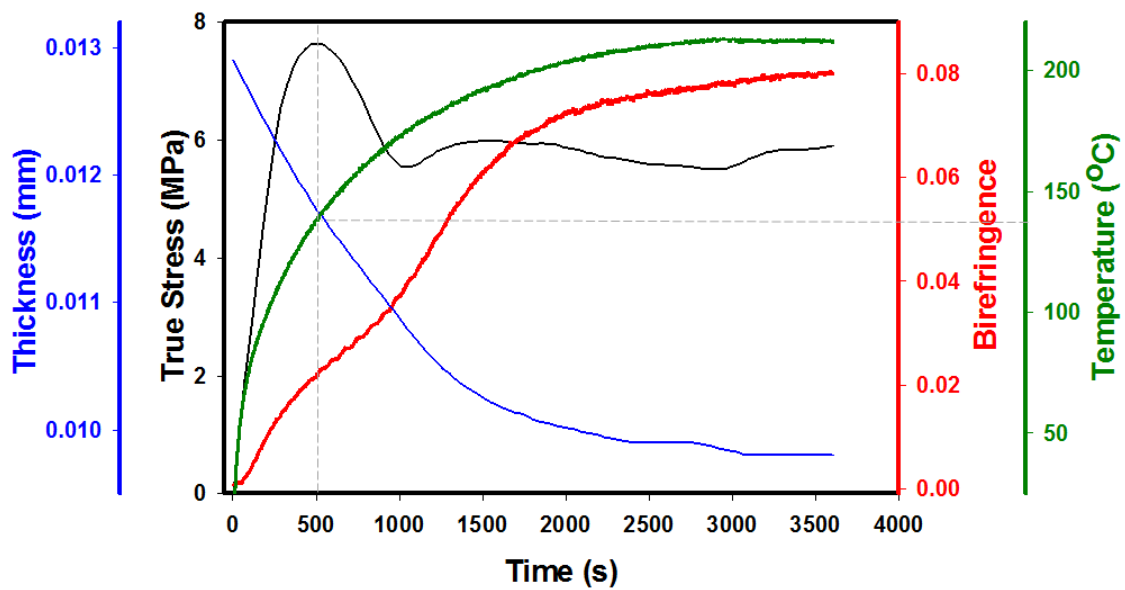
Figure VI-5 Real-time Rheo-optical data showing true stress, birefringence, thickness and temperature change during the thermal imidization reaction

Rheo-optical measurements during the imidization reaction are shown in Figure VI-5. The thickness of the sample decreases gradually as the temperature increases. This is due to decomplexation and evaporation of the bound solvent from the film. At the same time, true stress and birefringence increases from the beginning of experiment. The stress and orientation increase is attributed to the development of shrinkage due to evaporation of the bound solvent as film is held constrained at both ends. Imidization reaction is fastest at 150°C and when the temperature approaches that value, the stress goes through a maximum and before leveling off slightly relaxes after this point. At the same critical point, the slope of the birefringence curve decreases, followed by an increase at the same point where the stress levels off. At 200°C, the thickness, stress and

225

birefringence curves also level off as majority of the chemical conversion is completed.

Real-time IR spectra collected through URS-FT-IR equipment during the thermal imidization is shown in Figure VI-6 for 1780 cm^{-1} peak that belongs to polyimide (-C=O asymmetric stretching). Peak height values are color coded so as the height of the peak changes the color associated with that value changes. The equipment is capable of collecting vertical (parallel to the stretching direction) and horizontal (perpendicular to the stretching direction) spectra simultaneously, and both results are plotted on the same graph. The temporal evolution of the peak is shown as a function of time for both polarizations on the top-down view graphs. The onset of imidization is marked on these graphs around 500 seconds, which corresponds to the ~135°C in Figure VI-5 and also corresponds to mentioned regime changes as true stress shows a peak and start a decrease and birefringence slope temporarily decreases and when the stress begin to level off the birefringence start increasing with steeper slope.
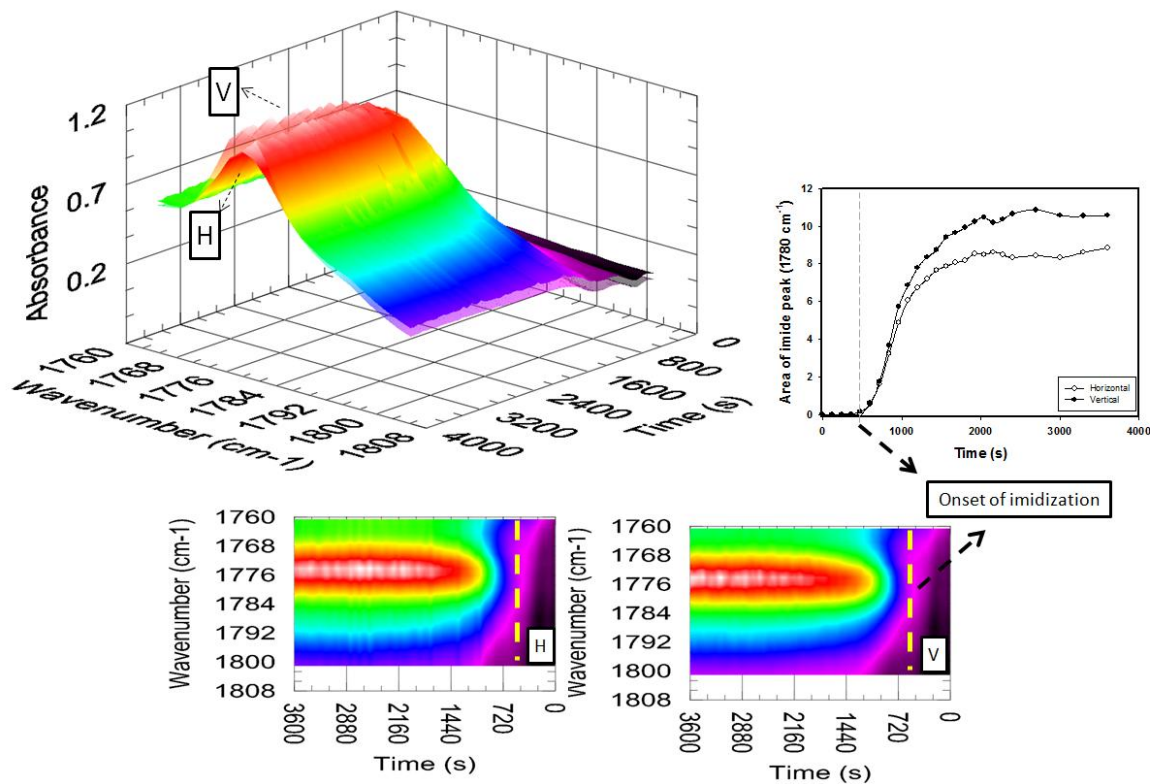
Figure VI-6 Time evolution of 1780 cm^{-1} peak for polyimide C=O asymmetric stretch during imidization reaction.

The vertical spectra are plotted semi-transparent on top of horizontal spectra shown as solid surface. The height and area difference of the two polarizations can be observed at the inset graph in Figure VI-6 for the 1780 cm^{-1} peak. The transition moment angle of this chemical group is parallel to the polymer chain, which indicates the preferential orientation of the polymer chains in the machine direction. [250]

For the same experiment, the range from 1320 cm^{-1} to 1470 cm^{-1} is shown in Figure VI-7. In this range, the peak centered at 1380 cm^{-1} belongs to –C-N stretching of PI and peak centered at 1408 cm^{-1} belongs to CH$_2$ stretching for

NMP solvent. The –C-N peak is saturated and not used for calculations in these experiments. However, the initiation of the imidization can be traced through the appearance of the peak. The NMP peak height decreases as time proceeds and temperature increases due to evaporation of the solvent. This data indicate that the imidization and bound solvent evaporation take place simultaneously, since there is still solvent remaining in the system at the onset of imidization reaction.[23,85,93,98,101,238].
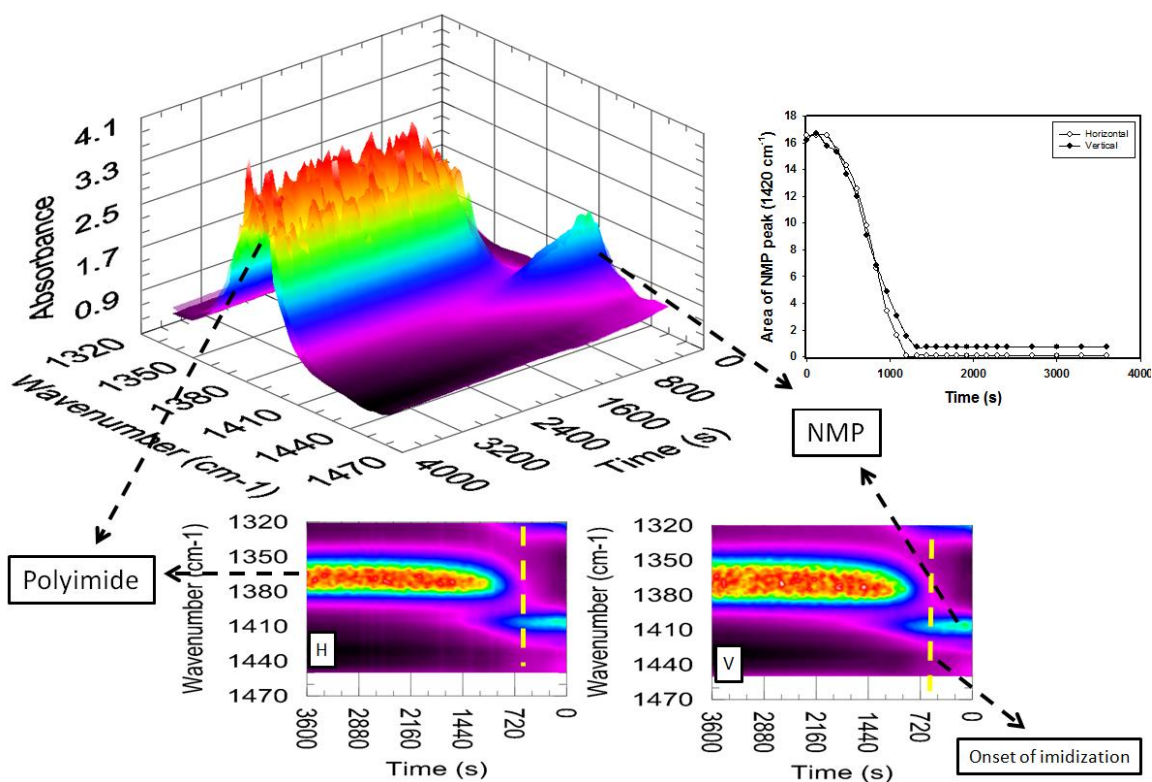
Figure VI-7Time evolution of 1375 cm^{-1} peak for C-N stretching and 1408 cm^{-1} for CH$_2$ stretching for NMP solvent during imidization reaction. The onset of imidization and simultaneous evaporation of solvent and during imidization reaction

The normalization of the imide and amic acid peaks are generally performed using the aromatic peak centered at 1500cm^{-1} as an internal reference. For this study, we used the peak centered at 1005 cm^{-1} instead, because the 1500 cm-1 peak was saturated. Figure VI-8 shows the temporal evolution of the 1005 cm-1 peak. Aromatic ring peaks are also affected by the orientation and we observed a slight difference in the parallel and perpendicular spectra, which can be observed at the inset graph in Figure VI-8. The vertical spectra (transparent curve) is slightly higher compared to the horizontal spectra (solid curve), which indicates the preferential orientation of this group along the stretching direction.[250] Since the reference peak we used also changed during the reaction due to orientation, we used a modified version of the Equation 1, in which we used the averages of the vertical and horizontal absorbance values for the calculations. Equation 11 shows the modified calculation procedure of degree of imidization. For solvent amount calculations, the area of the solvent peak is integrated and the initial and final bound solvent values are determined by the TGA results and the data normalized with respect to these results. The results from these calculations are shown in Figure VI-9 that shows the correlation of imidization and amount of bound solvent in the system.

$$Degree\ of\ imidization = \frac{\left(\dfrac{Average_{\parallel and \perp}1780\,cm^{-1}{}_T}{Average_{\parallel and \perp}1005\,cm^{-1}{}_T}\right)}{\left(\dfrac{Average_{\parallel and \perp}1780\,cm^{-1}{}_T{}'}{Average_{\parallel and \perp}1005\,cm^{-1}{}_T{}'}\right)} \qquad (11)$$
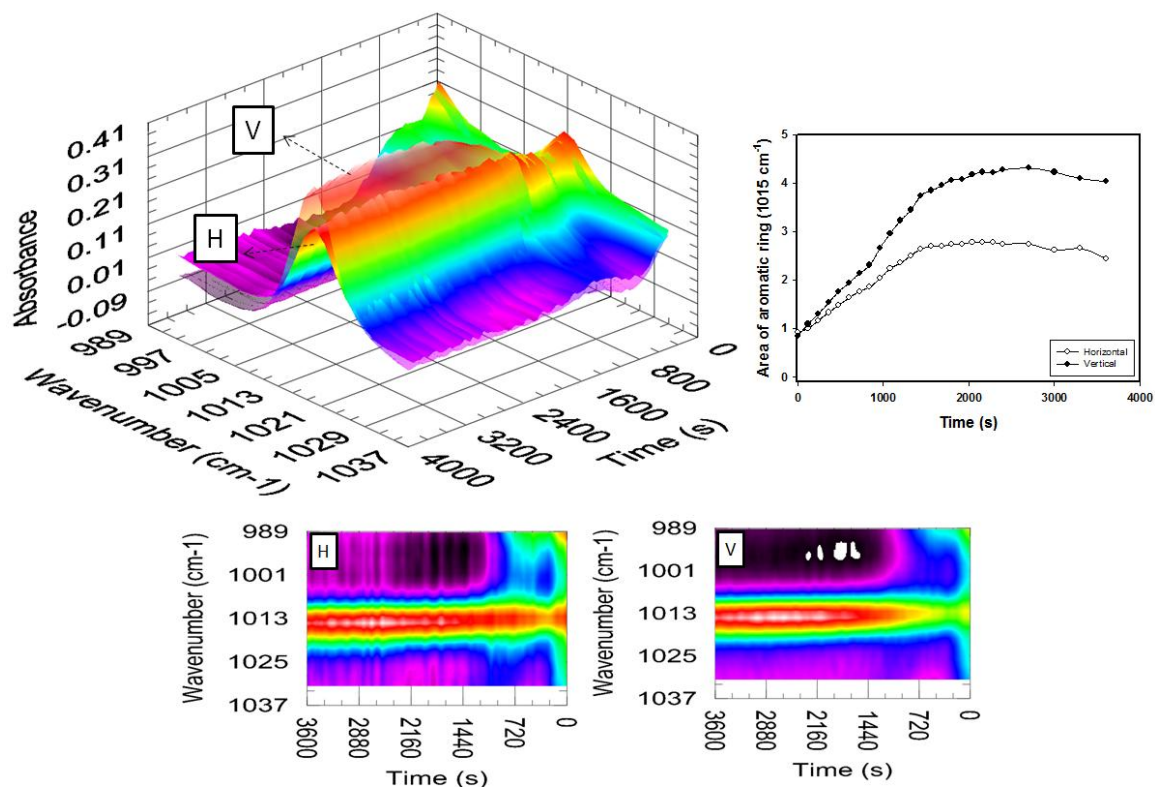
Figure VI-8 Time evolution of 1010 cm-1 peak for aromatic ring stretch during imidization reaction. The average of the H and V spectra of this peak is used as an internal reference

In Figure VI-9, the solvent starts to evaporate first and no imidization is taking place at the early stages. As more solvent evaporates, the imidization reaction starts at 35% bound solvent concentration and gradually accelerates as more solvent evaporates from the system. When almost all the solvent evaporated, the imidization reaction finalizes around 80%. The inset graph shows apparently that the two events are taking place simultaneously.
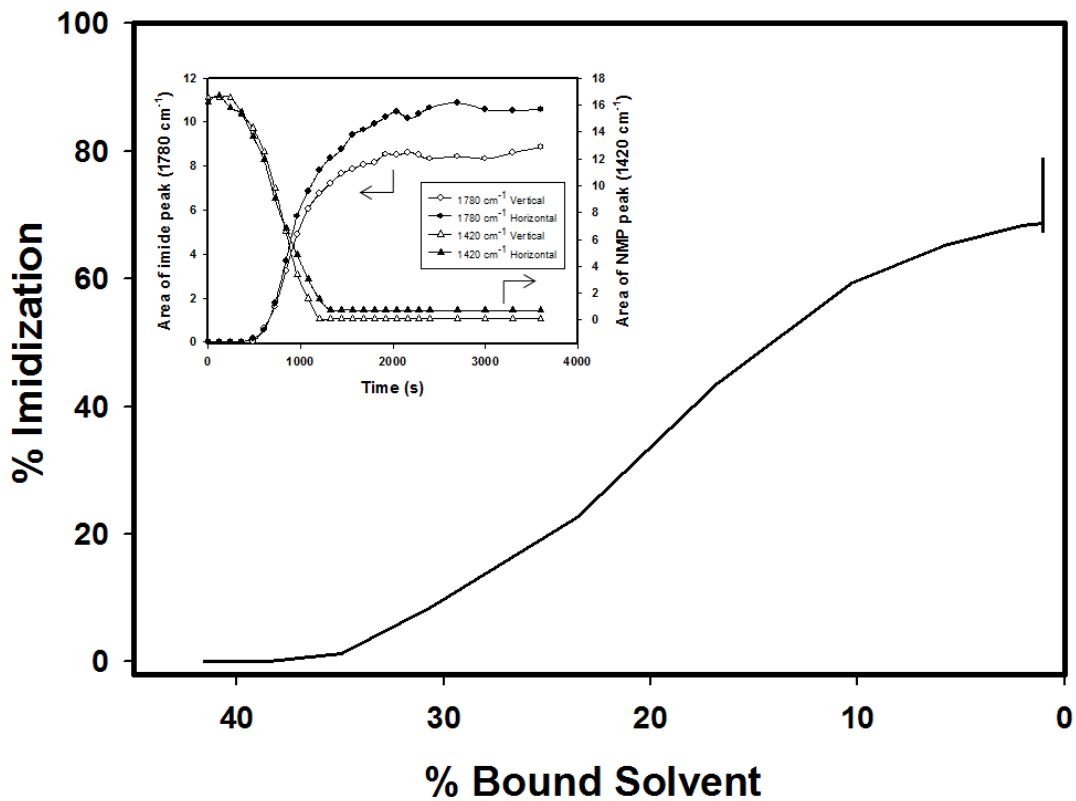
Figure VI-9 % imidization vs % bound solvent

6.4   Discussion

Time synchronized rheo-optical data (true stress and birefringence) and URS-FT-IR data (% imidization and % bound solvent) are combined in Figure VI-10. The first 2500 seconds of the experiment is focused on the graph, as most of the changes take place in this period. The critical regions are marked with gray-dashed lines and indicated "a" through "e".
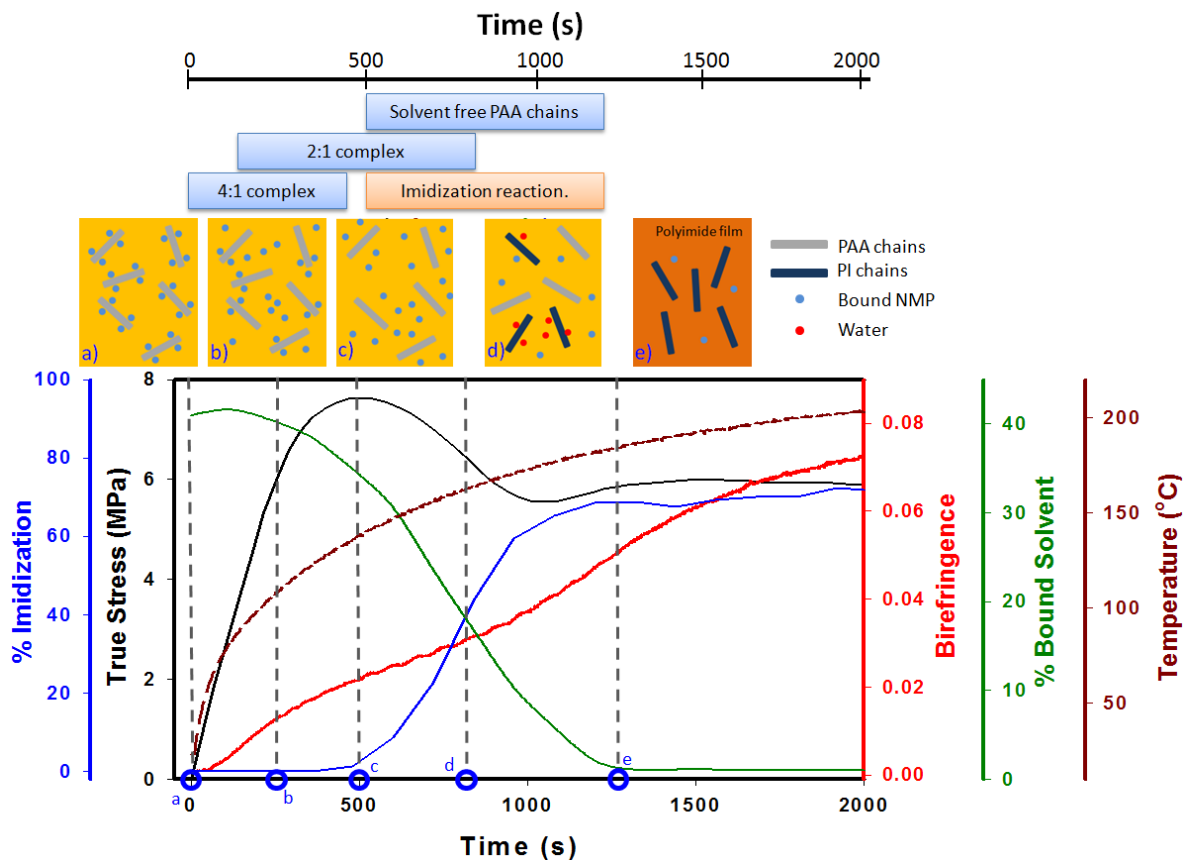
Figure VI-10Molecular mechanism through combined data

Initially, polyamic acid film contains significant amount of bound solvent (4:1 solvent:PAA repating unit) since it was dried a short period of time. From "a" to "b" the temperature (dark red dashed line) increases from room temperature to about 100°C in the first 250 seconds. At this stage, the bound solvent starts to decomplex from the PAA chains and gradually evaporates from the medium as indicated by the slight decrease on the % bound solvent graph (solid green line). As solvent evaporates, the film begins to shrink, however it is constrained uniaxially in the machine direction. This constraint is reflected as internal stress development that can be observed on the true stress (black curve) and

232

birefringence (red curve) increase. No imidization is observed at this stage (blue solid curve) as the temperature is lower than the initiation temperature of the reaction (T<120°C) and there is still considerable amount of solvent in the system blocking the reactive ends (amide and carboxylic acid groups).

The true stress and birefringence continue increasing up until point "c" and onset of imidization is observed. As the temperature increases to ~130°C, more solvent molecules gradually decomplex from the PAA chains and 5% evaporation is observed. The amount of bound solvent at this point is about 35% and majority of these molecules are now decomplexed from the PAA chains and diffuse through to film to evaporate. As they diffuse they plasticize the environment as seen from the slight relaxation at true stress curve and decreased slope change in the birefringence curve between points "c" and "d". After point "c", the temperature approaches to 150°C where the imidization reaction is fastest. The imidization takes off and the evaporation of solvent accelerates. At point "d", the imidization and bound solvent curves intersect, which indicates the two events take place simultaneously. After point "d", the birefringence increases at a higher rate, due to formation of rigid polyimide chains and evaporation of solvent, causing increase in T_g and formation of more rigid imide chains.

At point "e", true stress, imidization and bound solvent curves begin to level off. At this point, majority of the bound solvent evaporated from the medium and only a 2-3 % solvent remained. Imidization also levels off at 80% conversion. Higher temperatures (~300-350°C) are required for complete chemical conversion and remove the remaining bound solvent from the medium. The

birefringence increases at a slower rate after this point and reaches a plateau region around 2500 seconds (Figure 10).

6.5   Conclusions

For the first time real time dynamics and molecular mechanisms of the complex thermal imidization process was investigated by coupling rheo-optical measurements and polarized FT-IR spectrometer. It was observed that, at low temperatures solvent evaporation starts prior to imidization and the two events take place simultaneously as temperature increases. Evaporation of bound solvent causes thickness reduction and since the film is constrained the machine direction, the shrinkage translates into stress and orientation development before the conversion begins. As more solvent molecules decomplex they cause slight relaxation in the system just before leaving the film that was observed by the stress relaxation and change in the trend of orientation development.

CHAPTER VII

CONCLUSIONS

This research provides an in-depth analysis of complex, multi-step thermal imidization reaction, including casting, drying and imidization processes for PMDA/ODA polyamic acid in NMP solvent. Physical and chemical changes happening during the reaction are investigated using newly developed highly instrumented measurement systems. These instruments allow us to observe the dynamic relationship between the bound solvent evaporation that causes relaxation and chain orientation during the imidization.

The first instrument developed is a wind tunnel shaped drying tunnel that is designed to record the real time changes in physical parameters during the drying of solution cast films and coatings. A fully automated spectral birefringence measurement system is incorporated into the design of this machine for the first time. It is sensitive enough to measure very small optical retardation levels (~2-4nm) allowing this machine to be used with wide range of materials including those that exhibit small intrinsic birefringence. This instrument can be used to systematically study the effect of material variables including solvent types and mixtures and solid concentrations, and system variables including temperature, air speed and initial thickness. In addition, the sensors are

sensitive enough to track the changes in the physical characteristics of monomers during photocuring.

Drying and imidization of PMDA-ODA solutions in NMP were investigated by this wind tunnel shaped drying station and real time weight, thickness, surface temperature, in-plane and out-of-plane birefringence were recorded. At low temperature drying stage (T<120°C), the weight and thickness reductions occurred rapidly as a result of solvent evaporation. All the parameters started leveling off while the out of plane birefringence steadily increased and reached a plateau at longer drying times. When the temperature was increased for imidization reaction (T=200°C), additional weight loss accompanied by temporary reduction of birefringence was observed due to evaporation of bound solvent as solvent molecules decomplexed from the polymer chains and plasticized the film. During the latter stage, out-of-plane birefringence rose rapidly as the polymer chains increasingly became oriented with their chain axes were preferentially oriented in the film plane. Throughout the whole process the in-plane birefringence remained zero. For the first time, these real time measurements allowed us to quantitatively show the dynamics between chain relaxation due to evaporation of the decomplexed solvent molecules, and orientation development due to decreased chain mobility caused by imidization reaction and increasing Tg for the PMDA-ODA/NMP solutions. In addition, the dynamics of this interplay was investigated by varying the processing conditions: initial casting thickness and drying temperature.

It was shown how this competition between the two events was affected independently for each stage (drying, transition and imidization) in the imidization process by changing the processing parameters. The level of orientation development, weight loss and solvent evaporation was affected by the changing processing conditions of initial casting thickness and drying temperatures. This study showed that it is possible to fine tune the final orientation level during the drying and imidization stages simply by changing the processing conditions without the necessity of post-processing techniques.

The second instrument developed is a combination of a uniaxial stretcher and a polarized ultra-rapid-scan FT-IR (URS-FTIR) instrument that allows real-time tracking of true stress, true strain, birefringence and IR dichroism of uniaxially stretched/relaxed and/or annealed polymer films. The instrument is not only capable of monitoring physical changes such as chain orientation and crystallization but also monitors the chemical changes and reactions such as imidization. The URS-FTIR makes it possible to investigate very fast deformations at speeds up to 200 mm/min with a data acquisition rate of 300 complete spectra/second. Contribution of different phases to the averaged orientation of the bulk can be calculated, since the in-plane birefringence measurements are coupled with the IR dichroism measurements. This instrument can be used to systematically study the effect of processing variables; most importantly very high stretching rates, but also including stretching temperature, heating rates, stretching and relaxing (or annealing), stretching and retraction and stretching and strain cycling.

For the first time real time dynamics and molecular mechanisms of the complex thermal imidization process was investigated using this equipment. Chemical conversion, bound solvent and chain orientation that take place during thermal imidization of uniaxially constraint PMDA-ODA polyamic acid precursor was recorded up to 200°C. It was observed that, at low temperatures solvent evaporation starts prior to imidization and the two events take place simultaneously as temperature increases. Initially isotropic solution cast film developed stress and birefringence from the beginning while the solvent is decomplexed and evaporated. At a critical temperature (~130°C) onset of imidization reaction was observed as stress going true a maximum. Beyond this point, the evaporation and conversion took place simultaneously with steady increase in birefringence. At the end of the experiment, 80% conversion is achieved with 3% bound solvent remaining in the system

REFERENCES

(1)   Ratta, V. Crystallization, morphology, thermal stability and adhesive properties of novel high performance semicrystalline polyimides, Virginia Polytechnic Institute and State University: Blacksburg, 1999, Vol. PhD.

(2)   Mittal Ghosh, M. K., K. L. Polyimides, Fundementals and Applications **1996**.

(3)   Stone, C. D. A study of the morphology of PMDA-ODA polyimide films, North Carolina State University: Raleigh, 1992, Vol. Doktor of .

(4)   Sroog, C. E. *J. Polym. Sci., Macromol. Rev.* **1976**, *11*, 161–208.

(5)   Sroog, C. E.; Endrey, A. L.; Abramo, S. V; Berr, C. E.; Edwards, W. M.; Olivier, K. L. *J. Polym. Sci., Part A Gen. Pap.* **1965**, *3*, 1373–1390.

(6)   Bessonov Zubkov, V. A, M. I. Polyamic acids and poylimides. Synthesis, transformations and structure **1993**.

(7)   Bershtein, V.; Sukhanova, T.; Krizan, T.; Keating, M.; Grigoriev, A.; Egorov, V.; Yakushev, P.; Peschanskaya, N.; Vylegzhanina, M.; Bursian, A. *J. Macromol. Sci., Part B Phys.* **2005**, *44*, 613–639.

(8)   Jou, J.-H.; Lin, C.-P.; Sheu, W.-H. *J. Polym. Sci., Part B Polym. Phys.* **1995**, *33*, 1803–1811.

(9)   Sazanov, Y. N. *Russ. J. Appl. Chem.* **2001**, *74*, 1253–1269.

(10)   Takekoshi, T. Polyimides, Fundementals and Applications. *Synth. Polyimides, Chapter 2* **1996**.

(11)   Bower, G. M.; Frost, L. W. *J. Polym. Sci.* **1963**, *1*, 3135–3150.

(12)   Ando, S.; Sawada, T.; Sasaki, S. *Polym. Adv. Technol.* **1999**, *10*, 169–178.

(13) Hardaker, S. S.; Samuels, R. J. *J. Polym. Sci., Part B Polym. Phys.* **1997**, *35*, 777–788.

(14) Kaas, R. L. *J. Polym. Sci., Polym. Chem. Ed.* **1981**, *19*, 2255–2267.

(15) Flick, E. W. *Industrial Solvents Handbook*; 5th ed.; Noyes Data Corporation: New Jersey, 1998.

(16) Solomin, V. A.; Kardash, I. E.; Snagovskii, Y. S.; Messerle, P. E.; Zhubanov, B. A.; Pravednikov, A. N. *Dokl. Akad. Nauk SSSR* **1977**, *236*, 139–42 [Chem].

(17) Frost, L. W.; Kesse, I. *J. Appl. Polym. Sci.* **1964**, *8*, 1039–1051.

(18) Shin, T. J.; Lee, B.; Youn, H. S.; Lee, K.-B.; Ree, M. *Langmuir* **2001**, *17*, 7842–7850.

(19) Bell, V. L. *J. Polym. Sci., Polym. Chem. Ed.* **1976**, *14*, 225–235.

(20) Bell, V. L.; Stump, B. L.; Gager, H. *J. Polym. Sci., Polym. Chem. Ed.* **1976**, *14*, 2275–2291.

(21) Brandom, D. K.; Wilkes, G. L. *Polymer (Guildf).* **1994**, *35*, 5672–5677.

(22) Brink, M. H.; Brandom, D. K.; Wilkes, G. L.; McGrath, J. E. *Polymer (Guildf).* **1994**, *35*, 5018–5023.

(23) Kotera, M.; Nishino, T.; Nakamae, K. *Polymer (Guildf).* **2000**, *41*, 3615–3619.

(24) Nishino, T.; Kotera, M.; Inayoshi, N.; Miki, N.; Nakamae, K. *Polymer (Guildf).* **2000**, *41*, 6913–6918.

(25) Xu, Y.-K.; Zhan, M.-S.; Wang, K. *J. Polym. Sci., Part B Polym. Phys.* **2004**, *42*, 2490–2501.

(26) Kreuz, J. A.; Endrey, A. L.; Gay, F. P.; Sroog, C. E. *J. Polym. Sci., Part A-1 Polym. Chem.* **1966**, *4*, 2607–2616.

(27) Hsu, T. C. J.; Liu, Z. L. *J. Appl. Polym. Sci.* **1992**, *46*, 1821–1833.

(28) Brekner, M. J.; Feger, C. *J. Polym. Sci., Part A Polym. Chem.* **1987**, *25*, 2005–2020.

(29) Brekner, M. J.; Feger, C. *J. Polym. Sci., Part A Polym. Chem.* **1987**, *25*, 2479–2491.

(30) Laius, L. A.; Bessonov, M. I.; Kallistova, E. V; Adrova, N. A.; Florinskii, F. S. *Vysok. Soedin., Ser. A* **1967**, *9*, 2185–2192.

(31) Lavrov, S. V; Ardashnikov, A. Y.; Kardash, I. E.; Pravednikov, A. N. *Vysok. Soedin., Ser. A* **1977**, *19*, 1052–1057.

(32) Feger, C. *Polym. Eng. Sci.* **1989**, *29*, 347–351.

(33) Frayer, P. D. Co-solvent accelerator for conversion of polyamide-acid solution to polyimide , 1987.

(34) Okamoto, K.; Tanihara, N.; Watanabe, H.; Tanaka, K.; Kita, H.; Nakamura, A.; Kusuki, Y.; Nakagawa, K. *J. Polym. Sci., Part B Polym. Phys.* **1992**, *30*, 1223–1231.

(35) Verbicky Jr., J. W.; Williams, L. *J. Org. Chem.* **1981**, *46*, 175–177.

(36) Kudryavtsev, V. V Polyimide Synthesis by Chemical Cyclization of Polyamic Acids. *Polyam. Acids Polyimides Synth. Transform. Struct.* **1993**.

(37) Hsu, S. L. C.; Naiini, A.; Weber, W. D.; Blakeney, A. J. Chemical imidization reagent for polyimide synthesis, 1998.

(38) Zhai, Y.; Yang, Q.; Zhu, R.; Gu, Y. *J. Mater. Sci.* **2008**, *43*, 338–344.

(39) Endrey, A. L. Aromatic polyimide particles from polycyclic diamines, US Patent 3,179,631, 1965.

(40) Endrey, A. L. Aromatic Polyimides From Meta-Phenylene Diamine and Para-Phenylene Diamine, US Patent 3,179,633, 1965.

(41) Endrey, A. L. Ammonium salts of aromatic polyamide acids and polyimides therefrom, US Patent 3,242,136, 1966.

(42) Hendrix, W. R. Process for Preparing Polyimides by Treating Polyamide-Acids with Aromatic Monocarboxylic Acid Anhydrates, 1963.

(43) Hand, J. D.; Whitehouse, W. G. Polyimide prepolymer, 1972.

(44) Hand, J. D.; Whitehouse, W. G. Solution process for the preparation of polyimides from diamines and anhydrides, 1976.

(45) Simionescu, C. I.; Grigoras, M. *Prog. Polym. Sci.* **1991**, *16*, 907–976.

(46) Dine-Hart, R. A.; Wright, W. W. *Makromol. Chem.* **1971**, *143*, 189–206.

(47) Kotov, B. V; Gordina, T. A.; Voishchev, V. S.; Kolninov, O. V; Pravednikov, A. N. *Vysok. Soedin., Ser. A* **1977**, *19*, 614–618.

(48) Hasegawa, M.; Horie, K. *Prog. Polym. Sci.* **2001**, *26*, 259–335.

(49) Sakata, Y.; Yamashita, W.; Okawa, Y.; Tamai, S.; Matsuo, M.; Ishida, T.; Yamaguchi, K.; Yamaguchi, A. Preparation of fluorine-containing polyimides, 1995.

(50) St. Clair, A. K.; St. Clair, T. L. Essentially colorless polyimide film containing phenoxy-linked diamines, 1985.

(51) St. Clair, A. K.; St. Clair, T. L. Highly optically transparent/colorless aromatic polyimide film. US 4603061, 1985.

(52) Olivier, K. L. Melt-Fabricable End-Capped Aromatic Polyimides, 1966.

(53) St. Clair, A.; St Clair, T.; Slemp, W.; K.S., E. *Nasa Tech. Memo.* **1985, 87650**.

(54) Chalmers Everall, N. J., J. M. Qualitative and Quantitative Analysis of Plastics, Polymers and Rubbers by Vibrational Spectroscopy. *Vib. Spectrosc. Polym.* **2007**.

(55) Everall N. J. Griffiths P. R., C. J. M. Vibrational Spectroscopy of Polymers **2007**.

(56) Tashiro, K. Measurement of the Physical Characteristics of Polymers by Vibrational Spectroscopy. *Vib. Spectrosc. Polym.* **2007**.

(57) Buffeteau, T.; Pezolet, M. In *Vibrational spectroscopy of polymers: principles and practice*; Everall, N.; Chalmers, J.; Griffith, P., Eds.; John Wiley & Sons Ltd.: West Sussex, 2007; pp. 255–281.

(58) Jasse, B.; Koenig, J. L. *J. Polym. Sci., Polym. Phys. Ed.* **1979**, *17*, 799–810.

(59) Park, K. H.; Liang, Y.; Kim, S. H.; Lee, H. S. *Macromolecules* **2006**, *39*, 1832–1838.

(60) Fawcett, A. H. Polymer Spectroscopy **1996**.

(61) Hendra Maddams, W. F., P. J. Fourier Transform Infrared and Raman Spectroscopies in the Study of Polymer Orientation. *Polym. Spectrosc.* **1996**.

(62)   Chalmers, J. M. Spectra-Structure Correlations: Polymer Spectra. *Vib. Spectrosc. Polym.* **2007**.

(63)   Chalmers et al, J. M. Spectra-structure Correlations: Polymer Spectra. *Handb. Vib. Spectrosc.* **2002**, *3*, 1893–1918.

(64)   Chalmers Griffiths, P. R., J. M. Handbook of Vibrational Spectroscopy **2002**, *3.*

(65)   Scientific, T. F. FT-IR vs. Dispersive Infrared http://www.thermo.com/eThermo/CMA/PDFs/Product/productPDF_21615.pdf.

(66)   Manning, C. Tilt-compensated interferometer. 5,898,495, 1999.

(67)   Griffiths, P. R.; Hirsche, B. L.; Manning, C. J. *Vib. Spectrosc.* **1999**, *19*, 165–176.

(68)   Yang, H.; Griffiths, P. R.; Manning, C. J. *Appl. Spectrosc.* **2002**, *56*, 1281–1288.

(69)   Pellerin, C.; Prud'homme, R. E.; Pezolet, M.; Weinstock, B. A.; Griffiths, P. R. *Macromolecules* **2003**, *36*, 4838–4843.

(70)   Pellerin, C.; Pezolet, M.; Griffiths, P. R. *Macromolecules* **2006**, *39*, 6546–6551.

(71)   Garcia, D.; Serafini, T. T. *J. Polym. Sci., Part B Polym. Phys.* **1987**, *25*, 2275–2282.

(72)   Thomson, B.; Park, Y.; Painter, P. C.; Snyder, R. W. *Macromolecules* **1989**, *22*, 4159–4166.

(73)   Snyder, R. W.; Thomson, B.; Bartges, B.; Czerniawski, D.; Painter, P. C. *Macromolecules* **1989**, *22*, 4166–4172.

(74)   Marek Jr., M.; Schmidt, P.; Schneider, B.; Bednar, B.; Kralicek, J. *Makromol. Chem.* **1990**, *191*, 2631–2637.

(75)   Schneider, B.; Schmidt, P.; Marek Jr., M.; Straka, J.; Bednar, B.; Kralicek, J. *Eur. Polym. J.* **1990**, *26*, 941–945.

(76)   Matsuo, T. *Bull. Chem. Soc. Jpn.* **1964**, *37*, 1844–1848.

(77)   Vanclef, A.; Bouche, R. *Spectrosc. Lett.* **1979**, *12*, 371–385.

(78) Li, W. S.; Shen, Z. X.; Zheng, J. Z.; Tang, S. H. *Appl. Spectrosc.* **1998**, *52*, 985–989.

(79) Cheng, R. R.; Wunder, S. L. *J. Polym. Sci., Part B Polym. Phys.* **1996**, *34*, 435–448.

(80) Pryde, C. A. *J. Polym. Sci., Part A Polym. Chem.* **1989**, *27*, 711–724.

(81) Pryde, C. A. *J. Polym. Sci., Part A Polym. Chem.* **1993**, *31*, 1045–1052.

(82) Kim, H.-T.; Kim, S.-K.; Park, J.-K. *Polym. J.* **1999**, *31*, 154–159.

(83) Sawa, K.; Sumiyoshi, K.; Hirai, Y.; Tateishi, K.; Kamejima, T. *Jpn. J. Appl. Phys., Part 1* **1994**, *33*, 6273–6276.

(84) Johnson, C.; Wunder, S. L. *J. Polym. Sci., Part B Polym. Phys.* **1993**, *31*, 677–692.

(85) Coburn, J. C.; Pottiger, M. T. In *Polyimides, Fundementals and Applications*; Ghosh, M. K.; Mittal, K. L., Eds.; Marcel Dekker, Inc.: New York, 1996.

(86) Prest Jr., W. M.; Luca, D. J. *J. Appl. Phys.* **1979**, *50*, 6067–6071.

(87) Janeschitz-Kriegl, H. *Polymer melt rheology and flow birefringence*; Springer-Verlag: New York, 1983.

(88) Machell, J. S.; Greener, J.; Contestable, B. A. *Macromolecules* **1990**, *23*, 186–194.

(89) Greener, J.; Lei, H.; Elman, J.; Chen, J. *J. Soc. Inf. Disp.* **2005**, *13*, 835–839.

(90) Sosnowski, T. P.; Weber, H. P. *Appl. Phys. Lett.* **1972**, *21*, 310–311.

(91) Cherkasov, A. N.; Vitovskaya, M. G.; Bushin, S. V *Vysok. Soedin., Ser. A* **1976**, *18*, 1628–1634.

(92) Russell, T. P.; Gugger, H.; Swalen, J. D. *J. Polym. Sci., Polym. Phys. Ed.* **1983**, *21*, 1745–1756.

(93) Coburn, J.; Pottiger, M.; Noe, S.; Senturia, S. *J. Polym. Sci. Part B Polym. Phys.* **1994**, *32*, 1271.

(94) Li, B.; he, T.; Ding, M.; Zhang, P.; Gao, F.; Jing, F. *J. Mater. Res.* **1998**, *13*, 1368–1372.

(95) Prest Jr., W. M.; Luca, D. J. *J. Appl. Phys.* **1980**, *51*, 5170–5174.

(96) Echigo, Y.; Iwaya, Y.; Tomioka, I.; Yamada, H. *Macromolecules* **1995**, *28*, 4861–4865.

(97) Pottiger, M. T.; Auman, B. C.; Coburn, J. C.; Krizan, T. D. Preparing a polyimide film with a preselected coefficient of thermal expansion, 1992.

(98) Pottiger, M. T.; Coburn, J. C.; Edman, J. R. *J. Polym. Sci., Part B Polym. Phys.* **1994**, *32*, 825–837.

(99) Lee, C.; Seo, J.; Shul, Y.; Han, H. *Polym. J. (Tokyo, Jpn.)* **2003**, *35*, 578–585.

(100) Chen, P.-J.; Liu, T.-J.; Wu, P.-Y.; Tseng, C.-F.; Leu, C.-M. *AIChE J.* **2010**, *56*, 790–800.

(101) Morino, S.; Horie, K. *Polym. J.* **1999**, *31*, 707–710.

(102) Saraf, R. F. *Polym. Eng. Sci.* **1997**, *37*, 1195–1209.

(103) Elsner, G. *J. Appl. Polym. Sci.* **1987**, *34*, 815–828.

(104) Jou, J. H.; Huang, P. T. *Macromolecules* **1991**, *24*, 3796–3803.

(105) Jou, J. H.; Huang, P. T.; Chen, H. C.; Liao, C. N. *Polymer (Guildf).* **1992**, *33*, 967–974.

(106) Numata, S.; Fujisaki, K.; Kinjo, N. *Polymer (Guildf).* **1987**, *28*, 2282–2288.

(107) Numata, S.; Miwa, T. *Polymer (Guildf).* **1989**, *30*, 1170–1174.

(108) Hasegawa, M.; Shindo, Y.; Sugimura, T.; Yokota, R.; Kochi, M.; Mita, I. *J. Polym. Sci., Part B Polym. Phys.* **1994**, *32*, 1299–1303.

(109) Hasegawa, M.; Matano, T.; Shindo, Y.; Sugimura, T. *Macromolecules* **1996**, *29*, 7897–7909.

(110) Hasegawa, M.; Okuda, K.; Horimoto, M.; Shindo, Y.; Yokota, R.; Kochi, M. *Macromolecules* **1997**, *30*, 5745–5752.

(111) Ishii, J.; Shimizu, N.; Ishihara, N.; Ikeda, Y.; Sensui, N.; Matano, T.; Hasegawa, M. *Eur. Polym. J.* **2010**, *46*, 69–80.

(112) Ando, S.; Sawada, T.; Sasaki, S. *Polym. Adv. Technol.* **2001**, *12*, 319–331.

(113) Cha, C. Y.; Moghazy, S.; Samuels, R. J. *Polym. Eng. Sci.* **1992**, *32*, 1358–1365.

(114) Cha, C. Y.; Samuels, R. J. *J. Polym. Sci., Part B Polym. Phys.* **1995**, *33*, 259–267.

(115) Hardaker, S. S.; Moghazy, S.; Cha, C. Y.; Samuels, R. J. *J. Polym. Sci., Part B Polym. Phys.* **1993**, *31*, 1951–1963.

(116) Chen, X.; Mujumdar, A. S. *Drying technologies in food processing*; Wiley: Blackwell, 2008; p. 352.

(117) Sata, H.; Murayama, M.; Shimamoto, S. *Macromol. Symp.* **2004**, *208*, 323–334.

(118) Siemann, U. *Progr Colloid Polym Sci* **2005**, *130*, 1–14.

(119) Kesting, R. E. *Synthetic polymeric membranes: a structural perspective*; 2nd ed.; Wiley NY, 1985.

(120) Ulrich, R.; Weber, H. P. *Appl. Opt.* **1972**, *11*, 428–34.

(121) Kobayashi, H.; Saito, T. Method of manufacturing a polysulfone resin film and a retardation film. 5,611,985, 1997.

(122) Hosoi, M.; Nagoshi, T. Optical film and method for producing same. 6,222,003, April 24, 2001.

(123) Rickert, S. E.; Balik, C. M.; Hopfinger, A. J. *Adv. Colloid Interface Sci.* **1979**, *11*, 149–191.

(124) Sosnowski, T. P.; Weber, H. P. *Appl. Phys. Lett.* **1972**, *21*, 310–311.

(125) Cherkasov, A.; Vitovskaya, M.; Bushin, S. *Polym. Sci. USSR* **1976**, *18*, 1865–1873.

(126) Prest, W. M.; Luca, D. J. *J. Appl. Phys.* **1979**, *50*, 6067.

(127) Prest, W. M.; Luca, D. J. *J. Appl. Phys.* **1980**, *51*, 5170.

(128) Nasr, A. *Polym. Test.* **2002**, *21*, 303–306.

(129) Greener, J.; Lei, H.; Elman, J.; Chen, J. *J. Soc. Inf. Disp.* **2005**, *13*, 835.

(130) Chen, P. J.; Liu, T. J.; Wu, P. Y.; Tseng, C. F.; Leu, C. M. *AIChE J.* **2010**, *56*, 790–800.

(131) Shojaie, S. S.; Krantz, W. B.; Greenberg, A. R. *J. Memb. Sci.* **1994**, *94*, 255–280.

(132) Shojaie, S. S.; Krantz, W. B.; Greenberg, A. R. *J. Memb. Sci.* **1994**, *94*, 281–298.

(133) Vrentas, J.; Vrentas, C. *J. Polym. Sci. Part B Polym. Phys.* **1994**, *32*, 187–194.

(134) Ataka, M.; Sasaki, K. *J. Memb. Sci.* **1982**, *11*, 11–25.

(135) Tantekin, S. B.; Krantz, W. B.; Greenberg, A. R. *Polym. Prepr. Am. Chem. Soc. Div. Polym* **1989**, *30*, 36–37.

(136) Greenberg, A. R.; Shojaie, S. S.; Krantz, W. B.; Tantekin-Ersolmaz, S. B. *J. Memb. Sci.* **1995**, *107*, 249–261.

(137) Payne, J.; McCormick, A. *Rev. Sci. Instrum.* **1997**, *68*, 4564.

(138) Payne, J. A.; McCormick, A. V.; Francis, L. F. *J. Appl. Polym. Sci.* **1999**, *73*, 553–561.

(139) Toki, S.; Valladares, D.; Sen, T.; Cakmak, M. In *ANTEC 2001 Conference Proceedings*; 2001; p. 5.

(140) Sen, T. Z.; Toki, S.; Cakmak, M. In *ANTEC 2001 Conference Proceedings*; 2001; p. 5.

(141) Sen, T. Z. Ph. D. thesis, The University of Akron, 2003.

(142) Hassan, M.; Cakmak, M. In *ANTEC 2004 Conference Proceedings*; 2004; p. 3.

(143) Hassan, M. Ph. D. thesis, The University of Akron, 2004.

(144) Martins, C. I.; Cakmak, M. *Polymer (Guildf).* **2007**, *48*, 2109–2123.

(145) Stein, R. S. *J. Polym. Sci.* **1957**, *24*, 383–386.

(146) Schilling, M.; Colvin, V.; Dhar, L.; Harris, A.; Schilling, F.; Katz, H.; Wysocki, T.; Hale, A.; Blyler, L.; Boyd, C. *Chem. Mater.* **1999**, *11*, 247–254.

(147) Greene-Kelly, R. *Clay Miner.* **1970**, *8*, 405–419.

(148) Tadmor, Z.; Gogos, C. *Principles of polymer processing*; John Wiley & Sons: New Jersey, 2006.

(149) Bush, S. F. *Proc. Inst. Mech. Eng. Part E J. Process Mech. Eng.* **2000**, *214*, 217–232.

(150) Wiley *Characterization and Analysis of Polymers*; John Wiley & Sons: New Jersey, 2008.

(151) Reynolds, N.; Hsu, S. *Macromolecules* **1990**, *23*, 3463–3472.

(152) Lee, A.; Wool, R. P. *Macromolecules* **1986**, *19*, 1063–1068.

(153) Messé, L.; Pézolet, M.; Prud'homme, R. *Polymer (Guildf).* **2001**, *42*, 563–575.

(154) Estes, G.; Seymour, R.; Cooper, S. *Macromolecules* **1971**, *4*, 452–457.

(155) Alexandre, M.; Dubois, P. *Mater. Sci. Eng., R* **2000**, *R28*, 1–63.

(156) Förster, S.; Plantenberg, T. *Angew. Chem. Int. Ed. Engl.* **2002**, *41*, 689–714.

(157) Yalcin, B.; Cakmak, M. *Polymer (Guildf).* **2004**, *45*, 6623–6638.

(158) Cakmak, M.; Reneker, D. H.; Yalcin, B. HYBRID MANUFACTURING PLATFORM TO PRODUCE MULTIFUNCTIONAL POLYMERIC FILMS. 20090020921, 2009.

(159) Bistricic, L.; Leskovac, M.; Baranovic, G.; Blagojevic, S. L. *J. Appl. Polym. Sci.* **2008**, *108*, 791–803.

(160) Versteegen, R. M.; Kleppinger, R.; Sijbesma, R. P.; Meijer, E. W. *Macromolecules* **2006**, *39*, 772–783.

(161) Lin, S.; Hwang, K.; Tsay, S.; Cooper, S. *Colloid Polym. Sci.* **1985**, *263*, 128–140.

(162) Unsal, E.; Yalcin, B.; Yilgor, I.; Yilgor, E.; Cakmak, M. *Polymer (Guildf).* **2009**, *50*, 4644–4655.

(163) Graff, D. K.; Wang, H.; Palmer, R. A.; Schoonover, J. R. *Macromolecules* **1999**, *32*, 7147–7155.

(164) Yeh, F.; Hsiao, B. S.; Sauer, B. B.; Michel, S.; Siesler, H. W. *Macromolecules* **2003**, *36*, 1940–1954.

(165) Sup Lee, H.; Ra Yoo, S.; Won Seo, S. *J. Polym. Sci. Part B Polym. Phys.* **1999**, *37*, 3233–3245.

(166) Kaushiva, B. .; Wilkes, G. . *Polym. Commun.* **2000**, *41*, 6987–6991.

(167) Bretzlaff, R.; Wool, R. *Macromolecules* **1983**, *16*, 1907–1917.

(168) Tashiro, K.; Wu, G.; Kobayashi, M. *J. Polym. Sci. Part B Polym. Phys.* **1990**, *28*, 2527–2553.

(169) Tashiro, K.; Minami, S.; Wu, G.; Kobayashi, M. *J. Polym. Sci. Part B Polym. Phys.* **1992**, *30*, 1143–1155.

(170) Loo, L. S.; Gleason, K. K. *Macromolecules* **2003**, *36*, 6114–6126.

(171) Siesler, H. *Makromol. Chem., Makromol. Symp.* **1992**, *53*, 89–103.

(172) Siesler, H. W. *Polym. Bull.* **1983**, *9*, 382–389.

(173) Siesler, H. W. *Polym. Bull.* **1983**, *9*, 471–478.

(174) Siesler, H. W. *Polym. Bull.* **1983**, *9*, 557–562.

(175) Hoffmann, U.; Pfeifer, F.; Okretic, S.; Volkl, N.; Zahedi, M.; Siesler, H. W. *Appl. Spectrosc.* **1993**, *47*, 1531–1539.

(176) Kalkar, A. K.; Pfeifer, F.; Siesler, H. W. *Macromol. Chem. Phys.* **1998**, *199*, 667–675.

(177) Shigematsu, Y.; Takada, A.; Nemoto, N.; Nitta, K.-H. *Rev. Sci. Instrum.* **2001**, *72*, 3927.

(178) Song, Y.; Nitta, K.; Nemoto, N. *Macromolecules* **2003**, *36*, 8066–8073.

(179) Song, Y.; Nitta, K.; Nemoto, N. *Macromolecules* **2003**, *36*, 1955–1961.

(180) Song, Y.; Nitta, K.; Nemoto, N. *J. Soc. Rheol. Japan* **2003**, *31*, 131–141.

(181) Song, Y.; Shigemetsu, Y.; Nitta, K.; Nemoto, N. *Polym. J.* **2002**, *34*, 584–592.

(182) Song, Y.; Nemoto, N. *Polymer (Guildf).* **2005**, *46*, 6522–6530.

(183) Song, Y.; Nemoto, N. *Polymer (Guildf).* **2006**, *47*, 489–497.

(184) Manning, C. J. In *AIP Conference Proceedings*; 1998; pp. 84–95.

249

(185) Manning, C. Tilt-compensated interferometer. 6,967,722 B2, 2005.

(186) Koike, Y.; Sen, T. Z.; Cakmak, M. *Annu. Tech. Conf. - Soc. Plast. Eng.* **2002**, *60th*, 1550–1555.

(187) Koike, Y.; Cakmak, M. *Polymer (Guildf).* **2003**, *44*, 4249–4260.

(188) Koike, Y.; Cakmak, M. *Polymer (Guildf).* **2003**, *44*, 4249–4260.

(189) Kanuga, K.; Cakmak, M. *Macromolecules* **2005**, *38*, 9698–9710.

(190) Kanuga, K.; Cakmak, M. *Polymer (Guildf).* **2007**, *48*, 7176–7192.

(191) Sen, T. Z. Investigation of dynamics and structure development during uniaxial stretching of pet films at different molecular weights using fully automated spectral birefringence technique, University of Akron: Akron, 2003, Vol. PhD, p. 210 pp.

(192) Pluta, M. *Polymer (Guildf).* **1992**, *33*, 1553–1555.

(193) Hongladarom, K.; Burghardt, W.; Baek, S.; S., C.; Magda, J. J. *Macromolecules* **1993**, *26*, 772–784.

(194) Hongladarom, K.; Burghardt, W. *Macromolecules* **1993**, *26*, 785–794.

(195) Hongladarom, K.; Secakusuma, V.; Burghardt, W. *J. Rheol. (N. Y. N. Y).* **1994**, *38*, 1505.

(196) Hongladarom, K.; Burghardt, W. *Macromolecules* **1994**, *27*, 483–489.

(197) Beekmans, F.; de Boer, A. P. *Macromolecules* **1996**, *29*, 8726–8733.

(198) Galay, J.; Cakmak, M. *J. Polym. Sci. Part B Polym. Phys.* **2001**, *39*, 1147–1159.

(199) Galay, J.; Cakmak, M. *J. Polym. Sci. Part B Polym. Phys.* **2001**, *39*, 1107–1121.

(200) Venkatesvaran, H.; Cakmak, M. *Polym. Eng. Sci.* **2001**, *41*, 341–357.

(201) Hassan, M. K. Novel true stress-true strain-birefringence measurement systems for real time measurement during multiaxial deformation and heat setting of polymer films: "Application on PET films," 2004, p. 308 pp.

(202) Bicakci, S.; Cakmak, M. *Polymer (Guildf).* **2002**, *43*, 2737–2746.

(203) Cakmak, M.; Hassan, M. K.; Unsal, E.; Martins, C. I. *Rev. Sci. Instrum.* **2012**, *83*, 123901.

(204) Wang, H.; Palmer, R.; Manning, C. *Appl. Spectrosc.* **1997**, *51*, 1245–1250.

(205) Brault, J. W. *Appl. Opt.* **1996**, *35*, 2891–6.

(206) Siesler, H. *Adv. Polym. Sci.* **1984**, *65*, 1.

(207) Siesler, H.; Hoffmann, G.; Kolomiets, O.; Pfeifer, F.; Zahedi, M. In *Vibrational spectroscopy of polymers: principles and practice*; Everall, N.; Chalmers, J.; Griffith, P., Eds.; John Wiley & Sons Ltd.: West Sussex, 2007; pp. 313–347.

(208) Unsal, E.; Drum, J.; Yucel, O.; Nugay, I. *Rev. Sci. Instrum.* **2012**, *83*, 025114.

(209) Hanssen, L. M.; Zhu, C. In *Handbook of Vibrational Spectroscopy*; Chalmers, J. M.; Griffiths, P. R., Eds.; John Wiley & Sons Ltd: Chichester, 2002.

(210) Plyler, E.; Danti, A.; Blaine, L.; Tidwell, E. *J. Res. Natl. Bur. Stand. Phys. Chem.* **1960**, *64*, 29–48.

(211) Ghosh, M. K.; Mittal, K. L. *Polyimides: fundamentals and applications*; Marcel Dekker: New York, 1996; p. 891.

(212) Ree, M.; Chu, C.-W.; Goldberg, M. J. *J. Appl. Phys.* **1994**, *75*, 1410.

(213) Nielsen, L. E.; Buchdahl, R. *J. Appl. Phys.* **1950**, *21*, 488.

(214) Lefebvre, D.; Jasse, B.; Monnerie, L. *Polymer (Guildf).* **1983**, *24*, 1240–1244.

(215) Matsumoto, K.; Fellers, J. F.; White, J. L. *J. Appl. Polym. Sci.* **1981**, *26*, 85–96.

(216) Hada, Y.; Shikuma, H.; Ito, H.; Kikutani, T. *Fibers Polym.* **2005**, *6*, 19–27.

(217) Milagin, M.; Gabarayeva, A.; Shishkin, I. *Polym. Sci. USSR* **1970**, 513–519.

(218) Vancso, G.; Snétivy, D.; Tomka, I. *J. Appl. Polym. Sci.* **1991**, *42*, 1351–1359.

(219) Read, B.; Duncan, J.; Meyer, D. *Polym. Test.* **1984**, *4*, 143–164.

(220) Zbinden, R. *The Infrared Spectroscopy of High Polymers*; Academic Press: New York, 1964.

(221) Fraser, R. D. B. *J. Chem. Phys.* **1958**, *28*, 1113.

(222) St. Clair, A. K.; St. Clair, T. L. *US Pat. 4,603,061* **1986**.

(223) St. Clair, A. K.; St. Clair, T. L.; Slemp, W.; Ezzell, K. S. *Optically transparent/colorless polyimides*; Langley Res. Cent.,Natl. Aeronaut. Space Adm.,Hampton,VA,USA., 1985; p. 41 pp.

(224) Misawa, Y.; Kinjo, N.; Hirao, M.; Numata, S.; Momma, N. *IEEE Trans. Electron Devices* **1987**, *34*, 621–627.

(225) Sroog, C. E. *Prog. Polym. Sci.* **1991**, *16*, 561–694.

(226) Dine-• Hart, R.; Wright, W. *J. Appl. Polym. Sci.* **1967**, *11*, 609–627.

(227) Bell, V. Process for preparing thermoplastic aromatic polyimides. 4,094,862, 1978.

(228) Stephanie, J. G.; Rickerl, P. G. In *Polyimides, Fundementals and Applications*; Mittal, K. L.; Ghosh, M. K., Eds.; Marcel Dekker, Inc.: New York, 1996.

(229) Wachsman, E.; Frank, C. *Polymer (Guildf).* **1988**, *29*, 1191–1197.

(230) Pyun, E.; Mathisen, R.; Sung, C. *Macromolecules* **1989**, *22*, 1174–1183.

(231) Takahashi, N.; Yoon, D. Y.; Parrish, W. *Macromolecules* **1984**, *17*, 2583–2588.

(232) Ikeda, R. *J. Polym. Sci. Part B Polym. Lett.* **1966**, *4*, 353–359.

(233) Herminghaus, S.; Boese, D.; Yoon, D. Y.; Smith, B. a. *Appl. Phys. Lett.* **1991**, *59*, 1043.

(234) Hasegawa, M.; Horie, K. *Prog. Polym. Sci.* **2001**, *26*, 259–335.

(235) Ebisawa, S.; Ishii, J.; Sato, M.; Vladimirov, L.; Hasegawa, M. *Eur. Polym. J.* **2010**, *46*, 283–297.

(236) Li, B.; He, T.; Ding, M.; Zhang, P.; Gao, F.; Jing, F. *J. Mater. Res.* **1998**, *13*, 1368.

(237) Li, B.; He, T.; Ding, M. *Thin Solid Films* **1998**, *320*, 280–284.

(238) Coburn Pottiger Michael T., J. C. The influence of processing conditions on structure, properties and stress development in spin coated polyimide films **1990**.

(239) Unsal, E.; Nugay, I. I.; Offenbach, I.; Gross, M.; Manning, C.; Cakmak, M. *Rev. Sci. Instrum.* **2013**, *84*, 073901.

(240) Yucel, O.; Unsal, E.; Cakmak, M. *Macromolecules* **2013**, *46*, 7112.

(241) Yamada, H.; Fukudome, M.; Egawa, N.; Kondo, Y.; Maki, H. *US Pat. 6,264,866* **2001**.

(242) Sasaki, Y.; Inoue, H.; Negi, Y.; Sakai, K. *US Pat. 4,473,523* **1984**.

(243) Shigeru, T.; Yasumitsu, M. *JP,2000-302867,A* **2000**.

(244) Tetsuya, N.; Mikio, I.; Takehiro, N.; Haruhiko, M. *JP,2000-204178,A* **2000**.

(245) Tetsuya, N.; Egawa, N.; Haru *JP,2000-191806,A* **2000**.

(246) Machell, J. S.; Greener, J.; Contestable, B. A. *Macromolecules* **1990**, *23*, 186–194.

(247) Greener, J.; Lei, H.; Rao, Y.; Elman, J. F. *IDMC* **2007**, 402–405.

(248) Koo, Y.; Kim, H.; Kim, S.; Kim, J. *Korean J. Chem. …* **2002**, *19*, 474.

(249) Molis, S. E. In *Polyimides: Mater., Chem. Charact., Proc. Int. Conf. Polyimides, 3rd*; Feger, C.; Khojasteh, M.; McGrath, J. E., Eds.; E. I. duPont de Numours and Company: Amsterdam, 1989; pp. 659–672.

(250) Ha, K.; West, J. L. *J. Appl. Polym. Sci.* **2002**, *86*, 3072–3077.